Faculté de Médecine
Aix-Marseille Université

Inserm
La science pour la santé
From science to health

UNIVERSITE D'AIX-MARSEILLE

ECOLE DOCTORALE DES SCIENCES DE LA VIE ET DE LA SANTE

UNITE DE NEUROBIOLOGIE DES CANAUX IONIQUES ET DE LA SYNAPSE
INSERM UMR1072 UNIS

Thèse présentée pour obtenir le grade universitaire de docteur

Discipline : Neurosciences

Par

Yanis INGLEBERT

RÈGLE DE STDP EN CALCIUM PHYSIOLOGIQUE

Soutenue le 15/11/2018 devant le jury :

Dr. Desdemona Fricker	UMR 8119 – Université Paris Descartes	Rapportrice
Dr. Laurent Venance	UMR 7241 – U1050 – Collège de France	Rapporteur
Dr. Jean-Pierre Mothet	UMR 9188 – ENS Paris Saclay	Examinateur
Dr. Rosa Cossart	U 901 - INSERM	Examinatrice - Présidente
Dr. Dominique Debanne	UMR 1072 – Université Aix-Marseille	Directeur de thèse

Remerciements…

J'aimerais avant tout remercier **Dominique Debanne**, qui m'a offert la chance de réaliser une thèse à ses côtés sur un sujet que j'ai pris plaisir à découvrir et à porter. Je me souviens du premier cours que j'ai eu avec Dominique sur la plasticité synaptique, j'étais loin d'avoir tout compris. Finalement, cinq ans plus tard, j'écris une thèse sur ce qui à mes yeux me semblait bien obscur. J'ai appris énormément pendant ces années, évidemment d'un point de vue scientifique, mais aussi d'un point de vue personnel. Il a su me transmettre sa passion, moi l'étudiant un peu perdu sur mon avenir (et parfois sur mes manips qui ne fonctionnaient pas). Merci. Sincèrement.

Je remercie **Desdemona Fricker** et **Laurent Venance** d'avoir accepté d'évaluer mes travaux de thèse en acceptant d'en être rapporteurs. Un grand merci à **Jean-Pierre Mothet** d'avoir accepté d'être examinateur, et qui me suit depuis mon premier comité de suivi de thèse. Enfin, merci à **Rosa Cossart** d'avoir accepté d'être présidente et examinatrice de ma thèse.

J'ai une pensée toute particulière pour les membres de mon équipe qui ont été à mes côtés pendant ces quatre ans. Évidemment, je me dois de remercier **Michaël Russier** pour sa bonne (mauvaise ?) humeur et nos batailles autour de la machine à café. Un grand merci à **Laure Fronzaroli-Molinières** pour sa grande disponibilité, sa gentillesse et son aide au moindre souci. Je remercie aussi **Norah Boumedine**, toujours souriante malgré ma consommation parfois gourmande de cultures. Je ne peux pas oublier de remercier **Norbert Ankri** pour nos discussions révolutionnaires, au niveau sonore trop élevé, dès le matin dans le bus mais aussi au labo. Je remercie aussi **Aurélie Fekete**, avec qui j'ai partagé mon bureau, et qui nous a régulièrement nourris avec ses pâtisseries. Enfin, une petite pensée pour la dernière arrivée, **Johanna Extremet**, qui a toujours le sourire.

Je remercie aussi sincèrement ceux qui étaient avec moi au départ, mais que j'ai malheureusement dû voir partir au fur et à mesure. C'est probablement l'une des choses les plus difficiles dans la vie de laboratoire. Un grand merci à **Célia Gasselin**, ma maman en Master 2, qui m'a mis en selle pour la thèse. Je remercie sincèrement **Sylvain Rama**, pour nos rigolades et nos blagues informatiques qui ne faisaient rire que nous… et évidemment pour son aide de tous les jours lorsqu'il fallait réparer un microscope avec un trombone. Sans oublier **Mickaël Zbili**, mon compagnon d'expériences, qui transformait notre grotte en lieu de discussions politiques, philosophiques et parfois totalement absurdes. Enfin, une grosse pensée pour **Véréna Landel**, mon autre maman dans le laboratoire d'en face.

Un grand merci à **Oussama El Far**, toujours disponible quand j'avais des questions (stupides) en biochimie, ainsi que son équipe. En particulier **Marion Baudoux** et sa bonne humeur malgré son niveau moyen en badminton. Je remercie **Jean-Marc Goaillard** pour ses conseils ainsi que son équipe. En particulier, **Estelle** et **Monica** pour leur bonne humeur ainsi qu'**Alexis** et ses billards dans des endroits incongrus. Je remercie tout particulièrement **Jennifer Bedigian** qui a toujours été disponible (avec le sourire) bien que je n'aie jamais reçu ma lampe de bureau.

Je remercie aussi mes compagnons de thèse, mais aussi de vie, qui sont à mes côtés depuis le début (voire plus). En particulier, **Richard Desplantes**, pour nos séances de sport ridicules, nos discussions sans queue ni tête et nos heures de rigolade sous le regard parfois incrédule d'**Erika Boulant**, dont la gentillesse n'a d'égal que sa patience. Je remercie aussi **Jean-Michel Paumier**, pour nos soirées interminables et récurrentes à refaire le monde autour d'un verre, qui me laisseront des souvenirs impérissables. Merci les potes, vous êtes géniaux. Enfin, j'ai une pensée particulière (malgré la distance et le temps qui passe) pour **Vincent Hauet** et **Sébastien Rimbert**. Cette thèse marque une fin de parcours, et il n'aurait pas été le même sans vous et nos moments inoubliables à l'université.

Je remercie aussi une autre compagne de thèse particulière, **Fanny Gaudel**, probablement la meilleure chose que j'aie découverte pendant ces années marseillaises, toujours à mes côtés même dans les pires moments.

Je remercie aussi ma famille, particulièrement mon petit frère **Romain**, le futur vrai docteur en médecine, ainsi que ma grand-mère et ma mère pour leur soutien tout au long de mes études. J'ai une pensée toute particulière pour mon grand-père, même si tu n'es plus là, pas une semaine ne passe sans que je pense à toi.

Résumé

Il existe deux formes d'induction de la plasticité synaptique ; la première connue sous le nom de BCM (Bienenstock Cooper Munroe), dépend de la fréquence de stimulation des afférences synaptiques. En effet, une stimulation à haute fréquence (HFS) augmente la force synaptique alors qu'une stimulation à basse fréquence (LFS) diminue la force synaptique. La seconde dépend étroitement des interactions temporelles entre l'activité pré-synaptique et l'activité du neurone post-synaptique sous forme de potentiels d'action : la STDP (Spike Timing Dependent Plasticity). Suivant le postulat de Donald Hebb (1949), l'activation conjointe de l'élément pré- et post-synaptique renforce l'efficacité de la synapse, ce phénomène est appelé potentialisation à long terme (LTP). À l'inverse, la dépression à long terme (LTD) diminue l'efficacité de la synapse. Ensemble, LTP et LTD permettent une modification bidirectionnelle de la force synaptique. Expérimentalement, l'induction de cette plasticité peut se faire par différents niveaux de corrélation entre l'activité des neurones pré- et post-synaptiques. Une LTP peut être induite lorsque le neurone pré-synaptique décharge avant le neurone post-synaptique (corrélation positive), alors qu'une LTD est induite dans une situation inverse (corrélation négative) lorsque le neurone post-synaptique précède celle du neurone pré-synaptique. Les interactions temporelles entre les activités pré- et post-synaptiques sont très précises et la fenêtre de LTP comme celle de LTD sont généralement de l'ordre de 20-50 ms. La règle de STDP repose essentiellement sur le calcium comme messager intracellulaire. De ce fait, la concentration de calcium extracellulaire joue un rôle prépondérant. Le modèle de Lisman (1989) stipule que la LTP est associée à une forte entrée de calcium intracellulaire et la LTD à une plus faible entrée de calcium. La concentration de calcium extracellulaire est variable au cours du développement. Elle est comprise dans une gamme de de 1.3 à 1.8 mM. Or, toutes les études utilisent des concentrations élevées, très supérieures à la concentration physiologique (*i.e.* 2-3 mM). En conséquence, cela peut se traduire par une surévaluation de la plasticité, comme prédit par un modèle de STDP basé sur le calcium (Graupner et Brunel, 2012). L'utilisation de calcium en concentration physiologique pourrait diminuer ou supprimer tout phénomène de plasticité induite par la règle de STDP avec des protocoles standards. Dans la région CA1 de l'hippocampe, pour une concentration de calcium de 1.8 mM, nous observons une absence de LTP après corrélation positive, mais une LTD pour l'ensemble des délais étudiés. Pour 1.3 mM, ni LTP ni LTD ne sont observées dans nos conditions expérimentales. En plus du calcium, l'activité est une composante importante dans l'induction de la plasticité par STDP. En particulier, l'augmentation de la fréquence de stimulation pendant l'appariement ou l'augmentation du nombre de potentiels d'action post-synaptiques nous a permis de récupérer la LTP par corrélation positive à 1.3 et 1.8 mM. De la même manière, l'augmentation du nombre de potentiels d'action post-synaptiques ou de la fréquence de stimulation nous a permis de récupérer la fenêtre de LTD à 1.3 mM. Parallèlement à la modulation d'activité, nous avons testé un troisième facteur qui apparaît important : la neuromodulation. La règle de STDP serait modulée, en particulier, par l'activation des récepteurs dopaminergiques et noradrénergiques. La perfusion d'isoprénaline, un agoniste des récepteurs noradrénergiques, nous a permis de récupérer la fenêtre de LTP à 1.8 mM, contrairement à l'application de dopamine. Mes résultats montrent que la règle de STDP est profondément modifiée en calcium physiologique, mais que l'utilisation d'activités spécifiques ou l'application de neuromodulateurs sont capables de restaurer un profil de courbe normal.

Summary

Induction of synaptic plasticity can take two forms. The first plasticity rule, known as Bienenstock Cooper Rules (BCM rules) depends on the frequency of stimulation of synaptic afferences. High frequency stimulation (HFS) leads to an increase in synaptic strength while low frequency stimulation (LFS) leads to a decrease of synaptic strength. The second plasticity rule, known as STDP (Spike Timing Dependent Plasticity), relies on the timing between the pre- and postsynaptic neuron activity. Following the postulate of Donald Hebb (1949), joint activation of the pre- and postsynaptic element reinforces the efficacy of the synapse; this phenomenon is called long-term potentiation (LTP). Conversely, long-term depression (LTD) decreases the efficacy of the synapse. Together, LTP and LTD allow bi-directional modification of synaptic strength. Experimentally, this plasticity can be induced by various degrees of correlation between pre- and postsynaptic neuron activity. LTP can be induced when the presynaptic neuron discharges before the postsynaptic neuron (positive correlation), whereas LTD is induced in a reverse situation (negative correlation) when the postsynaptic activity precedes the presynaptic activity. Temporal interactions between pre and postsynaptic activities are very precise and both the LTP and LTD windows are generally in the order of 20-50 ms. The STDP rule is essentially based on calcium as an intracellular messenger. Therefore, the concentration of extracellular calcium plays a major role. Lisman's model (1989) states that LTP is associated with a high intracellular calcium entry and LTD is associated with a lower calcium entry. The concentration of extracellular calcium varies during development, ranging from 1.3 to 1.8 mM. However, all studies used high concentrations of calcium, much higher than physiological conditions (i.e. 2 to 3 mM). Consequently, this may have resulted in an overestimation of plasticity as predicted by a calcium-based STDP model (Graupner and Brunel, 2012). The use of calcium in physiological concentration may be able to reduce or eliminate any plasticity phenomenon induced by the STDP rule with standard protocols. In the CA1 region of the hippocampus, at a calcium concentration of 1.8 mM we observed an absence of LTP after positive correlation. Instead, LTD is observed for all the delays that were tested. At 1.3 mM, neither LTP nor LTD were observed under our experimental conditions. In addition to calcium, activity is an important component in the induction of plasticity by STDP. Notably, an increase in stimulation frequency during pairing or an increase in the number of postsynaptic action potential allowed us to rescue LTP induced by positive correlation at 1.3 and 1.8 mM. Similarly, an increase in the number of postsynaptic action potentials or the frequency of stimulation allowed us to rescue the LTD window at 1.3 mM. In parallel with activity modulation, we tested a third factor that showed a noticeable impact: neuromodulation. The STDP rule appeared to be predominantly modulated by the activation of dopaminergic and noradrenergic receptors. The perfusion of Isoprenaline, a noradrenergic receptor agonist, allowed us to rescue the LTP window whereas dopamine application at 1.8 mM did not rescue LTP. This study demonstrates that the STDP rule is profoundly changed under physiological calcium conditions; however, the use of specific activities or the application of neuromodulators restores a normal STDP profile.

Abréviations

AC : Adénylate Cyclase

Ach : Acétylcholine

AHP : After-spike-hyperpolarization

AMPc : Adénosine monophosphate cyclique

BAPTA : 1,2-bis(o-aminophenoxy)ethane-N,N,N',N'-tetraacetic acid

BCM : Bienenstock Cooper Munro

CAMKII : Calcium/calmoduline-dépendant protéine kinase 2

CREB : cAMP responsive element binding protein

DA : Dopamine

DCN : Noyau cochléaire dorsal

EGTA : Ethylene glycol-bis(2-aminoethylether)-NNNN'-tetraacetic acid ou acide egtazique

E-S : PPSE-Potentiel d'action

GABA : Acide gamma-aminobutyrique

HCN : Hyperpolarization-activated cyclic nucleotide-gated

HFS : Stimulation à haute fréquence

In1 : Inhibitor 1

IP3 : Inositol 1,4,5-triphosphate

LFS : Stimulation à basse fréquence

LTD : Dépression à Long Terme

LTP : Potentialisation à Long Terme

MAPK : Mitogen-activated protein kinases

mGluR : Récepteur métabotropique au glutamate

MSN : Medium-sized spiny neurons

NA : Noradrénaline

NMDA : N-Methyl-D-Aspartate

nNOS : Oxide nitrique synthase neuronale

PA : Potentiel d'Action

PiTx : Picrotoxine

PKA : Protéine Kinase A

PKC : Protéine Kinase C

PLC : Phospholipase C

PP1 : Protéine phosphatase 1

PPSE : Potentiel Post-Synaptique Excitateur

PPSI : Potentiel Post-Synaptique inhibiteur

STDP : Plasticité Synaptique Dépendant des interactions Temporelles

VDCC : Canaux calciques voltage-dépendants

SOMMAIRE

Plasticité de la transmission synaptique

1. Plasticité Hebbienne

La compréhension des mécanismes impliqués dans les phénomènes d'apprentissage et de mémorisation est un champ de recherche important en neurosciences. Plutôt que de créer ou supprimer constamment de nouvelles connexions synaptiques, il a été suggéré très tôt que les synapses déjà existantes étaient susceptibles de subir des modifications. Le terme de plasticité synaptique introduit par Jerzy Konorski (1948) décrit ces changements d'efficacité synaptique comme étant les bases du stockage de l'information dans le cerveau. Cette notion a été popularisée par Donald Hebb (1949) dont l'hypothèse suggère que ces renforcements concernent les synapses des neurones activés ensemble. Le postulat de Hebb est résumé par la phrase : « Des neurones qui s'excitent ensemble se lient entre eux » (Shatz, 1992). La théorie de Hebb a été utilisée dans de nombreux modèles théoriques, avec comme principale limite une saturation de l'ensemble des synapses du réseau par l'augmentation constante de l'efficacité synaptique. La solution, apportée par Christoph Von der Malburg (1973), propose une normalisation des poids synaptiques permettant que leur ensemble sur un même neurone reste constant durant l'apprentissage. Gunther Stent (1973) proposa une extension au postulat de Hebb en proposant que les synapses faiblement activées voient leur poids synaptique diminué quand le neurone post-synaptique est très actif. Le premier modèle mathématique, développé par Terrence Sejnowski (1977), prend en compte ces changements bidirectionnels en fonction de la corrélation entre l'activité pré- et post-synaptique. La force synaptique augmente lorsque l'activité est corrélée positivement et diminue lorsque l'activité est corrélée négativement. L'étude expérimentale des règles gouvernant la plasticité synaptique est un domaine de recherche qui a pris une grande importance en neurosciences depuis les années 1970.

2. Deux formes d'induction de la plasticité synaptique

Le postulat de Hebb a été vérifié expérimentalement avec la découverte de la potentialisation à long terme par Bliss et Lomo (1973), qui ont montré pour la première fois une augmentation de l'efficacité synaptique dans l'hippocampe **(Figure 1A)**. Son opposé, la dépression à long terme (LTD) sera découverte quelques années plus tard (Dudek and Bear, 1992; Dunwiddie and Lynch, 1978).

2.1 La règle de Bienenstock Cooper Munro (BCM)

Il existe deux grandes formes de plasticité synaptique basées sur leurs protocoles d'induction. La première est appelée BCM pour Bienenstock Cooper Munro, auteurs d'un article paru en 1982 (Bienenstock et al., 1982) et stipule l'existence d'un seuil flottant de modification qui dépend de l'activité. Cette règle, popularisée par Mark Bear, permet de faire le lien entre les modifications synaptiques et la fréquence de stimulation (Bear and Abraham, 1996; Dudek and Bear, 1992) Ainsi, la fréquence de stimulation des afférences pré-synaptiques détermine la plasticité de sortie **(Figure 1B)**. Dans l'hippocampe, les stimulations à basses fréquences des collatérales de Schaffer (1-5 Hz) induisent la LTD alors que les hautes fréquences (50 – 100 Hz) induisent la LTP (Dudek and Bear, 1992; Dunwiddie and Lynch, 1978; Mulkey and Malenka, 1992). Bien qu'universellement vérifiée dans pratiquement toutes les structures, l'induction de plasticité par des changements de fréquence est peu crédible sur le plan physiologique en raison d'une très faible activité *in vivo*(Epsztein et al., 2010).

2.2 Plasticité Synaptique dépendant des Interactions Temporelles (STDP)

La seconde forme de plasticité repose sur le principe de Hebb et associe la stimulation pré-synaptique à une dépolarisation post-synaptique. Il a en effet été montré dans les neurones pyramidaux du champ CA1 que l'activation pré-synaptique associée à une dépolarisation postsynaptique synchrone induit la LTP (Gustafsson et al., 1987) (**Figure 2A**). À partir de ce constat, l'idée de faire varier le timing entre l'activité pré- et post-synaptique a été émise.

A

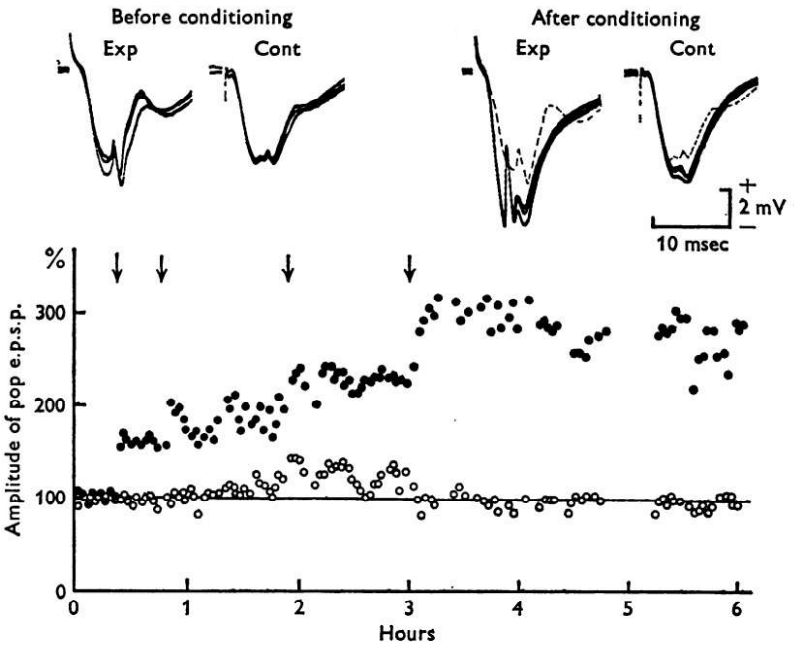

Bliss et Lomo, J. Physiol, 1973

B

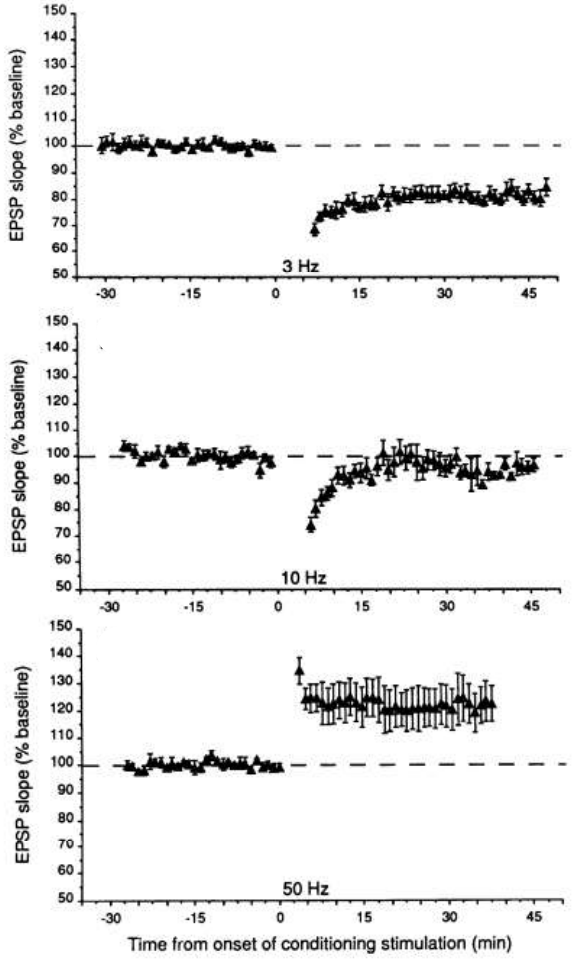

Dudek and Bear, 1992

Figure 1. La règle de Bienenstock Cooper Munro (BCM)

A. Première mise en évidence de la LTP par Bliss et Lomo en 1973 entre voie perforante et gyrus denté. La stimulation répétée de la voie perforante induit une augmentation durable de la réponse mesurée.

B. Dans la région CA1 de l'hippocampe, la fréquence de stimulation détermine les changements synaptiques. Une LTD est induite pour de faibles fréquences (< 10 Hz) alors qu'une LTP est induite pour de fortes fréquences (> 10 Hz).

A

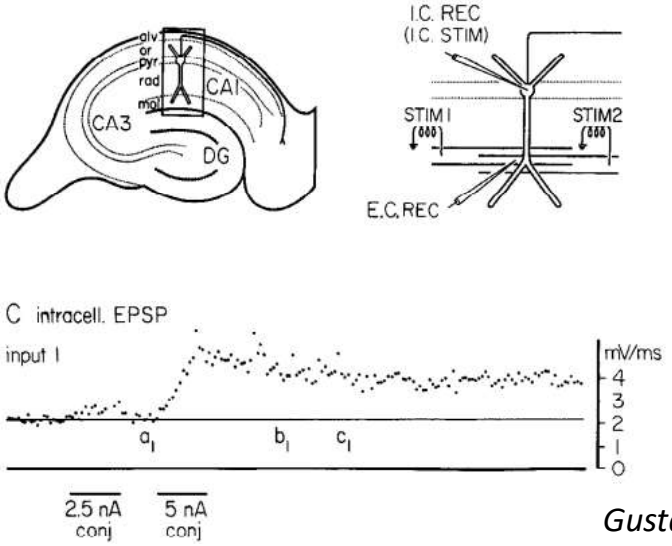

Gustaffson et al, 1987

B

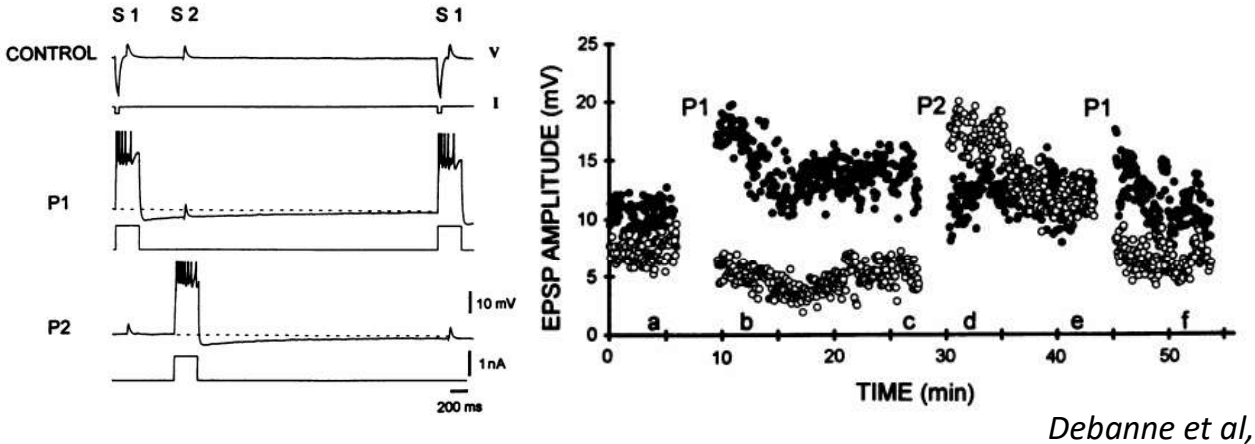

Debanne et al, 1994

C

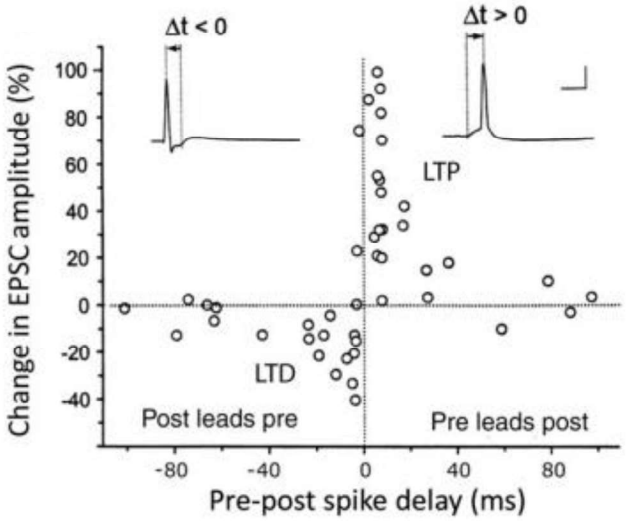

Bi and Poo, 1998

Figure 2. Plasticité Synaptique dépendant des Interactions Temporelles (STDP)

A. Première mise en évidence d'une LTP dépendante du délai entre activité pré- et post-synaptique dans l'hippocampe. L'activation pré-synaptique associée à une dépolarisation post-synaptique synchrone induit de la LTP.

B. Première mise en évidence d'une LTD dépendante du délai entre activité pré- et post-synaptique dans l'hippocampe. Lorsque l'activité n'est pas corrélée (post- avant pré-), une LTD est induite.

C. La règle de STDP conventionnelle. La LTP est induite lorsque l'activité pré-synaptique arrive avant l'activité post-synaptique. La LTD est induite lorsque l'activité pré-synaptique arrive après l'activité post-synaptique. Ces deux plasticités ont une fenêtre temporelle d'environ 100 ms.

Lorsque l'activité n'est pas corrélée, c'est-à-dire que l'activité post-synaptique précède l'activité pré-synaptique, la LTD est induite (Debanne et al., 1994) (**Figure 2B**). Ce principe a été vérifié par la suite dans de nombreuses synapses comme celles du cortex par enregistrement de paires de neurones connectés (L5-L5) (Markram et al., 1997). Ces deux plasticités présentent une fenêtre temporelle d'environ 100 ms, et sont dépendantes de la fréquence. L'augmentation de la fréquence d'appariement augmente l'amplitude de la LTP (Markram et al., 1997) et transforme la fenêtre de LTD en LTP pour des fréquences supérieures à 40 Hz (Sjöström et al., 2001). Cette règle, basée sur le délai entre l'activité pré- et post-synaptique a été nommée Plasticité Synaptique Dépendant des Interactions Temporelles (STDP) (Abbott and Nelson, 2000) et est maintenant extrêmement bien décrite dans les synapses glutamatergiques de l'hippocampe (Bi and Poo, 1998; Campanac et al., 2008; Wittenberg and Wang, 2006) (**Figure 2C**), du néocortex (Feldman, 2000; Sjöström et al., 2001, 2003) du tronc cérébral auditif (Tzounopoulos et al., 2004) ou encore aux synapses entre le thalamus et l'amygdale (Shin et al., 2006).

3. Diversité de la règle de STDP

La règle de STDP est, dans sa forme classique, bidirectionnelle avec une fenêtre de LTP lorsque l'activité pré-synaptique précède l'activité post-synaptique, et une fenêtre de LTD pour l'ordre inverse (Bi and Poo, 1998; Campanac et al., 2008; Dan and Poo, 2006; Feldman, 2000). Néanmoins, à travers les différentes régions et synapses du cerveau, il existe différentes formes de la courbe de STDP **(Figure 3).**

3.1 STDP classique

3.1.1 Dans les neurones excitateurs

Bien que les prérequis (activité spécifique ou neuromodulation) soient différents en fonction des régions étudiées, la forme classique de la STDP reste préservée dans de nombreuses

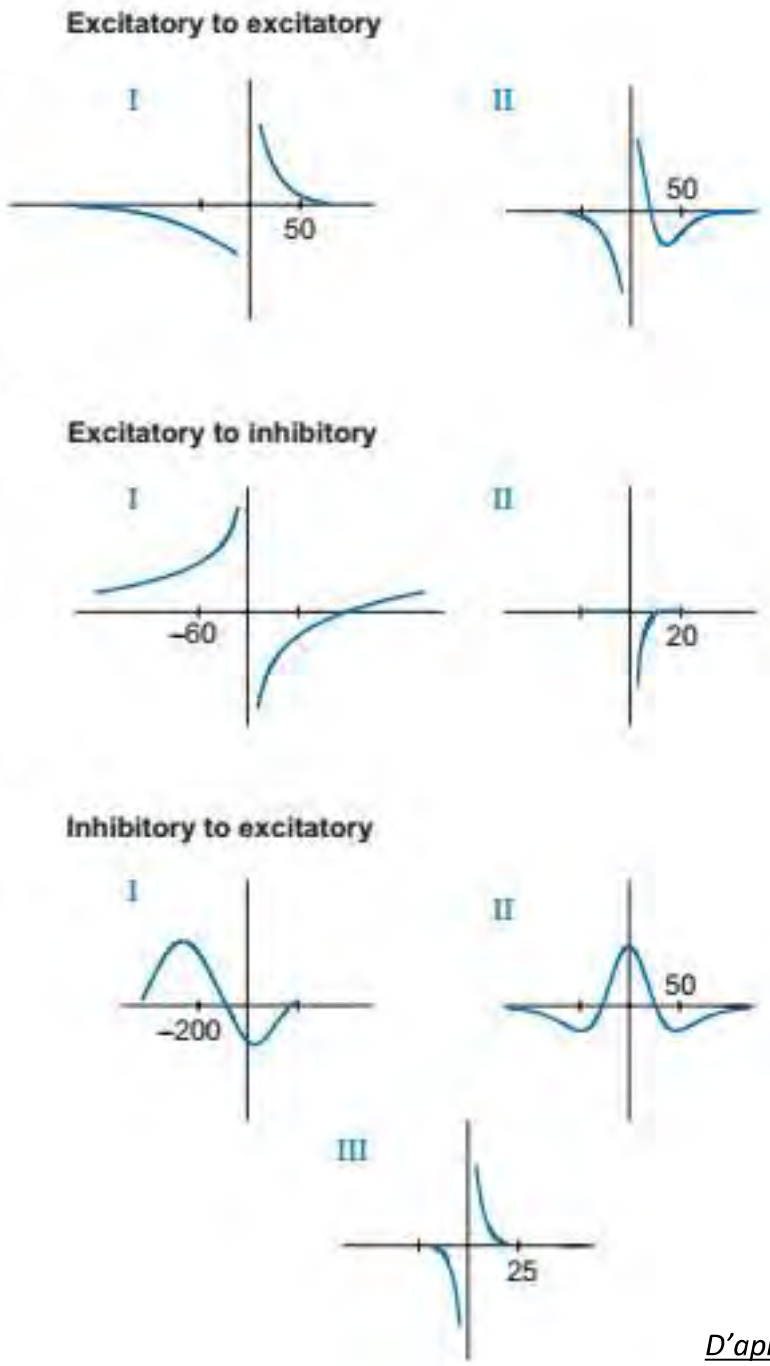

D'après Caporale et Dan, 2000

Figure 3. Diversité de la règle de STDP aux différentes synapses

En fonction de la synapse étudiée, la règle de STDP est variable. Généralement, les synapses excitatrices présentent une règle de STDP conventionnelle alors que les synapses excitatrices sur neurones inhibiteurs montrent une règle de STDP non-conventionnelle. Enfin, les synapses inhibitrices sur neurones excitateurs présentent plusieurs modalités possibles.

structures du cerveau mammifère, comme l'hippocampe ou le cortex. Le nombre de répétitions nécessaires pour induire de la LTP est plus faible que pour la LTD. Généralement, la LTP nécessite un nombre de répétitions moins important que la LTD (Debanne et al., 1994; Froemke et al., 2006). Par exemple, la LTD induite pour 30 répétitions est transitoire, alors qu'elle persiste pour 90 répétitions (Debanne et al., 1994) Ainsi, aux synapses CA3-CA1 de l'hippocampe, certaines études utilisent 100 répétitions pour la LTP contre 150 pour la LTD (Campanac et al., 2008). Tout comme le nombre de répétitions, la fréquence d'appariement est critique dans l'induction de la STDP classique (Markram et al., 1997). La fréquence d'induction pour la LTP influe grandement sur son amplitude (Markram et al., 1997; Sjöström et al., 2001). Par exemple, dans l'hippocampe **(Figure 4A),** de faibles fréquences (entre 0.3 et 1 Hz) suffisent pour induire de la LTP (Bi and Poo, 1998; Campanac et al., 2008) alors que le cortex nécessite des fréquences plus importantes (entre 10 et 20 Hz) pour observer une STDP classique (Sjöström et al., 2001).

La règle de STDP classique se retrouve dans le cortex **(Figure 4A)** comme par exemple au niveau des synapses excitatrices entre neurones pyramidaux L5 (Sjöström et al., 2001) et entre les synapses des neurones pyramidaux L4-L2/3 (Banerjee et al., 2014). Classiquement, la fréquence nécessaire à l'induction de la LTP est plus importante (>20 Hz) que dans l'hippocampe. Par exemple, dans le cortex, la LTP induite par une stimulation extracellulaire dépend fortement de la taille du PPSE évoqué (Sjöström et al., 2001). Pour de faibles fréquences, il est possible d'obtenir de la LTP uniquement avec un PPSE d'une taille importante (supérieure à 2.3 mV). Néanmoins, à faible fréquence, une dépolarisation post-synaptique permet tout de même de récupérer la LTP mais non la LTD. Par contre, pour des fréquences supérieures à 40 Hz, la fenêtre de la LTD se transforme en LTP (Markram et al., 1997; Sjöström et al., 2001). Cela illustre l'importance des fréquences utilisées dans l'induction de la plasticité par STDP, que nous discuterons par la suite.

3.1.2 Dans les neurones inhibiteurs

Certains neurones inhibiteurs présentent une forme de STDP classique. Dans le striatum, la majorité des neurones sont inhibiteurs (Fino et al, 2010) mais peuvent présenter sous certaines conditions une forme de STDP classique (Paille et al., 2013; Pawlak and Kerr, 2008). Les propriétés changent au cours du développement : alors qu'on observe une absence de LTP chez le jeune rat, on retrouve une courbe de STDP classique chez le rat plus âgé. Ce changement de propriétés provient d'un changement du tonus inhibiteur des neurones GABAergiques. Expérimentalement, il est possible de récupérer une STDP classique en bloquant l'inhibition chez le jeune animal ou l'animal âgé. Notons que les protocoles d'inductions se rapprochent de ceux décrits dans l'hippocampe avec un grand nombre de répétitions pour une faible fréquence (1 Hz) (Valtcheva et al., 2017). Néanmoins, les interneurones de type « fast-spiking » du striatum expriment naturellement une forme de STDP classique (Fino, 2010 ; **Figure 4B**).

On retrouve aussi une STDP classique au niveau des interneurones du noyau cochléaire dorsal (DCN) et du néocortex (Lu et al., 2007; Tzounopoulos et al., 2004). Dans le DCN, certaines synapses comme celles entre les fibres parallèles et les cellules fusiformes expriment une STDP classique (Tzounopoulos et al., 2004 ; **Figure 4B**). Dans le cortex, au niveau des synapses entre les cellules pyramidales et les interneurones de type bas-seuil (LTS), on retrouve une règle de STDP classique, alors que d'autres interneurones de la même région suivent une règle différente (Lu et al., 2007). Néanmoins, à ces synapses le protocole de STDP utilisé associe des trains de 5 potentiels d'action à 20 Hz.

3.1.3 Un cas particulier : la seconde fenêtre de LTD

Pour l'instant, seules 2 études expérimentales retrouvent une seconde fenêtre de LTD **(Figure 5A)**. Dans les neurones pyramidaux de la région CA1 de l'hippocampe, une seconde fenêtre

A

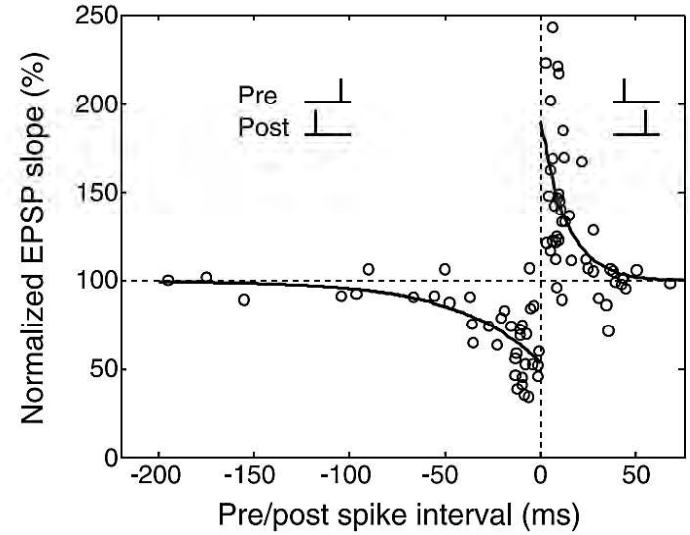

From Dan & Poo, 2006

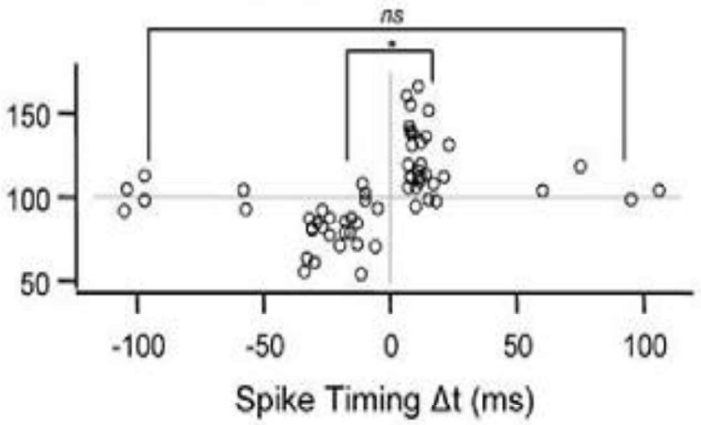

Campanac & Debanne, 2008

B

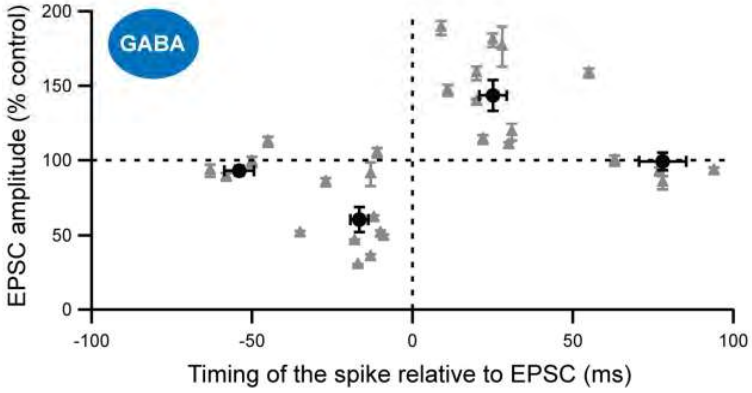

Fino et al, 2010

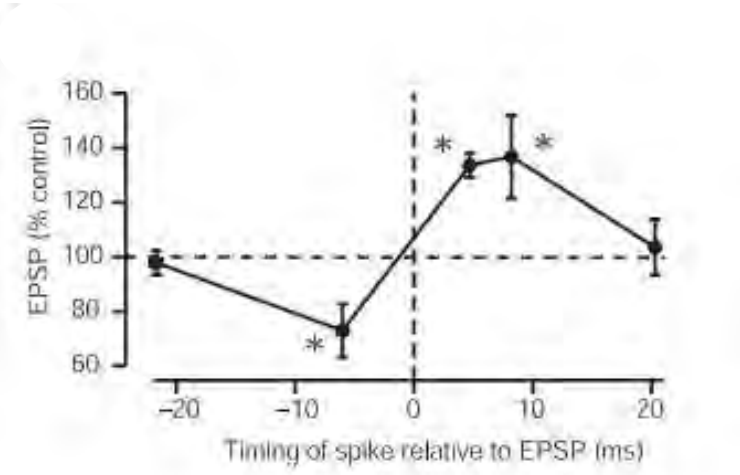

Tzounopoulos et al, 2004

Figure 4. La règle de STDP classique

A. Dans les neurones excitateurs, la règle de STDP classique est retrouvée avec une fenêtre de LTP pour les délais positifs, et une fenêtre de LTD pour les délais négatifs. Gauche : cortex visuel aux synapses de la couche 2/3 ; droite : hippocampe aux synapses CA3-CA1
B. Dans les neurones inhibiteurs, on peut retrouver une règle de STDP classique. Gauche : dans les interneurones fast-spiking du striatum. Droite : aux synapses entre fibres parallèles et cellules fusiformes du noyau cochléaire dorsal.

de LTD apparaît pour des délais d'environ +15/20 ms avec un protocole utilisant des fréquences thêta (5 Hz) pour induire la plasticité (Nishiyama et al., 2000; Wittenberg and Wang, 2006). On la retrouve aussi dans de nombreux travaux de modélisation (Graupner and Brunel, 2012; Karmarkar and Buonomano, 2002 ; **Figure 5B**) mais ses mécanismes sous-jacents sont encore inconnus. Comme nous le verrons par la suite, la STDP dépend étroitement du calcium selon le modèle de Lisman (1989) avec classiquement, une LTP associée à une forte entrée de calcium et une LTD associée à une entrée de calcium plus modérée. La présence d'une seconde fenêtre de LTD pour des intervalles de temps positifs signifie que l'on retrouve des niveaux de calcium post-synaptiques semblables aux délais négatifs, et donc orientant vers la LTD (Karmarkar and Buonomano, 2002). Les conditions expérimentales d'induction de la plasticité peuvent entraîner des biais expérimentaux (5 Hz, ions césium dans le neurone post-synaptique) car l'augmentation de la durée du potentiel d'action pourrait activer des canaux calciques dépendants du potentiel et induire une dépression synaptique (Zhou et al., 2005).

Néanmoins, la plupart des études consacrées à la STDP n'explorent que rarement des délais importants, ce qui pourrait fournir une explication à son absence dans de nombreuses études. La question de l'existence d'une seconde fenêtre de LTD doit être réexaminée dans les années à venir pour confirmer son existence, ses mécanismes et son rôle.

3.2 STDP non-conventionnelle

Il existe des règles de STDP non-conventionnelles, où un protocole pré-post induit de la LTD alors qu'un protocole post-pré induit de la LTP. A l'inverse du postulat de Hebb, les synapses GABAergiques sont un lieu important de cette forme de STDP, que l'on peut qualifier d'anti-Hebbienne, à travers de nombreuses régions cérébrales : hippocampe, cortex ou striatum.

A

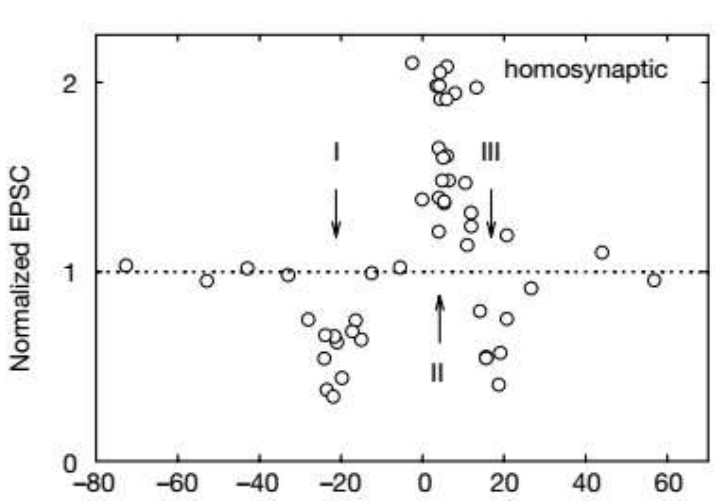

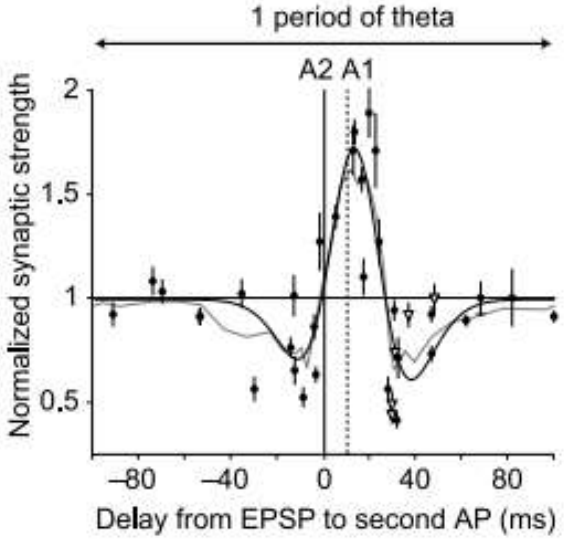

Nishiyama et al, 2000

Wittenberg et Wang, 2006

B

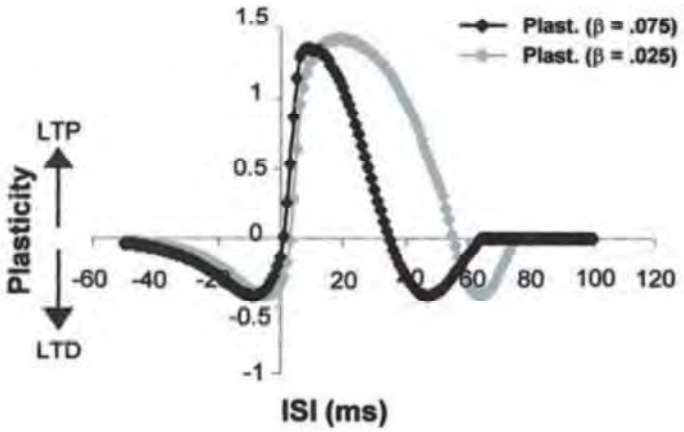

Karmarkar et Buonomano, 2002

Figure 5. Un cas particulier : la seconde fenêtre de LTD

A. Seulement 2 études expérimentales aux synapses CA3-CA1 retrouvent une seconde fenêtre de LTD pour des délais autour de +20 ms (gauche) ou +40 ms (droite) mais utilisant une fréquence d'appariement de 5 Hz.
B. La seconde fenêtre de LTD se retrouve aussi dans des études de modélisation pour un délai autour des 40 ms.

3.2.1 Au niveau des synapses excitatrices sur neurones inhibiteurs

On retrouve en particulier cette forme de STDP dans le striatum, où la majorité des neurones sont GABAergiques (Pour revue, voir Fino et al., 2010). Les synapses cortico-striatales entre les neurones de la couche V et les neurones MSN (medium-sized spiny neurons) du striatum expriment une STDP non-conventionnelle pour des faibles fréquences (1 Hz) avec un grand nombre de répétitions (Fino et al., 2005). Néanmoins, comme décrit précédemment, les conditions d'enregistrement aux synapses corticostriatales peuvent faire grandement varier la plasticité de sortie (Pawlak and Kerr, 2008). En fonction de la fréquence du protocole, les modalités d'expression de la STDP au sein du striatum sont différentes, ce qui sera discuté par la suite. D'autres types de neurones striataux expriment une STDP anti-Hebbienne, comme les interneurones cholinergiques **(Figure 6)**, et dans une certaine mesure les interneurones exprimant la nNOS (Oxide Nitrique Synthase neuronale) présentent une fenêtre de LTP décalée vers des valeurs temporelles plus importantes **(Figure 6)**. Ces interneurones développent la STDP pour les mêmes protocoles que les MSNs (faible fréquence, grand nombre de répétitions). La STDP non-conventionnelle se retrouve aussi dans d'autres régions cérébrales. Néanmoins, la majorité des formes non-conventionnelles de STDP présente uniquement une fenêtre de LTD asymétrique. Par exemple, contrairement aux cellules fusiformes, les cellules cartwheel du DCN expriment une forte LTD pour des corrélations positives (Tzounopoulos et al., 2004 ; **Figure 4**). Le même phénomène se retrouve dans le cortex au niveau des synapses entre neurones pyramidaux de la couche 2/3 et interneurones « fast-spiking » qui présentent une unique fenêtre de LTD. De même, cette forme de STDP se retrouve dans les dendrites distales des neurones corticaux de la couche 2/3 et 5, là où la coopérativité entre les entrées synaptiques est minimale (Sjöström and Häusser, 2006).

3.2.2 Au niveau des synapses inhibitrices sur neurones excitateurs

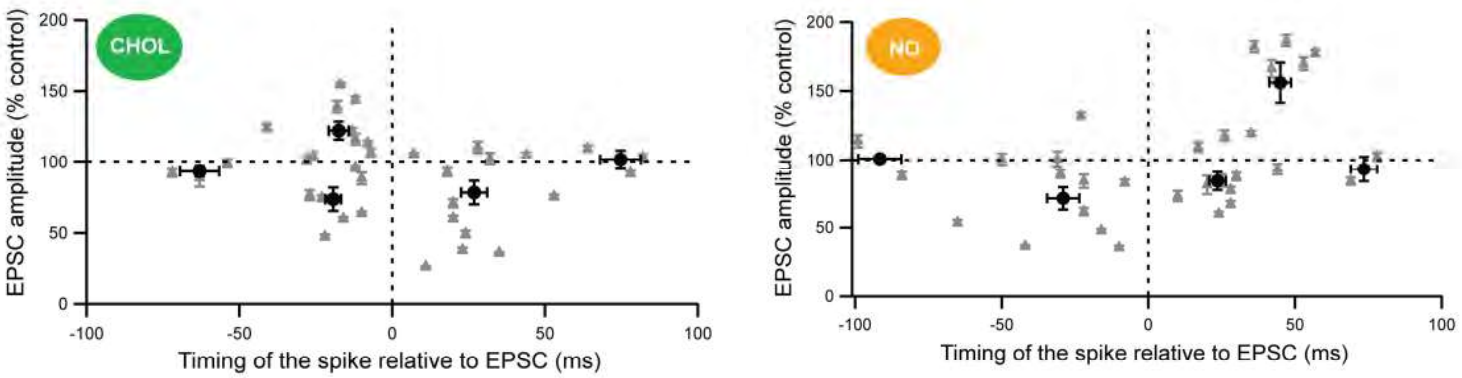

Fino et al, 2010

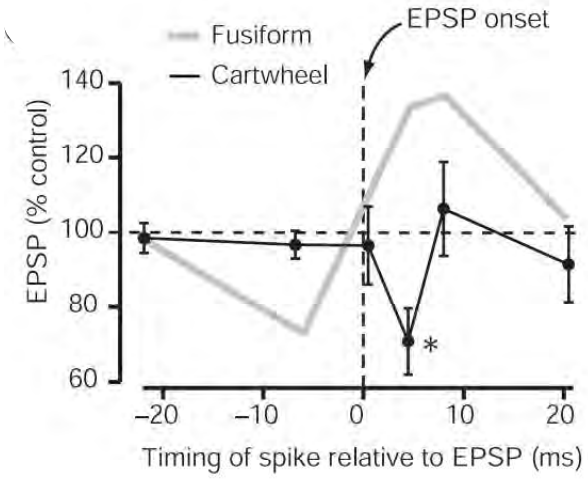

Tzounopoulos et al, 2004

Figure 6. La règle de STDP non-conventionnelle

Une règle de STDP non-conventionnelle se retrouve essentiellement aux neurones inhibiteurs, c'est le cas dans le striatum avec les interneurones cholinergiques **(gauche)** et les interneurones exprimant la nNOS (Oxide Nitrique Synthase neuronale) **(droite**). A l'inverse des cellules fusiformes, les cellules cartwheel (bas) présentent une STDP non-conventionnelle. Cette forme de STDP est caractérisée par l'inversion des deux fenêtres de plasticité ou l'absence totale de LTP et la présence d'une unique fenêtre de LTD.

Les synapses entre interneurones et neurones pyramidaux de la couche 2/3 du cortex présentent aussi une STDP non-conventionnelle. Un protocole pré-post utilisant des bouffées de potentiels d'action postsynaptiques à haute fréquence associés à une seule stimulation présynaptique induit de la LTD, alors qu'un protocole post-pré induit de la LTP (Holmgren and Zilberter, 2001). Une forme particulière de plasticité synaptique est retrouvée entre les synapses inhibitrices et les neurones pyramidaux CA1 de l'hippocampe, dont la plasticité est indépendante de l'ordre entre l'activité pré- et post-synaptique (Woodin et al., 2003). Dans une fenêtre de 20 ms, pour des corrélations positives ou négatives, on observe une diminution du courant post-synaptique inhibiteur GABAergique (CPSI).

Pour finir, on peut noter le manque d'études au niveau des synapses inhibitrices sur neurones inhibiteurs.

4. Aspect non-synaptique de la STDP

Bien que la STDP soit une forme de plasticité synaptique, elle peut s'accompagner dans certains cas de modifications non-synaptiques touchant l'intégration dendritique ainsi que l'excitabilité intrinsèque.

4.1 Intégration dendritique

En plus de changements d'excitabilité au niveau pré-synaptique, l'induction de LTP et LTD par STDP s'accompagne aussi de modifications de l'intégration dendritique post-synaptique. On parle de couplage PPSE-potentiel d'action (couplage E-S).

4.1.1 Couplage PPSE-potentiel d'action (E-S)

Le couplage E-S représente la capacité d'un PPSE à initier un potentiel d'action dans le neurone post-synaptique. Ce couplage est plastique et peut être augmenté, on parle d'E-S Potentialisation (ES-P) : un PPSE identique augmente la probabilité de déclencher un potentiel d'action. Il peut aussi être diminué, on parle d'E-S Dépression (ES-D) : un même

PPSE diminue la probabilité de déclencher un potentiel d'action. L'acteur central de cette forme de plasticité est le récepteur NMDA, capable d'induire des changements synaptiques mais aussi d'excitabilité. Bien que le récepteur NMDA soit le premier signal, ces modifications passent ensuite par des changements de conductance des canaux voltage-dépendants dendritiques comme I_H ou I_A mais aussi somatiques comme INaP (courant sodique persistant).

4.1.2 Modification du couplage E-S par la STDP

Le couplage E-S est modifié par l'activité synaptique. Dans l'hippocampe, l'induction de la LTP par HFS s'accompagne d'une augmentation de la probabilité de décharge ou ES-potentialisation (Abraham et al., 1980) alors que l'induction de LTD par LFS s'accompagne d'une diminution de la probabilité de décharge, soit une ES-Dépression (Daoudal et al., 2002 ; **Figure 7A**) Ces mêmes changements se retrouvent lors de l'induction d'une plasticité synaptique par STDP (Campanac and Debanne, 2008 ; **Figure 7B**). Ces modifications proviennent de changements de la conductance des canaux voltage-dépendants. L'ES-P repose sur une diminution du courant I_A ou I_H dendritique (Daoudal, 2003; Frick et al., 2004; Kim et al., 2007), mais aussi sur une augmentation de la conductance sodique somatique, INaP (Xu, 2005). L'ES-D provient de la régulation de ces mêmes canaux dans la direction opposée : augmentation du courant I_A et I_H, diminution du courant INaP.

Ces changements dans l'intégration dendritique partagent la même règle temporelle que les changements synaptiques induits par la règle de STDP ou BCM (Daoudal and Debanne, 2002 Campanac and Debanne, 2008 ; **Figure 7C**).

4.1.3 Rôle de l'inhibition

Le phénomène de couplage PPSE-potentiel d'action est aussi fortement dépendant de la transmission synaptique inhibitrice, impliquée aussi bien dans l'E-S Potentialisation que l'E-S

Dépression. Néanmoins, il est important de noter que l'étude des entrées excitatrices équivalentes passe par une réduction de l'intensité de stimulation après LTP, modifiant aussi la balance entre excitation et inhibition (Daoudal and Debanne, 2002).

4.1.4 Rôle de l'inhibition dans l'E-S Potentialisation (E-S P)

Le rôle de l'inhibition dans l'E-S P a longtemps été contradictoire. Certaines études déclaraient que l'E-S P était absente en présence de Picrotoxine (PiTX), un bloqueur du canal chlore du récepteur $GABA_A$ (Chavez-Noriega et al., 1989; Tomasulo and Ramirez, 1993), alors que d'autres études présentaient une E-S P résistante à la présence de PiTX (Daoudal et al., 2002; Jester et al., 1995). En réalité, l'E-S Potentialisation présente une composante sensible à la PiTX. Néanmoins, environ 40 % des changements observés dans l'intégration dendritique proviennent de modifications de l'excitabilité, et peuvent donc s'interpréter en termes de changements de conductances ioniques (Daoudal et al., 2002).

4.1.5 Rôle de l'inhibition dans l'E-S Dépression (E-S D)

Tout comme l'E-S P, environ 40 % des changements d'intégration dendritique observés après LTD proviennent de modifications de conductances ioniques (Daoudal et al., 2002). En effet, l'E-S D est toujours induite en présence de bloqueurs des récepteurs $GABA_A$ et $GABA_B$.

4.2 Modification de l'excitabilité intrinsèque

Des changements de l'excitabilité suite à une plasticité synaptique induite par la règle BCM ont déjà été montrés dans de nombreuses régions cérébrales (Daoudal, 2003; Debanne et al., 2018). Des modifications similaires se retrouvent dans l'hippocampe après un protocole de STDP.

4.2.1 Modification de l'excitabilité intrinsèque après LTP

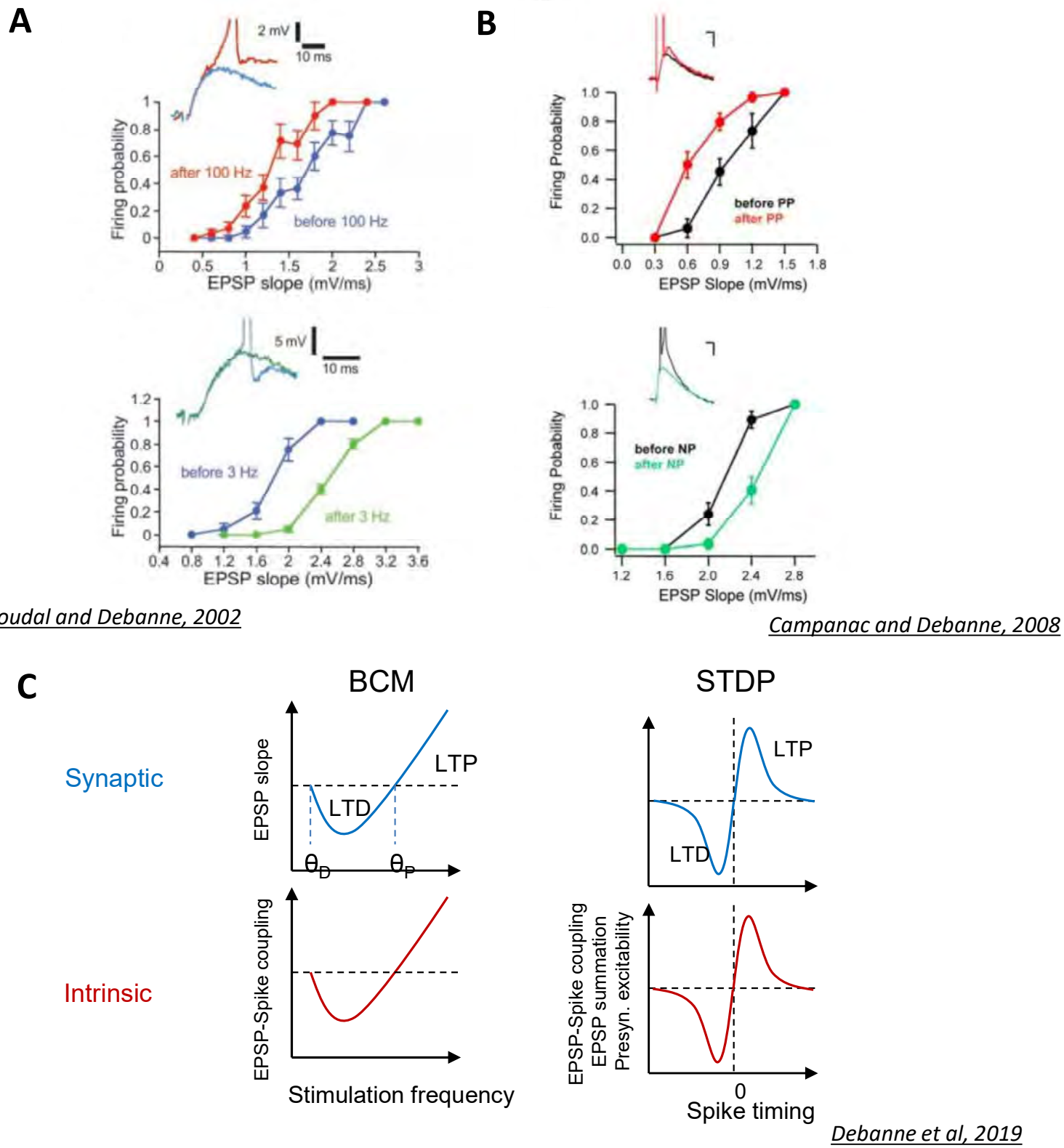

Daoudal and Debanne, 2002

Campanac and Debanne, 2008

Debanne et al, 2019

Figure 7. Couplage PPSE-potentiel d'action (ES) et plasticité synaptique

A. Observation d'ES-Potentialisation et d'ES-Dépression après LTP induite par HFS, et LTD induite par LFS aux synapses CA3-CA1. La LTP s'accompagne d'une augmentation de la probabilité de déclencher un potentiel d'action, la LTD s'accompagne d'une diminution de la probabilité d'induire un potentiel d'action.
B. Observation d'ES-P et d'ES-D après LTP et LTD par la règle de STDP aux synapses CA3-CA1. On observe les mêmes conséquences sur l'intégration dendritique.
C. Les changements dans l'intégration dendritique suivent la même règle temporelle que la règle BCM ou de STDP.

Dans des cultures de neurones d'hippocampe, la LTP s'accompagne d'une augmentation de l'excitabilité intrinsèque du neurone pré-synaptique (Ganguly et al., 2000), comme en témoigne l'augmentation du taux de décharge ainsi que la diminution du seuil de déclenchement du potentiel d'action **(Figure 8A)**. Cette augmentation de l'excitabilité est due à la diminution de l'inactivation de la conductance des canaux sodiques voltage-dépendants (Nav) et nécessite l'activation des récepteurs NMDA post-synaptiques, ainsi que la protéine kinase C (PKC) au niveau pré-synaptique (Ganguly et al., 2000). Au niveau post-synaptique, l'induction de LTP par STDP s'accompagne d'une réduction de l'excitabilité par une augmentation du courant hyperpolarisant de type H (I_H), et dépend des récepteurs NMDA post-synaptiques ainsi que des protéines kinases CaMKII. En effet, en présence de ZD7288, un bloqueur du courant I_H, cette diminution de l'excitabilité disparaît (Fan et al., 2005). Ensemble, ces modifications pourraient agir de manière synergique pour optimiser la production d'un message de sortie sous forme de potentiel d'action pour augmenter la spécificité synaptique.

4.2.2 Modification de l'excitabilité intrinsèque après LTD

De la même manière, dans des cultures d'hippocampes et tranches de cortex (L4), la LTD s'accompagne d'une diminution de l'excitabilité intrinsèque du neurone pré-synaptique **(Figure 8B).** Dans ce cas, cette diminution provient d'une augmentation de l'activation des canaux potassiques à inactivation lente, ainsi que de l'activité de la protéine kinase A (PKA) et C (PKC) (Li et al, 2004). Ces résultats ne se retrouvent pas aux synapses entre interneurones et cellules pyramidales de l'hippocampe (Li et al., 2004). Il est intéressant de souligner que ces résultats sont également retrouvés dans des tranches aigües, et pas seulement sur cultures neuronales qui présentent un fort taux de connexions synaptiques pouvant introduire un biais dans les résultats observés.

5. Conclusion

Bien que la STDP soit une règle universelle retrouvée à travers de nombreuses régions cérébrales, sa forme peut être différente en fonction de la structure étudiée et des conditions expérimentales. Enfin, si la règle de STDP s'accompagne avant tout de modifications de la transmission synaptique, tout comme les protocoles de LFS/HFS, elle est aussi vectrice de changements non-synaptiques à travers des modifications de l'excitabilité intrinsèque et de l'intégration dendritique (pour revue, voir Daoudal and Debanne, 2003). Néanmoins, les aspects non-synaptiques de la STDP suivent la même règle temporelle que les aspects synaptiques (Campanac and Debanne, 2008).

A

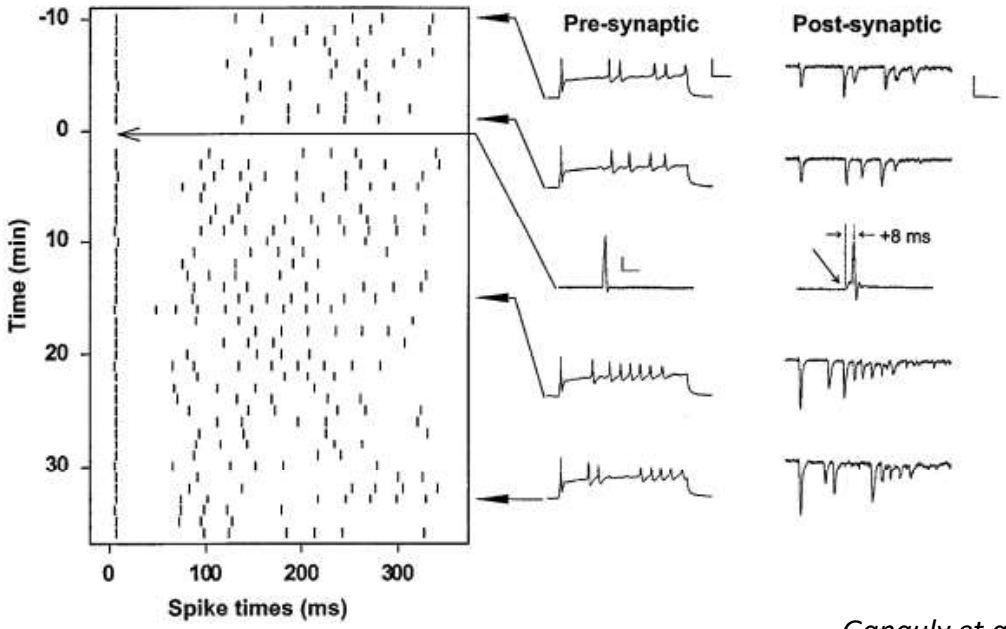

Ganguly et al, 2010

B

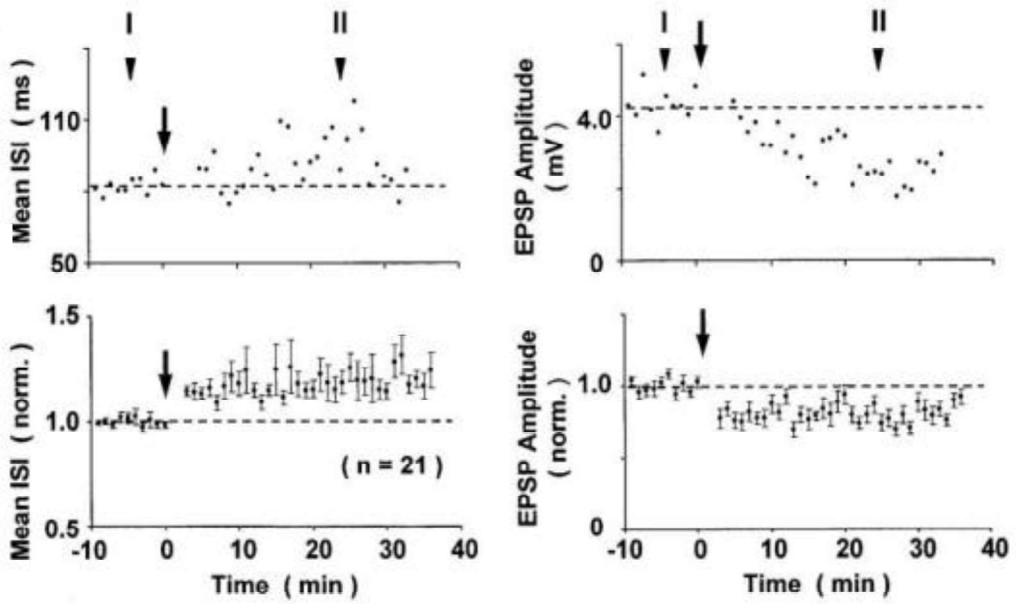

Li et al, 2004

Figure 8. Excitabilité intrinsèque et plasticité synaptique

A. Dans des cultures de neurones d'hippocampe, la LTP induite par STDP s'accompagne de changements dans les propriétés de décharge neuronale. On peut observer une augmentation du taux de décharge.
B. Dans des expériences de paires connectées (L4-L4) dans le cortex somato-sensoriel, on observe une réduction de l'excitabilité intrinsèque suite à une LTD induite par STDP, comme en témoigne l'augmentation de l'intervalle de temps entre deux potentiels d'action (ISI).

Mécanismes cellulaires de la STDP

1. Le rôle central du calcium

Le calcium est un acteur essentiel dans la plasticité synaptique. Il a été montré que l'application d'EGTA (Ethylene glycol-bis(2-aminoethylether)-NNNN'-tetraacetic acid, aussi appelé acide egtazique), un chélateur des ions Ca^{2+}, bloque l'induction de LTP par HFS dans les neurones CA1 de l'hippocampe (Lynch et al, 1983), tout comme la perfusion de BAPTA (1,2-bis(*o*-aminophenoxy)ethane-*N*,*N*,*N'*,*N'*-tetraacetic acid), un autre chélateur des ions Ca^{2+}, bloque l'induction de la LTD par LFS dans les neurones CA1 (Mulkey and Malenka, 1992). La LTD induite par STDP dans la région CA1 de l'hippocampe est aussi bloquée en présence de BAPTA dans la pipette d'enregistrement (Debanne et al., 1994). Depuis, l'étude des mécanismes sous-jacents de la plasticité synaptique et en aval de l'entrée de calcium représente un domaine de recherche qui s'est considérablement développé.

1.1 La théorie de Lisman

Selon le modèle de Lisman (1989), l'amplitude de l'influx calcique post-synaptique va déterminer l'orientation de la plasticité. D'après sa théorie, le sens de la plasticité synaptique est déterminé par l'activation spécifique de kinases ou de phosphatases. Une forte élévation du Ca^{2+} intracellulaire conduit à une activation de kinases sensibles au calcium (CaMKII, PKA…) alors qu'une élévation plus faible conduit à une activation de phosphatases (PP1, calcineurine...) En résumé, une forte entrée de calcium est associée à la LTP par activation des kinases, alors qu'une plus faible entrée de calcium est associée à la LTD par activation des phosphatases **(Figure 9A)**. La plupart des modèles mathématiques de plasticité synaptique basée sur le calcium (Graupner and Brunel, 2012; Shouval et al., 2002) utilise cette théorie pour déterminer l'orientation de la plasticité **(Figure 9B)** en réponse à divers stimuli (HFS, LFS, STDP). La source principale d'entrée calcique est le récepteur NMDA (N-Methyl-D-

A

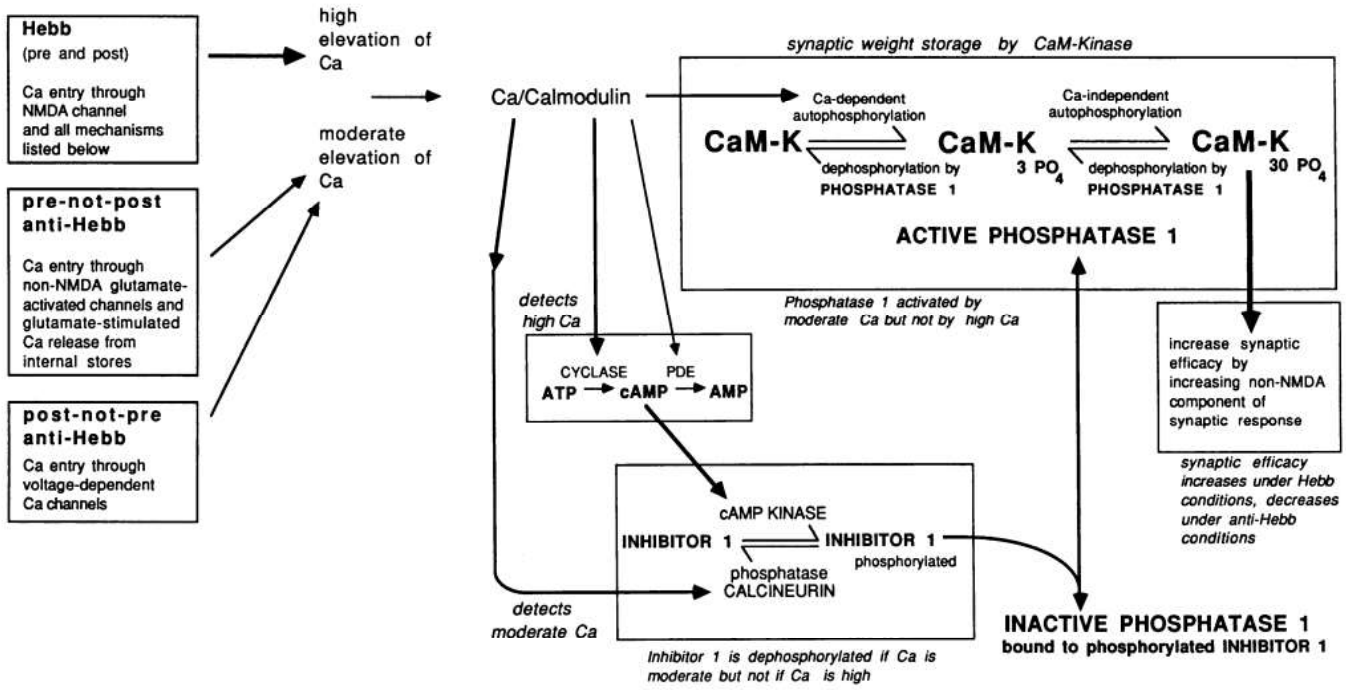

Lisman, PNAS, 1989

B

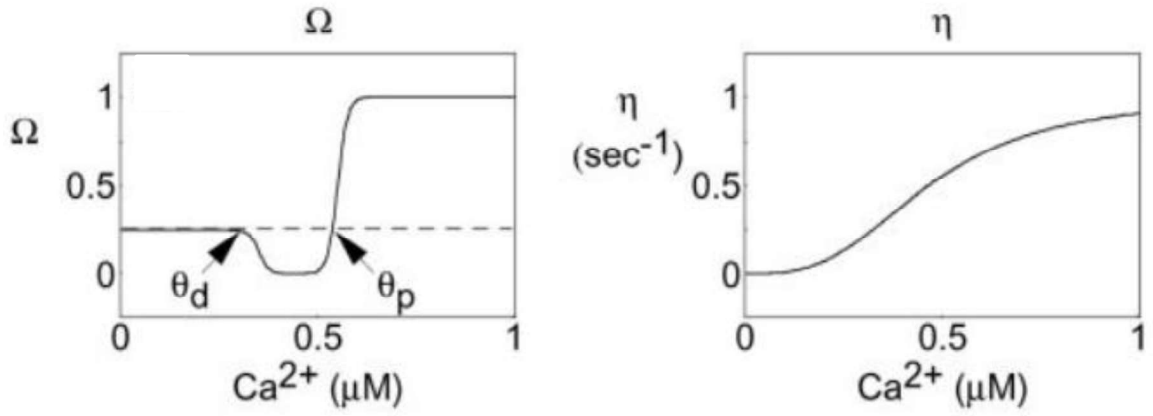

Shouval et al, 2002

Figure 9. L'influx calcique détermine l'orientation de la plasticité par STDP

A. Selon le modèle de Lisman (1989), une forte entrée de calcium active fortement les protéines kinases augmentant l'efficacité synaptique via la phosphorylation de la CaMKII, alors qu'une plus faible entrée de calcium active les protéines phosphatases, diminuant l'efficacité synaptique par déphosphorylation de la CaMKII.

B. La majorité des modèles de plasticité synaptique utilise la mesure du calcium comme indice de l'orientation de la plasticité. Le seuil de LTD (θD) est plus bas et nécessite une plus faible entrée de calcium alors le seuil de LTP (θP) est plus haut et nécessite une plus forte entrée de calcium.

Aspartate) post-synaptique et les canaux calciques dépendants du voltage (VDCC). Néanmoins, si d'autres sources de calcium existent, la plupart des modèles en font abstraction (Shouval et al., 2002). De plus, plusieurs études expérimentales montrent une corrélation directe entre le niveau de calcium mesuré dans les épines et l'orientation de la plasticité (Cho et al., 2001; Yang et al., 1999). Par exemple, des expériences de décageage de calcium aux épines des neurones CA1 de l'hippocampe montrent qu'une libération de calcium forte et brève oriente vers la LTP, alors qu'une libération de calcium plus faible et modérée oriente vers la LTD (Yang et al., 1999). Des résultats similaires sont retrouvés en imagerie calcique dans le cortex (Ismailov, 2004).

1.2 Limites du modèle de Lisman

La plupart des études utilise l'amplitude du signal calcique comme témoin de l'orientation de la plasticité. Néanmoins, plusieurs études n'observent pas cette corrélation (Neveu and Zucker, 1996; Nevian and Sakmann, 2006; Wang et al., 2005). Ensemble, ces travaux montrent que l'amplitude du signal calcique n'est pas une information suffisante pour déterminer le niveau de plasticité. Par exemple, dans la couche 2/3 du cortex, un même niveau de calcium peut induire de la LTP ou de la LTD (Nevian and Sakmann, 2006 ; **Figure 10A**). Néanmoins, si une élévation du calcium post-synaptique est nécessaire pour induire une plasticité et que le seuil nécessaire est plus haut pour la LTP que la LTD, la question demeure pour des élévations intermédiaires de calcium. Ainsi, il a été montré qu'un élargissement du potentiel d'action dans la couche 2/3 du cortex favorise la LTD plutôt que la LTP **(Figure 10B)** induite par STDP et le signal calcique provenant des VDCC, plus important, pourrait réorienter les voies métaboliques vers la LTD (Zhou et al., 2005).

A

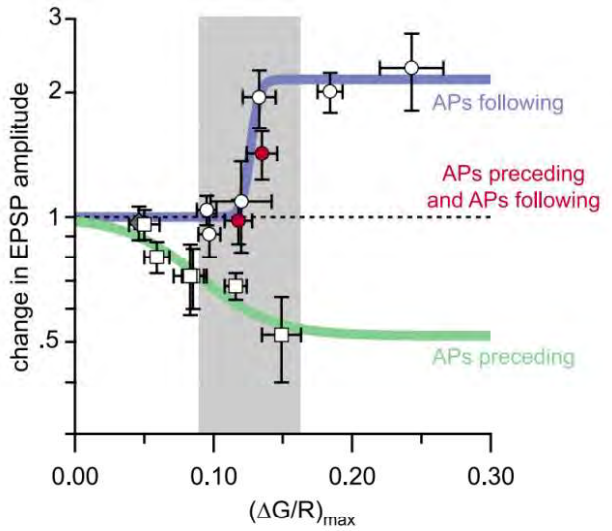

Nevian and Sakmann, 2006

B

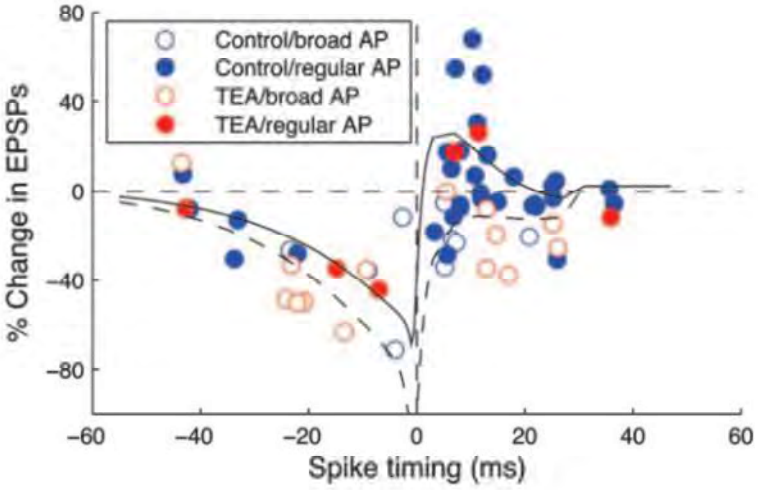

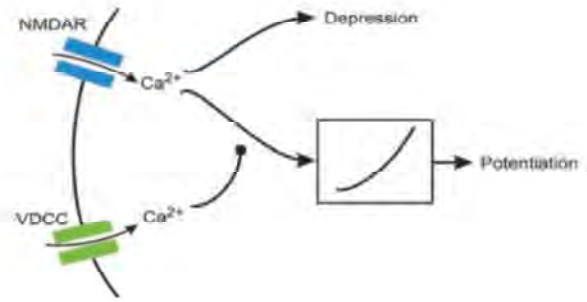

Zhang et al, 2005

Figure 10. Limite du modèle de Lisman

A. Dans la couche 2/3 du cortex, l'amplitude de l'entrée de calcium ne permet pas de prédire l'orientation de la plasticité vers la LTP ou la LTD. Pour des mêmes entrées de calcium (zone grise), on peut observer aussi bien de la LTD que de la LTP.
B. L'élargissement du potentiel d'action par l'application de TEA favorise l'induction de la LTD. L'entrée de calcium par les VDCC inhiberait le signal calcique provenant des récepteurs NMDA pour favoriser une voie métabolique orientant vers la LTD.

1.3 Les sources de calcium

L'élévation du calcium intracellulaire est un prérequis à l'induction d'une plasticité synaptique. Les sources de calcium sont à la fois extra- et intracellulaires.

1.3.1 Sources extracellulaires

Il existe deux sources majoritaires de calcium au niveau post-synaptique : le récepteur NMDA, et les canaux calciques voltage-dépendants (VDCC). L'influx calcique par les récepteurs NMDA est la source principale d'entrée de calcium dans le neurone, mais aussi l'acteur principal souvent requis pour l'induction de la LTP (Andrade-Talavera et al., 2016). Les VDCC représentent une source minoritaire de calcium qui n'est généralement pas nécessaire à l'induction de la LTP (Wyllie and Nicoll, 1994). Néanmoins les canaux calciques de type L semblent être nécessaires à l'induction de la LTD dans l'hippocampe (Andrade-Talavera et al., 2016).

1.3.2 Sources intracellulaires

Une source importante de calcium provient des stocks intracellulaires. La libération de calcium des stocks intracellulaires passe par la synthèse d'inositol triphosphate (IP3), l'activation des récepteurs à la ryanodine et/ou de l'IP3 par le calcium entrant, mais aussi par activation de la voie de la phospholipase C (PLC). Ainsi, le signal calcique provenant des récepteurs NMDA peut être amplifié fortement par la libération de calcium des stocks intracellulaires (Emptage et al., 1999) pour favoriser l'induction de la LTP. Dans l'hippocampe, l'induction de la LTD par corrélation négative nécessite la libération des stocks intracellulaires de calcium par la voie IP3/PLC (Andrade-Talavera et al., 2016).

2. Les acteurs cellulaires de la STDP

Les acteurs cellulaires de la STDP sont multiples, avec les récepteurs qui vont être le point d'entrée de l'élévation du calcium intracellulaire ainsi que les voies de signalisation intracellulaires qui vont orienter vers la LTP ou la LTD.

2.1 Lier calcium et changement synaptique

L'élévation post-synaptique du calcium active de nombreuses cascades de signalisation pour permettre les changements synaptiques (LTP ou LTP). Il existe trois voies principales de signalisation, identifiées majoritairement aux synapses CA3-CA1 de l'hippocampe : la voie activée par la protéine kinase Ca^{2+}/calmoduline, celle activée par le couple adénosine monophosphate cyclique (AMPc) et protéine kinase A (PKA), et enfin la voie dépendante de la calcineurine **(Figure 11)**. Bien que les voies d'induction de la plasticité puissent être différentes en fonction des régions cérébrales, l'hippocampe partage de nombreuses similarités avec le cortex (Kirkwood et al., 1993). Bien que d'autres protéines aient été suggérées comme impliquées dans la plasticité synaptique (protéine kinase C ou tyrosine kinase Src), nous ne couvrirons que les principales voies (Malenka and Bear, 2004).

2.1.1 Une balance phosphorylation – déphosphorylation

La plasticité synaptique dans l'hippocampe est une balance entre phosphorylation et déphosphorylation, entre protéines kinases et protéines phosphatases (Lisman, 1989). Généralement, la phosphorylation est synonyme de LTP, alors que la déphosphorylation est synonyme de LTD.

2.1.2 Protéine kinase Ca2+/calmoduline-dépendante (CaMKII)

Le niveau de phosphorylation de la CaMKII dépend directement du niveau d'activité du neurone. Elle est phosphorylée par la calmoduline (CaM), dont l'activation dépend de l'élévation du calcium intracellulaire par le récepteur NMDA et les VDCC (Hudmon and

Schulman, 2002). La CaMKII activée s'auto-phosphoryle pour maintenir son activité, et est capable de phosphoryler les récepteurs AMPA, augmentant leur conductance et favorisant leur insertion à la synapse (Derkach et al., 1999; Hayashi et al., 2000). Elle a un rôle important dans l'induction de la LTP par STDP. Dans l'hippocampe, en présence d'un bloqueur de la CaMKII, l'induction de la LTP est bloquée (Wang et al., 2005). Néanmoins, si son rôle dans l'induction de la LTP n'est pas sujet à discussion, sa fonction dans le maintien de cette dernière est débattue. Il a été montré que son activité diminue environ 10 à 15 minutes après induction de la LTP (Lengyel et al., 2004), mais pourtant la présence d'un inhibiteur non-compétitif de la CaMKII peut inverser la LTP (Sanhueza et al., 2007). Une composante de la CaMKII semble donc importante au maintien de la LTP dans la région CA1.

2.1.3 Le couple adénosine monophosphate cyclique (AMPc) – protéine kinase A (PKA)

Contrairement à la voie CaMKII, la voie AMPc-PKA semble plutôt impliquée dans le maintien de la LTP, en stimulant la synthèse de nombreuses protéines, et non dans son induction. L'activation de la voie dépend directement de la calmoduline, qui stimule la synthèse d'AMPc, qui active la PKA. La surexpression de l'adénylate cyclase, enzyme de synthèse de l'AMPc, augmente la LTP dans un modèle de souris transgéniques (Wang, 2004). L'échelle de temps est aussi très différente de la CaMKII. Dans l'hippocampe, on observe une augmentation de la synthèse protéique dépendante de la voie PKA environ 1 heure après induction de la LTP (Nguyen and Kandel, 1997). La PKA active d'autres voies de signalisation comme les MAPK (Mitogen-activated protein kinases), qui activeront CREB (cAMP-responsive element-binding protein) dans le noyau, qui contrôle la synthèse de protéines de la plasticité (Chen et al, 2003). Néanmoins, bien que la voie AMPc-PKA soit

majoritairement impliquée sur le long terme, certaines études mettent en évidence une élévation rapide de l'activité de la PKA dans le cortex visuel (Jay et al., 1998).

2.1.4 Calcineurine

Alors que la PKA est impliquée dans la LTP par son activité de phosphorylation de protéines clés de la plasticité synaptique, la calcineurine, par son activité de déphosphorylation, est plutôt impliquée dans la LTD. Par exemple, l'induction de LTD par STDP est bloquée dans l'hippocampe en présence d'inhibiteurs de la calcineurine (Wang et al., 2005).

2.1.5 Inhibitor 1 (In1) : point de convergence des voies PKA et calcineurine

Les voies de signalisation interagissent au niveau d'une protéine particulière, Inhibitor 1 (ou In1), dont l'état de phosphorylation est impliqué dans la plasticité synaptique. Alors que la LTD dans l'hippocampe est associée à une déphosphorylation d'In1 (Mulkey et al., 1994), la LTP est associée à une phosphorylation d'In1 (Blitzer et al., 1998). L'état d'activation d'In1 va activer (phosphoryler) ou non (déphosphoryler) une autre protéine, la protéine phosphatase 1 (PP1). En fait, In1 dans son état phosphorylé est un bloqueur de PP1. Par exemple, dans l'hippocampe, la LTD s'accompagne d'une déphosphorylation d'In1 qui amène à l'activation de PP1 (Mulkey et al., 1994).

2.1.6 Implication dans les modèles mathématiques de plasticité synaptique

Contrairement aux premiers modèles de STDP qui abordent uniquement les changements synaptiques en fonction des changements de calcium intracellulaire, qualifiés de phénoménologiques et qui ne prennent pas en compte les cascades de signalisation (pour revue, voir Graupner and Brunel, 2010), les modèles biologiques de STDP se basent essentiellement sur la voie CaMKII pour rendre compte des changements synaptiques en réponse à divers stimuli. Les premiers modèles ne peuvent pas rendre compte des

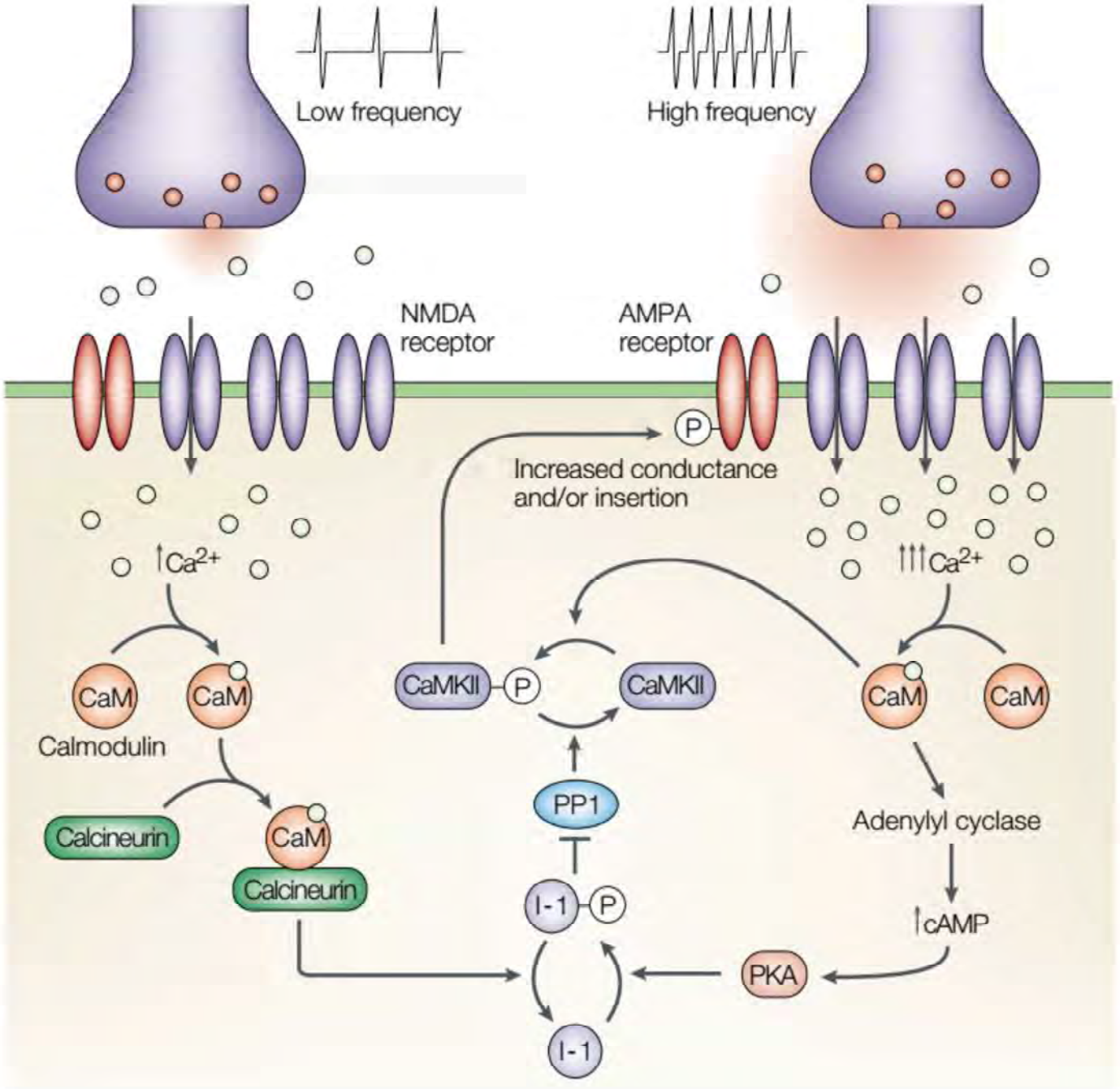

Winder and Sweatt, 2001

Figure 11. Lier calcium et plasticité synaptique

L'entrée modérée de calcium par les récepteurs NMDA et l'activation de la calcineurine désactive l'inhibiteur-1 (I-1) de la PP1. La PP1 va déphosphoryler la CaMKII et la rendre inactive. Une forte entrée de calcium active des protéines kinases, comme la PKA. La PKA active l'I-1, bloquant PP1 qui ne peut déphosphoryler la CaMKII. L'activation de la CaMKII phosphoryle les récepteurs AMPA et augmente leur conductance ou induit l'insertion de nouveaux récepteurs à la membrane.

changements synaptiques sur le long terme, alors que les seconds, incluant les voies biochimiques, et qui présentent en plus une propriété de synapses bistables (c'est-à-dire que la synapse se stabilise soit vers un état haut –potentialisé– soit vers un état bas –déprimé–) sont capables de rendre compte des changements synaptiques sur le long terme (Graupner and Brunel, 2012). Notons que cette vision « tout ou rien » des changements synaptiques s'appuie sur des travaux expérimentaux dans l'hippocampe au niveau des synapses CA3-CA1 (O'Connor et al., 2005; Petersen et al., 1998) avec stimulations minimales pour évoquer des évènements mono-synaptiques. Les résultats observés vont dans le sens de changements synaptiques «tout ou rien».

2.2 Les récepteurs synaptiques impliqués dans la plasticité synaptique

Bien que les transmissions excitatrice (glutamatergique) et inhibitrice (GABAergique) concernent des récepteurs différents, nous nous concentrons ici sur les récepteurs impliqués dans l'induction de la plasticité.

2.2.1 Récepteurs ionotropiques

Les récepteurs ionotropiques sont responsables de la transmission synaptique rapide, dont trois sont impliqués dans la transmission synaptique excitatrice : AMPA, Kaïnate et NMDA. Ils tiennent leur nom de leur affinité pour leur agoniste. Les récepteurs AMPA et NMDA sont particulièrement impliqués dans l'induction et le maintien de la plasticité.

2.2.1.1 Récepteur AMPA

Le récepteur AMPA est un hétérotétramère composé de plusieurs sous-unités (GluA1-4) qui changent fortement ses propriétés. Classiquement, le récepteur AMPA est responsable d'un courant sodique entrant rapide et d'un faible courant potassique sortant. Néanmoins, les récepteurs portant la sous-unité GluA2 sont imperméables au calcium (Hollmann et al., 1991). Les propriétés du récepteur AMPA peuvent être grandement modifiées en fonction de sa

phosphorylation. Ce récepteur est impliqué aussi bien dans l'induction que dans l'expression de la plasticité à long terme (Delgado et al., 2007; Hayashi et al., 2000).

2.2.1.2 Récepteur NMDA

Le récepteur NMDA (NMDA-R), activé par le N-Methyl-D-Aspartate, est un canal hétérotétramérique qui se compose de deux sous-unités GluN1 (le pore du récepteur) et associé avec deux autres sous-unités GluN2 (A-D) ou GluN3 (A-B). En l'absence de dépolarisation, le récepteur NMDA, perméable aux cations, est bloqué par un bouchon magnésium (Mg^{2+}). C'est ainsi qu'il est qualifié de détecteur de coïncidence, puisque son activité nécessite la présence d'une activité pré-synaptique (libération de glutamate) et post-synaptique (dépolarisation). Ce récepteur a une cinétique assez lente, et ses propriétés diffèrent selon les sous-unités le composant : affinité pour son agoniste, conductance, perméabilité au Ca^{2+} et sensibilité au blocage Mg^{2+} (Cull-Candy and Leszkiewicz, 2004). Par exemple, le récepteur NMDA de type NR1/2B est moins sensible au blocage par le Mg^{2+}. De plus, la glycine et la D-serine sont deux co-agonistes pouvant modifier les propriétés de ce récepteur (Mothet et al., 2015).

2.2.2 Récepteurs métabotropiques

Les récepteurs métabotropiques du glutamate sont responsables d'une transmission synaptique lente. Leur réponse est indirecte, car ils dépendent de l'activation d'une protéine G inhibitrice (Gαi) ou excitatrice (Gαs/q).

2.2.2.1 Récepteurs métabotropiques du glutamate (mGluRs)

Les récepteurs métabotropiques du glutamate font partie de la grande famille des récepteurs aux protéines G. Il existe 8 isoformes différentes du récepteur mGluR. Sa composition en sous-unités permet de distinguer trois groupes (Mukherjee and Manahan-Vaughan, 2013) : le

groupe I, composé de mGluR1 et mGluR5, augmente la quantité de calcium intracellulaire et active la protéine kinase C (PKC) via l'activation de protéines G stimulatrices stimulant la phospholipase C, provoquant la production de Diacylglycerol (DAG) ainsi que de 1,4,5-triphosphate (IP3) (Pin and Duvoisin, 1995). Les groupes II et III, respectivement composés des sous-unités mGluR2/3 et mGluR4/6/8 sont, eux, couplés à des protéines G inhibitrices, menant à la diminution de la concentration de calcium intracellulaire par inhibition de l'adénylate cyclase (Conn and Pin, 1997).

3. Induction et expression de la plasticité synaptique par STDP

3.1 Aux synapses glutamatergiques sur neurones glutamatergiques (STDP conventionnelle)

La STDP classique existant aux synapses excitatrices comme les synapses CA3-CA1 dépend étroitement du récepteur NMDA post-synaptique. On y trouve une forme de LTP et de LTD dépendante des récepteurs NMDA. Additionnellement, on y trouve une forme de LTD indépendante des récepteurs post-synaptiques mais reposant sur les récepteurs métabotropiques du glutamate (mGluR) et les récepteurs aux endocannabinoïdes de type 1 (CB1-R) **(Figure 12A)**.

3.1.1 LTP dépendante des récepteurs NMDA

3.1.1.1 Induction

La LTP NMDA-dépendante est associée à une forte entrée de calcium post-synaptique par le récepteur NMDA **(Figure 12B)**. Dans un protocole de STDP pré-post, la dépolarisation post-synaptique coïncide avec l'arrivée du PPSE, causant une entrée massive de calcium grâce au départ du blocage Mg^{2+} du récepteur NMDA (Kampa et al., 2004; Nevian and Sakmann, 2006), une meilleure propagation du signal dans les dendrites par inactivation du courant I_A, et l'activation des canaux sodium voltage-dépendants (Hoffman et al., 1997; Stuart and

A

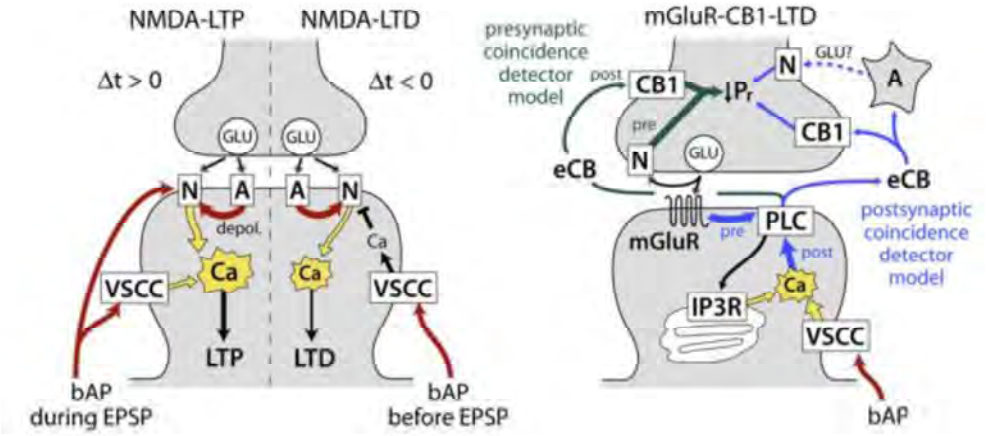

Feldman et al, 2012

B

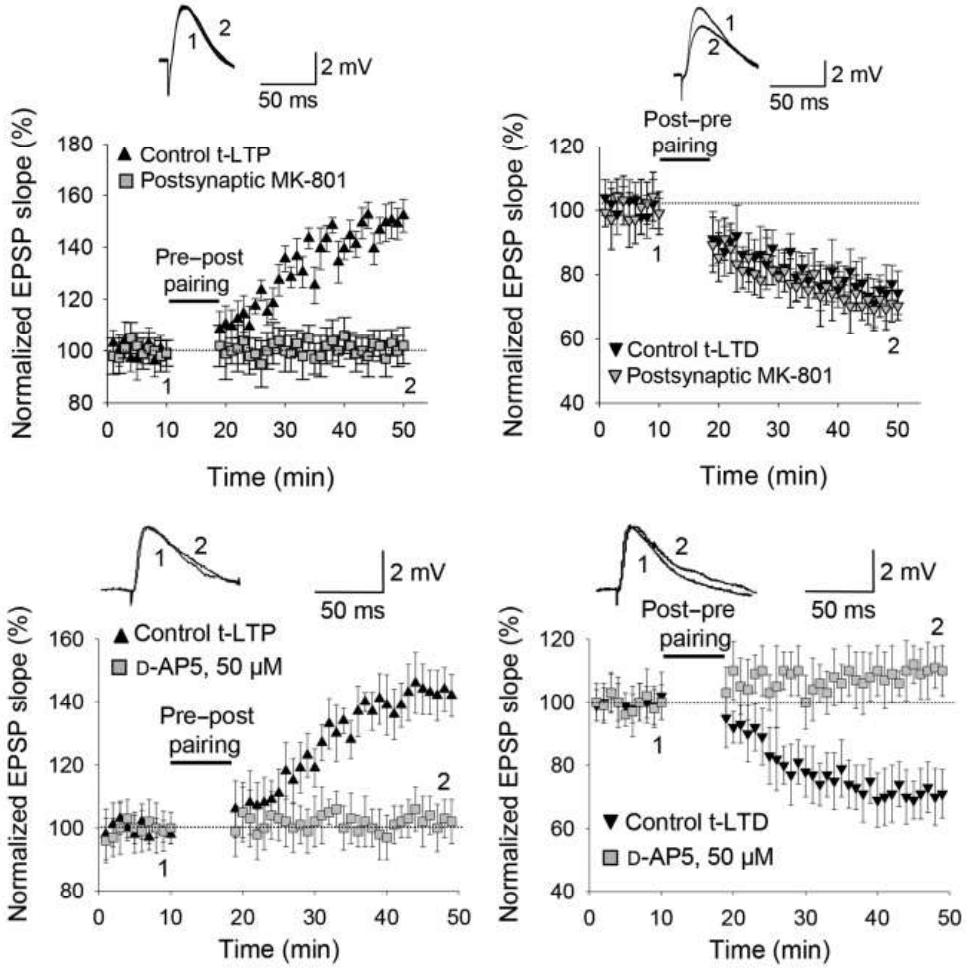

Andrade-Talavera et al, 2016

Figure 12. Induction et expression de la plasticité synaptique par STDP

A. L'induction de la LTP est essentiellement dépendante du récepteur NMDA post-synaptique, alors que les mécanismes d'induction de la LTD sont multiples. La LTD peut dépendre de l'activation du récepteur NMDA post-synaptique ou sur l'activation du récepteur métabotropique au glutamate (mGluR) ainsi que des récepteurs aux endocannabinoïdes de type 1 (CB1-R)

B. Dans l'hippocampe, aux synapses CA3-CA1, la perfusion de MK-801 -bloqueur des récepteurs NMDA- dans la pipette de patch empêche l'induction de la LTP mais pas de la LTD. La perfusion de D-AP5 dans le bain bloque l'induction de la LTP et de la LTD. Cette dernière repose donc sur l'activation des récepteurs NMDA pré-synaptiques.

Häusser, 2001), mais la dépolarisation véhiculée par le récepteur AMPA permet aussi une meilleure interaction entre le signal NMDA et l'EPSP (Fuenzalida et al., 2010; Holbro et al., 2010). On retrouve cette forme de plasticité dans l'hippocampe aux synapses CA3-CA1 (Nishiyama et al., 2000 ; Andrade-Talavera et al., 2016) ainsi que dans les couches II/III du cortex (Froemke et al., 2005) où l'utilisation d'un bloqueur des récepteurs NMDA, comme le MK801 ou l'APV, empêche l'induction de la LTP.

3.1.1.2 Expression

La phosphorylation des récepteurs AMPA et NMDA vont modifier et augmenter leur conductance (Lisman et al., 2012; Otmakhova et al., 2002). Un autre mécanisme concerne l'insertion de nouveaux récepteurs AMPA par exocytose (Malinow and Malenka, 2002). Dans la région CA1 de l'hippocampe, une insertion de nouveaux récepteurs NMDA après HFS a aussi été montrée (Carroll and Zukin, 2002).

3.1.2 LTD dépendante des récepteurs NMDA

3.1.2.1 Induction

La LTD NMDA-dépendante est associée à une plus faible entrée de calcium post-synaptique par le récepteur NMDA. Dans un protocole post-pré, la dépolarisation post-synaptique ne coïncide pas avec l'arrivée du PPSE. Les mécanismes à l'œuvre et cités précédemment dans le cadre de la LTP NMDA-dépendante n'existent pas, s'ensuit alors une entrée négligeable de calcium (Karmarkar and Buonomano, 2002; Shouval et al., 2002). Un autre mécanisme à l'œuvre est l'inactivation des récepteurs NMDA par l'entrée de calcium (Rosenmund et al., 1995) qui active la voie calcineurine (Tong et al., 1995). Cette inactivation des récepteurs NMDA induit donc un courant moins important en réponse à la stimulation pré-synaptique (Froemke et al., 2005) On retrouve cette forme de plasticité aux synapses CA3-CA1 de

l'hippocampe ainsi qu'à certaines synapses de la couche II/III du cortex (Nishiyama et al., 2000 ; Froemke et al., 2005).

3.1.2.2 Expression

L'induction de la LTD induit l'expression de phosphatases, qui vont déphosphoryler les récepteurs AMPA et NMDA et entraîner leur endocytose (Winder and Sweatt, 2001).

3.1.3 LTD dépendante du récepteur NMDA pré-synaptique

Le récepteur NMDA pré-synaptique est souvent requis pour l'induction de cette forme de LTD, et non le récepteur NMDA post-synaptique **(Figure 12B)**. Cette forme de plasticité a été mise en évidence pour la première fois par l'enregistrement de paires de neurones corticaux connectés (Sjöström et al., 2003 ; **Figure 13A**). Le récepteur NMDA pré-synaptique est capable de fortement moduler la transmission synaptique évoquée puisqu'il modifie cette dernière pour des fréquences de stimulation supérieures à environ 8 Hz (Abrahamsson et al., 2017). En effet, dans le néocortex et l'hippocampe, la perfusion de MK801 dans le neurone pré-synaptique empêche l'induction de la LTD mais pas de la LTP (Andrade-Talavera et al., 2016; Rodríguez-Moreno and Paulsen, 2008). Cette forme de LTD se retrouve dans de nombreuses régions cérébrales comme l'hippocampe (Andrade-Talavera et al., 2016), le cortex (Bender, 2006; Corlew et al., 2007; Nevian and Sakmann, 2006; Rodríguez-Moreno and Paulsen, 2008; Sjöström et al., 2003) et le striatum (Fino et al., 2010). Néanmoins, cette forme de LTD, qui est prépondérante dans le cortex chez l'animal jeune, disparaît chez l'animal âgé (Banerjee et al., 2009).

3.1.4 LTD dépendante des récepteurs mGluRs

3.1.4.1 Induction

- **Acteurs post-synaptiques**

Au niveau post-synaptique, cette forme de LTD requiert les récepteurs métabotropiques du glutamate (mGluR), la phospholipase C (PLC), les canaux calciques à bas seuil (VGCC de type T, R ou L), ainsi que la libération de calcium par les stocks intracellulaires via le récepteur à l'IP3. Le signal calcique provenant des canaux calciques ainsi que des stocks intracellulaires va conduire à l'activation de la PLC (Hashimotodani et al., 2005), qui va stimuler la production d'endocannabinoïdes (eCBs), messagers rétrogrades qui vont agir au niveau pré-synaptique (pour revue, Chevaleyre et al., 2006)

- **Acteurs pré-synaptiques**

Les eCBs, en tant que messagers rétrogrades, vont activer les récepteurs cannabinoïdes de type 1 (CB1R) pré-synaptiques pour diminuer la libération de neurotransmetteurs (Bender et al., 2006 ; Chevaleyre et al., 2006). Néanmoins, l'activation de récepteurs CB1 astrocytaires pourraient aussi contribuer à diminuer la libération de neurotransmetteurs par action sur les récepteurs NMDA pré-synaptiques (Min and Nevian, 2012).

3.1.4.2 Expression

L'expression de la LTD dépendante des récepteurs mGluRs nécessite deux détecteurs de coïncidence : l'un pré-synaptique, permettant de diminuer la libération de neurotransmetteurs, et l'autre post-synaptique induisant la production de messagers rétrogrades, représentés par les eCBs. Chaque dépolarisation post-synaptique serait à l'origine d'une rétro-propagation d'eCB qui coïnciderait avec l'activité pré-synaptique pour activer les récepteurs NMDA pré-synaptiques (Duguid and Sjöström, 2006) et réduire la libération de neurotransmetteurs. Le

signal calcique provenant des VDCCs, en synergie avec l'activité pré-synaptique, active la PLC pour permettre la production d'eCB qui va agir au niveau pré-synaptique.

3.1.5 Débat autour du récepteur NMDA présynaptique

Bien que le rôle du récepteur NMDA pré-synaptique semble établi dans certaines formes d'induction de la STDP **(Figure 13A)**, le débat est encore ouvert aujourd'hui, avec une récente étude montrant que les récepteurs NMDA pré-synaptiques ne sont pas nécessaires à la LTD par STDP entre les synapses L5-L2/3 (Carter and Jahr, 2016). Néanmoins, cette étude est en désaccord avec de nombreux autres travaux antérieurs (Sjöström et al., 2003 ; Rodriguez-Moreno et al., 2011 ; Min and Nevian, 2012). Récemment, une nouvelle étude a dévoilé que les voies de signalisation régulant la transmission synaptique évoquée et spontanée par le récepteur NMDA pré-synaptique sont différentes (Abrahamsson et al., 2017 ; **Figure 13B**). La régulation de la transmission synaptique évoquée passe par la protéine RIM1αβ, alors que la transmission synaptique spontanée est régulée par la voie JNK2. Cette étude est un premier pas pour comprendre le rôle du récepteur NMDA pré-synaptique. Pour revue sur la question, voir Bouvier et al., 2018.

3.2 STDP non-conventionnelle

La STDP prend diverses formes aux synapses montrant une STDP non-conventionnelle. Contrairement aux synapses glutamatergiques, il est difficile d'en déduire un mécanisme commun. Bien que les acteurs soient semblables, les prérequis sont divers en fonction de la synapse étudiée et doivent être considérés au cas par cas.

3.2.1 STDP des synapses excitatrices sur neurones inhibiteurs

Dans le noyau cochléaire dorsal, les synapses glutamatergiques sur les cellules glycinergiques à roue de charrette (cartwheel cells) dépendent du récepteur NMDA post-synaptique ainsi que du signal rétrograde des récepteurs CB1 pour l'induction de la LTD. Cependant, son

A

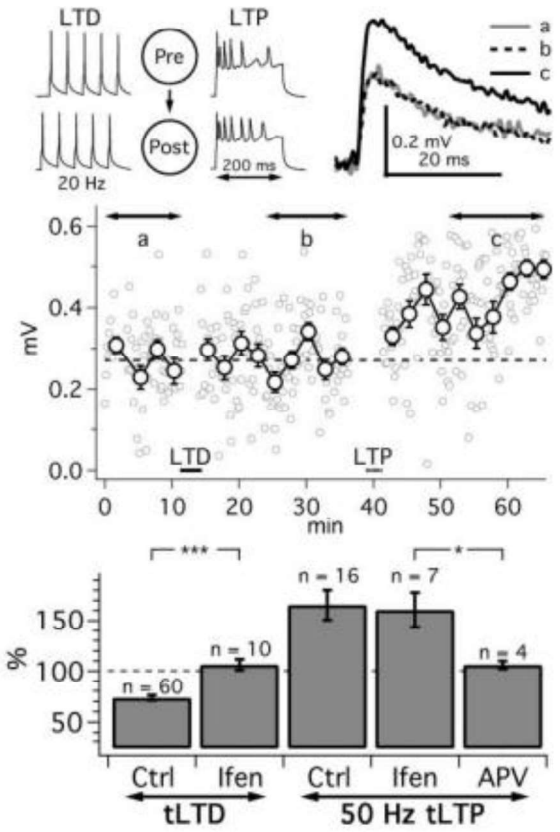

Sjöström et al, 2003

B

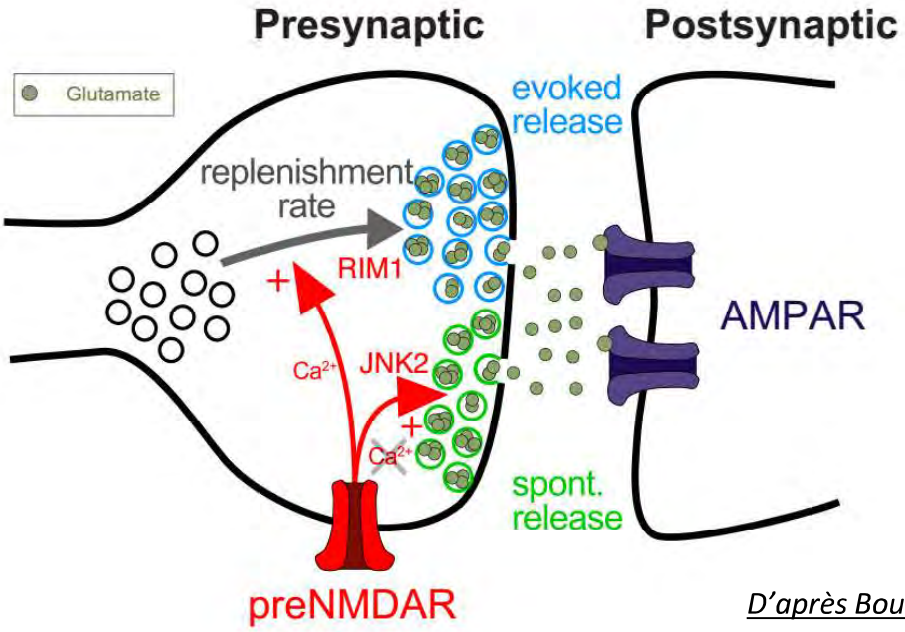

D'après Bouvier et al, 2018

Figure 13. Débat autour du rôle du récepteur NMDA pré-synaptique

A. Dans le cortex, En présence d'ifenprodil, un bloqueur spécifique de la sous-unité NR2B des récepteurs NMDA et spécifiquement exprimée au niveau pré-synaptique, l'induction de la LTD est bloquée, mais l'induction de la LTP est intacte.

B. Le récepteur NMDA contrôle la transmission synaptique par deux voies différentes. La transmission spontanée repose sur la protéine JNK2, alors que la transmission évoquée repose sur la protéine RIM1.

expression est pré-synaptique alors que la LTP dépend uniquement du récepteur NMDA post-synaptique et de la voie CaMKII (Tzounopoulos et al., 2007). Au niveau des synapses entre les fibres parallèles et les cellules de Purkinje du cervelet, la LTD est exprimée au niveau post-synaptique par internalisation des récepteurs AMPA, et dépend de l'action des récepteurs mGluRs post-synaptiques, mais aussi de l'activation des récepteurs CB1 pré-synaptiques (Safo and Regehr, 2008; Steinberg et al., 2006). Dans le cortex, les synapses corticales sur les interneurones fast-spiking nécessitent le récepteur mGluR post-synaptique et la voie IP3 pour l'induction de la LTD et est indépendante du récepteur CB1 (Lu et al., 2007). Pour finir, dans le striatum, lieu privilégié de la STDP non-conventionnelle, l'induction de LTD au niveau des interneurones cholinergiques dépend de l'activation des mGluR, concernant les interneurones nNOS, aucune étude n'a encore caractérisé les voies de signalisation (Fino, 2010; Fino et al., 2008).

3.2.2 STDP des synapses inhibitrices sur neurones excitateurs

Dans l'hippocampe, l'induction de la LTD au niveau des synapses entre interneurones et neurones pyramidaux CA1 nécessite un influx calcique par les VDCC de type L ainsi que la diminution de l'activité du co-transporteur K^+-Cl^- modifiant le potentiel de réversion du GABA (E_{GABA}) vers des valeurs plus positives (Woodin et al., 2003). Un autre mécanisme sans changement du E_{GABA} est présent dans le cortex, au niveau des synapses entre interneurones et neurones pyramidaux de la couche 2/3, où LTP et LTD nécessitent une élévation du Ca^{2+} post-synaptique (Holmgren and Zilberter, 2001).

4. Aspect biophysique de la STDP

4.1 Rôle du potentiel d'action rétro-propagé

Pour que le récepteur NMDA joue son rôle de détecteur de coïncidence, il est nécessaire que le potentiel d'action post-synaptique se rétro-propage jusqu'à la synapse considérée.

Néanmoins, l'arbre dendritique est grand, et la rétropropagation du potentiel d'action est limitée en distance (Golding et al., 2002). Généralement, dans les synapses proches dans l'arbre dendritique, la dépolarisation liée à la rétropropagation est suffisante pour induire de la LTP alors que les synapses plus éloignées, qui expriment généralement une STDP non-conventionnelle, vont avoir recours à des formes locales de dépolarisation dendritique comme les potentiels d'action calciques locaux **(Figure 14A,B)**.

4.2 Rôle des potentiels NMDA

Les récepteurs NMDA localisés dans les dendrites sont une source importante de dépolarisation permettant d'augmenter le signal qui diminue lors de sa progression dans l'arbre dendritique (Schiller and Schiller, 2001). Généralement, les potentiels NMDA, calciques, sont induits par l'activité synchrone de plusieurs synapses, mais plusieurs facteurs peuvent faciliter leur induction, comme l'appariement d'une activité pré- et post-synaptique (Schiller et al., 1998) ou une dépolarisation. Les potentiels NMDA peuvent être modulés par des conductances ioniques, comme les canaux SK qui diminuent leur seuil d'induction ainsi que leur amplitude (Bock and Stuart, 2016). On retrouve ce phénomène dans le cortex (Schiller et al., 1997) et dans l'hippocampe (Brandalise and Gerber, 2014). Plus récemment, il a été montré que les potentiels NMDA sont un prérequis à l'induction de la LTP par STDP aux synapses fibres moussues-CA3 (Brandalise et al., 2016 ; **Figure 14C**) mais aussi aux synapses distales du cortex entre la couche 2/3 et 5 (Sjöström et Häusser, 2006). Enfin, les synapses distales, contrairement aux synapses proximales, sont capables de coopération, facilitant l'induction de potentiels NMDA (Weber et al., 2016). Récemment, il a été mis en évidence une forme de plasticité synaptique, appelée plasticité synaptique à échelle de temps comportementale (BTSP), dans les cellules de lieu de l'hippocampe, où des plateaux de dépolarisations calciques sont suffisant pour induire une augmentation du poids synaptique indépendant du délai du potentiel d'action (Bittner et al., 2017). Dans des tranches aiguës,

cinq appariements d'une dépolarisation pré-synaptique sous-liminaire couplée à un plateau calcique permettent d'induire une potentialisation robuste.

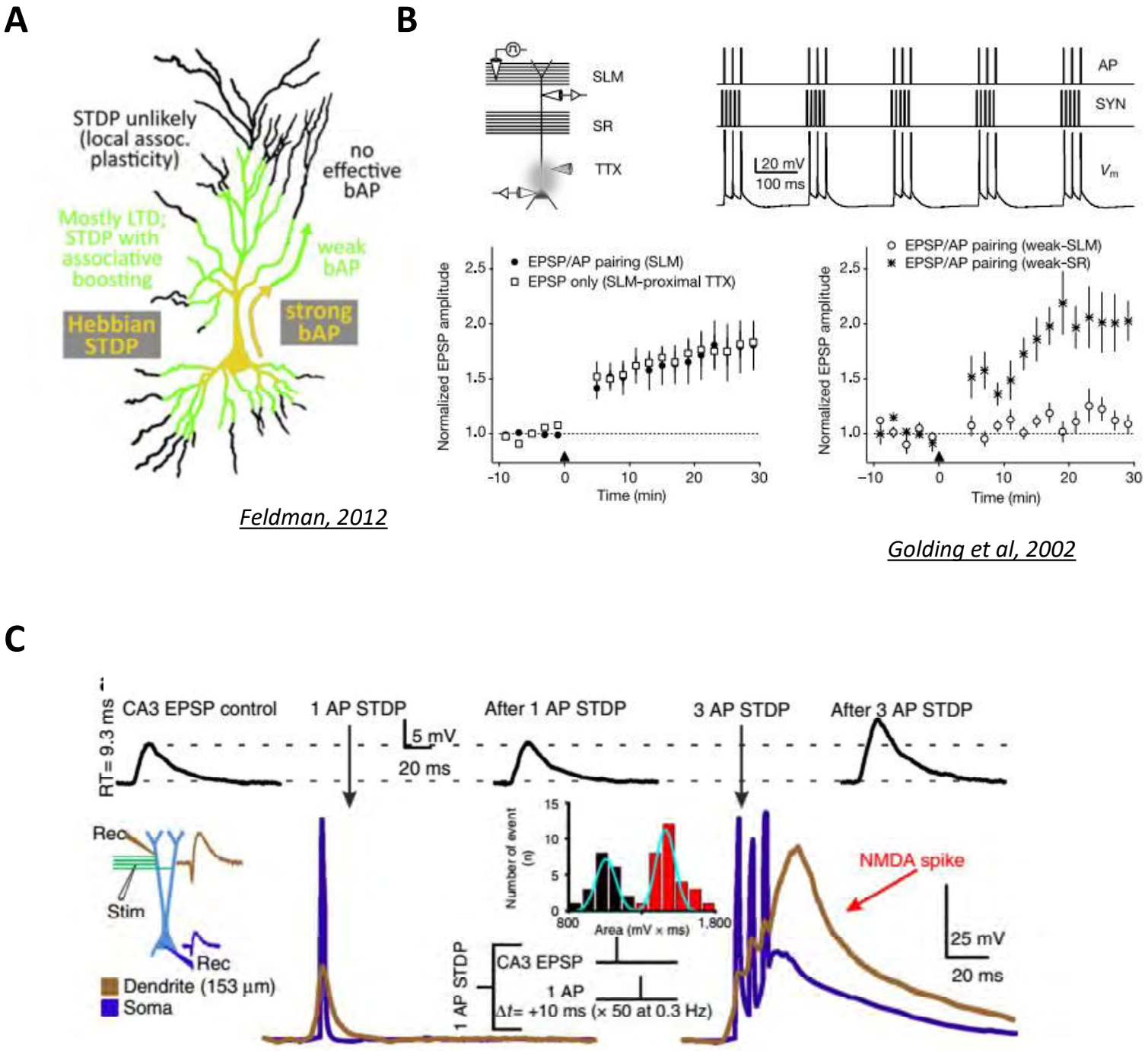

Feldman, 2012

Golding et al, 2002

Figure 14. Rôle du potentiel d'action rétro-propagé

A. La rétro-propagation du potentiel d'action est limitée dans l'arbre dendritique. La STDP classique est généralement limitée aux synapses proximales, alors que les synapses distales montrent une absence de LTD et présentent une STDP non-conventionnelle. Les synapses distales doivent avoir recours à des formes de dépolarisations locales.

B. Dans les dendrites distales des neurones pyramidaux CA1, la LTP ne repose pas sur la rétro-propagation du potentiel d'action mais nécessite des potentiels dendritiques. En présence de TTX et donc en l'absence de potentiels d'action, la LTP aux synapses distales n'est pas bloquée.

C. Dans les cellules pyramidales CA3, les potentiels NMDA sont nécessaires pour induire de la LTP par STDP. Un seul potentiel d'action n'est pas suffisant pour provoquer un potentiel NMDA, alors que trois potentiels d'action permettent d'évoquer un potentiel NMDA et l'induction de la LTP.

Modulation de la règle de STDP

La règle de STDP est multifactorielle. Bien que le timing soit un facteur important dans l'orientation de la plasticité, de nombreux autres facteurs, de deux types, sont capables de moduler la plasticité. Tout d'abord ceux liés à l'activité neuronale, c'est-à-dire : 1) le nombre de répétitions, 2) la fréquence de l'appariement pré- et post-synaptique, 3) le niveau de dépolarisation post-synaptique ou encore 4) le nombre de potentiels d'action post-synaptiques. Le second facteur est de nature externe et est représenté par les neuromodulateurs (dopamine, acétylcholine, noradrénaline, etc…) qui peuvent modifier la règle de STDP.

1. Modification de la règle de STDP par l'activité

1.1 Nombre de répétitions

1.1.1 Un seuil plus bas pour la LTP que pour la LTD

L'induction de changements synaptiques par STDP nécessite une répétition de l'appariement entre l'activité pré- et post-synaptique. Bien que les raisons nécessaires à ces multiples appariements soient encore floues, plusieurs effets du nombre de répétitions sur la STDP ont été observés. Il est généralement admis que le seuil de LTP nécessite moins de répétitions que le seuil de LTD. Dans l'hippocampe, aux synapses CA3-CA1, il est possible d'observer de la LTD pour 90 répétitions, alors qu'elle est absente avec 30 appariements (Debanne and Thompson, 1994 ; **Figure 15A**). Lorsque l'appariement est associé avec 2 potentiels d'action post-synaptiques, il est possible d'observer de la LTP pour seulement 30 répétitions dans les synapses CA3-CA1 (Wittenberg and Wang, 2006). Dans la couche 2/3 du cortex visuel, la LTP peut être observée à partir de seulement 12 répétitions contre 30 répétitions pour la LTD (Froemke et al., 2006 ; Figure 15B). Néanmoins, si le nombre de

répétitions semble influencer la probabilité d'induction de la plasticité, il n'a que peu d'effet sur l'amplitude de la plasticité induite qui sature à partir de 60 répétitions (Froemke et al., 2006).

1.1.2 Nombre de répétitions et probabilité d'induction

Plusieurs études suggèrent que les synapses modifient leurs poids synaptiques de manière digitale (phénomène tout ou rien), et que le niveau de modification possible serait déjà fixé pour chaque synapse (O'Connor et al., 2005; Petersen et al., 1998). Selon cette théorie, le nombre de répétitions serait un facteur important pour modifier la probabilité d'induction de la LTP ou LTD par STDP plutôt qu'un facteur influençant l'amplitude de la LTP. Dans la région CA1 de l'hippocampe, les travaux de Petersen et collaborateurs (1998) montrent que les synapses ont toutes un seuil différent à la LTP. En effet, certaines synapses potentialisent à partir de 10 répétitions contre 100 pour d'autres, alors que d'autres sont incapables de potentialiser. Cette hétérogénéité des connexions se retrouve aussi dans des expériences de paires de neurones CA3-CA3 connectées, où une grande variabilité dans l'amplitude de la LTP (jusqu'à 13 fois le poids synaptique initial), ainsi que l'absence de plasticité pour certaines synapses sont observées (Debanne et al., 1999). Tout comme la LTP, la LTD aux synapses CA3-CA1 semble aussi suivre un phénomène « tout ou rien » (O'Connor et al., 2005). Néanmoins, la plupart des études concernant la plasticité synaptique utilisent des stimulations extracellulaires recrutant un grand nombre de synapses et l'hétérogénéité des connexions font que l'augmentation du niveau de plasticité avec le nombre de répétitions ne serait que la somme de plusieurs synapses. De plus, selon certaines mesures, environ 70 % des synapses dans la région CA1 de l'hippocampe sont dans un état de dépression, ce qui peut expliquer la plus grande difficulté d'induire de la LTD et le nombre de répétitions plus important requis (O'connor et al., 2005). Certaines structures sont très sensibles au nombre de répétitions, c'est le cas du striatum au niveau des synapses cortico-

striatales où la forme de LTP induite dépend du nombre de répétitions. Pour un faible nombre de répétitions (< 10), une LTP dépendante des récepteurs CB1 est induite alors que pour un nombre plus important, c'est une LTP NMDA-dépendante qui est retrouvée (Cui et al., 2015, 2016).

1.2 Fréquence de répétition

LTP et LTD sont deux phénomènes dépendant étroitement de la fréquence de stimulation des afférences pré-synaptiques, comme décrit par la règle BCM. Les stimulations à hautes fréquences (> 10 Hz) induisent de la LTP alors que les basses fréquences (1 – 5Hz) induisent de la LTD (Bear and Abraham, 1996; Dudek and Bear, 1992). La STDP est aussi étroitement contrôlée par la fréquence de répétition de l'appariement entre l'activité pré- et post-synaptique (Markram et al., 1997 ; Sjöström et al., 2001).

1.2.1 Hétérogénéité de la fréquence d'appariement en fonction des synapses étudiées

Des expériences d'enregistrement de paires de neurones L5-L5 dans le cortex ont montré pour la première fois que la LTP dépend étroitement de la fréquence d'appariement (Markram et al., 1997). L'augmentation de la fréquence augmente l'amplitude de la LTP **(Figure 15C)** mais la STDP conventionnelle n'apparaît que pour des fréquences intermédiaires de l'ordre de 10-20 Hz, alors que des fréquences plus faibles (< 10 Hz) ou plus fortes (> 40 Hz) induisent respectivement uniquement de la LTD ou de la LTP quel que soit le délai utilisé (Sjöström et al, 2001 ; **Figure 15C**). Néanmoins, si la LTD peut être induite par des faibles fréquences (0.1 – 10 Hz), la LTP nécessite forcément des fréquences supérieures, contrairement à l'hippocampe, où une fréquence de 0.3 Hz est suffisante pour induire la LTP dans des expériences neurones connectés CA3-CA3 (Campanac and Debanne, 2008; Debanne

et al., 1998a) mais aussi les synapses retinotectales où une fréquence de 1 Hz est suffisante (Zhang et al., 1998).

1.2.2 Effet de l'augmentation de la fréquence d'appariement

L'augmentation de la fréquence (> 50 Hz) conduit à la transformation de la fenêtre de LTD en LTP, synonyme de la perte d'information du timing du potentiel d'action (Froemke et al., 2006; Sjöström et al., 2001). Dans certains cas, l'augmentation de la fréquence de l'appariement pré- et post-synaptique peut permettre de récupérer la fenêtre de LTP absente dans certaines conditions. Dans l'hippocampe, aux synapses CA3-CA1, l'utilisation d'une fréquence de 0.3 Hz ne permet pas d'obtenir une courbe de STDP conventionnelle mais présente uniquement une fenêtre de dépression. Néanmoins, l'utilisation d'une fréquence thêta (5 Hz) permet de récupérer la fenêtre de LTP (Wittenberg and Wang, 2006). Ce type de fréquence est aussi retrouvé *in vivo* pour induire de la LTP aux synapses thalamo-corticales dans le cortex visuel du chat (Frégnac et al., 2010). De plus, les modèles mathématiques de STDP basés sur le calcium montrent aussi qu'une augmentation de la fréquence conduit à la LTP (Graupner and Brunel, 2012; Shouval et al., 2002).

1.3 Modifications de l'activité post-synaptique

1.3.1 Nombre de potentiels d'action post-synaptiques

Les protocoles classiques de STDP associent un unique potentiel d'action post-synaptique avec l'activité pré-synaptique dans l'hippocampe (Bi and Poo, 1998; Debanne et al., 1998a). Néanmoins, certaines études aux synapses CA3-CA1 montrent qu'une activité en bouffées post-synaptiques permet de récupérer la fenêtre de LTP là où un seul potentiel d'action était incapable d'induire un changement synaptique (Pike et al., 1999 ; **Figure 15D**). Enfin, l'utilisation de 7 à 12 potentiels d'action permet d'étendre la fenêtre temporelle de LTD jusqu'à 1600 ms (Debanne et al., 1994; Sourdet and Debanne, 1999) alors qu'avec un

seul potentiel d'action, la fenêtre d'induction de la LTD est d'environ 200 ms (Debanne et al., 1998). On peut noter que pour une synchronisation des activités pré- et post-synaptiques, une LTD est induite avec un nombre inférieur à 4 potentiels d'action, alors qu'une LTP est induite pour un nombre supérieur à 4 potentiels d'action (Debanne et al., 1994 ; Sourdet and Debanne, 1999). Néanmoins, si les activités en bouffées semblent faciliter l'induction de la LTP dans l'hippocampe (Pike et al., 1999 ; Debanne et al., 1998), des résultats contradictoires sont retrouvés dans le cortex aux synapses entre la couche 2/3 et 5, où une activité en bouffées facilite l'induction de la LTD (Birtoli and Ulrich, 2004). Dans le cortex, pour une fréquence d'appariement de 0.2 Hz, une bouffée de 5 potentiels d'action post-synaptiques n'induit pas la même plasticité en fonction de la fréquence. Avec une fréquence de 10 ou 50 Hz, aucune LTP n'est observée, alors qu'une fréquence de bouffées de 100 Hz induit de la LTP (Froemke et al., 2006). Enfin, tout comme la fréquence d'appariement, une bouffée de potentiels d'action semble nécessaire pour l'induction de la LTP dans le cortex visuel *in vivo* (Frégnac et al., 2010).

1.3.2 Dépolarisation post-synaptique

Dans certains cas, indépendamment de l'augmentation du nombre de potentiels d'action post-synaptiques, une dépolarisation peut être suffisante pour récupérer la fenêtre de LTP. Dans le cortex, dans des expériences de paires de neurones L5-L5 connectés, l'injection d'un courant dépolarisant d'une durée de 100 ms dans le neurone post-synaptique précédant le potentiel d'action post-synaptique permet de récupérer la LTP pour de faibles fréquences (Sjöström et al., 2001).

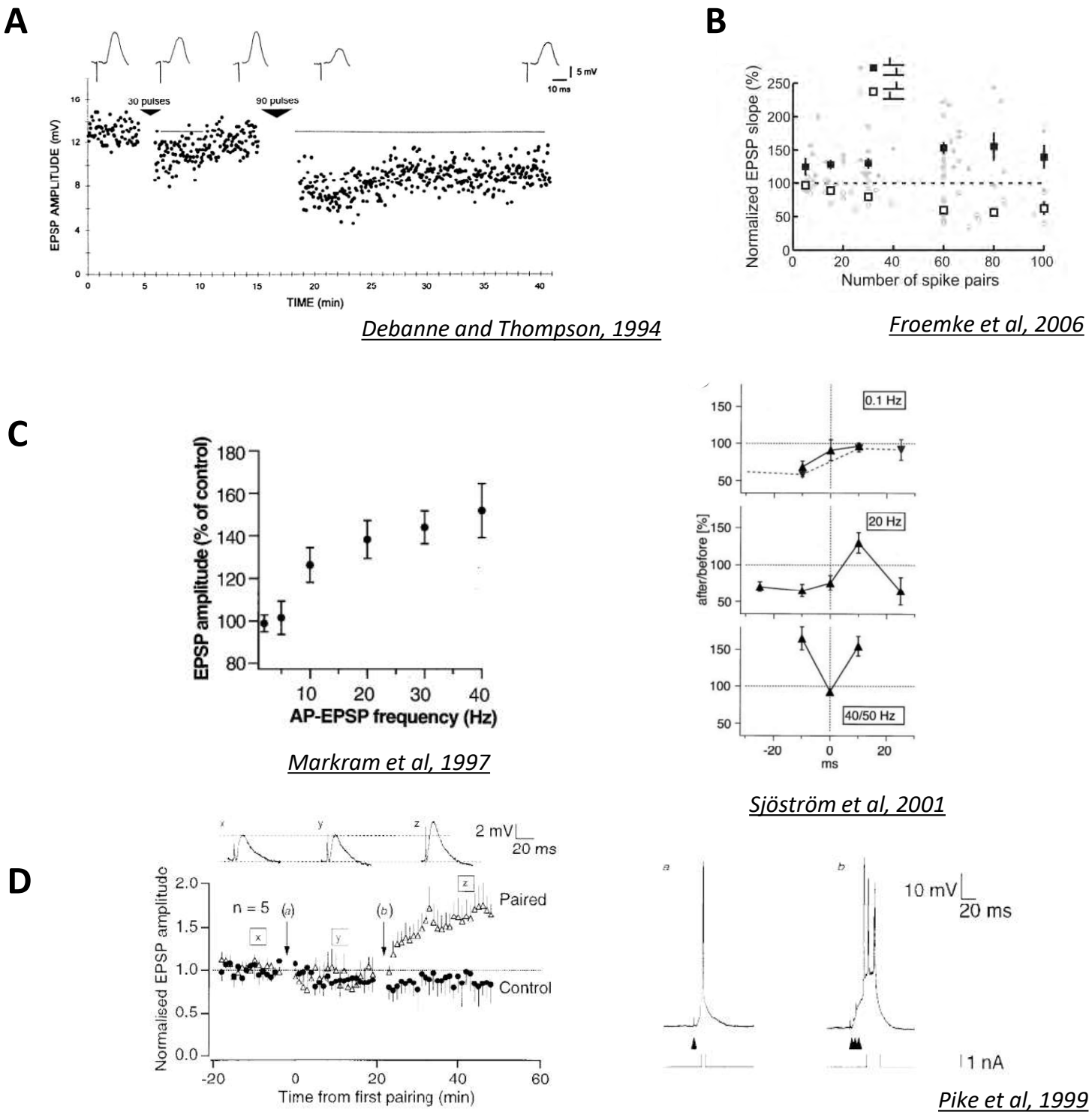

Figure 15. Modulation de la règle de STDP par l'activité

A. Aux synapses CA3-CA1 de l'hippocampe, 30 répétitions d'un protocole de LTD n'induisent qu'une dépression transitoire, alors que 90 répétitions permettent d'induire une LTD persistante.
B. Dans la couche 2/3 du cortex visuel, on peut observer LTP et LTD pour un très faible nombre de répétitions. La LTP apparaît pour seulement 12 répétitions, mais sature rapidement pour 60 répétitions, tout comme la LTD.
C. La LTP est très sensible à la fréquence d'appariement. L'augmentation de la fréquence augmente l'amplitude de la LTP (gauche). Dans le cortex, la STDP conventionnelle apparaît pour une fréquence d'appariement autour de 20 Hz, mais est absente pour des fréquences plus faibles. A haute fréquence, une STDP non-conventionnelle exprimant uniquement de la LTP est induite (droite).
D. Aux synapses CA3-CA1, une activité post-synaptique en bouffées permet de récupérer la fenêtre de LTP là ou un seul potentiel d'action n'est pas capable d'induire un changement synaptique.

1.4 Conclusion

Bien que le timing soit un facteur clé dans l'orientation de la plasticité, l'activité (fréquence, nombre de potentiels d'action, dépolarisation) peut modifier la plasticité de sortie. De plus, les effets sont différents en fonction de la structure étudiée.

2. Neuromodulation

En plus de l'activité, l'autre facteur pouvant fortement modifier la règle de STDP est la neuromodulation. La plupart des études portant sur la caractérisation de la règle de STDP ont été réalisées *in vitro*, mais *in vivo*, un neurone est soumis à une activité pré-synaptique importante, capable de générer un PA post-synaptique pouvant interagir avec un grand nombre de synapses. D'après les connaissances actuelles, l'association de ces activités pré- et post-synaptiques pourrait modifier continuellement l'efficacité d'une synapse, en l'augmentant ou en la diminuant. Devant ce constat, certaines études théoriques (Miller, 1981; Wickens, 1990) ont émis la possibilité d'un autre facteur, capable de sélectionner spatialement en plus de temporellement les entrées pouvant modifier la force synaptique. Ce facteur pourrait être la neuromodulation, avec de nombreux candidats : dopamine, noradrénaline ou encore acétylcholine. Bien que leur rôle ait été étudié dans la plasticité synaptique induite par HFS ou LFS dans l'hippocampe (Frey et al., 1990; Huerta and Lisman, 1993; Thomas et al., 1996), l'exploration du rôle de la neuromodulation sur la règle de STDP est assez récente (Foncelle et al., 2018; Palacios-Filardo and Mellor, 2019; Pawlak, 2010).

2.1 Dopamine

La dopamine (DA) est le neuromodulateur de loin le plus étudié du fait de son implication dans les mécanismes de récompense, la mémoire (McNamara et al., 2014), les comportements basés sur la motivation (Schultz, 1998; Suri and Schultz, 1999), ou encore la transmission synaptique (Rosen et al., 2015). Ceci en fait un candidat parfait pour résoudre les problèmes soulevés par les études théoriques (Foncelle et al., 2018).

2.1.1 Récepteurs

Il existe cinq récepteurs à la DA divisés en deux classes : D1 et D2. La famille de type D1 regroupe les récepteurs D1 et D5, alors que la famille de type D2 regroupe les récepteurs D2, D3 et D4. Les récepteurs à la DA sont métabotropiques, couplés à une protéine G. Les récepteurs de la classe D1 sont couplés positivement à l'adénylate cyclase (AC) par le biais d'une protéine G de type $G\alpha_s$ ou $G\alpha_{olf}$ provoquant la production d'AMP cyclique et l'activation de la voie de la protéine kinase A (PKA). À l'inverse, les récepteurs de la classe D2 sont couplés négativement à l'AC par couplage à une protéine G de type $G\alpha_i$ et $G\alpha_o$. Les récepteurs D1 et D2 agissent donc en opposition. Néanmoins, certaines études suggèrent que les récepteurs D2 peuvent stimuler l'activité de l'AC (Glass and Felder, 1997; Watts and Neve, 1997).

2.1.2 Projections dopaminergiques

La synthèse de dopamine se fait essentiellement au niveau de la substance noire et de l'aire tegmentale ventrale (ATV). Les neurones dopaminergiques projettent essentiellement au niveau des ganglions de la base, dont le striatum. Dans l'hippocampe, la source majoritaire de DA provient des projections du locus coeruleus (LC) (Kempadoo et al., 2016).

2.1.3 Effet sur la STDP

2.1.3.1 Effet des récepteurs D1

Globalement, du fait de leur couplage positif à l'AC et donc à la production d'AMPc, les récepteurs D1 sont associés majoritairement à une facilitation de l'induction de la LTP hippocampique. Ainsi, dans des cultures de neurones dissociés d'hippocampe, l'application de DA augmente la fenêtre temporelle d'induction de la LTP, réduit le nombre d'appariements nécessaires à son induction, et transforme la fenêtre de LTD en LTP (Zhang et al., 2009 ; **Figure 16A**). Cet effet se retrouve aussi dans le gyrus denté, aux synapses entre la voie

perforée et les neurones granulaires, où la fenêtre d'induction de la LTP est plus large (même pour des délais négatifs) en présence d'un agoniste spécifique des récepteurs D1, le SKF-91297 (Yang and Dani, 2014) en accord avec des résultats précédents selon lesquels l'activation des récepteurs D1 diminuait le seuil d'induction de la LTP (Hamilton et al., 2010). Dans ces expériences, l'application de DA a lieu pendant l'appariement, mais si elle est appliquée aux synapses CA3-CA1 après l'appariement post-pré, la fenêtre de LTD est transformée en LTP (Brzosko et al., 2015). Enfin, il apparaît que des conditions de préparation (préparation en sucrose) diminuant le niveau basal de DA dans les tranches aigües empêchent l'induction de la LTP aux synapses CA3-CA1 (Edelmann and Lessmann, 2011). Dans le striatum, lieu important des projections dopaminergiques, la DA est requise pour l'induction de la STDP *in vitro* et *in vivo* (Fisher et al., 2017). En effet, le blocage des récepteurs D1/D5 empêche l'induction de la LTD/LTP aux synapses cortico-striatales (Pawlak and Kerr, 2008; Shen et al., 2008 ; Figure 16B). Enfin, dans le cortex, les résultats sont disparates car l'application de DA permet l'induction de la LTP dans le cortex pré-frontal, mais pas dans le cortex visuel (He et al., 2015), probablement à cause d'une composition en récepteurs différente entre les deux régions.

2.1.3.2 Effet des récepteurs D2

Bien que les récepteurs D2 soient couplés négativement à l'AC, pouvant suggérer un rôle dans l'inhibition de la LTP, plusieurs études montrent que, tout comme les récepteurs D1, ce type de récepteurs à la DA facilite l'induction de la LTP. Dans l'amygdale latérale, l'application de DA permet d'induire de la LTP par activation des récepteurs D2 (Bissière et al., 2003). De la même manière, ils auraient un rôle dans l'induction de la LTP/LTD au niveau des synapses cortico-striatales (Shen et al., 2008), ainsi qu'à celui des synapses CA3-CA1 en synergie avec les récepteurs D1/D5 (Brzosko et al., 2015, 2017).

2.1.3.3 Coopération entre récepteurs D1 et D2

Dans certains cas, l'activation des récepteurs D1 et D2 est requise. Dans les neurones pyramidaux de couche 5 du cortex, l'application de DA permet l'induction de la LTP ainsi que l'augmentation de sa fenêtre temporelle d'induction (Xu and Yao, 2010). L'activation du récepteur D2, exprimé par les interneurones GABAergiques, bloque l'inhibition en synergie avec l'activation des récepteurs D1 situés sur le neurone post-synaptique **(Figure 16C).**

2.1.3.4 Mécanismes

Bien que les effets de la DA soient maintenant répertoriés dans plusieurs régions cérébrales (hippocampe, cortex, striatum), les mécanismes cellulaires à l'origine de la facilitation de la plasticité synaptique ne sont pas tout le temps étudiés dans la plupart des travaux qui se contentent de décrire les effets de l'application de DA (Zhang et al., 2009) ou d'agonistes spécifiques. Néanmoins, la plupart des études montre une dépendance au récepteur NMDA post-synaptique, qui disparaît en présence d'un bloqueur (D-AP5) de ce récepteur (Edelmann and Lessmann, 2011; Yang and Dani, 2014; Zhang et al., 2009). La plupart des études dans l'hippocampe citées précédemment rapportent des modifications des conductances de canaux voltage-dépendants, en particulier une inhibition du courant potassique de type A (I_A) facilitant la rétro-propagation du potentiel d'action dans l'arbre dendritique (Edelmann and Lessmann, 2011; Hamilton et al., 2010; Yang and Dani, 2014). De plus, certaines études suggèrent que le récepteur D2 pourrait avoir recours à des voies non-conventionnelles de signalisation pour promouvoir l'induction de la LTP dans les neurones pyramidaux CA1 (Brzosko et al., 2015).

Néanmoins, il est connu que les effets de la DA sont complexes à cause de ses voies de signalisation aux nombreux effets (Neve et al., 2004) et qu'elle est capable de modifier l'excitabilité neuronale par de nombreux mécanismes : augmentation du calcium

A

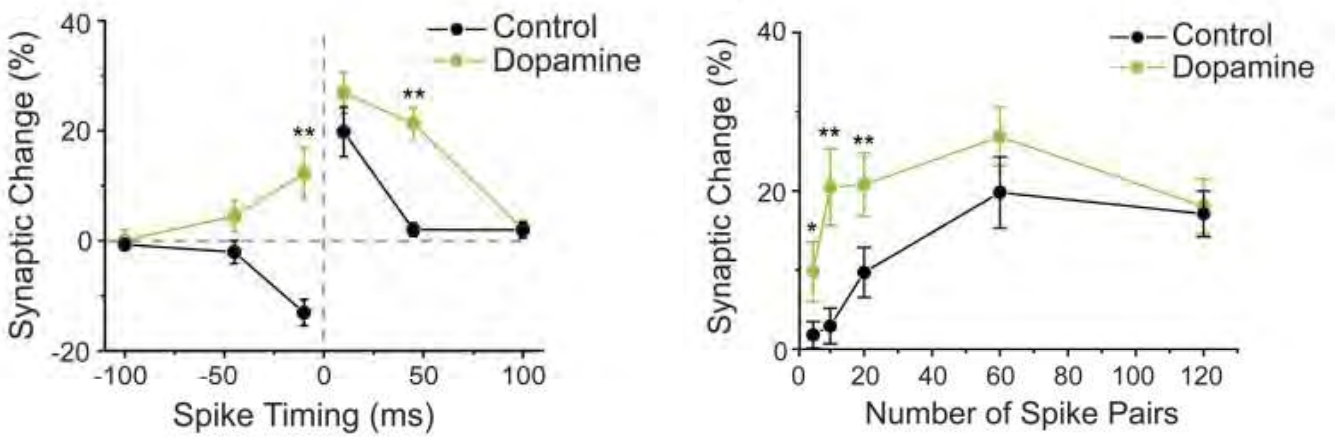

D'après Zhang et al, 2008

B

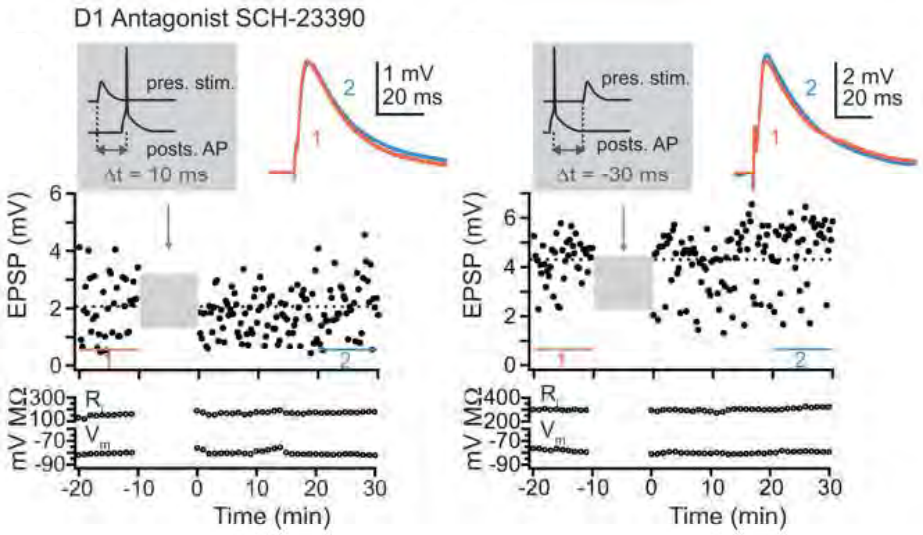

Pawlak and Kerr, 2008

C

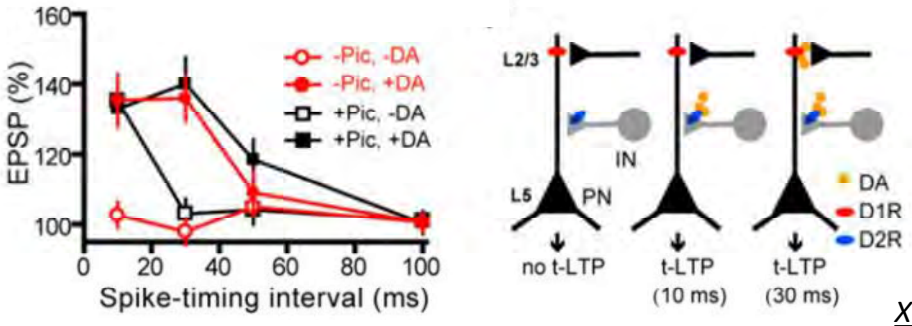

Xu and Yao, 2010

Figure 16. Modulation de la règle de STDP par la dopamine (DA)

A. Dans des neurones dissociés d'hippocampe, l'application de DA augmente l'amplitude de la LTP, augmente la fenêtre temporelle d'induction de la LTP, réduit le nombre d'appariements nécessaires à son induction, et transforme la fenêtre de LTD en LTP.
B. Dans le striatum, le blocage des récepteurs D1 par l'antagoniste SCH-23390 empêche l'induction de la STDP, LTP comme LTD.
C. Dans les neurones pyramidaux de la couche 5 du cortex, les effets de la DA dépendent de l'activation des récepteurs D1 post-synaptiques ainsi que des récepteurs D2 exprimés sur les interneurones pour réduire le tonus inhibiteur.

intracellulaire (Benardo and Prince, 1982; Lezcano and Bergson, 2002), diminution de la conductance des canaux sodiques voltage-dépendants (Cantrell et al., 1997), augmentation ou diminution de l'AHP après un potentiel d'action (Berretta et al., 1990; Gribkoff and Ashe, 1984; Malenka and Nicoll, 1986; Pedarzani and Storm, 1995), augmentation de l'activité des canaux HCN porteurs du courant I_H (Rosenkranz, 2006) et diminution de l'expression des canaux calciques de type T (Bender et al., 2010).

2.1.3.5 Rôle de l'inhibition

Dans certains cas, les effets de la DA passent par une diminution de l'inhibition GABAergique. C'est ainsi que dans le cortex, l'expression d'une STDP conventionnelle en présence de DA nécessite l'activation des récepteurs D2 au niveau des interneurones pour diminuer leur inhibition (Xu and Yao, 2010). De façon similaire, dans l'amygdale l'activation des récepteurs D2 exprimés par les interneurones supprime l'inhibition feed-forward (Bissière et al., 2003). La présence de l'inhibition dans l'étude de l'effet de la DA sur la plasticité synaptique est donc un facteur important, car classiquement, la plupart des études aux synapses excitatrices utilisent des bloqueurs des récepteurs GABAergiques (PiTx, gabazine, bicuculline,…).

2.2 Noradrénaline

La noradrénaline (NA) est aussi un neuromodulateur largement étudié. Elle est impliquée dans les processus d'attention, dans la perception mais aussi dans formation des souvenirs et la capacité à les retrouver (pour revue, Sara, 2009).

2.2.1 Récepteurs

Les récepteurs à la NA se décomposent en 3 familles : α1, α2, et β (β1-3). Les récepteurs α1 sont couplés à une protéine $G\alpha_q$, et stimulent la voie de la phospholipase C et la libération de calcium intracellulaire par la voie de l'IP3. Les récepteurs α2 sont couplés à une protéine $G\alpha_i$,

et inhibent la production d'AMPc, alors les récepteurs β sont couplés à une protéine $G\alpha_s$ qui stimule la production d'AMPc (O'Dell et al., 2015; Ramos and Arnsten, 2007). Notons que les récepteurs α1 ont une affinité plus importante (Ka = 330 nM) pour la NA que les récepteurs β (Ka = 740 nm).

2.2.2 Projections noradrénergiques

Les fibres noradrénergiques émergent du locus coeruleus (LC) et projettent dans de nombreuses régions cérébrales comme l'hippocampe, le cortex visuel, ou l'amygdale.

2.2.3 Effet sur la STDP

2.2.3.1 Activation du récepteur β

Tout comme la DA, la NA a des effets positifs sur l'induction de la LTP, en augmentant son amplitude ou encore sa fenêtre temporelle d'induction. Dans la région CA1 de l'hippocampe, l'activation des récepteurs β par un de leurs agonistes, l'isoprénaline (ISO), augmente la fenêtre temporelle d'induction de la LTP sans changement de l'amplitude de potentialisation (Lin et al., 2003 ; Figure 17A). D'autres études dans l'hippocampe semblent indiquer que la perfusion d'ISO ne permet pas la récupération de la LTP dans des conditions où elle est absente (Edelmann and Lessmann, 2011), contrairement à la couche 2/3 du cortex visuel (**Figure 17B**), où l'application d'ISO permet l'induction d'une LTP robuste (Guo et al., 2012; Seol et al., 2007) pour l'ensemble des délais (positifs et négatifs), abolissant la STDP conventionnelle. Notons qu'à ces synapses, il existe un effet dose-dépendant de la NA. Pour de faibles concentrations, la NA oriente vers la LTD en activant le récepteur α, alors qu'à de fortes concentrations, elle oriente vers la LTP par activation du récepteur β (Salgado et al., 2012).

A

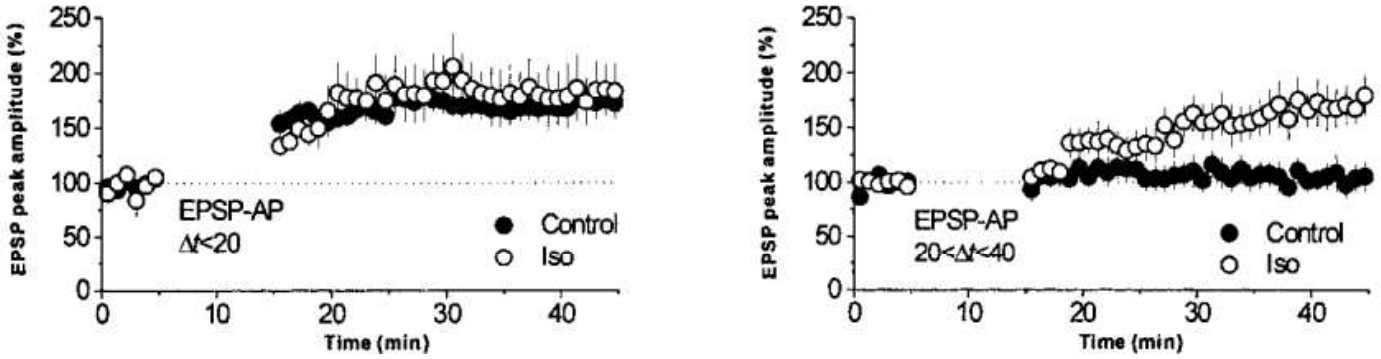

Lin et al, 2003

B

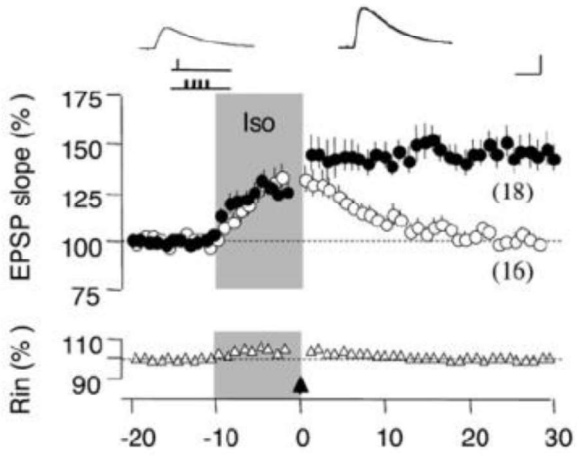

Seol et al, 2007

Figure 17. Modulation de la règle de STDP par la noradrénaline (NA)

A. Dans la région CA1 de l'hippocampe, l'application d'isoprénaline, un agoniste des récepteurs β-adrénergiques, augmente la fenêtre temporelle d'induction de la LTP sans modifier son amplitude. En effet, en présence d'ISO, la LTP est inductible pour des délais supérieurs à 20 ms.
B. Dans la couche 2/3 du cortex visuel, l'application d'isoprénaline permet l'induction d'une LTP robuste (ronds noirs). En l'absence d'ISO, la potentialisation n'est que transitoire (ronds blancs).

2.2.3.2 Coopération des récepteurs α et β

Il est parfois nécessaire que les récepteurs α et β soient co-activés pour obtenir une STDP conventionnelle. C'est le cas dans le cortex visuel, où l'activation de ces deux récepteurs est requise pour une STDP bidirectionnelle aux synapses excitatrices de la couche 2/3, mais aussi aux synapses entre neurones pyramidaux corticaux et interneurones de types fast-spiking ou à somatostatine (Huang et al., 2013, 2014). En effet, l'activation du récepteur α permet l'induction de la LTD, l'activation du récepteur β celle de la LTP et ensemble, les deux fenêtres de plasticité.

2.2.3.3 Mécanismes

Contrairement à la DA, l'effet de la NA sur la règle de STDP est encore peu étudié. Néanmoins, la majorité des effets de l'activation des récepteurs β nécessite l'action de la voie PKA (Lin et al., 2003), ainsi que l'élévation du Ca^{2+} intracellulaire (Seol et al., 2007). De plus, l'activation des récepteurs β est capable d'améliorer la rétro-propagation du potentiel d'action par l'inhibition de canaux potassiques voltage-dépendants, comme les Kv 1.1, Kv 4.2 (I_A) et SK (Faber et al., 2008; Liu et al., 2017; Yuan et al., 2002).

2.3 Acétylcholine

L'acétylcholine (Ach) est impliquée dans la mémoire et l'apprentissage (Blokland, 1995; Drever et al., 2011; Hasselmo, 1999). Dans l'hippocampe en particulier, les apprentissages hippocampo-dépendants augmentent le niveau extracellulaire d'Ach (Stefani and Gold, 2001; Yamamuro et al., 1995), de même que les processus nécessitant l'attention (Blokland, 1995).

2.3.1 Récepteurs

Les récepteurs à l'acétylcholine se décomposent en 2 familles : muscariniques et nicotiniques. On sépare les récepteurs muscariniques, couplés à des protéines G, en deux groupes : M1 (M1, M3 et M5) et M2 (M2 et M4). Les récepteurs M1 sont couplés à une protéine $G\alpha_q$ ou $G\alpha_{11}$, et activent la voie PKC, stimulant la libération de Ca^{2+} des stocks intracellulaires par la

voie IP3/PLC. Les récepteurs M2 sont couplés une protéine $G\alpha_i$ ou $G\alpha_o$ qui inhibent la production d'AMPc, et diminuent l'activité de la PKA (Thiele, 2013). À l'inverse, le récepteur nicotinique (nAchR) est un récepteur-canal cationique (Albuquerque et al., 2009).

2.3.2 Projections cholinergiques

La majorité des neurones cholinergiques sont situés à la base de prosencéphale et projettent vers de nombreuses structures comme l'hippocampe et le cortex. Dans le cortex, les fibres cholinergiques proviennent du septum médial.

2.3.3 Effet sur la STDP

2.3.3.1 Récepteurs muscariniques

Les résultats concernant le rôle des récepteurs muscariniques sur la STDP sont divers, et peuvent aussi bien favoriser l'induction de la LTP que celle de la LTD. Dans l'hippocampe, aux synapses CA3-CA1, l'application d'acétylcholine transforme la STDP conventionnelle en STDP non-conventionnelle présentant une unique fenêtre de dépression pour l'ensemble des délais étudiés (Brzosko et al., 2017 ; Figure 18A). À l'inverse, d'autres études dans la même région montre une facilitation de la LTP en présence d'ésérine **(Figure 18B)**, un inhibiteur de l'enzyme de dégradation de l'Ach (Sugisaki et al., 2011, 2016). De plus, il existe un effet dose-dépendant de l'Ach. Pour des concentrations intermédiaires, la STDP présente une unique fenêtre de potentialisation, et pour des concentrations extrêmes, la plasticité devient totalement absente (Sugizaki et al., 2011). Néanmoins, la plupart de ces études ne font pas de distinction entre les sous-types de récepteurs (M1 ou M2). Une étude au niveau de l'hippocampe montre que l'action des récepteurs M1 post-synaptiques est responsable d'une augmentation de l'amplitude de la LTP, qui disparaît chez les souris KO pour ces récepteurs (Shinoe, 2005).

2.3.3.2 Récepteurs nicotiniques

Dans les neurones pyramidaux de la couche V du cortex préfrontal, l'activation des récepteurs nicotiniques à l'acétylcholine (nAchR), augmente le seuil de LTP mais peut, à plus forte concentration, transformer la fenêtre de LTP en LTD (Couey et al., 2007). Néanmoins, l'augmentation du nombre de potentiels d'action post-synaptiques permet de retrouver la LTP. Dans ce cas, l'effet de l'Ach est dû à une augmentation de la transmission inhibitrice des interneurones.

2.3.3.3 Coopération avec d'autres neuromodulateurs

Dans le cortex visuel, l'Ach permet d'obtenir une règle de STDP bidirectionnelle, mais aussi de retrouver une fenêtre de LTD via l'activation des récepteurs M1 et en coopération avec l'activation des récepteurs β-adrénergiques par la NA (Seol et al., 2007). De la même manière, dans l'hippocampe, la co-activation des récepteurs à l'Ach et à la DA permet de retrouver une STDP conventionnelle (Brzosko et al., 2017).

2.3.3.4 Rôle de l'inhibition

Tout comme la DA, l'inhibition est à prendre en compte dans l'étude des effets de l'Ach sur la règle de STDP. Comme nous l'avons vu, certains effets sont médiés par une augmentation de la transmission inhibitrice (Couey et al., 2007). De la même manière, dans l'hippocampe, les effets de l'Ach sont en partie médiés par les interneurones, où l'activation des récepteurs muscariniques augmente le seuil d'induction de la LTP (Sugizaki et al., 2016).

2.3.3.5 Mécanismes

Tout comme la NA, des études supplémentaires sont requises pour comprendre les effets biologiques de l'Ach dans la modulation de la règle de STDP. On sait que les récepteurs M1 peuvent faciliter la rétro-propagation du potentiel d'action par l'inhibition des canaux

A

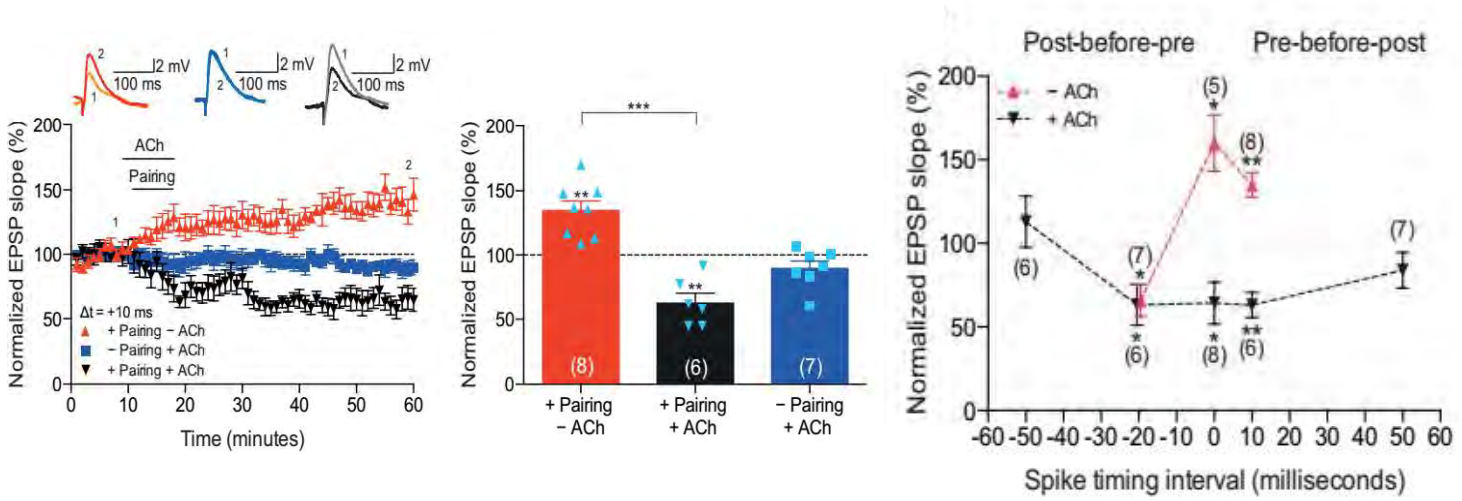

Brzosko et al, 2017

B

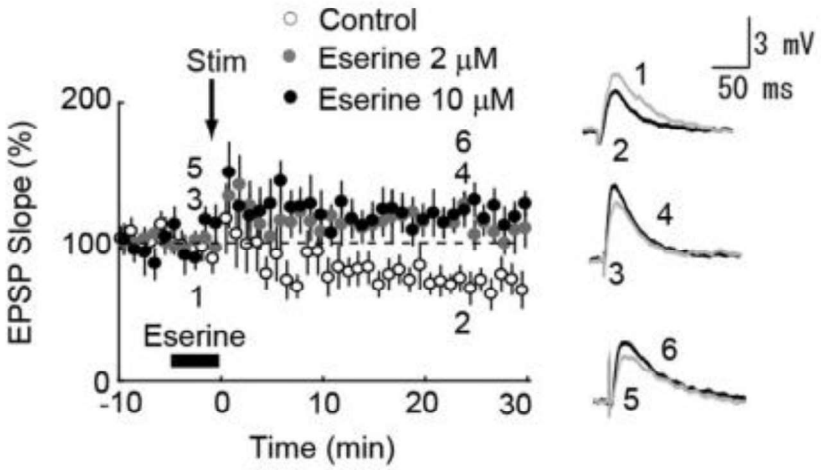

Sugizaki et al, 2011

Figure 18. Modulation de la règle de STDP par l'acétylcholine (Ach)

A. Dans la région CA1 de l'hippocampe, la perfusion d'Ach induit une STDP non-conventionnelle présentant une unique fenêtre de LTD pour l'ensemble des délais. Pour un délai de +10 ms, qui induit de la LTP (trace rouge), la présence d'Ach transforme la LTP en LTD (trace noire).
B. Dans la région CA1, la perfusion d'eserine, un inhibiteur de l'enzyme de dégradation de l'Ach, facilite l'induction de la LTP. Pour un délai de + 22 ms, de la LTD est induite en condition contrôle (ronds blancs) alors que de la LTP est induite en présence d'eserine (traces grises et noires).

calciques voltage-dépendants Kv7 (Petrovic et al., 2012), Kv 4.2 (Losonczy et al., 2008), et SK (Giessel and Sabatini, 2010). Néanmoins, la plupart des effets de l'activation des récepteurs muscariniques nécessitent l'activation de l'adénylate cyclase (Brzosko et al., 2017).

2.4 Neuromodulation et timing

La règle de STDP dépend étroitement du timing de l'activité pré- et post-synaptique. Si la neuromodulation est vue comme un troisième facteur permettant de promouvoir la STDP, la question du timing doit alors être aussi posée. Quand le signal de neuromodulation doit-il arriver afin de permettre à la synapse considérée de potentialiser ou déprimer ? Plusieurs hypothèses sont possibles : 1) le signal doit arriver avant l'activité pour permettre à la synapse d'être dans un «état» de plasticité, 2) le signal arrive après l'activité lorsque la synapse est dans un «état» permettant une plasticité. Quelques réponses sont apportées par des études perfusant le neuromodulateur après le protocole d'appariement, et qui permet dans une fenêtre relativement courte l'induction de la LTP dans l'hippocampe et le cortex (Brzosko et al., 2017; He et al., 2015).

2.5 Conclusion

Les neuromodulateurs peuvent drastiquement modifier la plasticité synaptique par la règle de STDP. Dans un cas, ils peuvent être nécessaires pour la plasticité et dans un autre, ils peuvent moduler plus finement la plasticité en augmentant ou abaissant le seuil de LTP et/ou LTD.

La règle de STDP *in vivo*

Les premières études sur la STDP ont été réalisées principalement *in vitro*, néanmoins de plus en plus de travaux s'attachent à retrouver et comprendre ses règles *in vivo*. Contrairement aux études *in vitro*, majoritairement sur tranches aigües ou cultures neuronales, l'expérimentation *in vivo* apporte d'autres contraintes qui pourraient limiter l'induction de la plasticité synaptique par STDP. En effet, la forte activité synaptique mesurée *in vivo* (excitatrice et inhibitrice) pourrait limiter le timing nécessaire à l'induction de la STDP ou la rétro-propagation du potentiel d'action, cruciale dans certains cas. De plus, la neuromodulation, contrôlée par l'expérimentateur *in vitro*, pourrait influencer fortement l'induction de LTP ou LTD *in vivo*. Plusieurs types d'expériences ont été réalisés pour tenter de reproduire la règle de STDP *in vivo*. Dans les études *in vitro,* l'activité pré- et post-synaptique est contrôlée directement par l'injection d'un courant dépolarisant ou par une électrode de stimulation extracellulaire, plusieurs protocoles différents sont retrouvés *in vivo* pour induire cette activité pré- et post-synaptique, que cela soit par stimulation électrique ou par des stimuli sensoriels (visuels, moteurs…). Néanmoins, quel que soit le protocole utilisé, de nombreuses études retrouvent une règle de plasticité dépendante du timing de l'activité pré- et post-synaptique qui rappelle fortement celle de STDP.

1. Diversité des études et protocoles

1.1 Avec stimulation électrique

Plusieurs études *in vivo* conservent l'injection d'un courant dépolarisant dans le neurone post-synaptique couplé à une activité pré-synaptique induite de manière électriques ou par stimulation sensorielle. La première étude prouvant l'existence d'une règle temporelle de plasticité a été réalisée dans le système rétino-tectal de la Xénope (Zhang et al., 1998). Il est possible d'observer de la LTP et de la LTD selon la règle temporelle de STDP

A

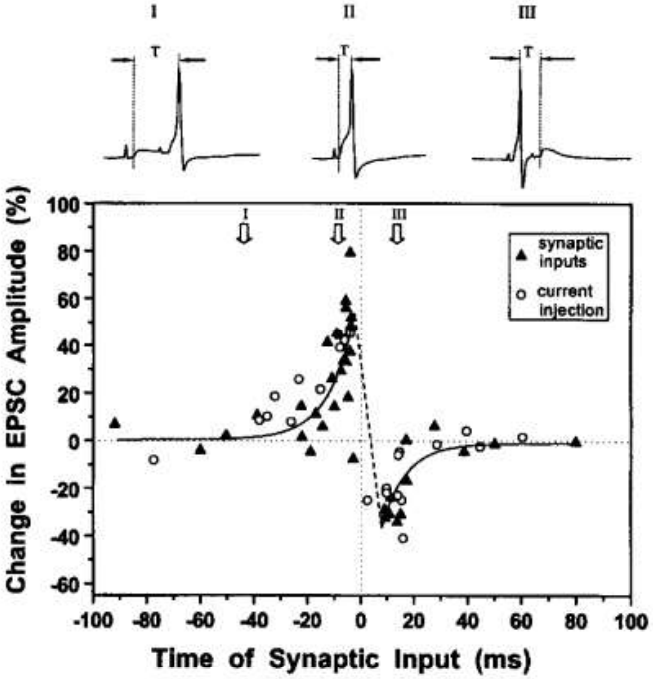

Zhang et al, 1998

B

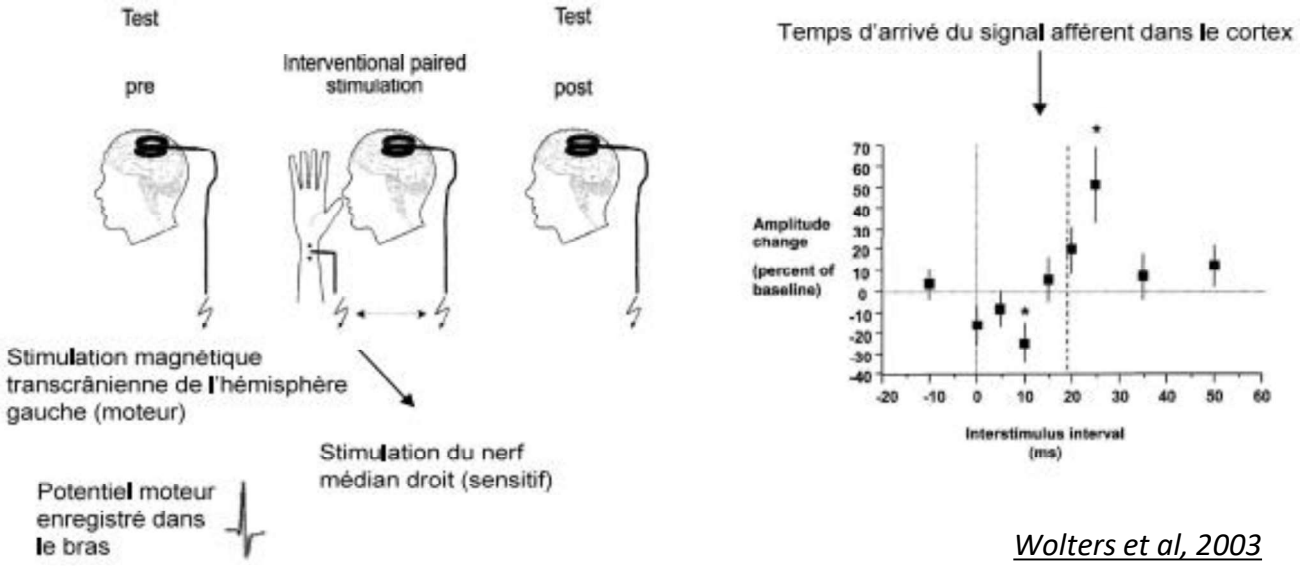

Wolters et al, 2003

Figure 19. La règle de STDP *in vivo*

A. On retrouve une règle de STDP classique dans le système visuel de Xénope : lorsque l'activité pré-synaptique arrive avant l'activité post-synaptique (I, II), on retrouve de la LTP, alors que lorsque l'activité post-synaptique arrive après (III), on retrouve de la LTD.
B. Chez l'homme, une règle de plasticité temporelle semblable à la STDP est retrouvée avec la stimulation du cortex moteur par TMS (pre) et d'un nerf périphérique (post). L'orientation des changements dans le potentiel moteur dépend du timing entre ces deux stimulations.

conventionnelle lorsque l'activité pré-synaptique est induite par stimulation électrique ou présentation d'un stimulus visuel espacé de ± 20ms avec l'activité post-synaptique **(Figure 19A)**. Les mêmes résultats sont retrouvés dans le cortex visuel, où une dépolarisation post-synaptique est couplée à la présentation d'un stimulus visuel, induisant potentialisation ou dépression en fonction de l'ordre de présentation (Meliza and Dan, 2006). On retrouve aussi une LTD dépendante du timing dans le cortex somato-sensoriel (S1) chez le rat anesthésié, où la stimulation d'une moustache, correspondant à l'activité pré-synaptique, précédée (17-33 ms) d'un potentiel d'action post-synaptique induit une dépression du potentiel post-synaptique (Jacob et al., 2007). Dans le cortex visuel de chaton, il est possible d'induire une plasticité des cartes visuelles en variant le timing entre les stimuli visuel et électrique dans le cortex, où l'on observe une augmentation ou une diminution de la réponse corticale suivant les mêmes règles temporelles que la STDP (Schuett et al., 2001). Ces expériences s'inspirent de celles réalisées par l'équipe de Y. Frégnac qui associaient un stimulus avec un niveau de décharge renforcé ou atténué selon le cas (Bringuier et al., 1992; Debanne et al., 1998b; Frégnac et al., 1988; Shulz and Frégnac, 1992). Enfin, on retrouve aussi une règle de plasticité temporelle chez l'homme de façon non-invasive grâce à la stimulation magnétique transcrânienne (TMS) pour stimuler le cortex moteur (pré) en association avec une stimulation nerveuse périphérique (post). L'orientation des changements dans le potentiel moteur dépend du timing entre ces deux stimulations **(Figure 19B)**, et permet d'obtenir une règle de plasticité temporelle (Stefan, 2000; Stefan et al., 2002; Wolters et al., 2003).

1.2 Avec stimulation sensorielle uniquement

Les études *in vivo* utilisant une injection de courant dans le neurone post-synaptique permettent un contrôle important du délai du potentiel d'action. Néanmoins, il est possible de retrouver des règles de plasticité dépendant des interactions temporelles avec uniquement des stimuli sensoriels (visuels, moteurs). Dans le cortex visuel du chat adulte, en l'absence de

A

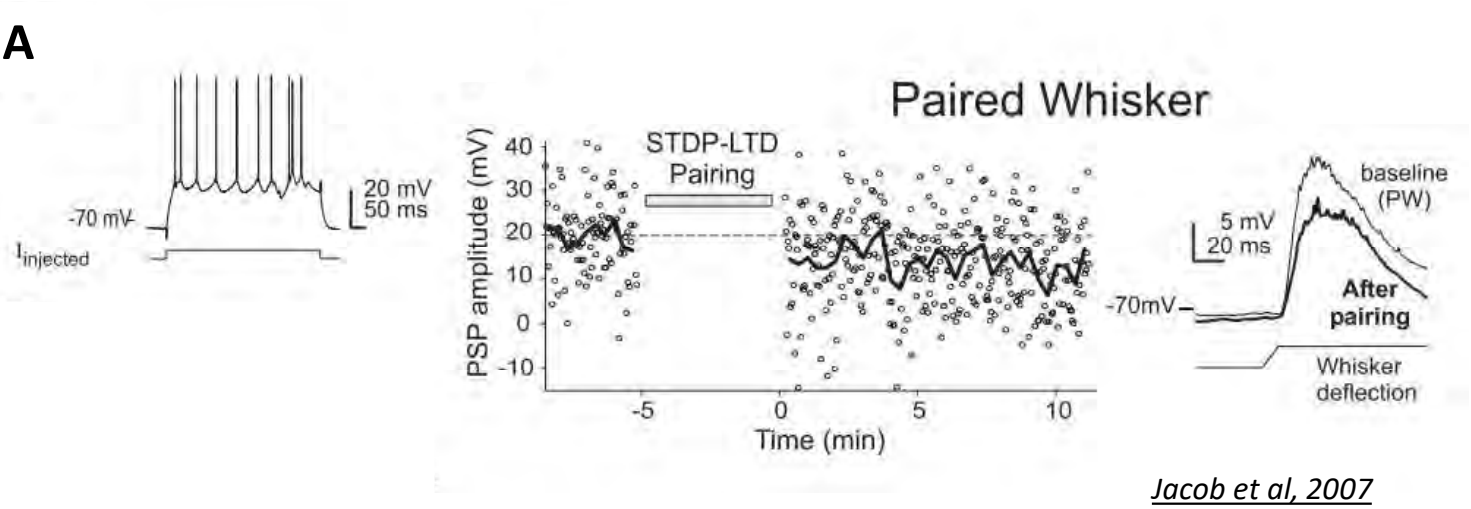

Jacob et al, 2007

B

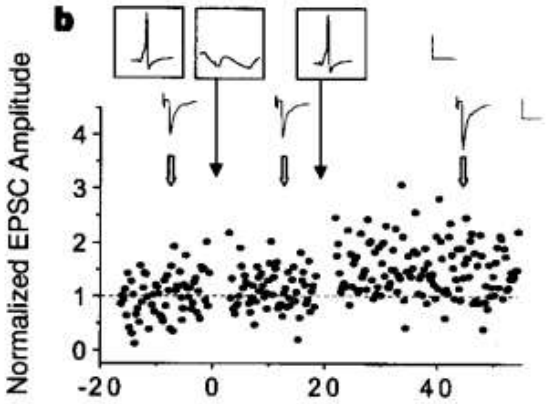

Zhang et al, 1998

Figure 20. Différence entre *in vivo* et *in vitro*

A. Il est possible d'induire une LTD dans le cortex en couplant une stimulation post-synaptique avec la déflection d'une moustache comme stimulation pré-synaptique, mais elle disparaît rapidement au bout de quelques minutes (5 – 10 minutes).
B. L'injection de courant hyperpolarisant de 25 mV pendant l'appariement bloque l'induction de la potentialisation. En l'absence d'hyperpolarisation, une potentialisation est induite.

toute stimulation électrique mais par la présentation de deux stimulations visuelles à intervalle régulier (40 ms), on peut observer une préférence vers l'un ou l'autre des stimuli en fonction de l'ordre de présentation (Yao and Dan, 2001). Ces résultats peuvent se retrouver dans un modèle incorporant la règle de STDP (Yao et al., 2004). Les mêmes observations se retrouvent dans le cortex visuel du chat adulte avec des signaux visuels en mouvement (plus physiologique), où le déplacement des champs réceptifs en opposition avec le mouvement des signaux visuels peut être prédit par un modèle incorporant la règle de STDP (Fu, 2004). Enfin, dans l'hippocampe, on retrouve une asymétrie des champs de lieu suite à l'exploration répétée de l'animal (Mehta et al., 2000). Ce développement de l'asymétrie peut être très simplement retrouvé dans un modèle incorporant la règle de STDP (Abbott et Blum, 1996). Enfin, on retrouve aussi la STDP chez les invertébrés. Des expériences chez le criquet ont montré qu'il est possible d'induire de la STDP conventionnelle dans le circuit olfactif en couplant une stimulation post-synaptique avec une stimulation pré-synaptique sous la forme de présentation d'une odeur dans une fenêtre de ± 25 ms (Cassenaer and Laurent, 2007, 2012).

2. Mécanismes

L'induction de la plasticité de la STDP conventionnelle repose essentiellement sur le récepteur NMDA post-synaptique. Cela semble aussi être le cas dans certaines études citées précédemment, où la potentialisation et la dépression sont abolies par la perfusion d'un bloqueur des récepteurs NMDA (Stefan et al., 2002; Wolters et al., 2003; Zhang et al., 1998). Notons que le blocage des VDCC prévient aussi l'induction de la dépression dans les expériences chez l'homme (Wolters et al., 2003). Il semble donc que les règles d'induction décrites *in vitro* se retrouvent aussi in *vivo*.

3. Différence entre *in vivo* et *in vitro*

3.1 Conséquence de l'activité spontanée

L'une des principales objections à l'existence de la STDP *in vivo* est la forte activité spontanée (inhibitrice et excitatrice) présente, contrairement aux études *in vitro* (Spruston, 2008). En effet, cela pourrait être un frein important à l'induction de la STDP avec les règles qu'on lui connaît (dépendance du timing, rôle de la rétropropagation). Cette objection se retrouve dans certaines études théoriques (Higgins et al., 2014). En effet, il est possible d'abolir les changements observés en présence d'une forte activité spontanée, d'une hyperpolarisation **(Figure 20B)**, ou de stimuli visuels (Zhang et al., 1998). De plus, les changements observés sont parfois de court terme. Contrairement à l'induction de la LTD *in vitro*, la LTD induite *in vivo* disparaît rapidement (entre 5 et 10 minutes) après le protocole d'induction (Jacob et al., 2007). La forte activité spontanée pourrait expliquer la disparition rapide de la LTD **(Figure 20A).**

3.2 Différences d'induction

Il semble parfois très difficile d'induire de la LTP, dont l'induction semble très aléatoire dans le cortex somato-sensoriel (Jacob et al., 2007). Néanmoins, dans le cortex visuel du chat, l'utilisation d'une fréquence d'appariement plus importante couplée à des potentiels d'action en bouffées dans le neurone post-synaptique est un moyen d'induire la LTP (Frégnac et al., 2010). Il semble donc qu'il ne soit pas forcément possible d'appliquer les mêmes protocoles *in vitro* et *in vivo*.

4. Conclusion

Bien qu'il soit parfois plus difficile d'induire de la plasticité *in vivo*, en particulier la LTP dans certains cas, on retrouve la règle de STDP dans de nombreuses conditions

expérimentales. Néanmoins, de nombreuses questions restent en suspens quant aux effets de la neuromodulation, difficiles à contrôler dans des conditions *in vivo*.

Le problème du calcium extracellulaire

Plusieurs objections ont été émises à l'encontre de l'existence de la règle de STDP. Malgré ces objections, nous avons vu que plusieurs études avaient pu induire de la plasticité synaptique par la règle de STDP en conditions physiologiques (*in vivo*). Néanmoins, un facteur important et pourtant rarement soulevé est le calcium extracellulaire. La STDP dépend étroitement de l'entrée de calcium dans le neurone post-synaptique, mais une différence majeure entre les études *in vivo* et *in vitro* est la concentration de calcium extracellulaire.

1. Rôle du calcium extracellulaire

1.1 Choisir la bonne concentration

La plupart des études, si ce n'est toutes, utilisent une concentration de calcium extracellulaire comprise entre 2 et 3 mM, or la concentration de calcium extracellulaire mesurée *in vivo* est comprise entre 1.3 et 1.8 mM, avec une valeur moyenne autour de 1.5 si l'on en croit la littérature. Globalement, l'ensemble des études pointe vers une concentration 1.2 à 2.3 fois inférieure à celles utilisées dans la majorité des études *in vitro*. Les différences de mesures entre les études s'expliquent par le modèle animal utilisé (singe, rat), la technique de calibration de la sonde, ainsi que la température (ambiante *vs* physiologique).

Référence	Concentration de calcium	Animal
Wong and Bradbury, Brain Research, 1975	1.3 – 1.4 mM	Rat (adulte)
Nicholson et al., PNAS, 1977	1 - 1.2 mM	Rat (adulte)
Heinemann et al., Exp. Brain Res., 1977	1.28 mM	Rat (adulte)
Harris et al., J. Cereb. Blood. Flow Metab., 1981	1.3 mM	Babouin
Jones and Keep, J Physiol., 1988	1.1 – 1.67 mM	Rat (adulte et jeune)

Silver and Erecinska, J Gen Physiol., 1990	1.49 – 1.56 mM	Rat (adulte)
Ding et al., Science, 2016	1.25 – 1.5 mM	Souris (8–12 semaines)

Tableau 1. Mesure du calcium extracellulaire dans le liquide cérébro-spinal

1.2 Les raisons derrière l'utilisation d'une concentration plus élevée

L'utilisation d'une concentration plus importante dans les précédentes études s'explique simplement par le besoin d'induire plus facilement de la LTP, mais aussi par les nombreuses études en paires de neurones CA3-CA3 ou L5-L5 qui permettaient d'obtenir des connexions de taille plus importante. Il reste à savoir si l'utilisation de ces concentrations ~2 fois supérieures pourrait modifier la règle de STDP. Or, en l'absence d'études expérimentales il faut se tourner vers les études théoriques.

Référence	**Concentration de calcium**	**Animal**
Debanne et al., 1994	2.8 mM	Rat (tranches en culture)
Bi and Poo., 1998	3 mM	Rat (cultures dissociées)
Markram et al., 1997	2 mM	Rat (14 – 16 jours)
Nishiyama et al., 2000	2 ou 2.6 mM	Souris ou Rat (26 – 33 jours)
Sjöström et al., 2001	2.5 mM	Rat (12 – 21 jours)
Froemke et al., 2006	2.5 mM	Rat (10 – 35 jours)
Witternberg and Wang., 2006	2 mM	Rat (14 – 21 jours)
Campanac and Debanne., 2008	3 mM	Rat (14 – 21 jours)

Pawlak and Kerr, 2008	2.5 mM	Rat (19 – 22 jours)

Tableau 2. Concentration de calcium extracellulaire utilisée dans les principales études sur la STDP

1.3 Apport de la modélisation

Les études concernant l'effet du calcium extracellulaire sur la règle de STDP sont absentes. Pour savoir si l'utilisation d'une concentration non-physiologique de calcium pourrait modifier la plasticité de sortie induite par STDP, il est nécessaire de se tourner vers des études théoriques qui se sont intéressées à ce problème.

1.3.1 Des effets importants sur la plasticité synaptique

Les travaux de Graupner et Brunel (2012) sont les premiers à étudier le rôle du calcium extracellulaire dans la STDP. Dans le modèle de STDP développé, la plasticité de sortie dépend de l'influx de calcium post-synaptique. On retrouve deux seuils de plasticité au sein du modèle, θ_p et θ_d, respectivement le seuil pour la potentialisation, et le seuil pour la dépression. Le calcium post-synaptique provient de deux sources : les récepteurs NMDA (Cpre), et les canaux calciques voltage-dépendants (Cpost). Pour différents protocoles, et en faisant varier l'entrée de calcium en modifiant les valeurs de Cpre et Cpost, il est possible d'obtenir une multitude de courbes de STDP : conventionnelle, non-conventionnelle, ou encore une absence totale de plasticité.

Pour des valeurs de calcium physiologiques, le modèle de Graupner et Brunel prévoit une absence de potentialisation ou une absence totale de plasticité. Cette étude semble donc indiquer que la diminution du calcium extracellulaire pour des valeurs physiologiques pourrait influencer grandement la plasticité de sortie vers une règle de STDP différente.

1.3.2 Effet du calcium extracellulaire sur le réseau

Dans une précédente étude théorique (Higgins et al., 2014), le rôle du calcium extracellulaire avait été soulevé pour une autre raison. L'étude de Higgins montre que de faibles concentrations de calcium peuvent aussi avoir d'importants effets sur la plasticité. Dans leurs modèles corticaux, ils prévoient qu'une concentration de 2.5 mM de calcium est synonyme d'une disparition des changements synaptiques au bout de quelques minutes, alors qu'une concentration de 1.5 mM de calcium permet de garder l'information pendant environ une heure. Or, comme nous l'avons décrit précédemment, l'une des critiques principales de la règle de STDP *in vivo* est sa sensibilité à l'activité spontanée (Zhang et al., 1998). Il est fort possible qu'elle limite la durée de la plasticité induite à quelques minutes (Jacob et al., 2007) malgré les conditions, par définition, physiologiques. Cela illustre la probable nécessité de prendre en compte d'autres facteurs, comme la neuromodulation ou des patrons d'activités spécifiques.

2. Conclusion

Il semble donc, selon les modèles de STDP basés sur le calcium, que la concentration extracellulaire puisse grandement influencer la plasticité synaptique. Néanmoins, aucune étude expérimentale n'a pour l'instant étudié les effets d'une concentration de calcium extracellulaire physiologique.

A

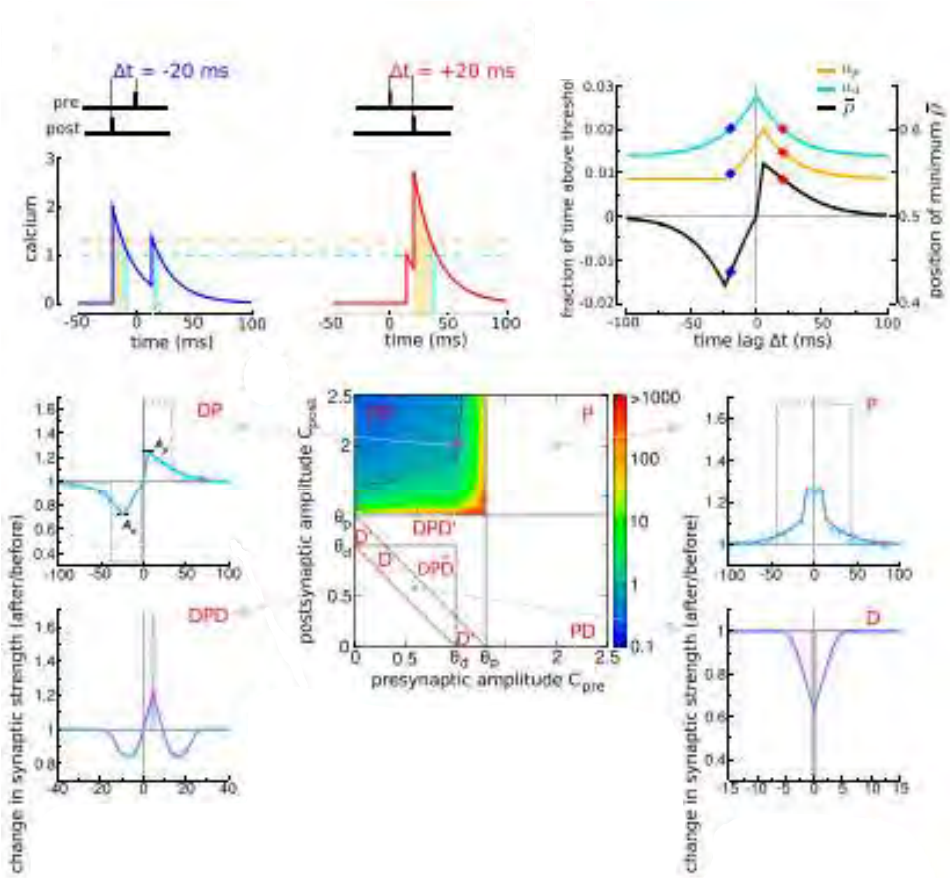

Graupner et Brunel, 2012

B

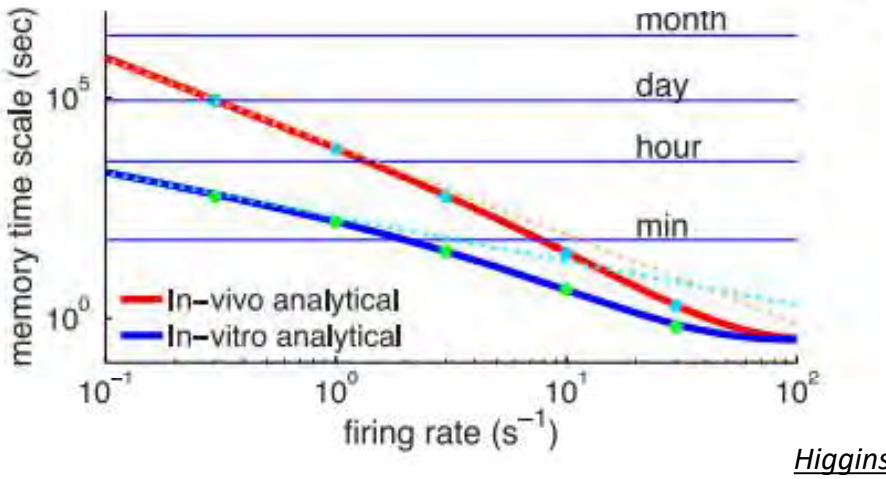

Higgins et al, 2014

Figure 21. Rôle du calcium extracellulaire et apport de la modélisation

A. Dans un modèle de STDP basé sur le calcium, la variation du calcium extracellulaire via la modification des paramètres Cpre et Cpost, qui représentent respectivement l'entrée de calcium par les récepteurs NMDA et VDCC, permet d'obtenir une multitude de courbes de STDP : classique (DP ou DPD), non-conventionnelle (D, D' ou P), voire une absence totale de plasticité.
B. Dans un modèle de réseau, l'utilisation de paramètres *in vivo* (rouge) permet de retenir l'information plus longuement en présence d'une forte activité spontanée. En particulier, les paramètres *in vivo* utilisent un faible calcium extracellulaire.

Problématique

L'utilisation de concentrations de calcium extracellulaire ~2 fois plus importantes que les concentrations physiologiques (voir Tableaux 1 et 2) pourrait amener à une surestimation de la plasticité en réponse aux protocoles classiques d'induction de la STDP à faible fréquence avec un seul potentiel d'action post-synaptique (Graupner and Brunel, 2012). Si la diminution des concentrations extracellulaires de calcium oriente la règle de STDP vers une absence de LTP ou de plasticité, nous savons que plusieurs études *in vivo* ont mis en évidence l'existence de LTP par STDP et par définition, dans des conditions physiologiques. Il serait donc tout à fait envisageable de récupérer la courbe conventionnelle de STDP (une fenêtre de LTD, une fenêtre de LTP) en jouant sur les facteurs d'induction de la STDP : activité (fréquence, nombre de potentiels d'action post-synaptiques) ou neuromodulation (dopamine, noradrénaline, acétylcholine).

Nous avons étudié la règle de STDP dans l'hippocampe entre les synapses CA3-CA1 dans des conditions physiologiques : calcium extracellulaire, sans blocage de l'inhibition et sans chélateur calcique dans la solution de patch. Après établissement des courbes de STDP pour différentes concentrations de calcium extracellulaire (physiologiques ou non), nous avons tenté de récupérer la fenêtre de LTP, et la fenêtre de LTD le cas échéant. En parallèle, dans le cadre d'une collaboration avec le groupe de Nicolas Brunel, nous avons développé un modèle mathématique de STDP basé sur le calcium post-synaptique, qui permettra dans l'avenir de mieux connaître les règles de plasticité en réponse à des variations de protocoles et de calcium extracellulaire.

Notre étude devrait permettre de mieux comprendre et cerner les règles de plasticité dans des conditions plus proches de la physiologie.

Matériels et Méthodes

1. Tranches aigües d'hippocampe de rat

Les tranches aigües d'hippocampe proviennent d'animaux âgés entre 14 et 20 jours. Les animaux sont profondément anesthésiés avec de l'hydrate de chloral par injection intra-péritonéale (400mg/kg) puis tués par décapitation. Des tranches de 350 µm sont réalisées dans une solution de coupe NMDG (concentration en mM : 92 NMDG, 2.5 KCl, 1.2 NaH_2PO_4, 30 $NaHCO_3$, 20 HEPES, 25 Glucose, 5 Sodium Ascorbate, 2 Thiouurea, 3 Sodium Pyruvate, 10 $MgCl_2$, 0.5 $CaCl_2$) à l'aide d'un vibratome (Leica VT1200S). Les tranches sont transférées pendant dans 30 minutes dans une solution de NMDG à 32° avant de reposer pendant 1 heure à température ambiante dans une solution artificielle de liquide cérébro-spinal (aCSF) oxygénée (95% O_2/5% CO_2). La composition de l'aCSF est la suivante (en mM) : 125 NaCl, 2.5 KCl, 0.8 NaH_2PO_4, 26 $NaHCO_3$, x $CaCl_2$, x $MgCl_2$ et 10 Glucose). Le ratio entre la concentration de calcium et magnésium est maintenu constant dans les différentes conditions expérimentales pour stabiliser la probabilité de relargage pré-synaptique. Les concentrations de calcium dans nos expériences étaient les suivantes : 3 mM Ca^{2+} / 2 mM Mg^{2+} ; 1.8 mM Ca^{2+} / 1.2 mM Mg^{2+} ; 1.3 mM Ca^{2+} / 0.9 mM Mg^{2+}. Pour l'enregistrement, les tranches sont transférées dans une chambre perfusée avec de l'aCSF dont la température est contrôlée et fixée à 30°C.

2. Electrophysiologie

Les neurones sont identifiés à l'aide un microscope Olympus BX 50WI avec un objectif 60x. Des neurones pyramidaux CA1 sont enregistrés en configuration cellule entière avec des pipettes contenant une solution intracellulaire de la composition suivante (en mM) : 120 K-Gluconate, 20 KCl, 10 HEPES, 2 $MgCl_2.6H_2O$ et 2 Na_2ATP. Les pipettes de stimulation extracellulaire sont remplies de solution saline (NaCl) et placées dans le *stratum radiatum*

pour stimuler les collatérales de Schaeffer. Les potentiels post-synaptiques excitateurs (PPSEs) sont évoqués à la fréquence de 0.1 Hz à l'aide un boîtier de stimulation digital (A385, World Precision Instruments). La résistance d'accès (RA) est enregistrée pendant l'ensemble de l'enregistrement et uniquement les enregistrements avec une RA stable sont conservés (changement < 20%).

3. Acquisition et analyse

Les enregistrements ont été obtenus à l'aide d'un amplificateur Multiclamp 700B (Molecular Devices) et du logiciel pClamp 10.4. Les données sont acquises à la fréquence de 10 kHz, filtrées à 3 kHz, et digitalisées grâce à une Digidata 1440A (Molecular Devices). Toutes les données ont été analysées par un logiciel maison écrit sur Igor Pro 6 (Wavemetrics). La pente des PPSEs mesurée sur les premières millisecondes sert de mesure pour la force des changements synaptiques. Les données sont représentées comme la moyenne +/- S.E.M. Les comparaisons statistiques ont été faites en utilisant le test de Wilcoxon ou Mann-Whitney de manière appropriée sur le logiciel Sigma Plot. La signification est considérée lorsque $p < 0.05$.

4. Induction de la STDP

Après l'enregistrement d'une ligne de base pendant une période d'au moins 10 à 15 minutes, un PPSE est couplé avec un protocole de STDP, avec 100 répétitions pour la LTP et 150 répétitions pour la LTD. Le nombre de potentiels d'action ainsi que la fréquence de d'appariement sont ajustés en fonction de l'expérience. La pente du PPSE est enregistrée au moins 20 minutes avant chaque appariement. Les valeurs de changements synaptiques sont mesurées sur les 10-15 dernières minutes de l'enregistrement.

5. Drogues

Toutes les drogues utilisées (dopamine hydrochloride, isoprénaline, d-AP5) ont été achetées chez Sigma Aldrich.

6. Imagerie calcique

Les neurones pyramidaux CA1 ont été imagés à l'aide d'un microscope confocal. Les neurones ont été remplis d'Oregon Green 488 BAPTA-1 (OGB-1 ; 50 µM). La fluorescence d'OGB-1 a été utilisée pour révéler la morphologie neuronale ainsi que pour l'imagerie calcique. La source laser pour l'excitation par fluorescence a été réglée à 494 nm et l'émission récupérée à 523 nm. La pipette de stimulation extracellulaire a été placée à proximité d'une épine identifiée visuellement. Les signaux de fluorescence OGB-1 acquis ont été convertis en valeurs $\Delta F/F$. L'amplitude maximale et le temps de décroissance des signaux Ca^{2+} ont été calculés à l'aide d'un programme d'analyse personnalisé écrit dans LabView.

Résultats

1. Spike timing dependent plasticity rules in physiological calcium

Yanis Inglebert, Johnatan Aljadeff, Nicolas Brunel, Dominique Debanne

En préparation

Abstract

Like many forms of long-term synaptic plasticity, spike-timing-dependent plasticity (STDP) depends on intracellular Ca2+ signaling for its induction. Yet, all in vitro studies devoted to STDP used abnormally high external Ca2+ concentration. We measured STDP at the CA3-CA1 hippocampal synapse under different extracellular Ca2+ concentrations and found that the sign, shape and magnitude of plasticity strongly depend on Ca2+. A pre-post protocol that results in robust LTP in high Ca2+, yielded only LTD or no plasticity in the physiological Ca2+ range. LTP could be restored by either increasing the number of post-synaptic spikes or increasing the pairing frequency. A calcium-based plasticity model in which depression and potentiation depend on postsynaptic Ca2+ transients was found to fit quantitatively all the data, provided. NMDA receptor-mediated non-linearities and short-term facilitation were implemented. In conclusion, STDP rule is profoundly altered in physiological Ca2+ but specific activity regimes restore a classical STDP profile.

Nature Neuroscience

Spike timing dependent plasticity rules in physiological calcium

Yanis Inglebert[1,4], Johnatan Aljadeff[2,3,4], Nicolas Brunel[2,3], Dominique Debanne[1]

[1] UNIS, INSERM Aix-Marseille Université, Marseille France

[2] University of Chicago, USA

[3] Duke University, USA

[4] these authors contributed equally to the work

Corresponding authors: dominique.debanne@inserm.fr or nicolas.brunel@duke.edu

Key words: STDP, synaptic plasticity, hippocampus, computational model, bistable synapse

29 pages, 6 figures, 15 supplementary figures, 6 tables

Abstract (150 max for Neuron & Nat Neurosci)

Like many forms of long-term synaptic plasticity, spike-timing-dependent plasticity (STDP) depends on intracellular Ca^{2+} signaling for its induction. Yet, all *in vitro* studies devoted to STDP used abnormally high external Ca^{2+} concentration. We measured STDP at the CA3-CA1 hippocampal synapse under different extracellular Ca^{2+} concentrations and found that the sign, shape and magnitude of plasticity strongly depend on Ca^{2+}. A pre-post protocol that results in robust LTP in high Ca^{2+}, yielded only LTD or no plasticity in the physiological Ca^{2+} range. LTP could be restored by either increasing the number of post-synaptic spikes or increasing the pairing frequency. A calcium-based plasticity model in which depression and potentiation depend on postsynaptic Ca^{2+} transients was found to fit quantitatively all the data, provided. NMDA receptor-mediated non-linearities and short-term facilitation were implemented. In conclusion, STDP rule is profoundly altered in physiological Ca^{2+} but specific activity regimes restore a classical STDP profile.

Introduction

Spike-timing-dependent plasticity (STDP) is a form of synaptic modification that is controlled by the relative timing between pre- and post-synaptic activity and depends on intracellular Ca^{2+} signaling (review in [1, 2]). Timing-dependent long-term synaptic potentiation (t-LTP) is induced when synaptic activity is followed by one or more backpropagating action potentials in the postsynaptic cell [3-8]. It involves post-synaptic Ca^{2+} influx through NMDA receptors that in turn activates protein kinases [3, 6, 8, 9]. Timing-dependent long-term synaptic depression (t-LTD) is expressed when synaptic activity is repeatedly preceded by one or more backpropagating action potentials [4-7, 10]. It depends on NMDA receptor activation, post-synaptic metabotropic glutamate receptors (mGluR), voltage-dependent calcium channels, protein phosphatases, cannabinoid receptor CB1 and astrocytic signaling [6, 9-16]. Calcium therefore represents potentially a key factor in the induction of STDP. The intracellular Ca^{2+} dependence of STDP suggests that extracellular Ca^{2+} might play a critical role in shaping STDP. Yet, most if not all *in vitro* STDP studies [6-10, 17-19] used non-physiological external Ca^{2+} concentrations ranging between 2 and 3 mM, whereas the physiological Ca^{2+} concentration ranges between 1.3 and 1.8 mM in the young rat hippocampus [20, 21]. Calcium-based models of synaptic plasticity [22] where Ca^{2+} transients result from backpropagating action potentials and EPSPs predict that the sign, shape and magnitude of STDP strongly depend on the amplitudes of calcium transients triggered by pre and post synaptic spikes, and therefore on external Ca^{2+} concentration [23] (see Figure 1). These modeling studies suggest that high Ca^{2+} concentrations used in experimental studies could lead to an overestimate of the *in vivo* levels of plasticity, or even to a lack of plasticity. We therefore set out to determine STDP rules in physiological Ca^{2+} at the CA3-CA1 synapse of the hippocampus *in vitro*.

We show here that the classical STDP rule (LTD for post-before-pre pairings, LTP for pre-before-post pairings) is obtained solely with a high external Ca^{2+} concentration (≥ 2.5 mM), whereas no plasticity could be induced for concentrations lower than 1.5 mM external Ca^{2+}, and only t-LTD could be induced by positive or negative time delays in 1.8 mM external Ca^{2+}. t-LTP could be restored only when bursts of 3 or 4 post-synaptic spikes were used

instead of single spikes, or when the pairing frequency was increased from 0.5 to 5 or 10 Hz. We used several variants of a Ca^{2+}-based plasticity model [23] in which both t-LTD and t-LTP depend on transient changes in postsynaptic Ca^{2+} (**Figure 1**) to fit the data. We found that the nonlinearity of transient Ca^{2+} changes conferred by NMDA receptor activation as well as short-term facilitation are critical to quantitatively account for the entire experimental dataset. Our results indicate that the STDP rule is profoundly altered in physiological Ca^{2+}, but that a classical STDP profile can be restored under specific activity regimes.

Results

STDP rule is altered in extracellular physiological calcium

Induction of STDP at the Schaffer collateral-CA1 cell synapse was examined under 3 different external Ca^{2+} concentrations (3, 1.8 and 1.3 mM) and in the presence of normal synaptic inhibition (i.e. without any $GABA_A$ receptor antagonist). In high Ca^{2+} (3 mM), t-LTP (124 ± 7% of the control EPSP slope, n = 14) was induced by repeatedly pairing (100 times, 0.3 Hz [24]; **Figure 2A**) the evoked excitatory post-synaptic potential (EPSP) and the post-synaptic action potential (AP) with a delay ranging between +5 and +25 ms (**Figure 2B**). t-LTD (68 ± 11%, n = 10) was induced by repeatedly pairing (150 times, 0.3 Hz [24]; **Figure 2A**) the EPSP and the post-synaptic AP with a delay ranging between -5 and -25 ms (**Figure 2B**). The plot of synaptic changes as a function of spike-timing provided a classical STDP curve in 3 mM external Ca^{2+} , with a LTP window in the [0,40ms] range surrounded by two LTD windows, one for negative delays and the other for positive delays at ~40-60 ms (**Figure 2A**). In contrast, only t-LTD was induced by positive or negative pairings in 1.8 mM external Ca^{2+} (respectively, 73 ± 6%, n = 13 & 71 ± 8%, n=11; **Figure 2C**) and no significant changes were observed in 1.3 mM external Ca^{2+} at any pairing (100 ± 12%, n = 13 after positive pairing and 106 ± 14%, n = 13 after negative pairing; **Figure 2D**). Thus, the STDP rules are highly altered in the physiological Ca^{2+} range (**Figure 2C** & **2D**).

In order to precisely determine the transition between LTD and no change on the negative correlation side, and the transition from LTP to LTD to no change on the positive correlation side, we tested the effects of positive and negative pairing in 1.5 mM and 2.5 mM external Ca^{2+}. The data show that negative pairing induced no plasticity in 1.5 mM external Ca^{2+} (95 ± 5%, n = 5, **Figure 2E**), whereas t-LTD was consistently observed in the 1.8-3 mM range (at 2.5 mM, 90 ± 3%, n = 5, **Figure 2E**).Positive pairing led to no change in 1.5 mM external Ca^{2+} (97 ± 5%, n = 6), t-LTD at 1.8 mM external Ca^{2+}, but t-LTP in 2.5 mM external Ca^{2+} (147 ± 13%, n = 6), with a switch from LTD to LTP occurring between 1.8 and 2.5 mM (**Figure 2E**). These data indicate that the STDP rule is profoundly altered in physiological calcium, with a lack of t-LTP in the whole range, and the appearance of t-LTD in a broad

range of timings in the upper limit of the physiological Ca^{2+} range.

Recovery of t-LTP in physiological calcium

The STDP rule in physiological Ca^{2+} is characterized by a complete lack of t-LTP and the predominance of t-LTD at 1.8 mM external Ca^{2+}, while no significant plasticity is observed at 1.3 mM. Therefore, we first tried to restore t-LTP in physiological Ca^{2+} by either using bursts of post-synaptic spikes, instead of individual spikes, during the pairing [18, 25] or increasing the frequency of single-spike pairing [18]. In 1.8 mM external Ca^{2+}, increasing the number of postsynaptic spike in a burst from 1 to 4 increased almost linearly the magnitude of potentiation as a function of the number of spikes per burst. While no net change was observed with 2 spikes (99 ± 15%, n = 11), significant potentiation was observed with 3 (116 ± 6%, n = 8) and 4 spikes (135 ± 13, n = 7; **Figure 3A**). In contrast, no potentiation was induced with 3 postsynaptic spikes in 1.3 mM external Ca^{2+} (88 ± 7%, n = 7; **Figure 3B**).

We next increased the frequency of single-spike pairing from 0.5 Hz to 3-10 Hz in physiological external Ca^{2+}. While no net change was observed when the frequency of stimulation was increased to 3 Hz (95 ± 4%, n = 8), significant potentiation was observed with 5 (138 ± 17%, n = 7) or 10 Hz (131 ± 9 %, n = 8) in 1.8 mM external Ca^{2+} (**Figure 3C**). Increasing the frequency of stimulation to 10 Hz also allowed to recover t-LTP in 1.3 mM external Ca^{2+} (129 ± 9%, n = 9, **Figure 3D**). We conclude that while STDP rules are strongly altered, t-LTP can be restored either by increasing the post-synaptic spike number or single-spike pairing frequency in physiological Ca^{2+}.

Recovery of t-LTD at negative delays in 1.3 mM calcium

While t-LTD induced by negative delays was observed at the upper limit of the physiological calcium range (i.e. 1.8 mM), it was absent in 1.3 mM external Ca^{2+} (106 ± 14%, n = 10; **Figure 4A**). We therefore examined the conditions for restoring t-LTD in 1.3 mM Ca^{2+} at negative delays. When the number of post-synaptic spikes was increased up to 3 during the pairing (delay of -25 ms), significant t-LTD was found to be induced (61 ± 7%, n = 7; **Figure**

4A). Similarly, when the pairing frequency was increased from 0.3 to 10 Hz, t-LTD was restored. We conclude that normal STDP profile can be restored even in 1.3 mM Ca^{2+} by either increasing the number of post-synaptic spikes during the pairing or the pairing frequency to 10 Hz.

Calcium-based synaptic plasticity model

We constructed a calcium-based model to quantitatively account for the experimental findings. Model parameters were fit to the results of the spike-pair protocols at a low pairing-frequency, and the model was then validated by making predictions for the burst and high frequency protocols. Following Graupner and Brunel (2012), our model describes two variables: the intra-cellular calcium transients in the post-synaptic spine resulting from the pre- and post-synaptic activity, and the dynamics of the synaptic efficacy (or synaptic *weight*).

Calcium fluxes mediated by NMDAR and VDCC are modeled as discrete jumps following each pre- and post-synaptic spike, respectively. The transients decay with timescale τ_{Ca} and their amplitudes are C_{pre} and C_{post} (see Methods). The extra-cellular calcium concentration enters our model *only* through scaling of the amplitude parameters: $C_{pre} \propto [Ca^{2+}]^2$ - due to the expected linear increase in flux with external concentration and the approximate linear relationship between the probability of pre-synaptic vesicle release and the extra-cellular calcium [26]; $C_{post} \propto [Ca^{2+}]$ - due to the increased flux with external concentration. A hallmark of the biophysics of calcium entry is its non-linearity: when pre- and post-synaptic neurons are co-active, calcium transients are markedly larger than what would be expected due to the sum of independent contributions [15, 27, 28]. This nonlinearity was characterized in the model by a single parameter, η. It is known that calcium transients attributed to nonlinear processes (such as dendritic NMDA spikes) decay on a longer timescale than transients following single spikes [28, 29], so the nonlinear term decays with timescale $\tau_{Ca,NMDA} > \tau_{Ca}$ (see Methods). Unless

noted otherwise, the intracellular calcium transient $c(t)$ is the sum of the above three contributions: pre- and post-synaptic, and the nonlinear term.

The model is characterized by a second variable, the synaptic weight, that increases at rate γ_p when the calcium transient $c(t)$ crosses the potentiation threshold θ_p, and decreases with rate γ_d when $c(t)$ crosses the depression threshold θ_d. This is consistent with the notion that high levels of calcium lead to LTP, whereas intermediate levels lead to LTD [22, 30]. We considered both a bi-stable synapse where the weight can be in an up- or down-state with high and low efficacy, respectively; and a graded synapse where any value of the weight is stable (see Methods for more details).

Nonlinear calcium transients are necessary to account for data in spike pair protocols

Graupner and Brunel (2012) showed that STDP curves at a single calcium concentration from various preparations can be well fit by a calcium-based model for which transients depend linearly on pre- and post-synaptic activity. We asked if such a model can be fit to the data at multiple calcium concentrations. The left column of **Supplementary Figure 1** shows that when the parameters of a linear model reproduce the depression - potentiation - depression profile at $[Ca^{2+}]$ = 3.0 mM, the model exhibits no plasticity for pairs of spikes at $[Ca^{2+}]$ = 1.8 mM. The poor fit of the linear model at $[Ca^{2+}]$ = 1.8, 3.0 mM is in fact a direct consequence of the assumptions we made on the scaling of the amplitudes C_{pre}, C_{post} with $[Ca^{2+}]$ (see Methods for details). We therefore focus henceforth on models that include a nonlinear term. **Figure 5** shows the fitted STDP curves at multiple concentrations for the bi-stable and the graded synapse models.

The model with bi-stable synaptic weight dynamics yielded the lowest fitting error (see **Supplementary Figure 2** and **Tables 1, 2** for model parameters, fitting and prediction errors for all models tested). The resulting STDP curves have a square shape (blue and green lines in **Figure 5**), a consequence of the small inferred ratio between the noise parameter (representing the probability of "spontaneous" transitions between the up- and down-states) and the potentiation and depression rates (γ_p, γ_d). This suggests that a small number of

repeats could be sufficient to induce transitions between the up- and the down-states of individual synaptic contacts, consistent with direct tests of the bi-stability of these synapses [31] and the efficiency observed for some short induction protocols with only 10 repeats [32]. These sharp transitions further imply a relatively small ratio change between the efficacy of the up- and the down-state, which in all tested versions was between 1.4 and 1.5. These rapid transitions are nonetheless consistent with the typical smooth shape of STDP curves (**Figure 2**, right) because plotting the average STDP curve obtained by varying the parameters randomly in the neighborhood of the best fitting parameters yields a curve similar to the experimental one (**Figure 5**, light blue shaded region; Methods). This reflects the fact that each data point corresponds to a measurement of a different synapse, and suggests that the parameters our fitting procedure finds are not fine-tuned.

We also fitted parameters for a model with graded synaptic weight dynamics (**Figure 5**, see Methods for definitions). The error of the best fitting graded model is higher than the bi-stable one, but since it has less free parameters (**Table 1**), the model selection criterion we used does not strongly favor one over the other (Methods, **Supplementary Figure 2** and **Table 2**).

Residual LTD at [Ca^{2+}] = 1.3 mM

The STDP curve at the lowest concentration we measured showed non statistically significant LTD at positive relative timing (**Figure 2E**, see results for [Ca^{2+}] = 1.3 mM, Δt = +10ms). The models we inferred from the data show a small window for the induction of LTD at 1.3 mM (**Figure 5**, bottom), that disappears at [Ca^{2+}] = 0.92 mM for both the graded and bi-stable models. We note that the window for induction of LTD exhibited by both models is consistent with the data, when the variability is taken into account (**Figure 5**, bottom). We also searched for parameters that fit well STDP curves for intermediate and high concentrations, but that are constrained to exhibit no LTD at [Ca^{2+}] = 1.3 mM (see Methods). We found that models that satisfy this constraint fit poorly to the STDP curves at [Ca^{2+}] = 1.8 mM (see **Supplementary Figure 3**). Under this constraint the window for induction of LTD is

much narrower than in the data and in unconstrained models (compare middle panels in **Figure 5** and in **Supplementary Figure 3**).

Note that the long time scale $\tau_{Ca,NMDA}$ was chosen to be fixed, since the spike-pair data does not put strong constraints on this parameter. Varying this parameter in the range [60,130 ms] consistent with published data regarding decay of calcium transients following dendritic NMDA spikes (see [33] for a review) did not change significantly fitting errors for spike-pair data (**Supplementary Figure 4** for both the bi-stable and graded models). The main effect on the remaining free parameters is the decrease in η for longer $\tau_{Ca,NMDA}$, and the main difference between the models is the quality of predictions they give for the held-out data, which we address next.

Model predictions for protocols with burst stimuli and high pairing-frequencies

We then asked whether models that were fit using STDP curves for spike-pairs at low frequency give accurate predictions for plasticity measured following induction protocols with burst stimulation of the post-synaptic neuron and/or high pairing-frequencies.

We generated predictions for the burst protocols for each parameter set that lies in a *local* minimum of the fitting error (i.e., error with respect to the spike-pair STDP). We then computed the *prediction* error with respect to the burst protocols. **Supplementary Figures 5, 6, 7** show the fitting and prediction errors plotted against one another for the bi-stable and graded models. We focused on the parameter sets within these scatter plots that represent the model with the smallest *total* error (combining the spike-pair and burst data, dark blue), and the smallest *fitting* error (light blue).

For each model, both parameter sets generated predictions that are in good quantitative agreement with the data (**Figure 6**, left and **Supplementary Figures 5, 6, 7**), suggesting that our model does not suffer from over-fitting. Our model correctly predicts that at $[Ca^{2+}]$ = 1.8 mM, increasing the number of post-synaptic spikes that follow a pre-synaptic spike from one to four leads to a change in the direction of plasticity from LTD to LTP; and that at $[Ca^{2+}]$ = 1.8 mM, a single pre-synaptic spike followed by a burst of three post-synaptic

spikes leads to LTP, while the reverse order of the same stimulation pattern leads to LTD (**Figure 6**). We note however that models that have the smallest fitting error to the pair data do not predict the magnitude of LTD for a protocol with a burst of 3 post-synaptic spikes *before* a pre-synaptic spike at $[Ca^{2+}]$ = 1.3 mM. Choosing the model that gives the lowest *total* error on the pair and burst data leads only to a very small increase in the fitting error (compare light blue and blue circles in **Supplementary Figures 5, 6, 7**, panels **A, F**)

We next tested the model predictions for protocols with pairing-frequencies higher than 0.3 Hz. For spike-pairs, we focused on positive relative timing Δt = +10 ms for which we observed LTP at $[Ca^{2+}]$ = 3.0 mM, LTD at $[Ca^{2+}]$ = 1.8 mM and non-statistically significant LTD at $[Ca^{2+}]$ = 1.3 mM. Our model correctly predicts that for the physiological concentrations (1.3 and 1.8mM), the sign of plasticity changes from LTD to LTP at a sufficiently high pairing frequency (**Figure 6**, right). However, it does not produce an accurate prediction for the frequency at which this change in the sign of plasticity occurs. At 1.8 mM our data indicates that the change occurs between 3-5 Hz, compared to a frequency between 7-8 Hz predicted by our model whereas at 1.3 mM, our data indicates that the change occurs at a frequency smaller than 10 Hz, compared to a frequency larger than 15 Hz predicted by our model (see blue and red lines in **Figure 6** for the bi-stable and graded models, respectively).

Model with short-term plasticity

The model we have described thus far explains a broad set of measurements of *long-term* synaptic plasticity, while the high pairing-frequency protocols we used are within the range of frequencies where short-term plasticity (STP) is expected to play a role. To incorporate STP into our model, we multiplied the amplitude associated with transients following pre-synaptic activity (C_{pre}) by a frequency dependent factor $q_{ST}(f)$. Measurements of STP in hippocampal slices suggest that short-term *facilitation* dominates in the frequency range relevant to our experiments (3-10 Hz) (Debanne et al., 1996, deKay et al., 2006). Therefore we chose $q_{ST}(f)$ to have a simple sigmoidal form: for the baseline frequency (f = 0.3 Hz) the short-term factor is unity. For high frequencies, in accordance with the literature, we assumed it saturates at 3,

although the exact value of the saturation is not important for our purposes, due to the saturation of Δw in the bi-stable model. We varied the crossover frequency f_0 in the range 1-9 Hz.

When f_0 is chosen to be 3 Hz, our model predictions are in excellent agreement with the data (**Figure 5**, dark blue and dark red lines for bi-stable and graded models that include STP, respectively). The measurements we report in this study do not allow us to explicitly fit this parameter in our model, nor can we fit $\tau_{Ca,NMDA}$ (for similar reasons). It will be interesting to see how future experiments might allow construction of a model where short- and long-term plasticity effects are parameterized and fit to data more directly.

Discussion

Our study reveals that the STDP curve at the Schaffer collateral-to-CA1 pyramidal cell synapse measured in external physiological calcium (1.3-1.8 mM) and in the presence of normal synaptic inhibition does not follow the classical asymmetric shape reported at non physiological calcium. Rather, we show that no significant plasticity occurs in the lower range of the physiological calcium range, while only depression occurs in the upper range, when single EPSPs and post-synaptic spikes are paired. Thus, there is a complete lack of potentiation at external Ca^{2+} concentration ranging between 1.3 and 1.8 mM. We then find that t-LTP can be restored in physiological Ca^{2+} either by increasing the number of post-synaptic spikes (from 1 to 3-4) or by increasing the pairing frequency (from 0.3 to 10 Hz). Likewise, t-LTD can be restored at 1.3mM by increasing the number of post-synaptic spikes during the pairing from 1 to 3.

t-LTP and physiological external calcium

We report here that t-LTP could not be induced by positive correlation between single pre- and post-synaptic spikes in physiological external calcium. Rather, t-LTD and no plasticity was respectively induced at 1.8 and 1.3 mM calcium. It is noteworthy that for positive delay (+5/+25 ms), the synaptic plasticity goes from no change at the lower limit of calcium range (1.3 mM) through a depression phase at the upper limit of calcium range (1.8 mM) before reaching the potentiation level for non-physiological, high calcium (2.5 and 3 mM). Such biphasic behavior was predicted by calcium-based theoretical studies of synaptic plasticity [22, 23, 30].

t-LTP at positive delay could be restored in physiological calcium by either increasing the number of post-synaptic spike from 1 to 3 or 4 (at 1.8 mM but not at 1.3 mM calcium) or by increasing the pairing frequency from 0.3 to 10 Hz (at 1.3 or 1.8 mM calcium). Such recovery of t-LTP had been already reported in previous studies [18, 25], but the data reported in these studies were obtained in non-physiological calcium and in the absence of synaptic inhibition. This finding suggests that the minimal paradigm for inducing robust t-LTP *in vivo*

would be to pair EPSPs associated with spike bursting at theta frequency. In fact, this type of pairing has been shown to induce synaptic potentiation of thalamo-cortical EPSPs in the cat visual cortex *in vivo* [34].

t-LTD and physiological external calcium

At 3 mM calcium, t-LTD was induced by negative delays (-5/-50 ms) and for positive delays (+40/+60 ms). This second LTD window has been predicted by calcium-based models [22, 23, 35] and had been reported previously in a few experimental studies in which calcium transients were enhanced by spike broadening [8, 13] or by multiple spike-pairing at 5 Hz [18]. t-LTD was also observed for any spike timing at 1.8 mM but no significant t-LTD was observed for negative delays (-5/-25 ms) at 1.3 mM and 1.5 mM calcium. Nevertheless, t-LTD could be restored at 1.3 mM calcium when the number of postsynaptic spikes was increased from 1 to 3.

Comparison of experimental data and calcium-based models

The successive transitions from a STDP curve with both LTD and LTP first to a curve with LTD only, and then to a curve with no plasticity, are generic predictions of calcium-based models in which potentiation occurs at high calcium concentrations, while depression occurs at intermediate calcium concentrations [22, 23]. Furthermore, these models also generically predict that increasing frequency, or number of spikes in a burst, will lead eventually to LTP [22, 23]. Here, we have a made a major step beyond these generic predictions, by fitting quantitatively experimental data at various calcium concentrations with several variants of calcium-based synaptic plasticity models (linear and non-linear, bistable and analog). The data reported here measured at multiple concentrations allowed us to show that non-linear summation of transient calcium contributions is necessary to reproduce quantitatively the experimental findings. We chose the non-linear interaction term to be quadratic for simplicity. This non-linearity describes in a schematic fashion the biophysical properties of the NMDA receptor, that needs a coincidence of both presynaptic (for glutamate binding) and

postsynaptic (for magnesium block relief) activity in order to maximize opening probability. It has been directly observed in calcium imaging experiments (e.g. [15, 27]).

Furthermore, we found the non-linear term should have a decay timescale of approximately 100 ms (longer than that of transients due to pre- or postsynaptic activity alone, ~20 ms) for the model to make accurate predictions for high pairing-frequency protocols. A model with nonlinear transients that decay fast fits well data measured at a low pairing frequency (0.3 Hz), but it fails to capture quantitatively the pairing-frequency dependence of plasticity. These conclusions are consistent with the recent work of Brandalise et al. (2016) where it was shown that dendritic NMDA spikes following coincident stimulation of pre and post synaptic activity lead to calcium transients that decay slowly, and that blocking these NMDA spikes abolishes LTP measured in the control protocol. Note however that these experiments were carried out in recurrent CA3 synapses and not in CA3 to CA1 synapses.

These results call for a radical reevaluation of classic `STDP rules' (and of the experimental conditions under which they are measured), in which pairs of single pre and post-synaptic spikes modify synaptic efficacy; rather, they show that such pairs (even if repeated many times at low frequency) are not likely to elicit any changes of synaptic strength in physiological conditions. They indicate that plasticity can only be triggered when bursts of spikes are used, or neurons fire at sufficiently high frequency, and invalidate popular phenomenological models of STDP in which plasticity is triggered by pairs of single pre and post-synaptic spikes. Qualitatively similar findings have been obtained in synaptic plasticity experiments in granule cell to Purkinje cell synapses, where bursts of pre-synaptic spikes are required to induce both LTD [36] and LTP [37]; and in area RA of songbirds [38]. In cortical slices, it has been shown that pairing single spikes at low frequencies only induce LTD but not LTP [17].

Beyond spiking activity, the recent work of Bittner et al. (2017) serves as another example of how LTP can be induced reliably in physiological conditions: these authors have shown that a plateau potential in a CA1 neuron can lead to potentiation (and, in fact, `creation' of a new place field) even when the preceding presynaptic activity occurs up to a second before it [39].

The large calcium influx during the plateau potential suggests that it might be possible to construct a biophysical, calcium-based model that will parsimoniously describe plasticity due to both spiking activity and plateau potentials in the hippocampus.

Methods

Acute slices of rat hippocampus

Hippocampal slices were obtained from 14- to 20-day-old rats according to institutional guidelines (Directive 86/609/EEC and French National Research Council) and approved by the local health authority (# D1305508, Préfecture des Bouches-du-Rhône, Marseille). Rats were deeply anaesthetized with chloral hydrate (intraperitoneal 400mg/kg) and killed by decapitation. Slices (350 µm) were cut in a N-methyl-D-glucamine (NMDG)-solution (in mM: 92 NMDG, 2.5 KCl, 1.2 NaH_2PO_4, 30 $NaHCO_3$, 20 HEPES, 25 glucose, 5 sodium ascorbate, 2 thiourea, 3 sodium pyruvate, 10 $MgCl_2$, 0.5 $CaCl_2$) on a vibratome (Leica VT1200S) and were transferred at 32°C in NMDG-solution for 30min before resting for 1 h at room temperature in oxygenated (95% O_2/5% CO_2) artificial cerebro-spinal fluid (ACSF; in mM: 125 NaCl, 2.5 KCl, 0.8 NaH_2PO_4, 26 $NaHCO_3$, x $CaCl_2$, x $MgCl_2$, and 10 D-glucose). The ratio of $CaCl_2$ and $MgCl_2$ concentration was maintained constant to stabilize presynaptic release probability [40, 41] and external Ca^{2+} concentration was set to either 3 mM (Mg^{2+}: 2 mM), 1.8 mM (Mg^{2+}: 1.2 mM) or 1.3 mM (Mg^{2+}: 0.9 mM). For recording, each slice was transferred to a temperature-controlled (30°C) chamber with oxygenated ACSF.

Electrophysiology

Neurons were identified with an Olympus BX 50WI microscope using Differential Interference Contrast (DIC) x60 optics. Whole-cell recordings were made from CA1 pyramidal neurons, electrodes were filled with a solution containing the following (in mM): 120 K-gluconate, 20 KCl, 10 HEPES, 2 $MgCl_26H_2O$, and 2 Na_2ATP. Stimulating pipettes filled with extracellular saline were placed in the stratum radiatum (Schaffer collaterals). In control and test conditions, Excitatory Post-Synaptic Potentials (EPSPs) were elicited at 0.1 Hz by a digital stimulator that fed a stimulation isolator unit (A385, World Precision Instruments). Access resistance was monitored throughout the recording and only experiments with stable resistance were kept (changes<20%).

Acquisition and data analysis

Recordings were obtained using a Multiclamp 700B (Molecular Devices) amplifier and pClamp10.4 software. Data were sampled at 10 kHz, filtered at 3 kHz, and digitized by a Digidata 1440A (Molecular Devices). All data analyses were performed with custom written software in Igor Pro 6 (Wavemetrics). EPSP slope was measured as an index of synaptic strength. Pooled data are presented as mean ± SEM. Statistical comparisons were made using Wilcoxon or Mann-Whitney test as appropriate with Sigma Plot software. Data were considered as significant when $P<0.05$.

STDP induction protocols

After obtaining a stable EPSP baseline for a period of 10-15 minutes, single EPSPs were paired with a STDP protocol was applied on the input with 100 repetitions for LTP and 150 repetitions for LTD. The number of postsynaptic spikes and the pairing frequencies were adjusted depending on the experiment. The postsynaptic spikes(s) were evoked by a brief somatic current pulse. EPSP slopes were monitored at least for 20 minutes after each pairing episode. Values of synaptic change were measured in the time window between 15 and 25 minutes after pairing.

Synaptic plasticity model

Calcium transients

The calcium transients in the model depend on the pre- and post-synaptic spiking activity, and indirectly on the extra-cellular calcium concentration (through parameter scaling with $[Ca^{2+}]$. The pre- and post-synaptic spike trains are denoted by $s_{pre}(t) = \Sigma_i \, \delta(t-t_{i,pre})$ and $s_{post}(t) = \Sigma_i \, \delta(t-t_{i,post})$, respectively. The temporal evolution of the pre- and post-synaptically induced calcium transients is given by:

$$(d/dt)\, c_{pre}(t) = -c_{pre}(t) / \tau_{Ca} + C_{pre}\, s_{pre}(t - D), \quad \text{and} \quad (d/dt)\, c_{post}(t) = -c_{post}(t) / \tau_{Ca} + C_{post}\, s_{post}(t)$$

where C_{pre} and C_{post} are parameters describing the magnitude of jumps in calcium following a pre- and a post-synaptic spike, D is a pre-synaptic delay parameter and τ_{Ca} is the decay

timescale of calcium transients.

The equation for the time evolution of the nonlinear contribution $c_{NL}(t)$ is

$$(d/dt)\, c_{NL}(t) = -c_{NL}(t) / \tau_{Ca,NMDA} + \eta\, c_{pre}(t)\, c_{post}(t)$$

where $\tau_{Ca,NMDA}$ is the decay timescale of the nonlinear transients and η is a parameter describing the strength of the nonlinearity. The total transient $c(t)$ is then

$$c(t) = c_{pre}(t) + c_{post}(t) + c_{NL}(t).$$

The parameters C_{pre} (C_{post}) scale quadratically (linearly) with the extra-cellular calcium concentration:

$$C_{pre}([Ca^{2+}]_1) / C_{pre}([Ca^{2+}]_2) = ([Ca^{2+}]_1) / [Ca^{2+}]_2)^2,$$

$$C_{post}([Ca^{2+}]_1) / C_{post}([Ca^{2+}]_2) = [Ca^{2+}]_1) / [Ca^{2+}]_2 .$$

In addition to the full nonlinear model described by the equations above, we considered linear models where the calcium transient is a sum over pre- and post-synaptic contributions only, i.e., $c(t) = c_{pre}(t) + c_{post}(t)$ (equivalently, one can set $\eta = 0$).

We also considered a model in which there is no linear post-synaptic contribution. The equations for the time evolution of calcium transients in that case are the same as above, with $C_{post} = 1$ and $c(t) = c_{pre}(t) + c_{NL}(t)$ (note that the post-synaptic transient must still be computed to then compute the nonlinear one).

Synaptic weight dynamics- Graded synapse

When the synapse is graded, any value of the weight is stable in the absence of stimulation, within the allowed range. We assume that the weight variable ρ is restricted to be between 0 and 1, which is enforced by two soft thresholds. The equation for the time evolution of ρ is

$$(d/dt)\, \rho(t) = + \gamma_p\, [1-\rho(t)]\, \Theta[c(t) - \theta_p] - \gamma_d\, \rho(t)\, \Theta[c(t) - \theta_d].$$

Here, Θ is the heaviside step function; γ_p and γ_d are the potentiation and depression rates, respectively; and θ_p and θ_d are the potentiation and depression thresholds above which the synaptic weight variable increases or decreases.

Synaptic weight dynamics- Bistable synapse

The dependence of the synaptic weight variable on the calcium variable is similar in the bi-stable case and in the graded case. Here we introduce two terms to the equation for the time evolution of ρ: one implements the underlying bi-stability and the other is the noise term. The equation is now:

$$(d/dt)\,\rho(t) = -1/\tau\,(\partial/\partial\rho)\,U[\rho(t)] + \gamma_p\,[1-\rho(t)]\,\Theta[c(t)-\theta_p] - \gamma_d\,\rho(t)\,\Theta[c(t)-\theta_d] + \sigma\,\tau^{-1/2}\,\xi(t)$$

where $U(\rho)$ is the "double-well" potential: $U(\rho) = \rho^2(1-\rho)^2/4$, and τ describes the timescale of the dynamics in the double-well potential.

Fitting model parameters

A detailed description of the procedure and formulas we used to fit the different models is included in the supplementary mathematical note.

Constraints on model parameters

Table 2 includes the range of values within which we optimized the model parameters, and the values we used (for parameters that were fixed).

Qualitative features of the model and the STDP curve help constrain the parameters

The parameters C_{pre} and C_{post}

For the transient amplitude parameters C_{pre} and C_{post} the constraints we used ensure that a single spike by a pre- or post-synaptic neuron cannot lead to a calcium transient that exceeds the depression threshold at the highest calcium concentration we used in our experiments ($[Ca^{2+}] = 3.0$mM).

If one is interested in fitting a model for only a single calcium concentration, this constraint can be relaxed. One can then ensure that a pair of well separated pre- and post-synaptic spikes do not lead to changes in the synapse by requiring that the product of the time spent above threshold (T_p, T_d) and the corresponding rate (γ_p, γ_d) are equal. If transients

induced by single spikes can cross threshold, this requires tuning either γ_p or γ_d such that indeed $\gamma_d \, T_d = \gamma_p \, T_p$.

This scheme cannot be used when one is interested in fitting the model for multiple levels of the extra-cellular calcium. The reason is that if one fixes, say, γ_d such that potentiation and depression balance each other for a pair of spikes at one concentration, the same value will lead to imbalance at a different concentration.

Understanding the limitations of the linear model

We show in **Supplementary Figure 1** that a linear model fails to simultaneously reproduce the STDP curve at intermediate and high calcium concentrations. We can understand that this must be the case, given the constraints on the amplitude parameters C_{pre}, C_{post} and the assumptions we made on their scaling with the concentration. The constraint that a single pre- or post-synaptic spike does not lead to a transient that crosses the depression threshold at $[Ca^{2+}] = 3.0$mM implies that $C_{pre} \leq \theta_d / 3^2$, and $C_{post} \leq \theta_d / 3$. On the other hand, a perfectly aligned pre-post pair (including the effect of the pre-synaptic delay) at $[Ca^{2+}] = 1.8$mM *should* cross the depression threshold, i.e., $1.8^2 \, C_{pre} + 1.8 \, C_{post} \geq \theta_d$. Substituting in the maximal values we allow for the amplitudes and dividing by θ_d we get a contradiction: $(1.8 / 3)^2 + (1.8 / 3) = 0.96 \geq 1$, implying that a linear model cannot simultaneously satisfy the single spike constraints at high calcium concentrations *and* produce LTD at intermediate concentration. Note however that this conclusion strongly depends on our assumptions on how C_{pre} and C_{post} depend on calcium concentration – if for instance the presynaptic transients depend linearly on extracellular calcium concentration, then parameters can be found for which all three constraints can be satisfied (for instance, $C_{pre} = C_{post} = 0.3 \; \theta_d$).

The parameters τ_{Ca} and $\tau_{Ca,NMDA}$

We assumed that the calcium transients following a single pre- and post-synaptic spike decay on the same timescale, τ_{Ca}, while the time-scale associated with the nonlinear term, $\tau_{Ca,NMDA}$, is longer. This assumption can be justified, at least qualitatively, by inspection of the

STDP curve we measured at $[Ca^{2+}]$ = 3.0 mM and the fact that increasing the pairing-frequency above a few Hz leads to strong changes in the resulting plasticity.

From the shape of Δw as a function of Δt at high concentration we conclude that the calcium transients in the model must carry information about the relative timing of pre- and post-synaptic spikes at a resolution of approximately 20ms. In other words, the fact that changing the relative timing of a pair of spikes by 20ms leads to significant changes to the resulting plasticity implies that the calcium transients in the model must preserve the timing information on that timescale.

On the other hand, the impact that increasing the pairing-frequency has on the resulting plasticity implies that the model must consist of at least one transient that decays on a timescale significantly longer than 20 ms.

We further inspect the shape of the STDP curve measured at $[Ca^{2+}]$ = 3.0 mM. Especially noteworthy is the second LTD window at positive Δt. The width of that window is comparable with the first LTD window at negative Δt. Moreover, consider reflecting the data about a vertical axis at the center of the LTP window, $\Delta t \approx 20$ ms. The resulting data points give an STDP curve that overlaps the original curve, suggesting a degree of symmetry played by the pre-synaptic neuron (including the delay D) and the post-synaptic neuron. This symmetry (which is also respected by the STDP curves measured at $[Ca^{2+}]$ = 1.3, 1.8 mM) implies that one cannot associate the pre-synaptic transients with a short decay timescale and the post-synaptic transients with a long decay timescale, or vice versa.

Therefore, assuming there are no intermediate timescales between τ_{Ca} and $\tau_{Ca,NMDA}$ that need to be explicitly introduced to the model, the only way to associate the timescales with transients that respects this symmetry is to let the pre- and post-synaptic transients decay with timescale τ_{Ca}, and let the nonlinear transient decay with timescale $\tau_{Ca,NMDA}$. We note that this qualitative argument yields a model that is in good agreement with the known biophysics of calcium entry in hippocampal neurons.

Numerical optimization

We binned the spike-pair data (gray points in **Figure 4**) into ~15 bins of the relative timing Δt for each of the calcium concentrations $[Ca^{2+}]$ = 1.3, 1.8, 3.0 mM. The fitting error is defined to be RMS error over the binned data points (black crosses in **Figure 4**), weighted by the number of data points used to compute Δw in each bin. When a bin contained more than one data point, we set the corresponding Δt value to the average of data points in that bin.

The fitting error is highly nonlinear in terms of the model parameters, and therefore we cannot expect it to be convex. Hence, for each model and for each value of a parameter that was fixed, we initialized a gradient descent routine at 2500 points chosen uniformly at random within the allowed parameter hyper-cube. We used the nonlinear constrained optimization built-in to the Matlab software, choosing the *interior-point* algorithm. Using a different optimization algorithm (*active-set*) had impact on the time it took to find (local) minima and the fraction of initial conditions of the parameter set that "exited" the allowed hyper-cube, due to the differences in how step sizes are computed in different algorithms. However, using a different algorithm did not affect the properties of parameter sets with small fitting errors for both the graded and bi-stable models (**Supplementary Figures 8, 9**).

Parameter variation

To study the effect of varying model parameters in the neighborhood of the best fitting parameter set we multiplied each model parameter and the timescales τ_{Ca}, $\tau_{Ca,NMDA}$ by a factor $1 + 0.2x$, where x is drawn at random (independently for each parameter and each repetition of this procedure) from a standard normal distribution. For the models with bi-stable synaptic weight dynamics, we considered a more heavy-tailed distribution for variations of the parameter describing the ratio of the efficacy of the up- and down-state (denoted b). Specifically, b was multiplied in each repetition by a number drawn from a log-normal distribution with parameters $\mu = 0$, $\sigma = 0.4$. In instances where this gave a value $b<1$ (which is nonsensical, since the down-state cannot have a higher efficacy than the up-state) we set b to its original value found by the fitting procedure.

With these randomized parameter sets in hand, we computed the STDP curves and the changes in synaptic efficacies following all experimental protocols. These were then used to compute the error bars and shaded areas around the curves showing Δw as a function of Δt and Δw as a function of the pairing-frequency f.

Model selection and estimation of the Akaike Information Criterion (AIC)

We considered a number of different model structures that each has a different number of free parameters which were fit to data. Additionally, some models were fit using a number of different values for fixed parameters. To make comparisons between the models, we used the AIC. Computing the AIC directly requires having a probabilistic model that can specify the the likelihood of the data points given the model parameters. For highly nonlinear models like ours, such a probabilistic description is not feasible.

Instead, we used the following procedure to *estimate* the AIC. The error $\varepsilon_{i,m}$ of the i-th spike pair data point and m-th model (without binning, total 143 points at $[Ca^{2+}]$ = 1.3, 1.8, 3 mM) was computed. The standard deviation of the data was estimated to be

$$\sigma_i^2 = 0.1^2 + \mathrm{Var}\{\Delta w_{i,1}\},$$

where the variance is computed over 100 randomized parameter sets in the neighborhood of the nonlinear, bi-stable model with the best fitting parameter set and $\tau_{Ca,NMDA}$ = 95ms. Using variance computed from the predictions of a different model does not change the results substantially nor does choosing a different "baseline" variance (instead of 0.1^2). This assumes that the noise is increased for pre-post timing that produces LTD or LTP, but some residual variance is added by hand. The errors were then assumed to follow a Gaussian distribution, such that the likelihood of a given model is

$$L_m = \prod_i \left(2\pi\sigma_i^2 \right)^{-1/2} \exp(-\varepsilon_{i,m}^2 / 2\sigma_i^2)$$

The resulting AIC value for each model is

$$\mathrm{AIC}_m = 2k_m - 2 \log (L_m),$$

where k_m is the number of free parameters in model m. This index is shown in

Supplementary Figure 2 (gray bars, most of which have negative values) and the actual values appear in **Table 2**. All nonlinear bistable models (with and without linear post-synaptic transients), except those that are constrained to have no LTD at $[Ca^{2+}]$ = 1.3 mM, have similar AIC values implying that this statistical criterion does not favor one model over the other in a significant way. Nonlinear graded models have somewhat larger AIC values, but given the fact that these are estimates, we think our results cannot rule out the possibility that the synapses' behavior is graded. The choice of the timescale $\tau_{Ca,NMDA}$ does not have a strong effect for the bi-stable models (i.e., choosing among $\tau_{Ca,NMDA}$ = 60, 95, 130ms does not lead to large changes in the AIC). For the nonlinear, graded model changing this timescale does lead to noticeable changes. We remind the reader that the AIC is computed using only the spike-pair data, so it reflects information about the "goodness of fit." It does not contain information about the quality of predictions to the burst and/or high-frequency protocols. While some models exhibit low sensitivity to the value of $\tau_{Ca,NMDA}$ in the context of fitting (especially the bi-stable models), all models are sensitive to this timescale in the context of predicting the outcome of the high-frequency protocols.

In conclusion, our fitting procedure, model selection criterion and computation of the prediction error strongly favor a nonlinear model with a long timescale of approximately 100 ms associated with nonlinearly induced transients. Despite the inclusion of a long timescale in the model, an accurate prediction for the high pairing-frequency protocols requires a short-term-facilitation factor to the model, in agreement with previously reported results. Finally, our results do not strongly favor bi-stable synaptic weight dynamics over graded dynamics.

Eliminating the linear post-synaptic contribution.

Previous results have indicated that repeated post-synaptic stimulation, even at high frequencies, does not lead to long-term synaptic plasticity if the pre-synaptic neuron does not fire [42]. Qualitatively, the model described above is inconsistent with this observation, since the post-synaptically induced calcium transient alone will summate and cross the LTD/LTP threshold for high enough frequency. We therefore asked whether our model can be modified

such that it will predict no change in the synaptic efficacy for protocols where only the post-synaptic neuron is stimulated, while still achieving low fitting error for the data reported here. In **Figure 5** (purple lines) and **Supplementary Figure 10** we show that a model where the linear post-synaptic contribution is eliminated from the overall intra-cellular calcium transient can account for the STDP data at all calcium concentrations. The post-synaptic component of the transient is still used for the purposes of computing the nonlinear contribution. The fitting error is indistinguishable from the model described above that does include the linear post-synaptic contribution. Moreover, we found that it is not necessary to re-fit the model without the linear post-synaptic contribution. Removing this contribution from the "full" model carries a negligible effect on the results, as the overall calcium transient is dominated by the nonlinear term (compare green and blue lines in **Figure 5**). We focus our discussion on the "full" model (that includes linear dependence on post-synaptic activity), but we emphasize that the data can be fit equally well with a model with such linear dependence.

Scaling of pre-synaptic amplitude parameter

Throughout the paper we used a model in which the pre-synaptic amplitude parameter C_{pre} scales quadratically with the extra-cellular calcium. This relies on the assumption that the probability of vesicle release scales linearly with $[Ca^{2+}]$. This assumption is supported by data reported by Murthy et al. (1997). However, the conclusions reached from our modeling work do not depend on this assumption. To show this, we fit the four main types of models discussed in the main text (linear graded, linear bistable, nonlinear graded, nonlinear bistable) with the important variants, and used the fitted parameters to produce predictions for the burst and high pairing-frequency data. While the parameters themselves depend on the scaling, the quality of the fits and predictions, and consequently the conclusions we have reached do not depend on this choice. Results for models where C_{pre} scales linearly with the extra-cellular calcium are shown in **Supplementary Figures 9-16** and **Table 3-6**.

Figure legends

Figure 1. Calcium-based model of Spike-Timing Dependent Plasticity

Cartoon qualitatively showing that a calcium-based model of synaptic plasticity implies that the shape of STDP (and sign of plasticity) will depend on extra-cellular calcium concentration. Synaptic changes depend on two plasticity thresholds, one for LTP (blue) and one for LTD (red). In response to a pre-post protocol, the post-synaptic calcium transient determines the orientation of plasticity. The reduction of extracellular calcium reduces the post-synaptic calcium transient, and leads to LTP for average values and an absence of plasticity for low values.

Figure 2. Spike-Timing Dependent Plasticity under various calcium concentration

(A) LTP and LTD are induced at low frequency (0.3 Hz). The pre-post protocol is repeated 100 times while the post-pre protocol is repeated 150 times. The action potential is induced by the injection of a depolarizing current into a CA1 neuron recorded in a whole cell configuration. The PPSE is induced by a stimulation electrode placed in the Schaffer collaterals. The delay (Δt) is varied according to the experiments. (B) In 3 mM extracellular calcium, a pre-post protocol (positive delays; $+5 < \Delta t < +25$ ms ; red) leads to LTP for positive and a post-pre (negative delays; $-25 < \Delta t < -5$ ms ; green) protocol leads to LTD for. Note the presence of a second LTD window at around +40 / + 50 ms. (C) In 1.8 mM extracellular calcium, a pre-post protocol ($+5 < \Delta t < +25$ ms; red) leads to LTD while a post-pre protocol ($-25 < \Delta t < -5$ ms ; green) leads to LTD . The LTP window is absent under these conditions. (D) In 1.3 mM extracellular calcium, on average, no plasticity is induced regardless of the delay. The LTP and LTD window are missing under these conditions. (E) Left, synaptic changes for a pre-post protocol at +10 ms. No plasticity is induced for calcium concentrations of 1.3 and 1.5 mM. For 1.8, 2.5 and 3 mM calcium, LTP is induced. Right, synaptic changes for a post-pre protocol at -25 ms. No plasticity is induced in 1.3 and 1.5 mM calcium. For 1.8, 2.5 and 3 mM calcium, a LTD is induced. Note the difference between the results in the range of physiological calcium concentration (green squares) and the results in non-physiological calcium concentration.

Figure 3. Recovery of t-LTP in physiological calcium

(A) Role of postsynaptic spike number for inducing synaptic changes by a pre-post protocol at +10 in 1.8 mM extracellular calcium. With only one action potential (blue), an LTD is induced. With two action potentials (red), on average, no plasticity is induced. Note the large variability in the plasticity. With three (green) or four (purple) action potentials LTP is induced. The increase in the number of post-synaptic action potential allows the LTP window to be restored. (B) Role of postsynaptic spike number for inducing synaptic changes by a pre-post protocol at +10 in 1.3 mM extracellular calcium. With only one action potential (black), no change is induced. With three action potentials (orange), no change is induced. The increase in the number of post-synaptic action potentials does not allow the LTP window to be restored. (C) Effects of the stimulation frequency on synaptic changes induced by a pre-post protocol at +10 ms with a single post-synaptic action potential in 1.8 mM extracellular calcium. For 0.3 Hz, an LTD is induced. For 3 Hz, no synaptic changes are induced. For 5 or 10 Hz, a LTP is induced. Increasing the pairing frequency restores the LTP window. (D) Effects of the stimulation frequency on synaptic changes induced by a pre-post protocol at +10 ms with a single post-synaptic action potential in 1.3 mM extracellular calcium. For 0.3 Hz, no synaptic change is induced. For 10 Hz, a LTP is induced. Increasing the pairing frequency restores the LTP window.

Figure 4. Recovery of t-LTD at negative delays in 1.3 mM calcium

(A) Role of postsynaptic spike number on synaptic changes induced by a post-pre protocol at -25 ms at a pairing frequency of 0.3 Hz in 1.3 mM extracellular calcium. For a single action potential, no change is induced (black). For three action potentials, LTD is induced (orange). The increase in the number of post-synaptic action potentials allows the recovery of the LTD window. (B) Effects of stimulation frequency on the induction of synaptic plasticity by a post-pre protocol at -25 ms with a single post-synaptic action potential in 1.3 mM extracellular calcium. For 0.3 Hz, no change is induced (black). For 10 Hz, LTD is induced (orange). The

increase in the pairing frequency allows the recovery of the LTD window.

Figure 5. Models that include a contribution to calcium transients that is nonlinear in the pre- and postsynaptic activity can be fit well to spike-pair data for multiple extra-cellular calcium concentrations

(A-C) Fits to the STDP data at [Ca2+] = 3, 1.8, 1.3mM for a number of variants of the nonlinear calcium-based plasticity model. Each measured synapse is represented by a gray circle. Black crosses represent binned data-points used for fitting. Red– nonlinear, graded model; Solid blue– nonlinear, bistable model. Dashed blue– average over 100 STDP curves for models with perturbed parameter values in the neighborhood of the best fitting nonlinear, bistable model (shaded area shows the standard deviation). Eliminating the linear contribution of post-synaptic spikes to the calcium transients in the bistable model does not cause a significant change in the fit (magenta). Further, one can also fit a model without a linear term to the data directly, again leading to good fits (green). All models have two LTD windows at [Ca2+] = 3mM, and residual LTD at 1.3mM.

Figure 6. Nonlinear calcium-based models produce accurate fits to the plasticity measured using burst and high pairing-frequency protocols.

(A) At [Ca2+] = 1.8mM, all models capture the change in sign of plasticity as a function of the number of spikes in the post-synaptic burst, and the reverse in sign when a post-synaptic burst of three spikes preceeds a pre-synaptic spike. (B) At [Ca2+] = 1.3mM, LTD is restored at a low pairing-frequency by a burst of three post-synaptic spikes (regardless of they arrive closely before or after the pre-synaptic spike), compared to a spike-pair protocol where no significant change was observed. This is captured by all nonlinear model variants, although the graded model shows a weaker effect than the experiment and the bistable models. The graded model also fails to reproduce the effect of a burst protocol at high pairing frequency, unless the effect of short-term plasticity are taken into account. (C-D) For spike pair protocols with _t = 10ms, the resulting plasticity depends strongly on the pairing frequency for both [Ca2+] = 1.8mM (top) and 1.3mM (bottom). The models capture the switch in sign of

plasticity, but the frequency at which this happens is over-estimated unless short-plasticity is taken into account. Key: Red– nonlinear, graded model; Blue– nonlinear, bistable model. Open red and blue symbols correspond to averages over 100 variations in the neighborhood of the best fitting parameters for the graded and bistable models, respectively. Brown and dark blue symbols correspond to the graded and bistable models, respectively, when short-term plasticity is taken into account. Magenta– bistable model where the linear contribution of post-synaptic spikes to the calcium transients were eliminated; Green– Bistable model fit directly without a linear post-synaptic term.

References

1. Dan, Y. & Poo, M.M. Spike timing-dependent plasticity: from synapse to perception. *Physiol Rev* **86**, 1033-48 (2006).
2. Feldman, D.E. The spike-timing dependence of plasticity. *Neuron* **75**, 556-71 (2012).
3. Gustafsson, B., Wigstrom, H., Abraham, W.C. & Huang, Y.Y. Long-term potentiation in the hippocampus using depolarizing current pulses as the conditioning stimulus to single volley synaptic potentials. *J Neurosci* **7**, 774-80 (1987).
4. Markram, H., Lubke, J., Frotscher, M. & Sakmann, B. Regulation of synaptic efficacy by coincidence of postsynaptic APs and EPSPs. *Science* **275**, 213-5 (1997).
5. Debanne, D., Gahwiler, B.H. & Thompson, S.M. Long-term synaptic plasticity between pairs of individual CA3 pyramidal cells in rat hippocampal slice cultures. *J Physiol* **507 (Pt 1)**, 237-47 (1998).
6. Bi, G.Q. & Poo, M.M. Synaptic modifications in cultured hippocampal neurons: dependence on spike timing, synaptic strength, and postsynaptic cell type. *J Neurosci* **18**, 10464-72 (1998).
7. Feldman, D.E. Timing-based LTP and LTD at vertical inputs to layer II/III pyramidal cells in rat barrel cortex. *Neuron* **27**, 45-56 (2000).
8. Nishiyama, M., Hong, K., Mikoshiba, K., Poo, M.M. & Kato, K. Calcium stores regulate the polarity and input specificity of synaptic modification. *Nature* **408**, 584-8 (2000).
9. Wang, H.X., Gerkin, R.C., Nauen, D.W. & Bi, G.Q. Coactivation and timing-dependent integration of synaptic potentiation and depression. *Nat Neurosci* **8**, 187-93 (2005).
10. Debanne, D., Gahwiler, B.H. & Thompson, S.M. Asynchronous pre- and postsynaptic activity induces associative long-term depression in area CA1 of the rat hippocampus in vitro. *Proc Natl Acad Sci U S A* **91**, 1148-52 (1994).
11. Normann, C. et al. Associative long-term depression in the hippocampus is dependent on postsynaptic N-type Ca2+ channels. *J Neurosci* **20**, 8290-7 (2000).
12. Sjostrom, P.J., Turrigiano, G.G. & Nelson, S.B. Neocortical LTD via coincident activation of presynaptic NMDA and cannabinoid receptors. *Neuron* **39**, 641-54 (2003).
13. Zhou, Y.D., Acker, C.D., Netoff, T.I., Sen, K. & White, J.A. Increasing Ca2+ transients by broadening postsynaptic action potentials enhances timing-dependent synaptic depression. *Proc Natl Acad Sci U S A* **102**, 19121-5 (2005).
14. Bender, V.A., Bender, K.J., Brasier, D.J. & Feldman, D.E. Two coincidence detectors for spike timing-dependent plasticity in somatosensory cortex. *J Neurosci* **26**, 4166-77 (2006).
15. Nevian, T. & Sakmann, B. Spine Ca2+ signaling in spike-timing-dependent plasticity. *J Neurosci* **26**, 11001-13 (2006).

16. Min, R. & Nevian, T. Astrocyte signaling controls spike timing-dependent depression at neocortical synapses. *Nat Neurosci* **15**, 746-53 (2012).
17. Sjostrom, P.J., Turrigiano, G.G. & Nelson, S.B. Rate, timing, and cooperativity jointly determine cortical synaptic plasticity. *Neuron* **32**, 1149-64 (2001).
18. Wittenberg, G.M. & Wang, S.S. Malleability of spike-timing-dependent plasticity at the CA3-CA1 synapse. *J Neurosci* **26**, 6610-7 (2006).
19. Edelmann, E. et al. Theta Burst Firing Recruits BDNF Release and Signaling in Postsynaptic CA1 Neurons in Spike-Timing-Dependent LTP. *Neuron* **86**, 1041-1054 (2015).
20. Jones, H.C. & Keep, R.F. Brain fluid calcium concentration and response to acute hypercalcaemia during development in the rat. *J Physiol* **402**, 579-93 (1988).
21. Silver, I.A. & Erecinska, M. Intracellular and extracellular changes of [Ca2+] in hypoxia and ischemia in rat brain in vivo. *J Gen Physiol* **95**, 837-66 (1990).
22. Shouval, H.Z., Bear, M.F. & Cooper, L.N. A unified model of NMDA receptor-dependent bidirectional synaptic plasticity. *Proc Natl Acad Sci U S A* **99**, 10831-6 (2002).
23. Graupner, M. & Brunel, N. Calcium-based plasticity model explains sensitivity of synaptic changes to spike pattern, rate, and dendritic location. *Proc Natl Acad Sci U S A* **109**, 3991-6 (2012).
24. Campanac, E. & Debanne, D. Spike timing-dependent plasticity: a learning rule for dendritic integration in rat CA1 pyramidal neurons. *J Physiol* **586**, 779-93 (2008).
25. Pike, F.G., Meredith, R.M., Olding, A.W. & Paulsen, O. Rapid report: postsynaptic bursting is essential for 'Hebbian' induction of associative long-term potentiation at excitatory synapses in rat hippocampus. *J Physiol* **518 (Pt 2)**, 571-6 (1999).
26. Murthy, V.N., Sejnowski, T.J. & Stevens, C.F. Heterogeneous release properties of visualized individual hippocampal synapses. *Neuron* **18**, 599-612 (1997).
27. Svoboda, K., Denk, W., Kleinfeld, D. & Tank, D.W. In vivo dendritic calcium dynamics in neocortical pyramidal neurons. *Nature* **385**, 161-5 (1997).
28. Brandalise, F., Carta, S., Helmchen, F., Lisman, J. & Gerber, U. Dendritic NMDA spikes are necessary for timing-dependent associative LTP in CA3 pyramidal cells. *Nat Commun* **7**, 13480 (2016).
29. Sabatini, B.L., Oertner, T.G. & Svoboda, K. The life cycle of Ca(2+) ions in dendritic spines. *Neuron* **33**, 439-52 (2002).
30. Lisman, J. A mechanism for the Hebb and the anti-Hebb processes underlying learning and memory. *Proc Natl Acad Sci U S A* **86**, 9574-8 (1989).
31. O'Connor, D.H., Wittenberg, G.M. & Wang, S.S. Graded bidirectional synaptic plasticity is composed of switch-like unitary events. *Proc Natl Acad Sci U S A* **102**, 9679-84 (2005).
32. Petersen, C.C., Malenka, R.C., Nicoll, R.A. & Hopfield, J.J. All-or-none potentiation at CA3-CA1 synapses. *Proc Natl Acad Sci U S A* **95**, 4732-7 (1998).
33. Antic, S.D., Zhou, W.L., Moore, A.R., Short, S.M. & Ikonomu, K.D. The decade of the dendritic NMDA spike. *J Neurosci Res* **88**, 2991-3001 (2010).
34. Fregnac, Y. et al. A Re-Examination of Hebbian-Covariance Rules and Spike Timing-Dependent Plasticity in Cat Visual Cortex in vivo. *Front Synaptic Neurosci* **2**, 147 (2010).
35. Karmarkar, U.R. & Buonomano, D.V. A model of spike-timing dependent plasticity: one or two coincidence detectors? *J Neurophysiol* **88**, 507-13 (2002).
36. Bidoret, C., Ayon, A., Barbour, B. & Casado, M. Presynaptic NR2A-containing NMDA receptors implement a high-pass filter synaptic plasticity rule. *Proc Natl Acad Sci U S A* **106**, 14126-31 (2009).
37. Bouvier, G. et al. Burst-Dependent Bidirectional Plasticity in the Cerebellum Is Driven by Presynaptic NMDA Receptors. *Cell Rep* **15**, 104-116 (2016).
38. Mehaffey, W.H. & Doupe, A.J. Naturalistic stimulation drives opposing heterosynaptic plasticity at two inputs to songbird cortex. *Nat Neurosci* **18**, 1272-80 (2015).
39. Bittner, K.C., Milstein, A.D., Grienberger, C., Romani, S. & Magee, J.C. Behavioral time scale synaptic plasticity underlies CA1 place fields. *Science* **357**, 1033-1036 (2017).

40. Hubbard, J.I. The effect of calcium and magnesium on the spontaneous release of transmitter from mammalian motor nerve endings. *J Physiol* **159**, 507-17 (1961).
41. Debanne, D., Guerineau, N.C., Gahwiler, B.H. & Thompson, S.M. Paired-pulse facilitation and depression at unitary synapses in rat hippocampus: quantal fluctuation affects subsequent release. *J Physiol* **491 (Pt 1)**, 163-76 (1996).
42. Kullmann, D.M., Perkel, D.J., Manabe, T. & Nicoll, R.A. Ca2+ entry via postsynaptic voltage-sensitive Ca2+ channels can transiently potentiate excitatory synaptic transmission in the hippocampus. *Neuron* **9**, 1175-83 (1992).

Figure 1 - Cartoon

A

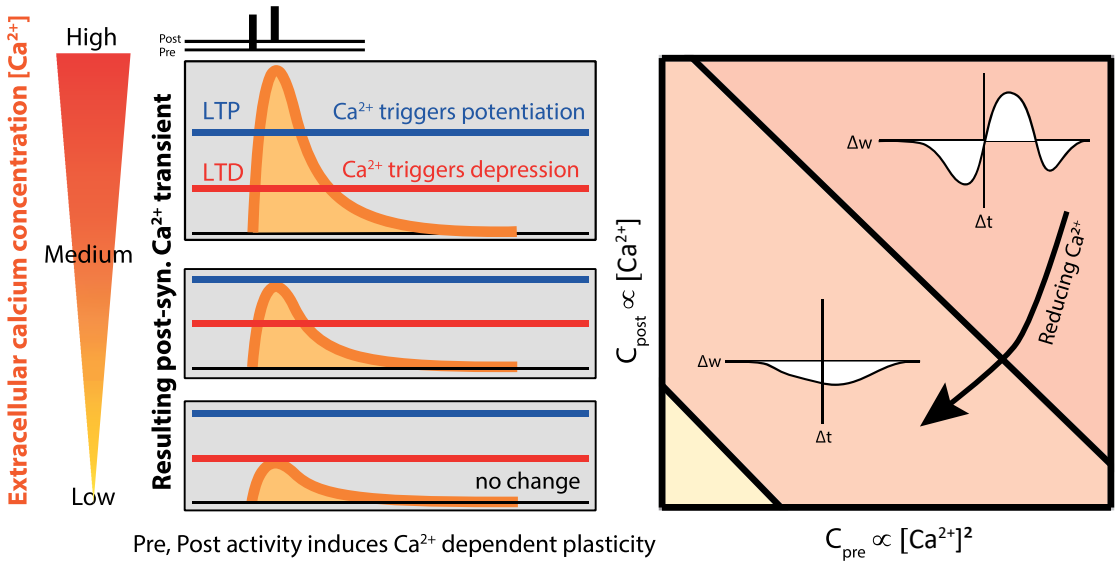

Pre, Post activity induces Ca^{2+} dependent plasticity

Figure 2. STDP Curves under various extracellular calcium concentration

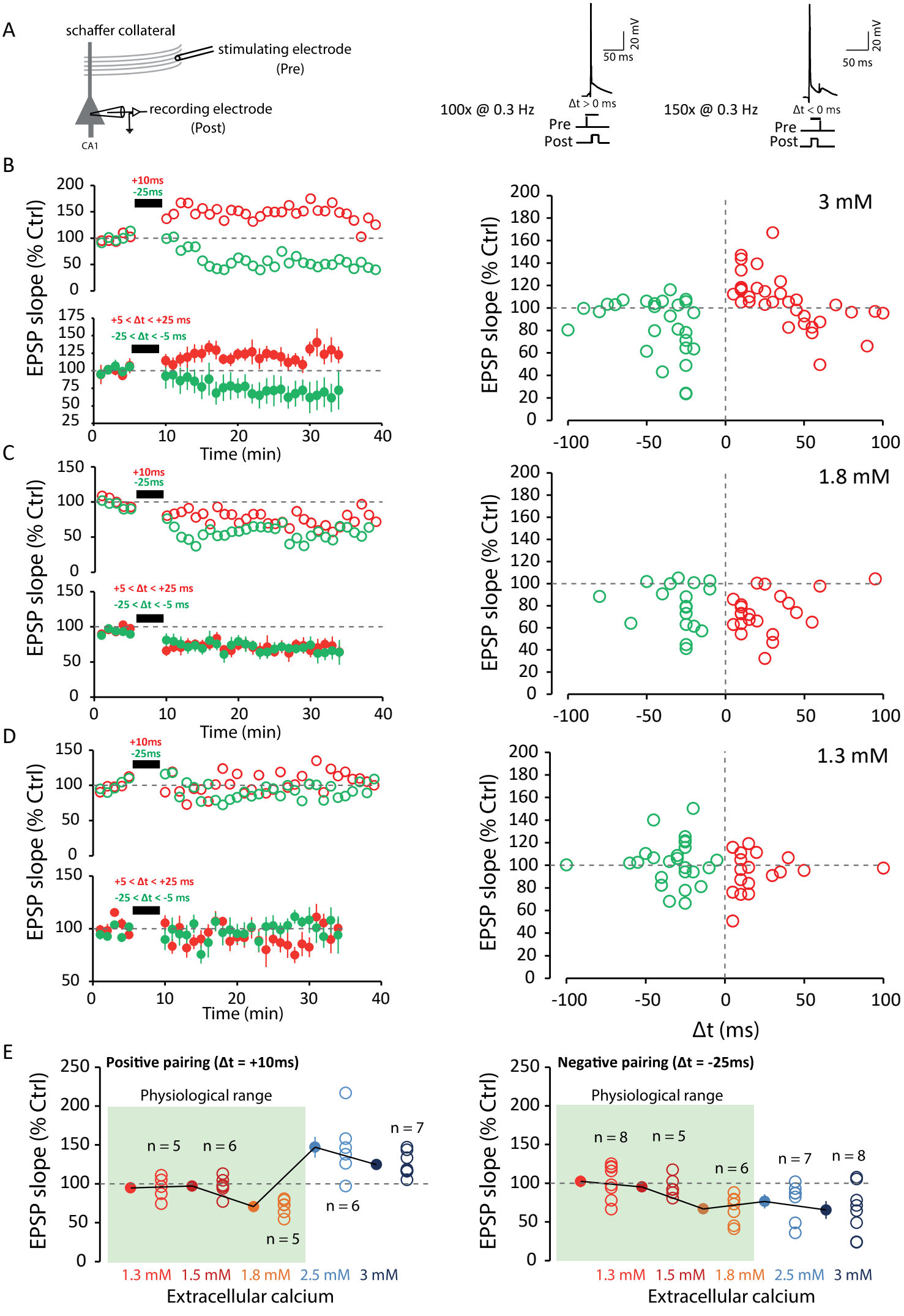

Figure 3. Burst and high frequency data

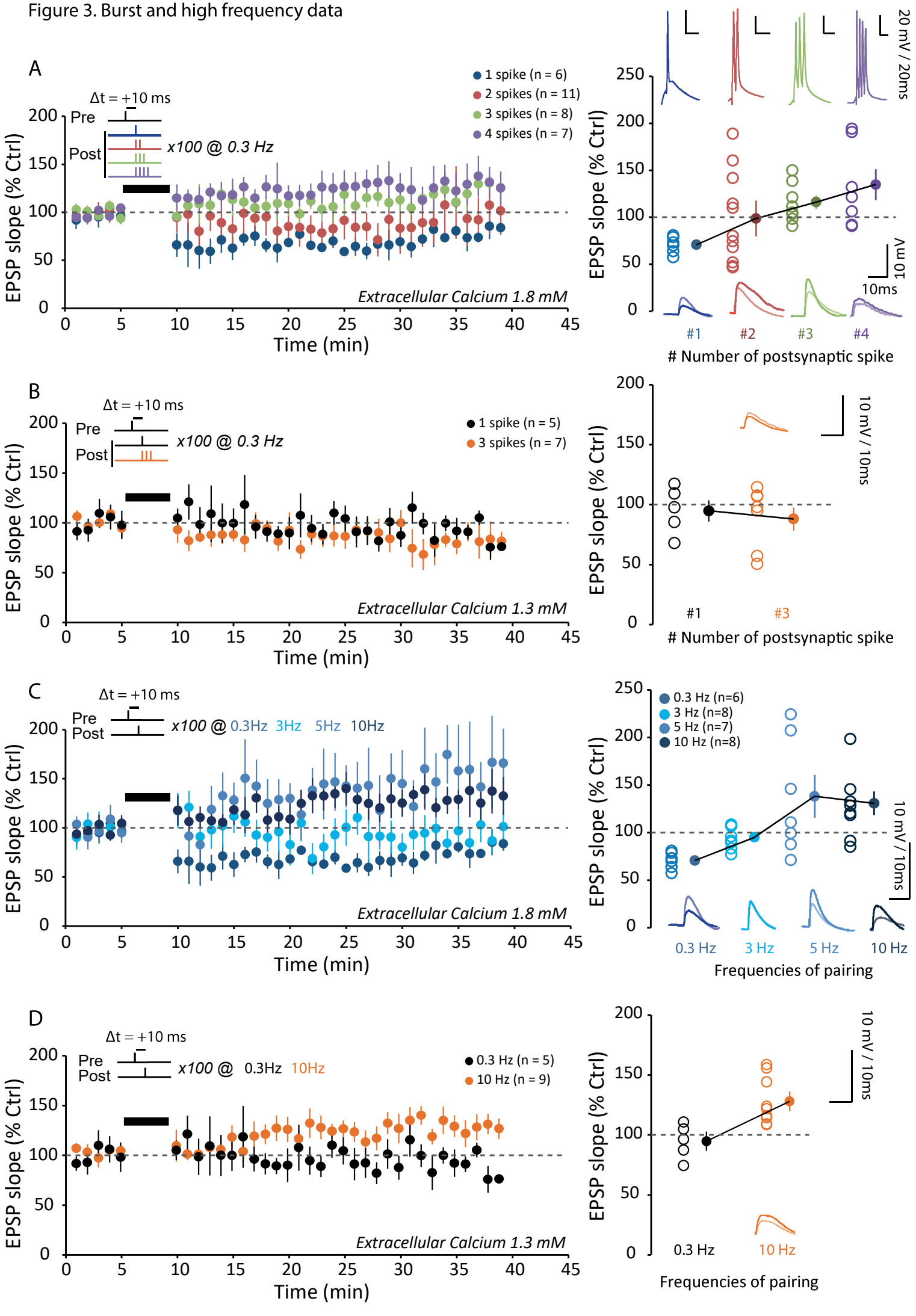

Figure 4. Increasing spike number or pairing frequency restores LTD in 1.3 mM Ca2+

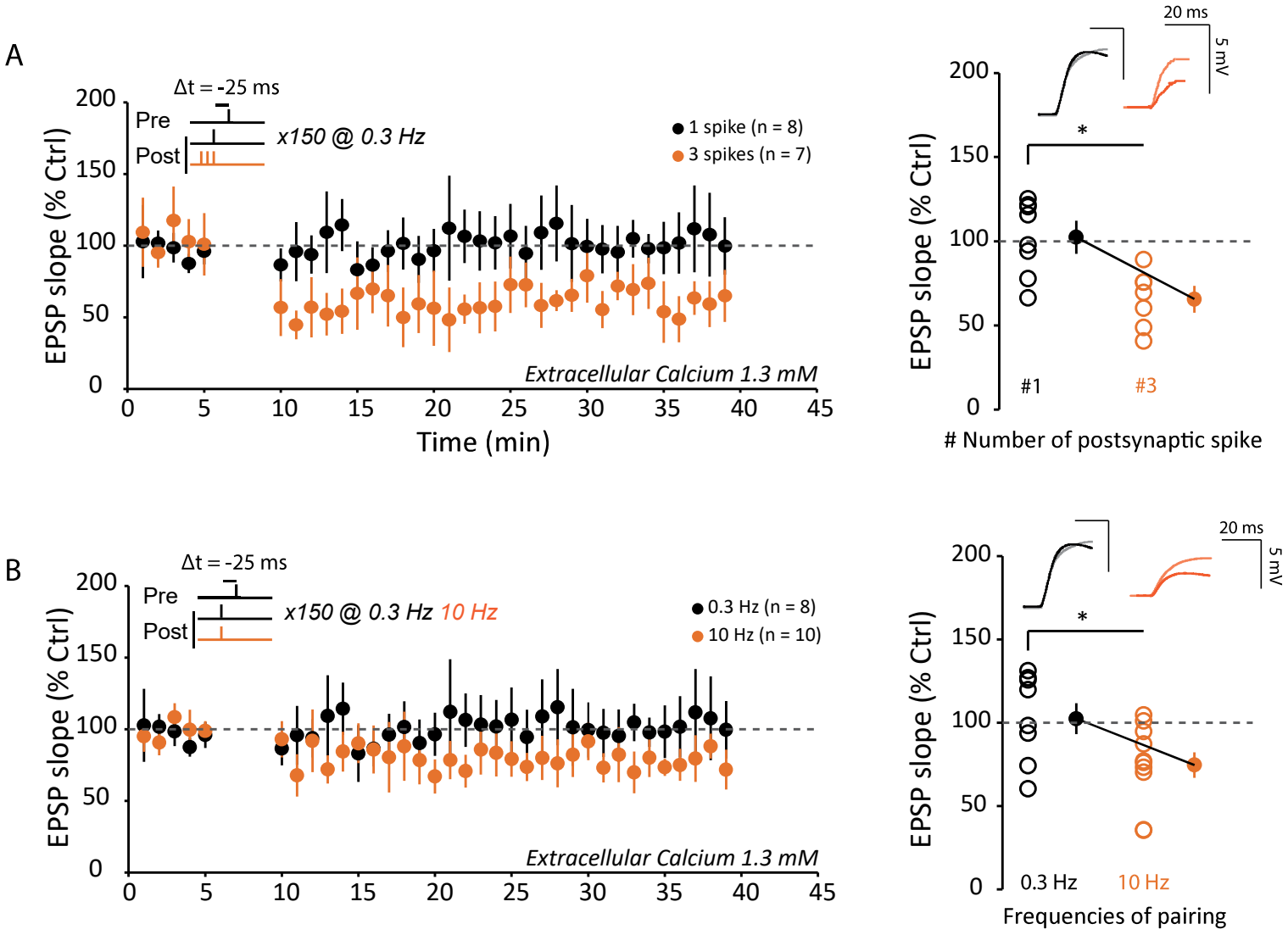

Figure 5. Models that include a contribution to calcium transients that is nonlinear in the pre- and postsynaptic activity can be fit well to spike-pair data for multiple extra-cellular calcium concentrations

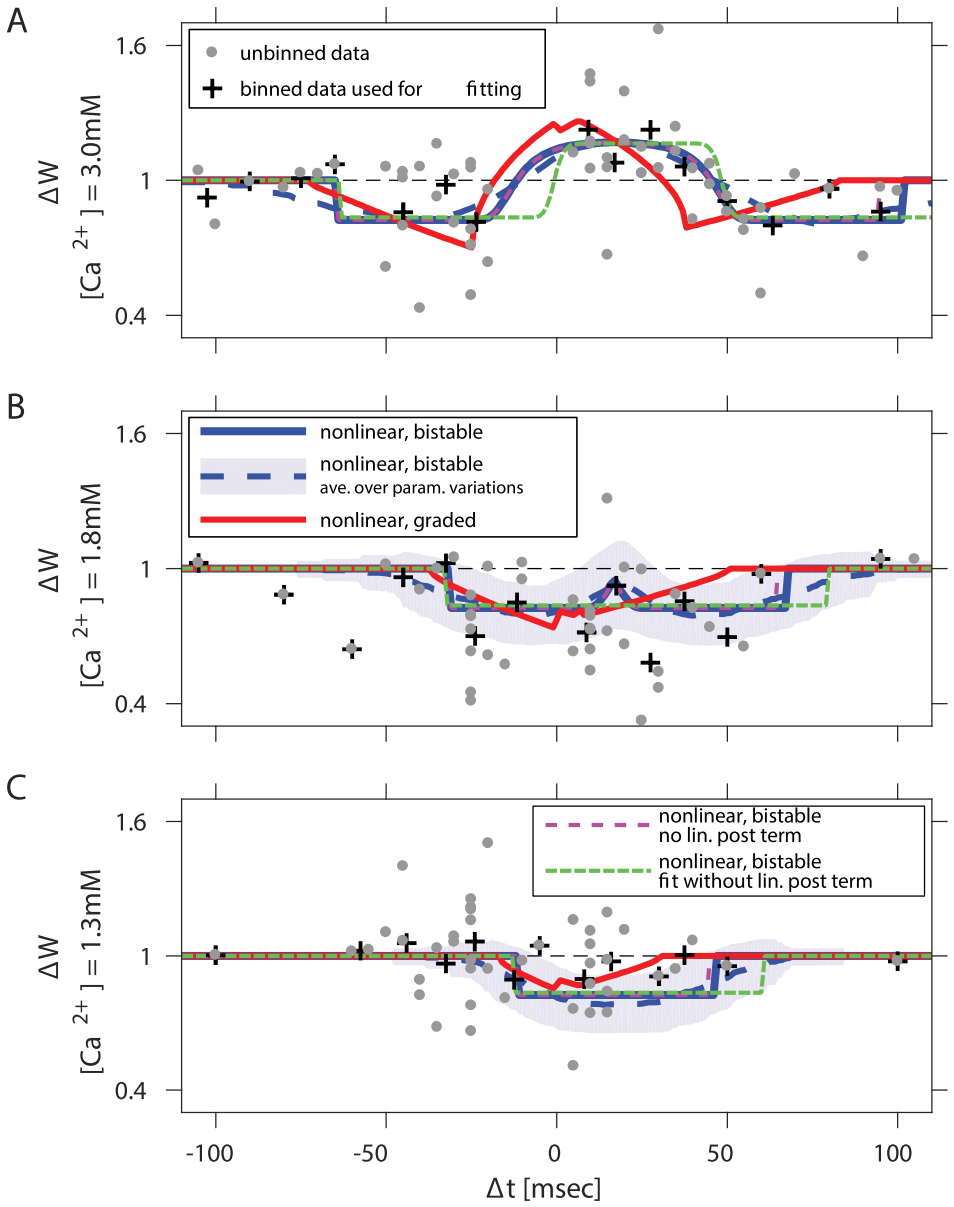

Figure 6. Nonlinear calcium-based models produce accurate fits to the plasticity measured using burst and high pairing-frequency protocols.

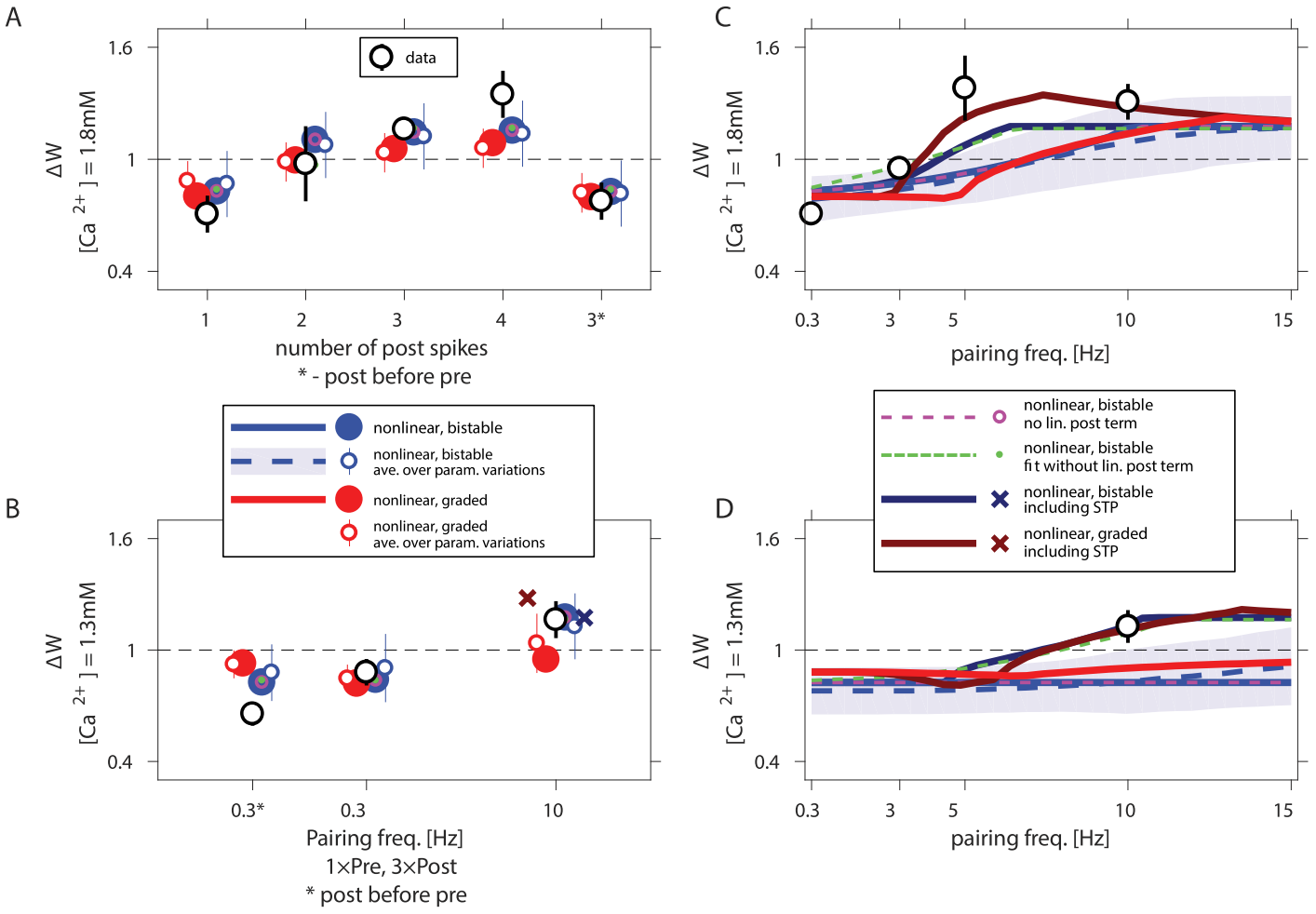

Supplementary Text, Figures and Tables(4/18)

Model fitting

We fit the calcium based plasticity model to the binned experimental STDP curves at three calcium concentrations using the procedure described below. The central part of the fitting procedure is to mathematically express the relative change in synaptic efficacy Δw as a function of the induction protocol, the extra-cellular calcium concentration $[Ca^{2+}]$ and the model parameters.

The function Δw is computed in two steps as a function of these variables. First we compute the time the intra-cellular calcium variable $c(t)$ spends above the depression and potentiation thresholds: T_d and T_p, respectively. In the second step we use T_d, T_p and the rest of the variables and parameters to compute Δw.

Computation of calcium transients and time spent above threshold

The calcium transient $c(t)$ is a sum of three contributions: pre-synaptic, post-synaptic and nonlinear, unless noted otherwise. The contributions to the total calcium transient evolve according to the differential equations:

$$\frac{d}{dt}c_{\text{pre}}(t) = -\frac{1}{\tau_{\text{Ca}}}c_{\text{pre}}(t) + C_{\text{pre}}s_{\text{pre}}(t-D) \quad (1)$$

$$\frac{d}{dt}c_{\text{post}}(t) = -\frac{1}{\tau_{\text{Ca}}}c_{\text{post}}(t) + C_{\text{post}}s_{\text{post}}(t) \quad (2)$$

$$\frac{d}{dt}c_{\text{NL}}(t) = -\frac{1}{\tau_{\text{Ca,NMDA}}}c_{\text{NL}}(t) + \eta c_{\text{pre}}(t)c_{\text{post}}(t) \quad (3)$$

Where $C_{\text{pre}}, C_{\text{post}}$ are the pre- and post-synaptic amplitude parameters, $s_{\text{pre}}(t) = \sum_{t_{\text{pre}}}\delta(t-t_{\text{pre}})$, $s_{\text{post}}(t) = \sum_{t_{\text{post}}}\delta(t-t_{\text{post}})$ are the pre- and post-synaptic spike trains (i.e., sums over Dirac-delta functions centered at the spike times), D is the delay parameter and η is the nonlinearity parameter.

For induction protocols with low pairing frequencies one can assume that the transient calcium returns to baseline before each repetition. This assumption holds for a paring frequency of 0.33Hz used for most of our measurements (and *all* the data used for model fitting purposes), making it sufficient to compute transients for a single repetition of each protocol. Furthermore, when a protocol consists of a single pre- and a single post-synaptic spike occurring at $t = 0$, $t = \Delta t$, respectively, Eqs. (1-3) can be solved analytically:

$$c_{\text{pre}}(t) = \Theta(t-D)C_{\text{pre}}\exp\left(-\frac{t-D}{\tau_{\text{Ca}}}\right) \quad (4)$$

$$c_{\text{post}}(t) = \Theta(t-\Delta t)C_{\text{pre}}\exp\left(-\frac{t-\Delta t}{\tau_{\text{Ca}}}\right) \quad (5)$$

$$c_{\text{NL}}(t) = \Theta\left(t-\max(D,\Delta t)\right)\tilde{\tau}_{\text{Ca}}\eta C_{\text{pre}}C_{\text{post}}\exp\left(-\frac{t}{\tau_{\text{Ca,NMDA}}}+\frac{D+\Delta t}{\tau_{\text{Ca}}}\right)\left[\exp\left(-\frac{\max(D,\Delta t)}{\tilde{\tau}_{\text{Ca}}}\right)-\exp\left(-\frac{t}{\tilde{\tau}_{\text{Ca}}}\right)\right] \quad (6)$$

Here $\Theta(\cdot)$ is the Heaviside step function and $\tilde{\tau}_{\text{Ca}}$ is the effective time constant:

$$\tilde{\tau}_{\text{Ca}} = \frac{1}{\frac{2}{\tau_{\text{Ca}}}-\frac{1}{\tau_{\text{Ca,NMDA}}}}. \quad (7)$$

The calcium transient was computed using these expressions:

$$c(t) = c_{\text{pre}}(t) + c_{\text{post}}(t) + c_{\text{NL}}(t), \quad (8)$$

with temporal resolution $dt = 0.25$ms.

For protocols with a post-synaptic burst of spikes, c_{post} and c_{NL} were computed by replacing Δt in Eqs (5,6) with the times of the spikes in the post-synaptic burst (relative to the pre-synaptic spike at $t = 0$) and summing over all the spikes in the burst of the post-synaptic neuron[1].

[1]This is only valid because there was a single pre-synaptic stimulation in every repetition of the induction protocol. Had there been more than a single pre-synaptic stimulation then computing c_{NL} requires solving Eqs. (4-6) explicitly.

For protocols with high pairing frequency where the calcium transient does not necessarily return to baseline following each repeat of the induction protocol, the transients were computed using the Euler method with time-step $dt = 0.25$ms. Using a smaller time-steps made fitting considerably slower but it did not change the results.

The time spent above the depression and potentiation thresholds (during each repeat of the induction protocol of duration T) is then

$$T_d = \int_0^T \Theta(c(t) - \theta_d)dt \tag{9}$$

$$T_p = \int_0^T \Theta(c(t) - \theta_p)dt. \tag{10}$$

The integrals were approximated by counting temporal bins in which $c(t)$ exceeded the threshold and multiplying by dt. Note that for the linear model ($\eta = 0$), T_d and T_p can be computed analytically (see Graupner and Brunel, 2012).

Computation of Δw

Graded model. Recall that for models with graded dynamics the synaptic weight variable evolves according to

$$\frac{d}{dt}\rho(t) = \gamma_p(1 - \rho(t))\Theta\left[c(t) - \theta_p\right] - \gamma_d\rho(t)\Theta\left[c(t) - \theta_d\right]. \tag{11}$$

From this, one can show that if the initial value $\rho_(t = 0) = \rho_0$ and the protocol is repeated n times, the synaptic weight variable at the end of the protocol $\rho_f = \rho(t = nT)$ is

$$\rho_f = \bar{\rho} + (\rho_0 - \bar{\rho})\exp(-n/\tau_{\text{eff}}), \tag{12}$$

where

$$\bar{\rho} = \frac{\gamma_p T_p}{\gamma_p T_p + \gamma_d T_d} \tag{13}$$

$$\tau_{\text{eff}} = \frac{T}{\gamma_p T_p + \gamma_d T_d}. \tag{14}$$

The relative change in synaptic efficacy as a function of the protocol and the model parameters is simply

$$\Delta w = \rho_f/\rho_0. \tag{15}$$

Bistable model. The bistable model is stochastic, so computing the change in synaptic efficacy relies on averaging over the transition probabilities from the down to the up state, and vice versa. These probabilities in turn depend on the time spent above the depression and potentiation thresholds explained above.

We use the exact same expressions as in Graupner and Brunel to compute Δw given T_d and T_p. We include these expressions here for completeness but refer the reader to that paper for a detailed explanation of the full derivation.

Here ρ evolves according to

$$\tau\frac{d}{dt}\rho(t) = -\frac{\partial}{\partial\rho}U[\rho(t)] + \gamma_p(1 - \rho(t))\Theta\left[c(t) - \theta_p\right] - \gamma_d\rho(t)\Theta\left[c(t) - \theta_d\right] + \sigma\sqrt{\tau}\xi(t) \tag{16}$$

$$U(\rho) = \frac{1}{4}\rho^2(1 - \rho)^2. \tag{17}$$

The distribution of the synaptic weight variable ρ at time t is

$$P\left(\rho, t|\rho_0\right) = \frac{1}{\sqrt{\pi\sigma_\rho^2\left[1 - \exp\left(-\frac{2t}{\tau_{\text{eff}}}\right)\right]}}\exp\left\{-\frac{\left(\rho - \bar{\rho} + (\bar{\rho} - \rho_0)\exp\left(-\frac{t}{\tau_{\text{eff}}}\right)\right)^2}{\sigma_\rho^2\left[1 - \exp\left(-\frac{2t}{\tau_{\text{eff}}}\right)\right]}\right\} \tag{18}$$

$$\sigma_\rho^2 = \frac{\sigma^2\left(T_p + T_d\right)}{\gamma_p T_p + \gamma_d T_d} \tag{19}$$

$$\tau_{\text{eff}} = \frac{\tau T}{\gamma_p T_p + \gamma_d T_d} \tag{20}$$

Note that the setting $\tau = 1$ gives an effective time constant for the bistable model (Eq. 20) that is equal to the one for the graded model (Eq. 14).

The probability $\mathcal{U}$ that the system will converge to the up state is the integral over this distribution from the potential's unstable fixed point ($rho^\star = 1/2$ in our case) to $+\infty$. Similarly, the probability $\mathcal{D}$ that the system will converge to the down state is the integral over this distribution from $-\infty$ to the unstable fixed point:

$$\mathcal{U} = \frac{1}{2}\left[1 + \mathrm{erf}\left(-\frac{\left(\rho_\star - \bar{\rho} + (\bar{\rho} - \rho_0)\exp\left(-\frac{nT}{\tau_{\mathrm{eff}}}\right)\right)^2}{\sigma_\rho^2\left[1 - \exp\left(-\frac{2nT}{\tau_{\mathrm{eff}}}\right)\right]}\right)\right] = 1 - \mathcal{D}. \tag{21}$$

To relate these quantities to Δw, recall the parameter b– the ratio of the synaptic efficacy in the up state ($w_{\mathcal{U}}$) and down state ($w_{\mathcal{D}}$). The efficacy at the end of the protocol is $w = w_{\mathcal{D}} + \rho(w_{\mathcal{U}} - w_{\mathcal{D}})$. Given b and β, the fraction of synapses initially in the down state ($\beta = 1/2$ under our assumptions), Δw is

$$\Delta w = \frac{[(1-\mathcal{U}) + \mathcal{D}(1-\beta)] + b\,[\mathcal{U}\beta + (1-\mathcal{D})(1-\beta)]}{\beta + (1-\beta)b} \tag{22}$$

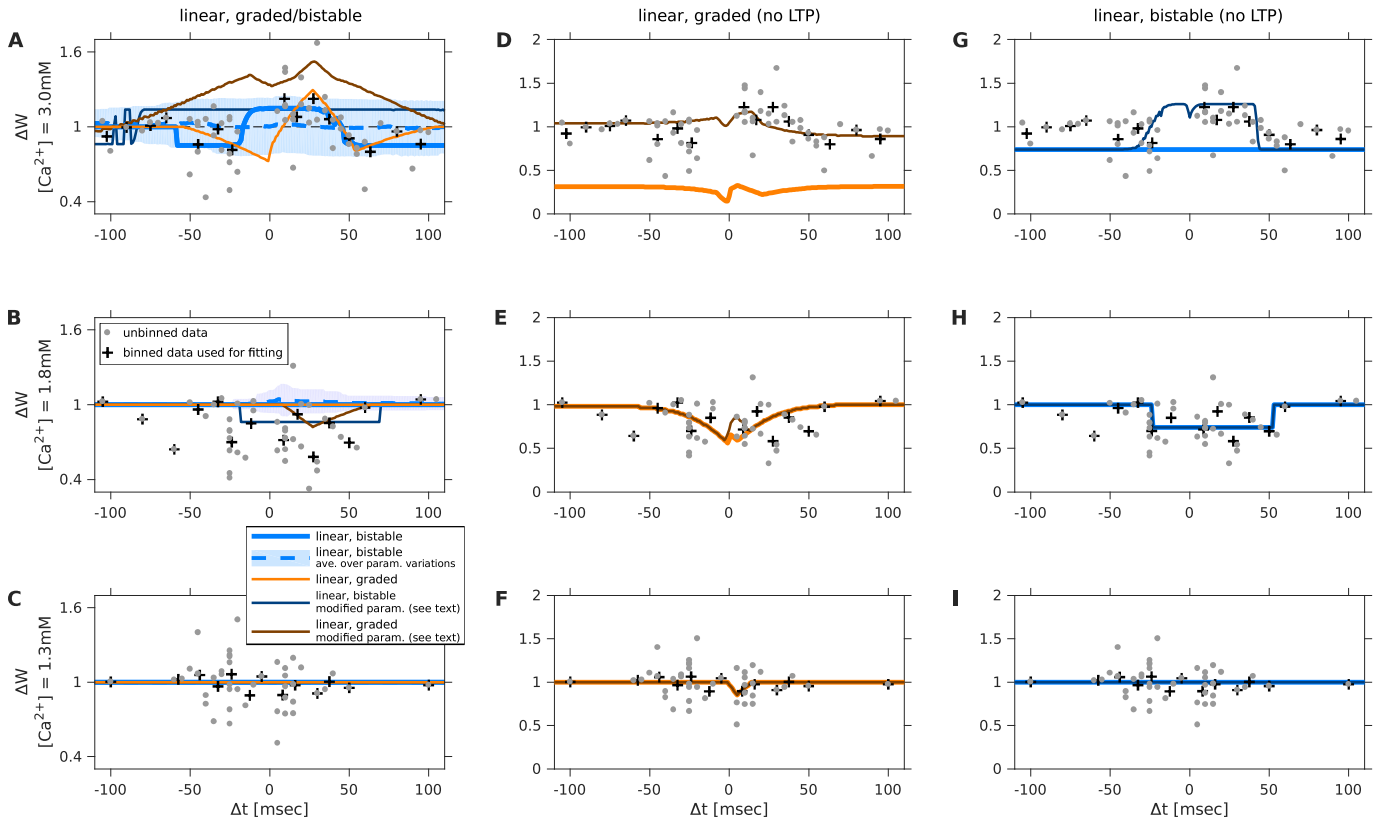

Figure S1: **Models without a nonlinear NMDA term contributing to calcium transients do not fit the STDP data at multiple [Ca^{2+}] concentrations.** (**A-C**) Fits to the STDP data at [Ca^{2+}] = 3, 1.8, 1.3mM for a graded (orange) and bistable (light blue) models in which the calcium transient depends linearly on the pre- and post-synaptic activity. The models are able to fit relatively well the depression-potentiation-depression shape of the STDP curve at [Ca^{2+}] = 3mM. However the scaling of the amplitdue parameters C_{pre}, C_{post} with [Ca^{2+}] implies that at a concentration of 1.8mM the model predicts no plasticity. When the best fitting amplitude parameters are increased by a factor of 1.55 while the rest of the parameters stay the same (brown for the graded model, dark blue for the bistable model) the depression [Ca^{2+}] = 1.8mM is reproduced, but the STDP curve at 3mM qualitatively differs from the experimental results. (**D-F**) Fits to the STDP data for a graded with no LTP yield good fits at [Ca^{2+}] = 1.3, 1.8mM but, by definition, cannot reproduce the experimental results at 3mM (orange lines). "Manually" reinserting LTP into the model by setting $\theta_p = 1.6$ and $\gamma_p = 2\gamma_d$ produces predictions for the STDP curve that strongly disagree with the experiments (brown line). (**G-I**) same as (**D-F**) for a bistable model without LTP (light blue) and a model where LTP is reinserted manually (dark blue). The failure of multiple versions of the linear calcium based model supporting the notion that a nonlinear term is necessary to fit the data.

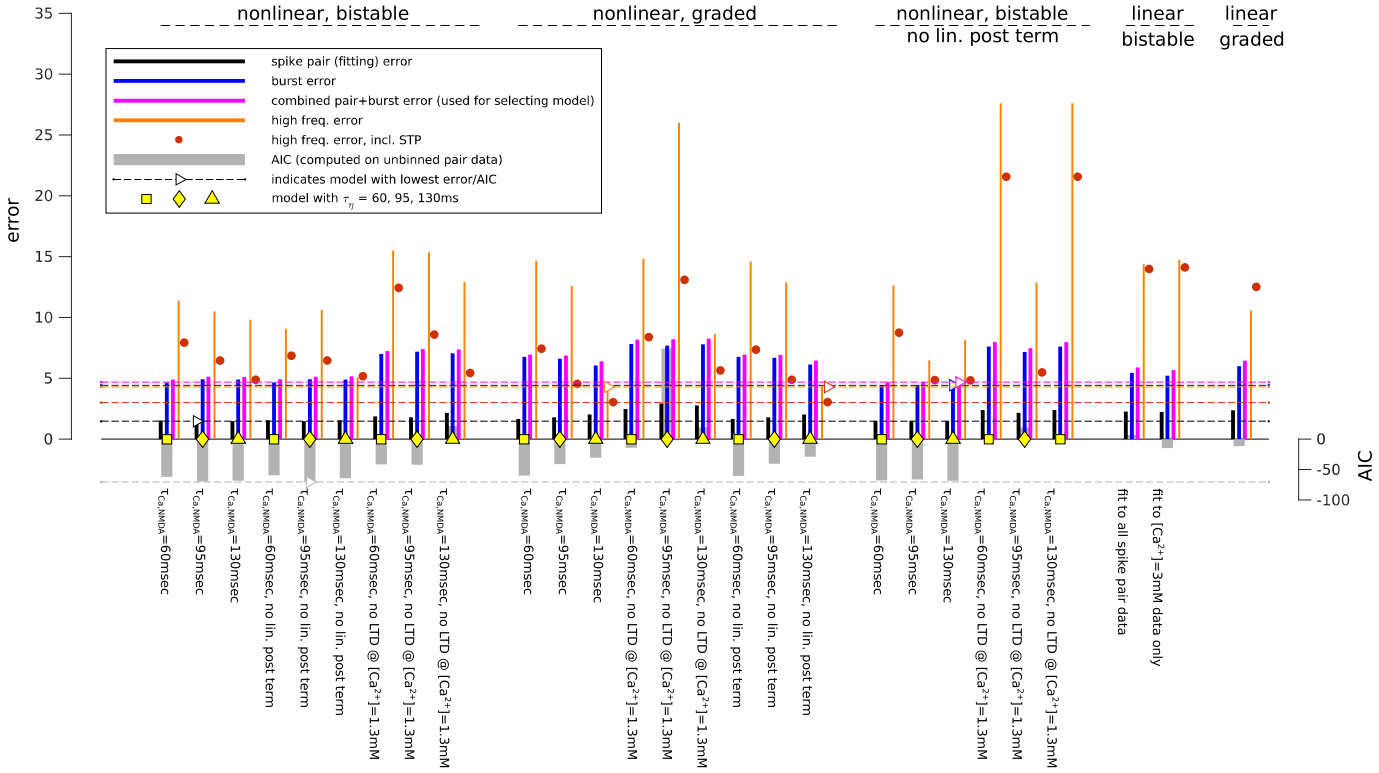

Figure S2: **Summary statistics for models with quadratic (linear) scaling of the pre- (post-) synaptic calcium amplitude.** Bar plots show the fitting errors on pair data (black), errors for burst data (blue), total error (on pair and burst data, magenta), error on high pairing frequency data (orange and red for models with and without short-term plasticity, respectively) and the model selection criterion AIC (gray). Results are shown for (from left to right) nonlinear, bistable models with multiple values of the timescale of the NMDA nonlinearity $\tau_{\mathrm{Ca,NMDA}}$, models where the linear post-synaptic contribution was set to 0 "manually" and models constrained to show no LTD at $[Ca^{2+}] = 1.3$mM; nonlinear, graded models with the same variations as the bistable model; nonlinear bistable models fit without a linear post-synaptic term contributing to calcium transients; linear, bistable and a linear, graded model. The model with the lowest error (of each "type") and the lowest AIC is indicated by a white triangle.

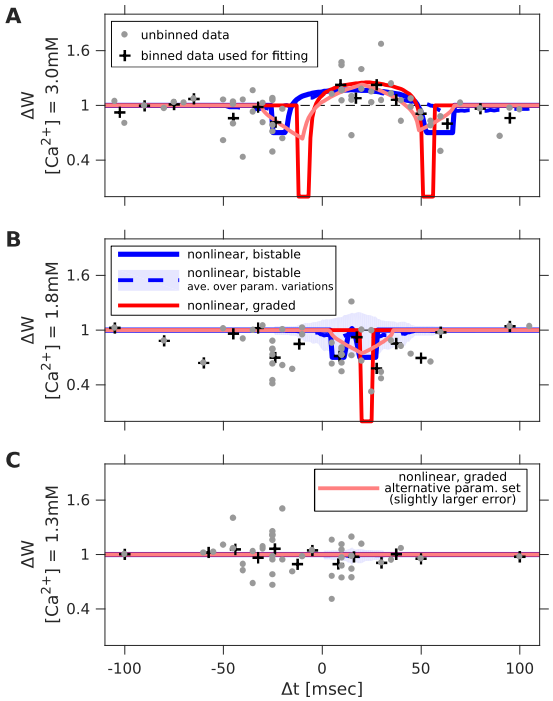

Figure S3: **Nonlinear models contrained to show no LTD at [Ca^{2+}] = 1.3mM.** (**A-C**) Fits to the STDP data at [Ca^{2+}] = 3, 1.8, 1.3mM for graded (red) and bistable (blue) models where the pre- and postsynaptic transient amplitude parameters C_{pre}, C_{post} and the nonlinearity parameter η are constrained such that there is no LTD at [Ca^{2+}] = 1.3mM. The constraint implies poor fits to both the intermediate concentration where STDP was measured (**B**, [Ca^{2+}] = 1.8mM), where the window for inducing depression was substanstially wider in the experiment than in the model. The graded model that satisfies this constraint has two narrow windows for inducing very strong LTD. This parameter set was found since the fitting error is essentially unaffected by this feature. Plotting the STDP curve for a model with slightly larger fitting error (pink) shows that the failure to qualitatively match the data while satisfying the constraint at [Ca^{2+}] = 1.3mM is not caused by problems with the fitting procedure.

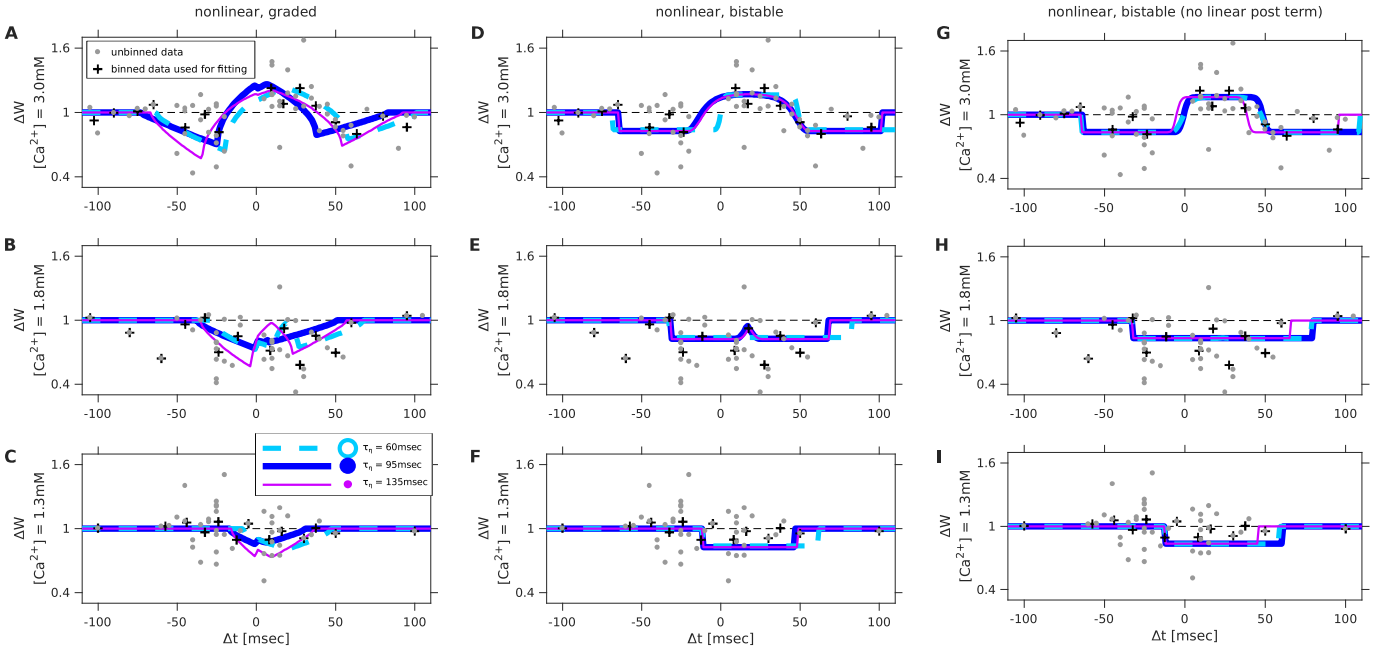

Figure S4: **Nonlinear models can be fit well to spike-pair data for a range of nonlinear decay time-scales.** (**A-C**) Fits to the STDP data at $[Ca^{2+}] = 3$, 1.8, 1.3mM for graded models with multiple values of the decay timescale of the nonlinear contribution to the calcium transients ($\tau_{\mathrm{Ca,NMDA}} = 60$, 95 130ms shown in light blue, blue and magenta, respectively). The longer this timescale is, the wider the window is for inducing potentiation/depression. The qualitative shape of the curve does not change. (**D-F**) same as (**A-C**) for a nonlinear, bistable model. (**G-I**) same as (**A-C**) for a nonlinear, bistable model with no linear post-synaptic contribution to the calcium transients.

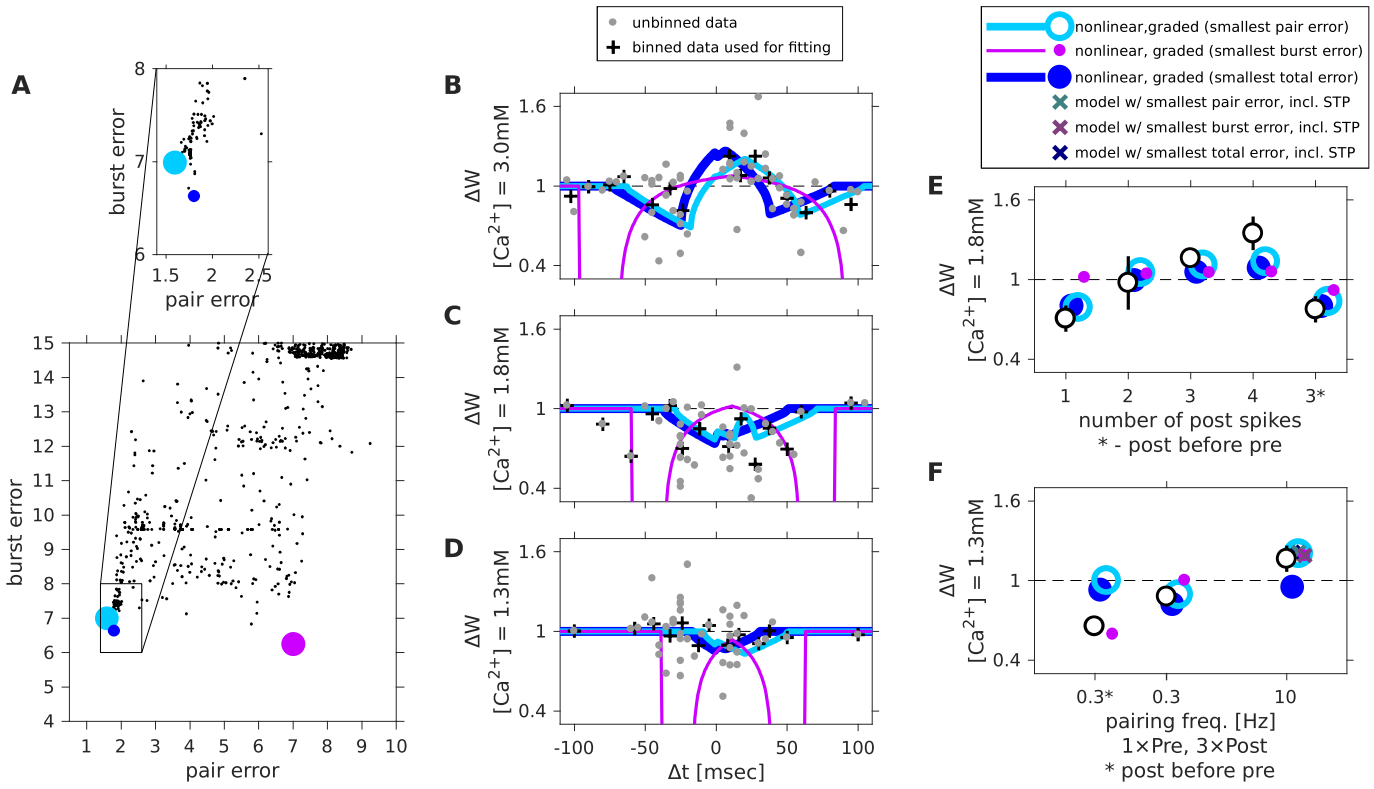

Figure S5: **Nonlinear graded models with smallest spike-pair, burst and combined errors.** Error values and predictions for nonlinear, graded models with smallest spike-pair data errors, combined error and error for burst data only are shown in light blue, blue and magenta, respecitively. (**A**) For each random initialization of the optimization procedure we plot the final fitting error (horizontal axis) and the prediction error for burst data given by that parameter set (vertical axis). The parameter set at the global minimum of the spike-pair error surface (light blue) yields a prediction associated with pair and burst errors close to a model with smallest total error (blue). (**B-D**) STDP curves at $[Ca^{2+}] = 3$, 1.8, 1.3mM for the model with smallest spike-pair error is very similar to that with the smallest total error. (**E**) At $[Ca^{2+}] =$ 1.8mM, both the model with smallest spike-pair error and the one with smallest total error match well the burst data. (**F**) At $[Ca^{2+}] = 1.3$mM, the model with smallest spike-pair error does not accurately predict the plasticity resulting from a burst of three post-synaptic spikes before a pre-synaptic spike at a low pairing frequency. The model with smallest combined error fails to predict the effect of a burst of post-synaptic spikes after a pre-synaptic spike at a high pairing frequency, but this discrepancy is eliminated when taking into account the effect of short-term plasticity (dark blue). For all models shown, $\tau_{\mathrm{Ca,NMDA}}$=95msec.

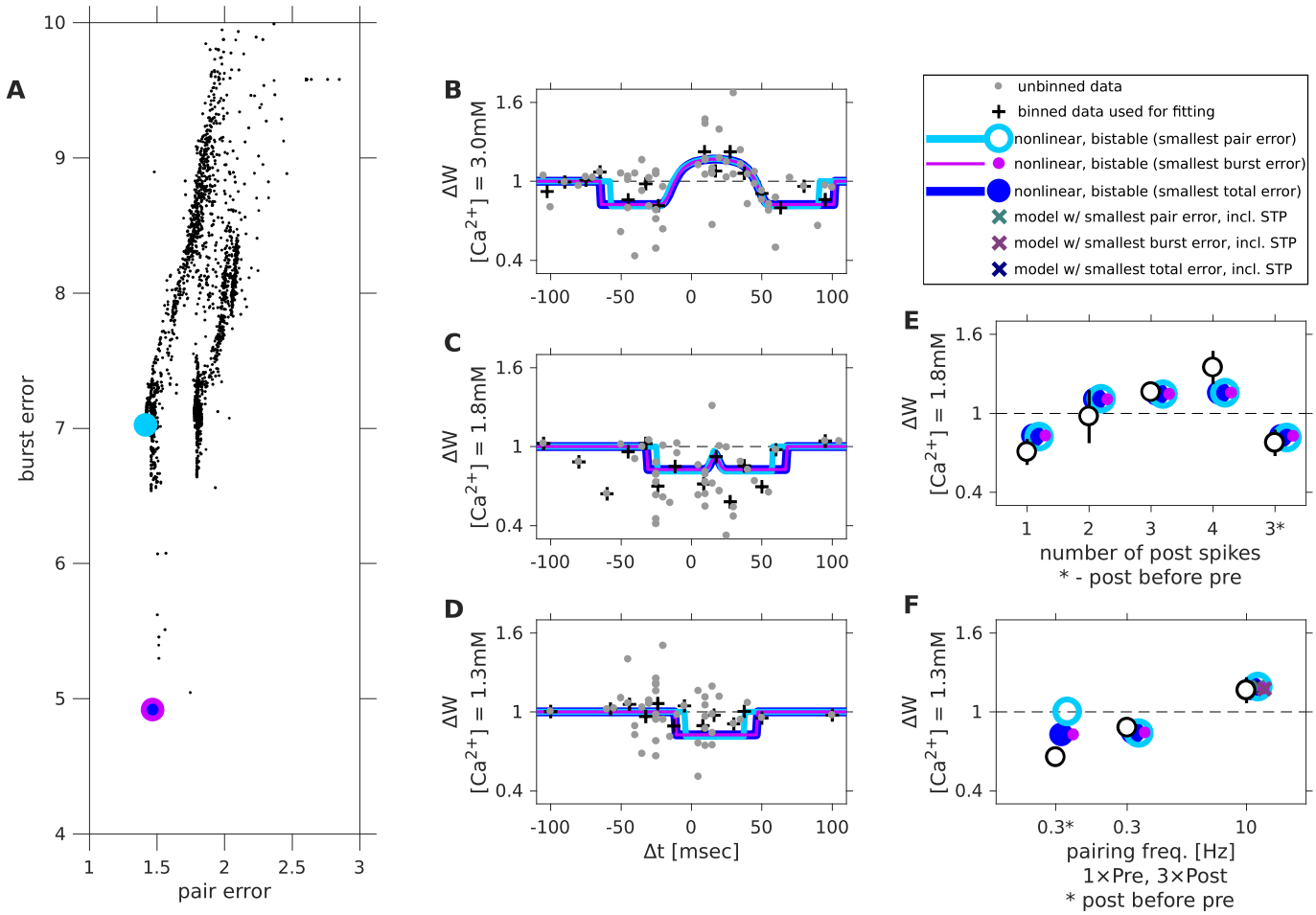

Figure S6: **Nonlinear bistable models with smallest spike-pair, burst and combined errors.** Error values and predictions for nonlinear, bistable models with smallest spike-pair data errors, combined error and error for burst data only are shown in light blue, blue and magenta, respecitively. (**A**) For each random initialization of the optimization procedure we plot the final fitting error (horizontal axis) and the prediction error for burst data given by that parameter set (vertical axis). The parameter set with the smallest combined error has a fitting error that is very close to the global minimum. (**B-D**) STDP curves at $[Ca^{2+}] = 3$, 1.8, 1.3mM for the model with smallest spike-pair error is very similar to that with the smallest total error. (**E**) At $[Ca^{2+}] = 1.8$mM, the model with smallest spike-pair error and the one with smallest total error yield essentially identical predictions to the burst protocols that match well the experimental results. (**F**) At $[Ca^{2+}] = 1.3$mM, the model with smallest spike-pair error does not accurately predict the plasticity resulting from a burst of three post-synaptic spikes before a pre-synaptic spike at a low pairing frequency. The model with smallest combined error correctly reproduces the LTD found under that condition. For all models shown, $\tau_{Ca,NMDA}$=95msec.

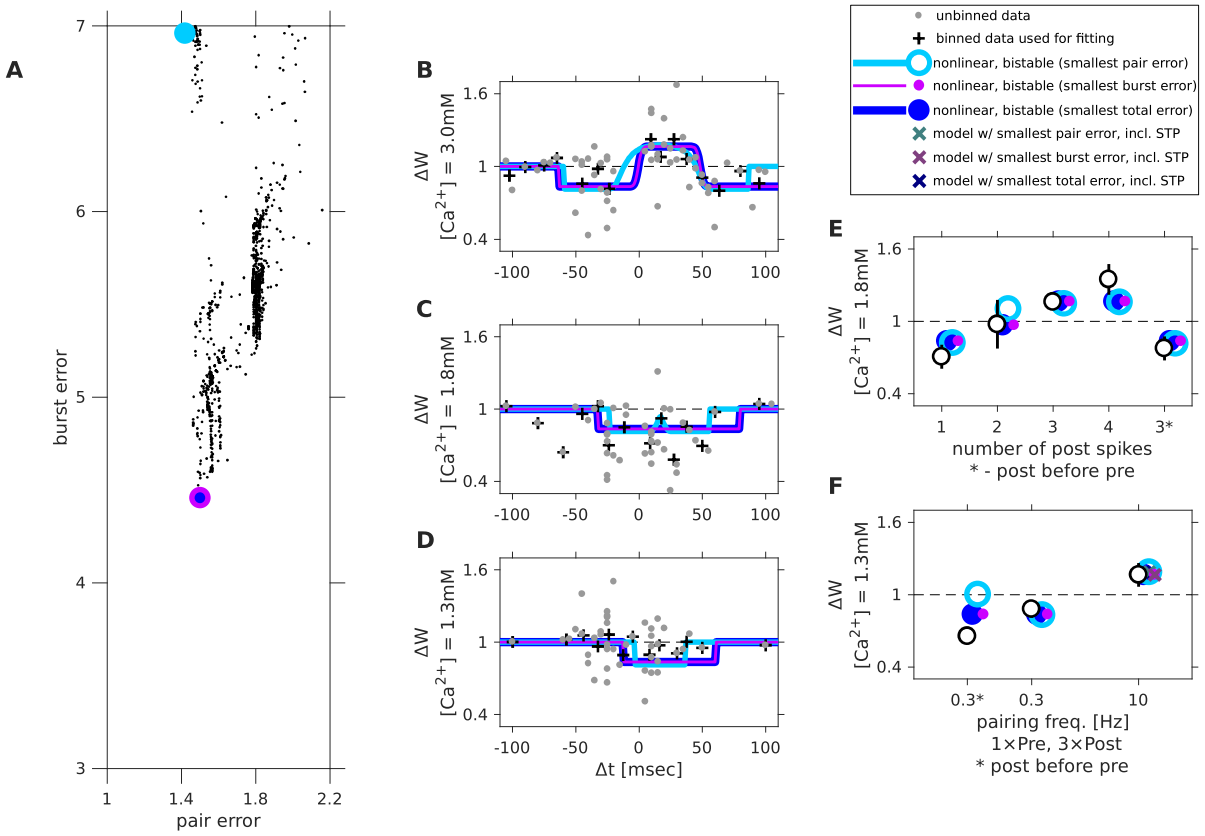

Figure S7: **Nonlinear bistable models without a linear post-synaptic term contributing to calcium transients, that have the smallest spike-pair, burst and combined errors.** Error values and predictions for nonlinear, bistable models without linear post-synaptic term, that have the smallest spike-pair data errors, combined error and error for burst data only are shown in light blue, blue and magenta, respecitively. (**A**) For each random initialization of the optimization procedure we plot the final fitting error (horizontal axis) and the prediction error for burst data given by that parameter set (vertical axis). The parameter set with the smallest combined error has a fitting error that is very close to the global minimum. (**B-D**) STDP curves at $[Ca^{2+}] = 3$, 1.8, 1.3mM for the model with smallest spike-pair error is very similar to that with the smallest total error. (**E**) At $[Ca^{2+}] = 1.8$mM, the model with smallest spike-pair error and the one with smallest total error yield essentially identical predictions to the burst protocols that match well the experimental results. (**F**) At $[Ca^{2+}] = 1.3$mM, the model with smallest spike-pair error does not accurately predict the plasticity resulting from a burst of three post-synaptic spikes before a pre-synaptic spike at a low pairing frequency. The model with smallest combined error correctly reproduces the LTD found under that condition. For all models shown, $\tau_{Ca,NMDA}$=95msec.

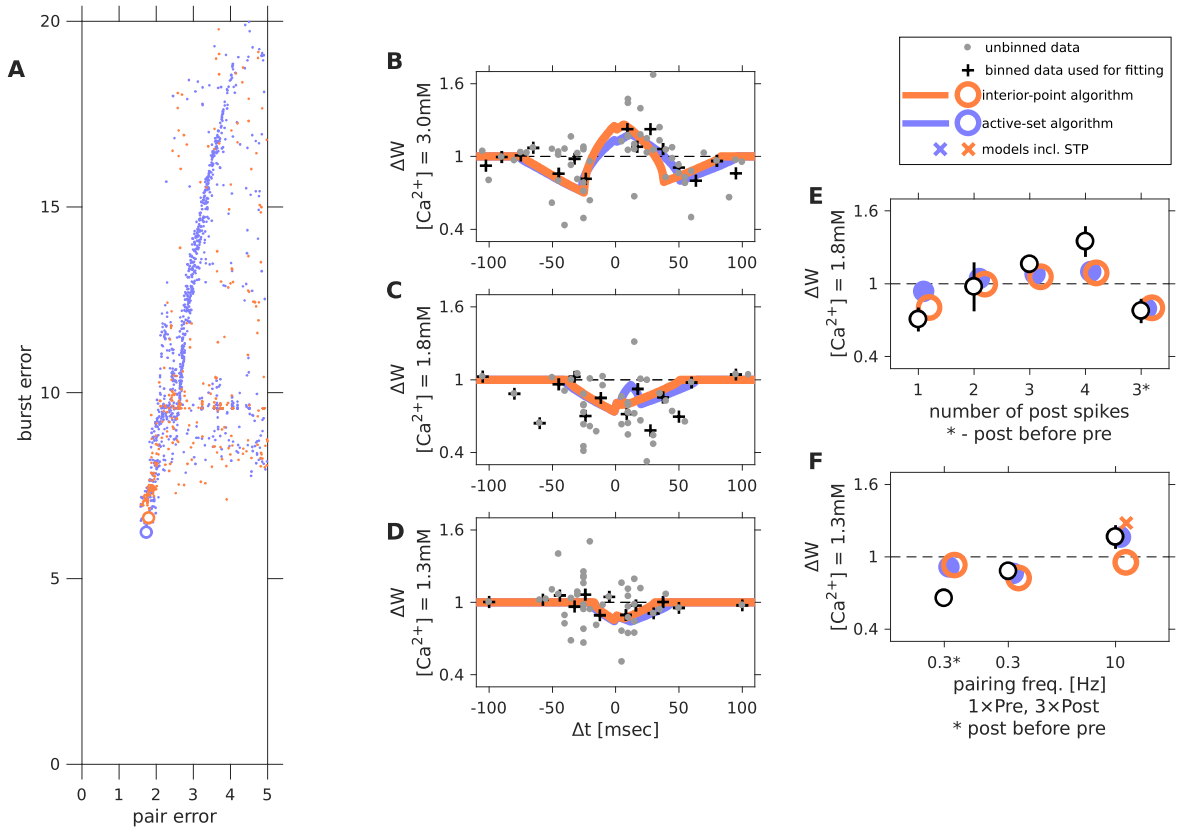

Figure S8: **Nonlinear graded models fit using different numerical optimization algorithms.** We fit the nonlinear, graded model using the interior-point (orange) and the active-set (purple) optimization methods (built-in to the MATLAB software). (**A**) For each random initialization of the optimization procedure we plot the final fitting error (horizontal axis) and the prediction error for burst data given by that parameter set (vertical axis). (**B-D**) STDP curves at $[Ca^{2+}] = 3$, 1.8, 1.3mM for models with smallest combined spike-pair and burst errors fit using the two algorithms. The parameter set found using the active-set algorithm (with the smallest combined spike-pair and burst error) corresponds to a STDP curve with a very wide window for induction of plasticity, extending beyond $\Delta t = 110$msec and thus a substantially larger fitting error. (**E-F**) At $[Ca^{2+}] = 1.8$, 1.3mM, the models fit using both algorithms produce predictions that match well the experimental measurements. For all models shown, $\tau_{Ca,NMDA}$=95msec.

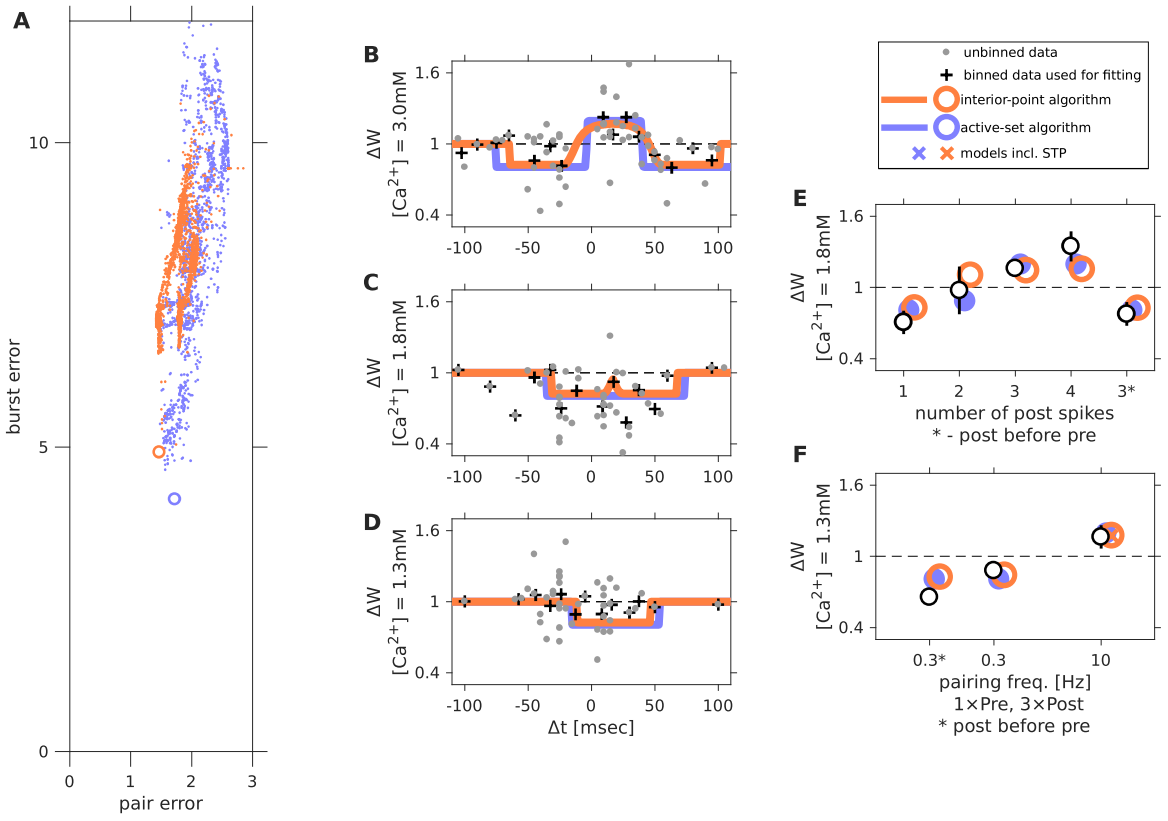

Figure S9: **Nonlinear bistable models fit using different numerical optimization algorithms.** We fit the nonlinear, bistable model using the interior- point (orange) and the active-set (purple) optimization methods (built-in to the MATLAB software). (**A**) For each random initialization of the optimization procedure we plot the final fitting error (horizontal axis) and the prediction error for burst data given by that parameter set (vertical axis). (**B-D**) The STDP curves at $[Ca^{2+}] = 3$, 1.8, 1.3mM for models with smallest combined spike-pair and burst errors are very similar for the two algorithms. (**E-F**) At $[Ca^{2+}] = 1.8$, 1.3mM, the models fit using both algorithms produce predictions that match well the experimental measurements. The exception to this is the prediction of the model fit using the interior-point algorithm for the effect of a burst of post-synaptic spikes after a pre-synaptic spike at $[Ca^{2+}] = 1.3$mM with a high pairing frequency. This discrepancy is eliminated when taking into account the effect of short-term plasticity. For all models shown, $\tau_{Ca,NMDA}$=95msec.

Summary tables for models with $C_{\text{pre}} \propto [\text{Ca}^{2+}]^2$

Nonlinear, Bistable fixed $\tau = 10^5$ms	C_{pre}	C_{post}	γ_d	γ_p	θ_p	D [ms]	σ^2 [ms^2]	b	η [ms^{-1}]
$\tau_{\text{Ca,NMDA}}$=60ms	0.0847	0.262	1.1e+04	2.07e+04	5.18	24.3	0.828	1.39	16.4
$\tau_{\text{Ca,NMDA}}$=95ms	0.0533	0.231	7.97e+03	2.44e+04	6.42	16.8	104	1.42	19.3
$\tau_{\text{Ca,NMDA}}$=130ms	0.0604	0.206	4.82e+03	1.47e+04	6.53	18	61.9	1.43	19.1
$\tau_{\text{Ca,NMDA}}$=60ms, no lin. post term	0.0507	0.3	7.21e+03	1.25e+04	5.07	17.7	1.47	1.38	28.5
$\tau_{\text{Ca,NMDA}}$=95ms, no lin. post term	0.0533	0.231	7.97e+03	2.44e+04	6.42	16.8	104	1.42	19.3
$\tau_{\text{Ca,NMDA}}$=130ms, no lin. post term	0.0926	0.16	1.54e+04	2.2e+04	2.7	20	3.93	1.39	23.2
$\tau_{\text{Ca,NMDA}}$=60ms, no LTD @ [Ca^{2+}]=1.3mM	0.111	0.333	2.37e+03	4.04e+03	1.86	25	1.49	1.42	1.25
$\tau_{\text{Ca,NMDA}}$=95ms, no LTD @ [Ca^{2+}]=1.3mM	0.0121	0.313	1.13e+04	2.36e+04	1.4	14.8	1.05e+03	1.84	8.77
$\tau_{\text{Ca,NMDA}}$=130ms, no LTD @ [Ca^{2+}]=1.3mM	0.06	0.135	25.2	2.39e+03	2.77	3.36	218	1.36	5.6
Nonlinear, Graded	C_{pre}	C_{post}	γ_d	γ_p	θ_p	D [ms]	η [ms^{-1}]		
$\tau_{\text{Ca,NMDA}}$=60ms	0.0684	0.2	2.06e-05	6.81e-05	6.75	18.9	17.2		
$\tau_{\text{Ca,NMDA}}$=95ms	0.0788	0.149	1.02e-05	4.72e-05	8.01	6.52	15.4		
$\tau_{\text{Ca,NMDA}}$=130ms	0.025	0.27	1.6e-05	4.22e-05	4.8	9.5	28.4		
$\tau_{\text{Ca,NMDA}}$=60ms, no LTD @ [Ca^{2+}]=1.3mM	0.0222	0.213	6.78e-05	0.000134	1.51	12.2	6.7		
$\tau_{\text{Ca,NMDA}}$=95ms, no LTD @ [Ca^{2+}]=1.3mM	0.0412	0.0851	0.0357	0.0699	1.31	22.5	6.88		
$\tau_{\text{Ca,NMDA}}$=130ms, no LTD @ [Ca^{2+}]=1.3mM	0.0534	0.293	0.000148	0.00023	1.03	2.61	0.821		
$\tau_{\text{Ca,NMDA}}$=60ms, no lin. post term	0.0684	0.2	2.06e-05	6.81e-05	6.75	18.9	17.2		
$\tau_{\text{Ca,NMDA}}$=95ms, no lin. post term	0.0788	0.149	1.02e-05	4.72e-05	8.01	6.52	15.4		
$\tau_{\text{Ca,NMDA}}$=130ms, no lin. post term	0.025	0.27	1.6e-05	4.22e-05	4.8	9.5	28.4		
Nonlinear, Bistable fixed $\tau = 10^5$ms, no lin. post term	C_{pre}	γ_d	γ_p	θ_p	D [ms]	σ^2 [ms^2]	b	η [ms^{-1}]	
$\tau_{\text{Ca,NMDA}}$=60ms	0.0404	1.05e+04	2.42e+04	7.41	23.3	12.5	1.4	9.36	
$\tau_{\text{Ca,NMDA}}$=95ms	0.0221	1.74e+04	2.5e+04	2.87	23.8	0.537	1.39	16.4	
$\tau_{\text{Ca,NMDA}}$=130ms	0.0283	9.9e+03	2.22e+04	5.65	16.6	2.86	1.4	8.55	
$\tau_{\text{Ca,NMDA}}$=60ms, no LTD @ [Ca^{2+}]=1.3mM	0.0727	7.29	1.76e+04	2.96	19	2.95e+04	2.79	0.465	
$\tau_{\text{Ca,NMDA}}$=95ms, no LTD @ [Ca^{2+}]=1.3mM	0.0149	63	95.2	1.59	2.86	0.0113	1.36	3.47	
$\tau_{\text{Ca,NMDA}}$=130ms, no LTD @ [Ca^{2+}]=1.3mM	0.0727	7.29	1.76e+04	2.96	19	2.95e+04	2.79	0.465	
Linear, Bistable fixed $\tau = 10^5$ms	C_{pre}	C_{post}	γ_d	γ_p	θ_p	D [ms]	σ^2 [ms^2]	b	τ_{Ca} [ms]
fit to all spike pair data	0.0727	0.321	1.63e+04	1.76e+04	1.02	0.86	0.0196	1.32	56.8
fit to [Ca^{2+}]=3mM data only	0.0783	0.332	1.88e+04	2.4e+04	1.07	7.42	4.31	1.35	54.7
Linear, Graded	C_{pre}	C_{post}	γ_d	γ_p	θ_p	D [ms]	τ_{Ca} [ms]		
	0.0968	0.286	0.000183	0.000854	1.32	27.2	42.7		

Table 1: Best fitting parameters for all model variations discussed in the manuscript with $C_{\text{pre}} \propto [\text{Ca}^{2+}]^2$

Nonlinear, Bistable fixed $\tau = 10^5$ms	ϵ_{pair}	ϵ_{burst}	$\epsilon_{\text{pair+burst}}$	$\epsilon_{\text{freq.}}$	$\epsilon^{\text{STP}}_{\text{freq.}}$	AIC
$\tau_{\text{Ca,NMDA}}$=60ms	1.54	4.65	4.9	11.4	7.72	-61.9
$\tau_{\text{Ca,NMDA}}$=95ms	1.47	4.92	5.13	10.5	6.11	-69.3
$\tau_{\text{Ca,NMDA}}$=130ms	1.47	4.89	5.11	9.81	4.57	-68.4
$\tau_{\text{Ca,NMDA}}$=60ms, no lin. post term	1.56	4.67	4.92	9.08	6.66	-59.3
$\tau_{\text{Ca,NMDA}}$=95ms, no lin. post term	1.47	4.92	5.14	10.6	6.11	-70.3
$\tau_{\text{Ca,NMDA}}$=130ms, no lin. post term	1.55	4.91	5.15	5.05	5.05	-64
$\tau_{\text{Ca,NMDA}}$=60ms, no LTD @ [Ca^{2+}]=1.3mM	1.88	7	7.25	15.5	12.3	-41.4
$\tau_{\text{Ca,NMDA}}$=95ms, no LTD @ [Ca^{2+}]=1.3mM	1.81	7.19	7.41	15.3	7.77	-41.9
$\tau_{\text{Ca,NMDA}}$=130ms, no LTD @ [Ca^{2+}]=1.3mM	2.16	7.05	7.37	12.9	5.41	21.6
Nonlinear, Graded	ϵ_{pair}	ϵ_{burst}	$\epsilon_{\text{pair+burst}}$	$\epsilon_{\text{freq.}}$	$\epsilon^{\text{STP}}_{\text{freq.}}$	AIC
$\tau_{\text{Ca,NMDA}}$=60ms	1.66	6.76	6.96	14.7	6.95	-60.1
$\tau_{\text{Ca,NMDA}}$=95ms	1.81	6.62	6.87	12.6	3.68	-40.9
$\tau_{\text{Ca,NMDA}}$=130ms	2.03	6.07	6.4	4.3	2.88	-30.3
$\tau_{\text{Ca,NMDA}}$=60ms, no LTD @ [Ca^{2+}]=1.3mM	2.48	7.81	8.19	14.8	7.46	-14
$\tau_{\text{Ca,NMDA}}$=95ms, no LTD @ [Ca^{2+}]=1.3mM	2.92	7.68	8.22	26	7.99	149
$\tau_{\text{Ca,NMDA}}$=130ms, no LTD @ [Ca^{2+}]=1.3mM	2.76	7.79	8.26	8.63	5.55	19.7
$\tau_{\text{Ca,NMDA}}$=60ms, no lin. post term	1.66	6.76	6.96	14.6	6.84	-60.2
$\tau_{\text{Ca,NMDA}}$=95ms, no lin. post term	1.81	6.68	6.92	12.9	3.68	-40.3
$\tau_{\text{Ca,NMDA}}$=130ms, no lin. post term	2.03	6.13	6.45	4.32	2.88	-28.8
Nonlinear, Bistable fixed $\tau = 10^5$ms	ϵ_{pair}	ϵ_{burst}	$\epsilon_{\text{pair+burst}}$	$\epsilon_{\text{freq.}}$	$\epsilon^{\text{STP}}_{\text{freq.}}$	AIC
$\tau_{\text{Ca,NMDA}}$=60ms	1.51	4.44	4.69	12.6	8.51	-67.8
$\tau_{\text{Ca,NMDA}}$=95ms	1.5	4.46	4.7	6.47	4.82	-65.9
$\tau_{\text{Ca,NMDA}}$=130ms	1.49	4.44	4.68	8.17	4.8	-68.3
$\tau_{\text{Ca,NMDA}}$=60ms, no LTD @ [Ca^{2+}]=1.3mM	2.41	7.61	7.98	27.6	21.5	-2.56
$\tau_{\text{Ca,NMDA}}$=95ms, no LTD @ [Ca^{2+}]=1.3mM	2.16	7.16	7.48	12.9	5.45	19.3
$\tau_{\text{Ca,NMDA}}$=130ms, no LTD @ [Ca^{2+}]=1.3mM	2.41	7.61	7.98	27.6	21.5	-2.56
Linear, Bistable fixed $\tau = 10^5$ms	ϵ_{pair}	ϵ_{burst}	$\epsilon_{\text{pair+burst}}$	$\epsilon_{\text{freq.}}$	$\epsilon^{\text{STP}}_{\text{freq.}}$	AIC
fit to all spike pair data	2.27	5.45	5.9	14.4	13.9	7.02
fit to [Ca^{2+}]=3mM data only	2.25	5.23	5.69	14.7	14	-14.8
Linear, Graded	ϵ_{pair}	ϵ_{burst}	$\epsilon_{\text{pair+burst}}$	$\epsilon_{\text{freq.}}$	$\epsilon^{\text{STP}}_{\text{freq.}}$	AIC
	2.36	6.02	6.46	10.6	11.9	-11.5

Table 2: Fitting errors, prediction errors and AIC values for all model variations discussed in the manuscript with $C_{\text{pre}} \propto [\text{Ca}^{2+}]^2$

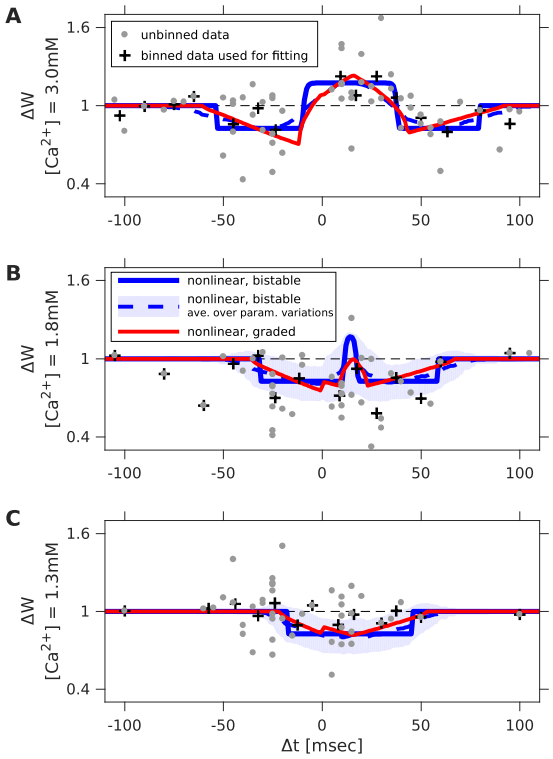

Figure S10: **Models with a nonlinear NMDA term contributing to calcium transients fit well the STDP data at multiple [Ca^{2+}] concentrations.** We plot the spike-pair STDP curves for a nonlinear models where the pre-synaptic amplitude parameter C_{pre} scales *linearly* with the extra-cellular concentration (instead of the quadratic scaling used in the main text and in Supplementary Figures 1-9). (**A-C**) Fits to the STDP data at [Ca^{2+}] = 3, 1.8, 1.3mM for a graded (red) and bistable (blue) models. The models fit well the data at all concentrations where the STDP was characterized experimentally.

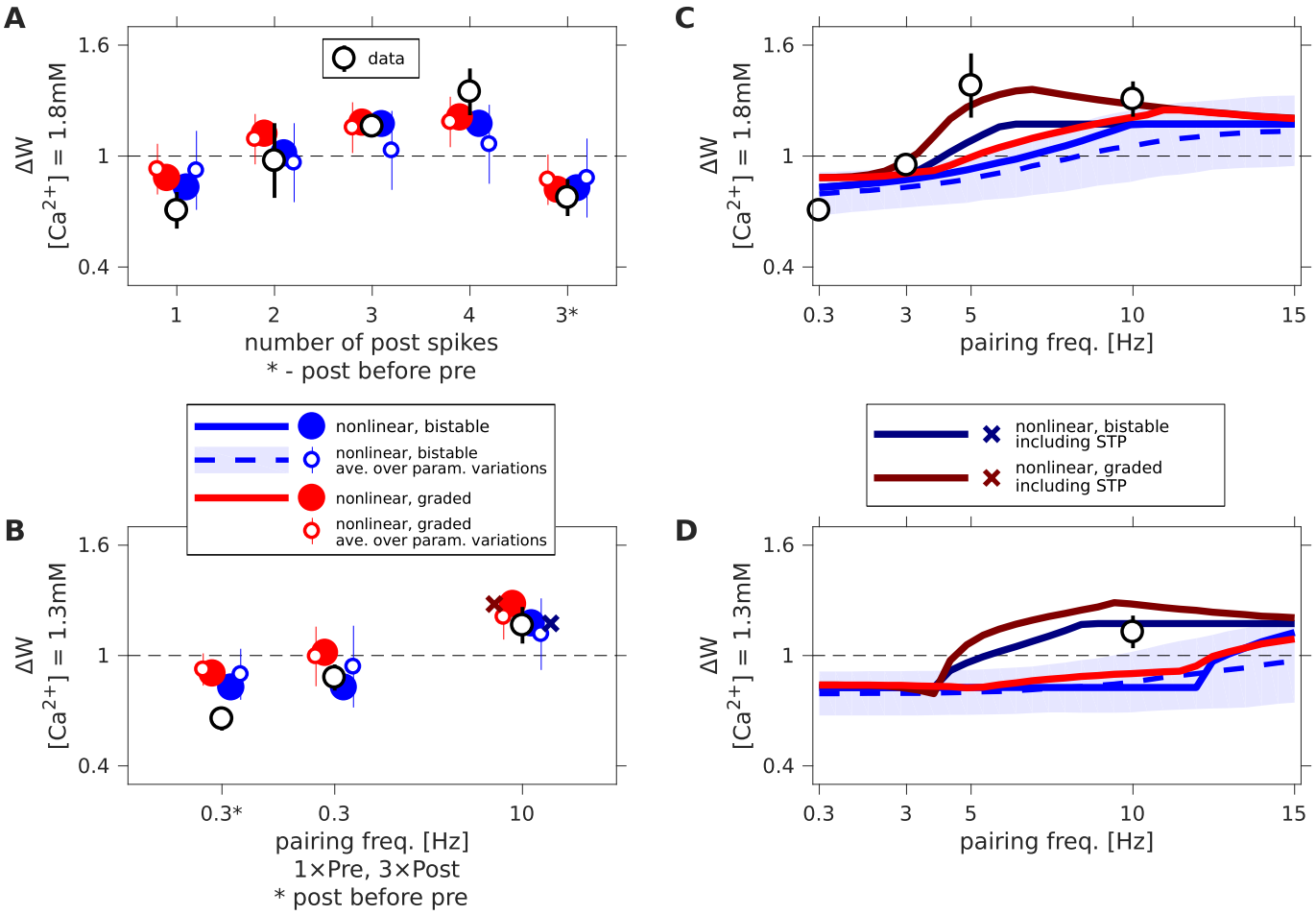

Figure S11: **Models with a nonlinear NMDA term contributing to calcium transients fit well the burst data at multiple [Ca^{2+}] concentrations and require including the effect of short-term plasticity to reproduce the effects seen at high pairing frequencies.** We plot results for nonlinear models where the pre-synaptic amplitude parameter C_{pre} scales *linearly* with the extra-cellular concentration (instead of the quadratic scaling used in the main text and in Supplementary Figures 1-9). (**A-B**) Both the nonlinear graded (red) and nonlinear bistable (blue) models fit well the burst data at [Ca^{2+}] = 1.8, 1.3mM. For the graded model, the change in synaptic efficacy for depends more weakly on the number of spikes in the burst compared with the data and the bistable model. (**C-D**) Both models predict a change in the sign of plasticity as a function of the pairing frequency for a pair of spikes with Δt =10ms, but the frequency at which this change occurs is over-estimated when short-term plasticity is not taken into account. Including STP in the model produces plasticity-frequency curves that are match the experimental measurements (brown– graded model, dark blue– bistable).

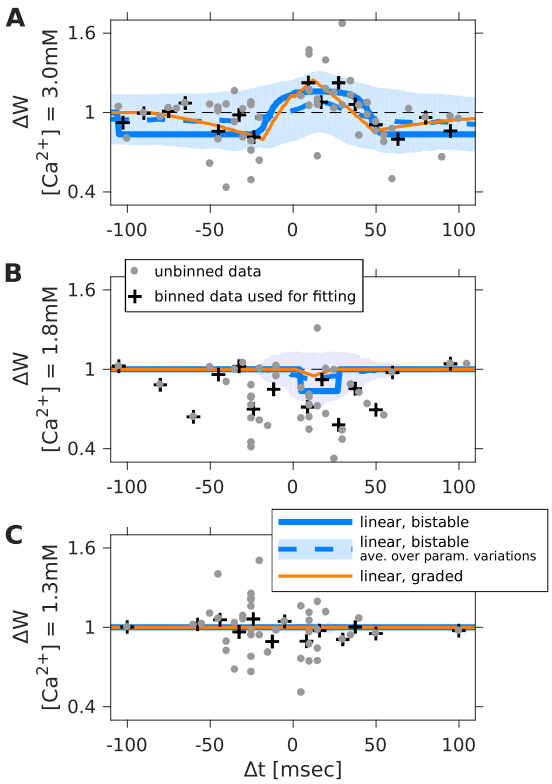

Figure S12: **Models without a nonlinear NMDA term contributing to calcium transients do not fit the STDP data at multiple [Ca^{2+}] concentrations.** We plot the spike-pair STDP curves for a linear model where the pre-synaptic amplitude parameter C_{pre} scales *linearly* with the extra-cellular concentration (instead of the quadratic scaling used in the main text and in Supplementary Figures 1-9). (**A-C**) Fits to the STDP data at [Ca^{2+}] = 3, 1.8, 1.3mM for a graded (orange) and bistable (light blue) models in which the calcium transient depends linearly on the pre- and post-synaptic activity. The models are able to fit relatively well the depression-potentiation-depression shape of the STDP curve at [Ca^{2+}] = 3mM. However the scaling of the amplitdue parameters C_{pre}, C_{post} with [Ca^{2+}] implies that at a concentration of 1.8mM the model predicts LTD that is weaker and induced in a narrower window than what we found experimentally.

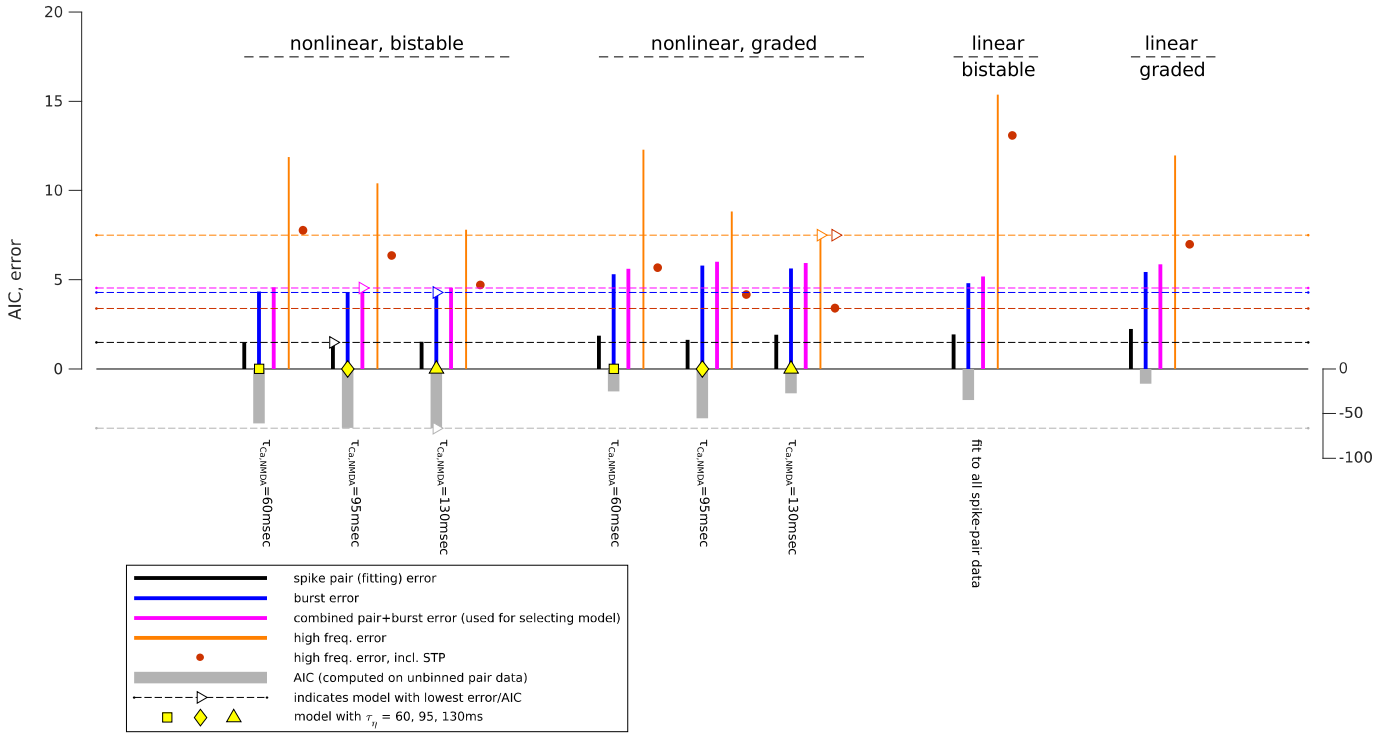

Figure S13: **Summary statistics for models with linear scaling of the pre- and post-synaptic calcium amplitude.** Bar plots show the fitting errors on pair data (black), errors for burst data (blue), total error (on pair and burst data, magenta), error on high pairing frequency data (orange and red for models with and without short-term plasticity, respectively) and the model selection criterion AIC (gray). Results are shown for (from left to right) nonlinear, bistable models with multiple values of the timescale of the NMDA nonlinearity τ_η; nonlinear, graded models with the same variations as the bistable model; linear, bistable and a linear, graded model. The model with the lowest error (of each "type") and the lowest AIC is indicated by a white triangle.

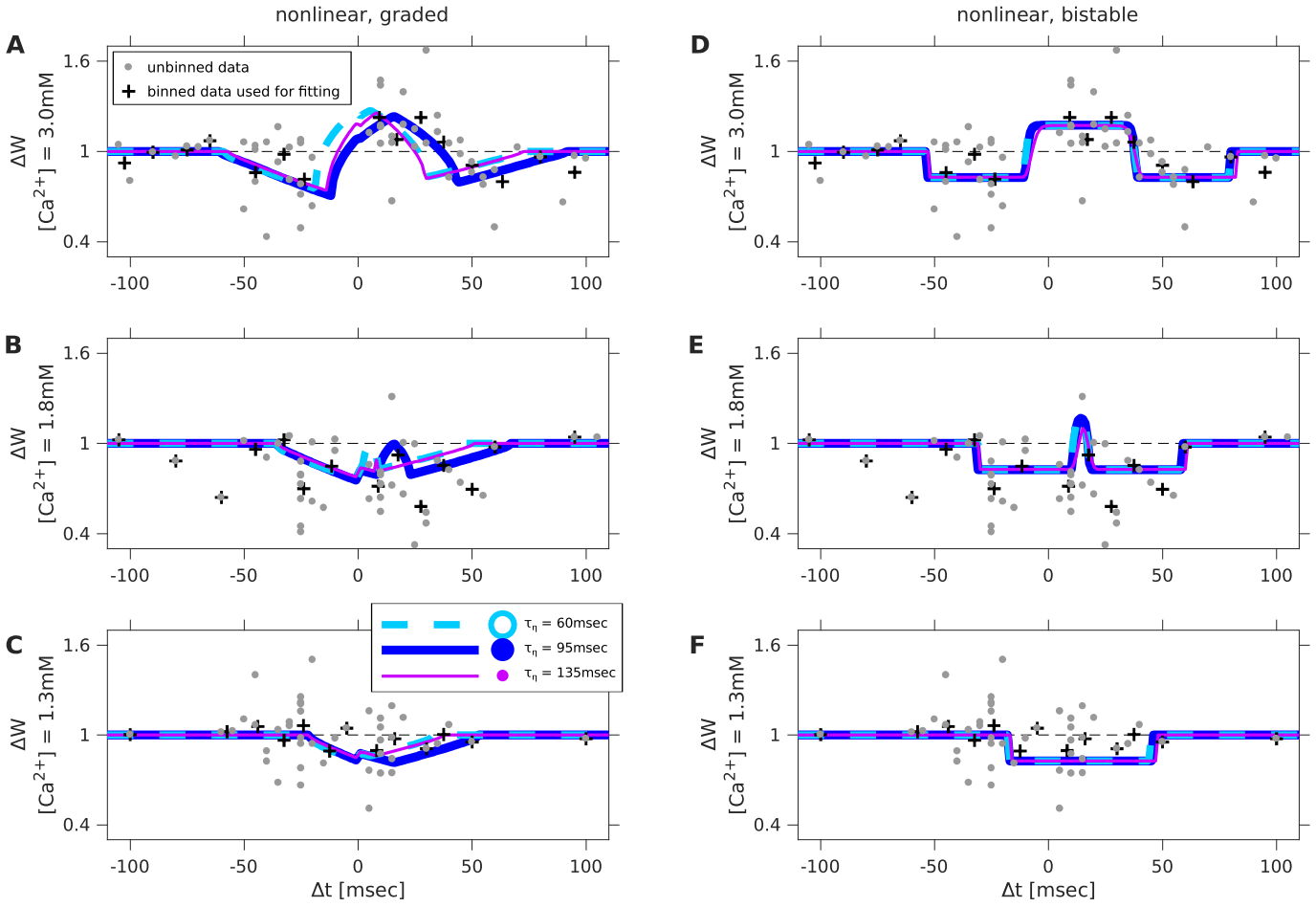

Figure S14: **Nonlinear models can be fit well to spike-pair data for a range of nonlinear decay time-scales.** We plot the spike-pair STDP curves for nonlinear models where the pre-synaptic amplitude parameter C_{pre} scales *linearly* with the extra-cellular concentration (instead of the quadratic scaling used in the main text and in Supplementary Figures 1-9). (**A-C**) Fits to the STDP data at $[Ca^{2+}] = 3$, 1.8, 1.3mM for graded models with multiple values of the decay timescale of the nonlinear contribution to the calcium transients ($\tau_\eta = 60$, 95 130ms shown in light blue, blue and magenta, respectively). The longer this timescale is, the wider the window is for inducing potentiation/depression. The qualitative shape of the curve does not change. (**D-F**) same as (**A-C**) for a nonlinear, bistable model.

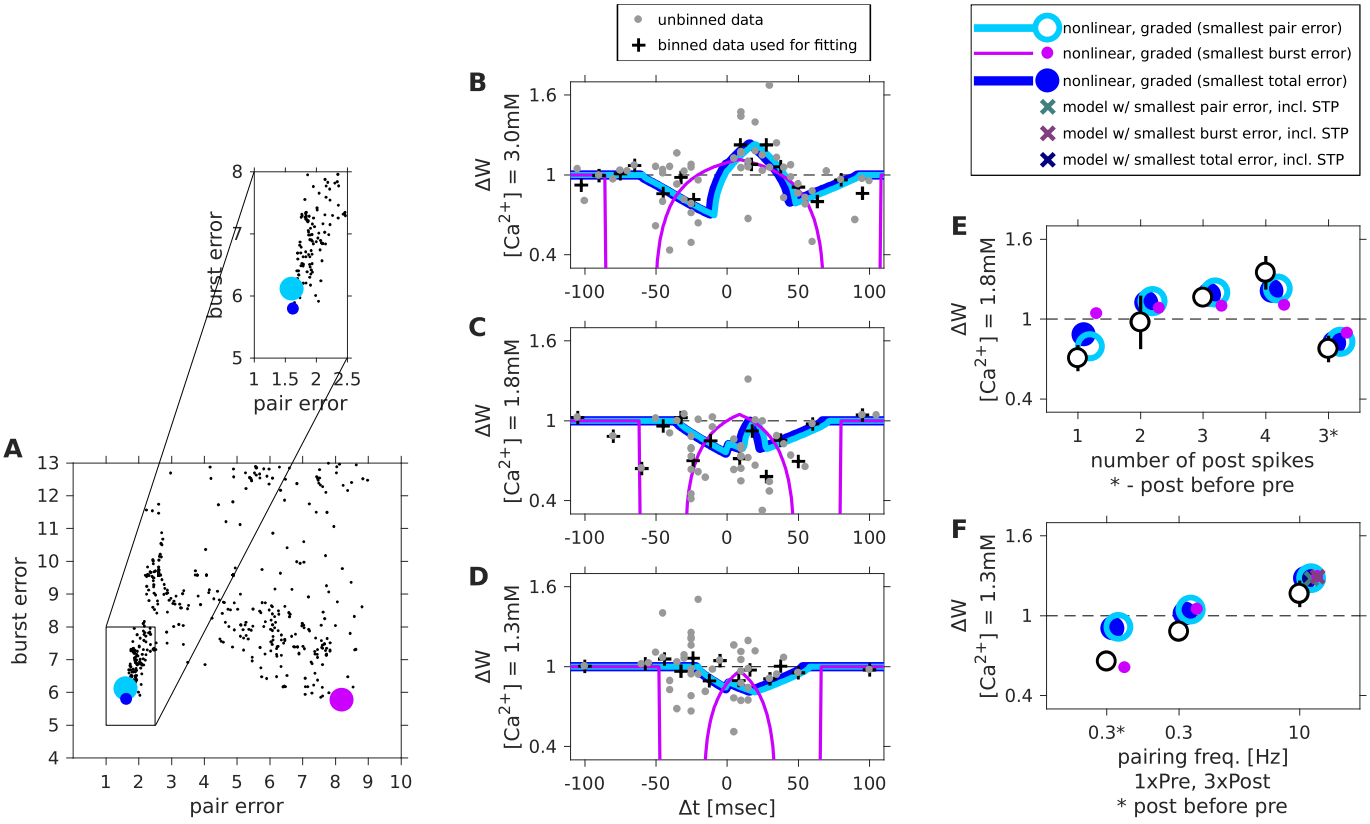

Figure S15: **Nonlinear graded models with smallest spike-pair, burst and combined errors.** Error values and predictions for nonlinear, graded models with smallest spike-pair data errors, combined error and error for burst data only are shown in light blue, blue and magenta, respecitively. We plot the results for models where the pre-synaptic amplitude parameter C_{pre} scales *linearly* with the extra-cellular concentration (instead of the quadratic scaling used in the main text and in Supplementary Figures 1-9). (**A**) For each random initialization of the optimization procedure we plot the final fitting error (horizontal axis) and the prediction error for burst data given by that parameter set (vertical axis). The parameter set at the global minimum of the spike-pair error surface (light blue) yields a prediction associated with pair and burst errors close to a model with smallest total error (blue). (**B-D**) STDP curves at $[Ca^{2+}] = 3, 1.8, 1.3$mM for the model with smallest spike-pair error is very similar to that with the smallest total error. (**E-F**) At $[Ca^{2+}] = 1.8, 1.3$mM, both the model with smallest spike-pair error and the one with smallest total error match well the burst data. For all models shown, $\tau_{\text{Ca,NMDA}}$=95msec.

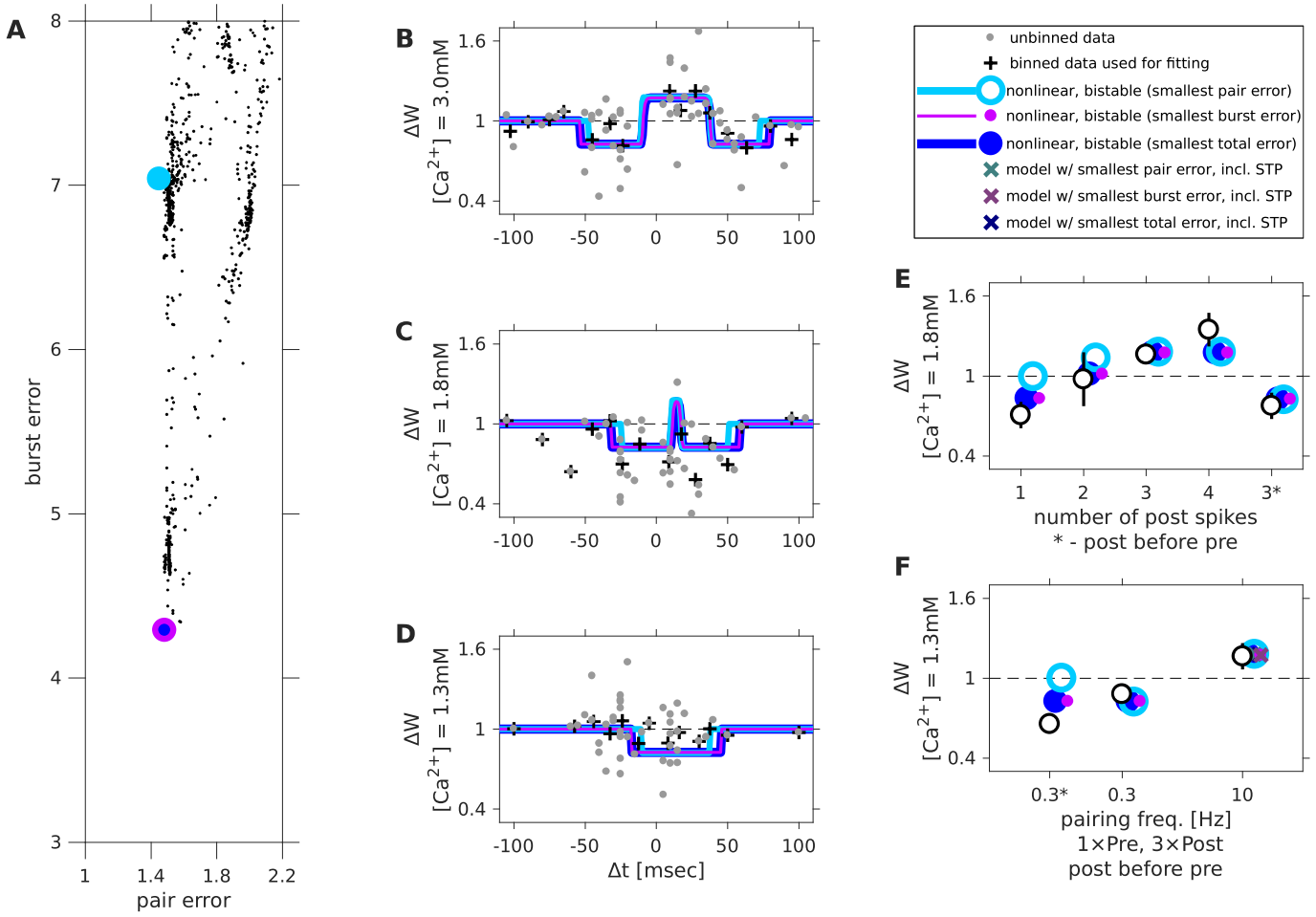

Figure S16: **Nonlinear bistable models with smallest spike-pair, burst and combined errors.** Error values and predictions for nonlinear, bistable models with smallest spike-pair data errors, combined error and error for burst data only are shown in light blue, blue and magenta, respecitively. We plot the results for models where the pre-synaptic amplitude parameter C_{pre} scales *linearly* with the extra-cellular concentration (instead of the quadratic scaling used in the main text and in Supplementary Figures 1-9). (**A**) For each random initialization of the optimization procedure we plot the final fitting error (horizontal axis) and the prediction error for burst data given by that parameter set (vertical axis). The parameter set with the smallest combined error has a fitting error that is very close to the global minimum. (**B-D**) STDP curves at $[Ca^{2+}] = 3$, 1.8, 1.3mM for the model with smallest spike-pair error is very similar to that with the smallest total error. (**E**) At $[Ca^{2+}] = 1.8$mM, the model with smallest spike-pair error predicts a smaller effect for increasing the number of post-synaptic spikes from 1 to 4 compared with the data, and the model with smallest combined error. (**F**) At $[Ca^{2+}] = 1.3$mM, the model with smallest spike-pair error does not accurately predict the plasticity resulting from a burst of three post-synaptic spikes before a pre-synaptic spike at a low pairing frequency. The model with smallest combined error correctly reproduces the LTD found under that condition. For all models shown, $\tau_{\text{Ca,NMDA}}$=95msec.

Summary tables for models with $C_{\text{pre}} \propto [\text{Ca}^{2+}]$

Nonlinear, Bistable fixed $\tau = 10^5$ms	C_{pre}	C_{post}	γ_d [ms]	γ_p [ms]	θ_p	D [ms]	σ^2 [ms^2]	b	η [ms^{-1}]
$\tau_{\text{Ca,NMDA}}$=60ms	0.189	0.135	5.18e+03	2.26e+04	5.73	14	19.9	1.42	14
$\tau_{\text{Ca,NMDA}}$=95ms	0.172	0.106	2.52e+03	1.99e+04	6.81	14.2	45.1	1.42	19
$\tau_{\text{Ca,NMDA}}$=130ms	0.154	0.157	6.54e+03	2.44e+04	5.43	15.3	22	1.42	14.1
Nonlinear, Graded	C_{pre}	C_{post}	γ_d	γ_p	θ_p	D [ms]	η [ms^{-1}]		
$\tau_{\text{Ca,NMDA}}$=60ms	0.176	0.195	1.4e-05	7.29e-05	5.88	5.31	8.62		
$\tau_{\text{Ca,NMDA}}$=95ms	0.262	0.252	1.03e-05	4.72e-05	7.8	15.7	6.51		
$\tau_{\text{Ca,NMDA}}$=130ms	0.148	0.133	6.78e-06	4.11e-05	7.6	7.92	15.2		
Linear, Bistable fixed $\tau = 10^5$ms	C_{pre}	C_{post}	γ_d [ms]	γ_p [ms]	θ_p	D [ms]	σ^2 [ms^2]	b	τ_{Ca} [ms]
fit to all spike pair data	0.311	0.317	4.8e+03	1.2e+04	1.24	16	239	1.39	45.6
Linear, Graded	C_{pre}	C_{post}	γ_d	γ_p	θ_p	D [ms]	τ_{Ca} [ms]		
fit to all spike pair data	0.291	0.331	9.28e-05	0.000477	1.4	12.5	48		

Table 3: Best fitting parameters for all model variations discussed in the manuscript with $C_{\text{pre}} \propto [\text{Ca}^{2+}]$

Nonlinear, Bistable fixed $\tau = 10^5$ms	ϵ_{pair}	ϵ_{burst}	$\epsilon_{\text{pair+burst}}$	$\epsilon_{\text{freq.}}$	$\epsilon^{\text{STP}}_{\text{freq.}}$	AIC
$\tau_{\text{Ca,NMDA}}$=60ms	1.48	4.33	4.58	11.9	7.53	-61.1
$\tau_{\text{Ca,NMDA}}$=95ms	1.48	4.29	4.54	10.4	6.02	-66.2
$\tau_{\text{Ca,NMDA}}$=130ms	1.51	4.28	4.54	7.79	4.64	-66.5
Nonlinear, Graded	ϵ_{pair}	ϵ_{burst}	$\epsilon_{\text{pair+burst}}$	$\epsilon_{\text{freq.}}$	$\epsilon^{\text{STP}}_{\text{freq.}}$	AIC
$\tau_{\text{Ca,NMDA}}$=60ms	1.86	5.3	5.62	12.3	5.65	-25.1
$\tau_{\text{Ca,NMDA}}$=95ms	1.63	5.79	6.01	8.82	4.14	-55.2
$\tau_{\text{Ca,NMDA}}$=130ms	1.91	5.62	5.94	7.5	3.38	-27.5
Linear, Bistable fixed $\tau = 10^5$ms	ϵ_{pair}	ϵ_{burst}	$\epsilon_{\text{pair+burst}}$	$\epsilon_{\text{freq.}}$	$\epsilon^{\text{STP}}_{\text{freq.}}$	AIC
fit to all spike pair data	1.94	4.8	5.18	15.4	13	-34.9
Linear, Graded	ϵ_{pair}	ϵ_{burst}	$\epsilon_{\text{pair+burst}}$	$\epsilon_{\text{freq.}}$	$\epsilon^{\text{STP}}_{\text{freq.}}$	AIC
fit to all spike pair data	2.23	5.42	5.87	12	6.64	-16.6

Table 4: Fitting errors, prediction errors and AIC values for all model variations discussed in the manuscript with $C_{\text{pre}} \propto [\text{Ca}^{2+}]$

Nonlinear, Bistable, fixed $\tau = 10^5$ms	C_{pre}	C_{post}	γ_d	γ_p	θ_p	D [ms]	σ^2 [ms^2]	b	η [ms^{-1}]
$\tau_{\text{Ca,NMDA}}$=60, 95, 130ms*	[0.010, 0.111]	[0.010, 0.333]	[1, 25000]	[1, 25000]	[1, 10]	[0, 40]	[0.002, 10^5]	[1, 10]	[10^{-8}, 30]
Nonlinear, Graded	C_{pre}	C_{post}	γ_d	γ_p	θ_p	D [ms]	η [ms^{-1}]		
$\tau_{\text{Ca,NMDA}}$=60, 95, 130ms*	[0.010, 0.111]	[0.010, 0.333]	[10^{-8}, 0.1]	[10^{-8}, 0.1]	[1, 10]	[0, 40]	[10^{-8}, 30]		
Nonlinear, Bistable fixed $\tau = 10^5$ms, no L post contrib	C_{pre}	γ_d	γ_p	θ_p	D [ms]	σ^2 [ms^2]	b	η [ms^{-1}]	
$\tau_{\text{Ca,NMDA}}$=60, 95, 130ms§	[0.010, 0.111]	[1, 25000]	[1, 25000]	[1, 10]	[0, 40]	[0.002, 10^5]	[1, 10]	[10^{-8}, 30]	
Linear, Bistable, fixed $\tau = 10^5$ms	C_{pre}	C_{post}	γ_d	γ_p	θ_p	D [ms]	σ^2 [ms^2]	b	τ_{Ca} [ms]
	[0.010, 0.111]	[0.010, 0.333]	[1, 25000]	[1, 25000]	[1, 2]	[0, 40]	[0.002, 10^5]	[1, 10]	[15, 60]
Linear, Graded	C_{pre}	C_{post}	γ_d	γ_p	θ_p	D [ms]	τ_{Ca} [ms]		
	[0.010, 0.111]	[0.010, 0.333]	[10^{-8}, 0.1]	[10^{-8}, 0.1]	[1, 2]	[0, 40]	[15, 60]		

Table 5: Allowed parameter ranges for fitting models with $C_{\text{pre}} \propto [\text{Ca}^{2+}]^2$.

Nonlinear, Bistable, fixed $\tau = 10^5$ms	C_{pre}	C_{post}	γ_d	γ_p	θ_p	D [ms]	σ^2 [ms^2]	b	η [ms^{-1}]
$\tau_{\text{Ca,NMDA}}$=60, 95, 130ms	[0.010, 0.333]	[0.010, 0.333]	[1, 25000]	[1, 25000]	[1, 10]	[0, 40]	[0.002, $4 \cdot 10^5$]	[1, 10]	[10^{-8}, 30]
Nonlinear, Graded	C_{pre}	C_{post}	γ_d	γ_p	θ_p	D [ms]	η [ms^{-1}]		
$\tau_{\text{Ca,NMDA}}$=60, 95, 130ms	[0.010, 0.333]	[0.010, 0.333]	[10^{-8}, 0.1]	[10^{-8}, 0.1]	[1, 10]	[0, 40]	[10^{-8}, 30]		
Linear, Bistable, fixed $\tau = 10^5$ms	C_{pre}	C_{post}	γ_d	γ_p	θ_p	D [ms]	σ^2 [ms^2]	b	τ_{Ca} [ms]
	[0.010, 0.333]	[0.010, 0.333]	[1, 25000]	[1, 25000]	[1, 2]	[0, 40]	[0.002, $4 \cdot 10^5$]	[1, 10]	[15, 60]
Linear, Graded	C_{pre}	C_{post}	γ_d	γ_p	θ_p	D [ms]	τ_{Ca} [ms]		
	[0.010, 0.333]	[0.010, 0.333]	[10^{-8}, 0.1]	[10^{-8}, 0.1]	[1, 2]	[0, 40]	[15, 60]		

Table 6: Allowed parameter ranges for fitting models with $C_{\text{pre}} \propto [\text{Ca}^{2+}]$.

* Models with linear pre and post contributions constrained to have no LTD at $[\text{Ca}^{2+}] = 1.3$mM were fit using the same parameter ranges with the additional constraint: $1.3^2 \times C_{\text{pre}} + 1.3 \times C_{\text{post}} + 1.3^3 \times C_{\text{pre}} \times C_{\text{post}} \times \eta \leq \theta_d = 1$.

§ Models with no linear post contribution constrained to have no LTD at $[Ca^{2+}] = 1.3$mM were fit using the same parameter ranges with the additional constraint: $1.3^2 \times C_{\text{pre}} + 1.3^3 \times C_{\text{pre}} \times \eta \leq \theta_d = 1$.

2. Neuromodulation

Pour une concentration extracellulaire de calcium de 1.8 mM, l'application de dopamine (DA) à une concentration de 20 µM pendant l'appariement pré-post à Δt=+10ms, avec une fréquence de 0.3 Hz et 100 répétitions ne permet pas la récupération de la fenêtre de LTP (80 +/- 11 %, n = 8; Figure 1A). L'application d'isoprénaline (ISO), un agoniste des récepteurs β-adrénergiques, à une concentration de 10 µM pendant l'appariement pré-post à Δt=+10ms avec une fréquence de 0.3 Hz et 100 répétitions, montre une tendance vers la récupération de la fenêtre de LTP (121 +/- 9 %, n = 5 ; ns ; Figure 1A). L'application d'ISO mais non de DA permet de récupérer la fenêtre de LTP pour une concentration extracellulaire de calcium de 1.8 mM.

3. Implication des récepteurs NMDA pré-synaptiques

Pour une concentration extracellulaire de calcium de 3 mM, l'application de MK-801 (1 mM) dans la pipette de patch abolit la LTP observée (103 +/- 7 %, n= 9; Figure 1B) pour un appariement pré-post à Δt= +10 ms mais pas la LTD observée (63 +/- 8 %, n = 4; Figure 1B) pour un appariement post-pré à Δt= -25ms. Dans ces conditions, la LTP mais non la LTD dépend des récepteurs NMDA post-synaptiques. De manière surprenante, pour une concentration extracellulaire de calcium de 1.8 mM, l'application de MK-801 dans la pipette de patch n'abolit pas la LTD observée (68 +/- 7 %, n = 6; $p < 0.05$; Figure 1B) pour un appariement pré-post à Δt=+10ms, alors que l'application de D-AP5 (50 µM) dans le milieu extracellulaire bloque l'induction de la LTD (89 +/- 5 %, n = 7; Figure 1B). Dans ces conditions, la LTD repose sur les récepteurs NMDA pré-synaptiques.

4. Imagerie Calcique

L'enregistrement du signal calcique avec une concentration de calcium extracellulaire à 1.3 mM au sein d'une épine d'un neurone pyramidal de la région CA1 de l'hippocampe montre

une absence de sommation pour une fréquence de 0.3 Hz, alors qu'il existe une sommation du signal calcique à 10 Hz. En accord avec notre modèle, cette sommation permet de franchir le seuil d'induction de la LTP, et donc sa récupération en calcium extracellulaire physiologique.

Figure 1 - Pharmacologie

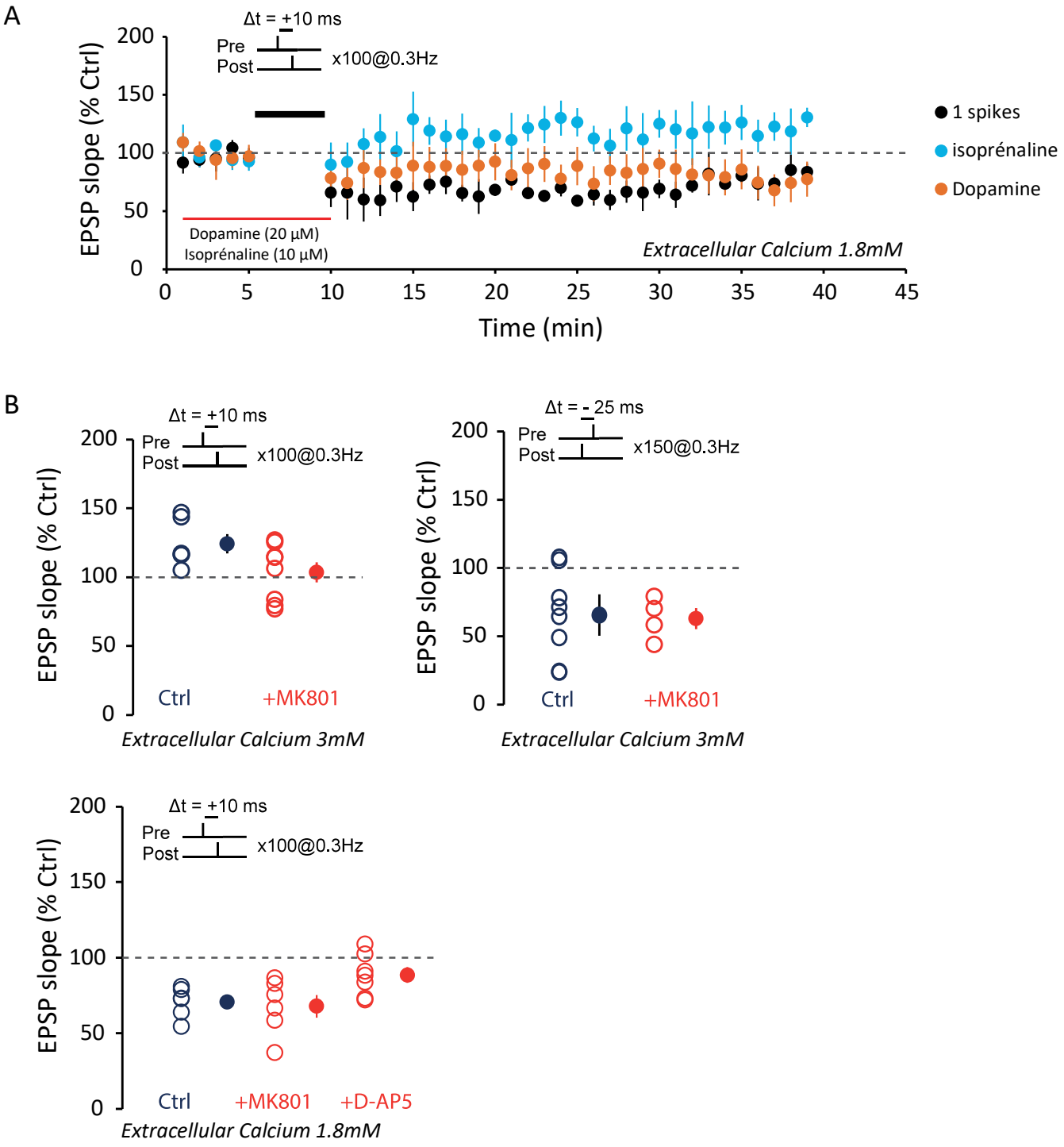

Figure 2 - Imagerie Calcique

Extracellular calcium : 1.3 mM

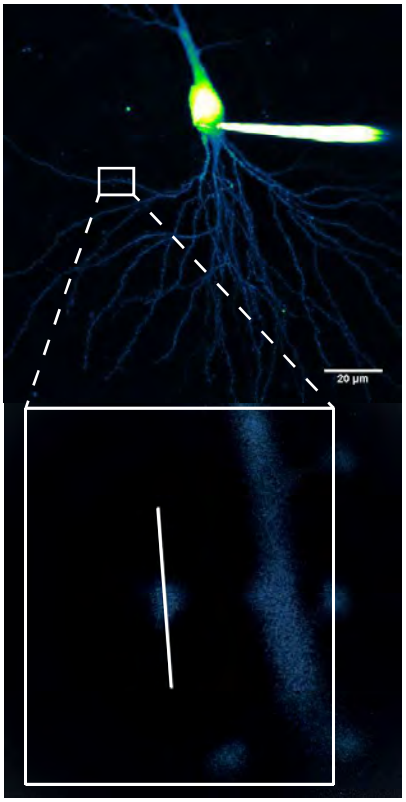

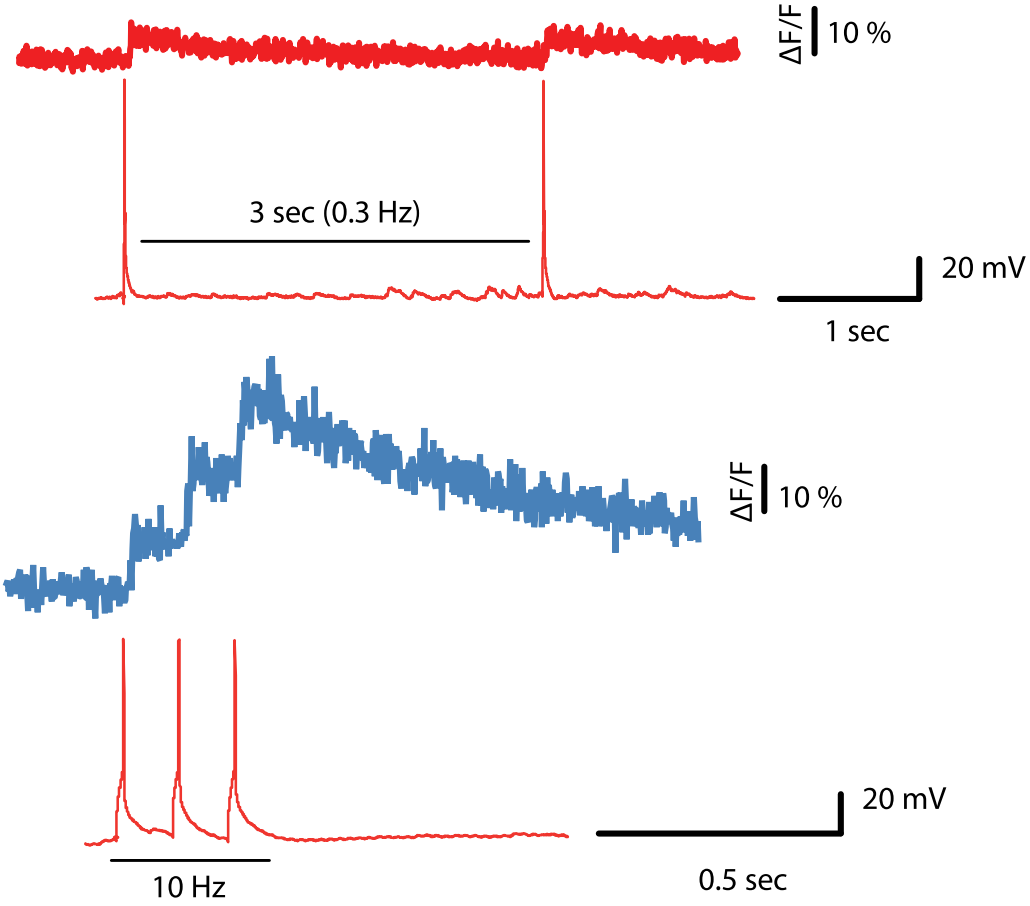

Discussion

La règle de STDP est universelle et présente expérimentalement dans de nombreuses régions comme le cortex (Feldman, 2000; Sjöström et al., 2001, 2003), l'hippocampe (Bi and Poo, 1998; Campanac and Debanne, 2008) ou encore dans le tronc cérébral auditif (Tzounopoulos et al., 2007). Néanmoins, elle se retrouve sous différentes formes, globalement conventionnelle aux neurones excitateurs et non-conventionnelle aux neurones inhibiteurs. La règle de STDP est fortement modulée par l'activité (fréquence d'appariement, nombre de répétitions, nombre de potentiels d'action post-synaptiques) et par la neuromodulation. Pourtant, elle est retrouvée dans de nombreuses expériences *in vivo* (Zhang et al., 1998) mais son induction est parfois difficile et peu durable (Frégnac et al., 2010 ; Jacob et al., 2007). Cela s'explique probablement par divers facteurs présents *in vivo* mais absents *in vitro* comme la forte activité spontanée (Higgins et al., 2014) ou la neuromodulation. Néanmoins, une différence majeure oubliée jusqu'à maintenant concerne la concentration de calcium extracellulaire ($[Ca^{2+}]_e$). La concentration physiologique de calcium est d'environ 1.5 mM **(Tableau 1)** alors que la majorité des études, voire la totalité, a utilisé des concentrations entre 2 et 3 mM **(Tableau 2)**. Nos résultats ont montré que la règle de STDP, en conditions de $[Ca^{2+}]_e$ physiologique, est profondément altérée aux synapses CA3-CA1 en réponse à des protocoles classiques (faible fréquence, un seul potentiel d'action post-synaptique). Cependant, l'utilisation d'activités spécifiques (triplet, fréquence θ) ou de neuromodulateurs (noradrénaline) nous ont permis de récupérer une plasticité classique.

1. Implication pour les autres études

Nos résultats indiquent que le protocole minimal pour induire une LTP robuste *in vivo* doit utiliser des potentiels d'action en bouffée couplés à une fréquence θ. Ces observations se retrouvent déjà dans certaines études *in vivo*, dans le cortex visuel de chat où ce type

d'appariement permet d'induire de la LTP (Frégnac et al., 2010). Cela pourrait expliquer la difficulté d'induire de la LTP dans certaines études ainsi que la LTD peu durable (Jacob et al., 2007). Notre étude se limite aux synapses CA3-CA1 de l'hippocampe, mais de par l'universalité de la règle de STDP, son étude en $[Ca^{2+}]_e$ physiologique devrait s'étendre à d'autres régions, mais aussi à d'autres synapses, en particulier au niveau des interneurones.

2. Le rôle de l'activité

L'activité module fortement la règle de STDP. Nos résultats montrent que l'augmentation du nombre de potentiels d'action post-synaptiques ou de la fréquence d'appariement permettent la récupération d'une courbe de STDP conventionnelle dans nos différentes conditions de calcium extracellulaire. Néanmoins, pour mieux comprendre la règle de STDP dans l'hippocampe dans des conditions *in vivo*, il serait intéressant d'utiliser des patrons d'activités provenant d'enregistrements *in vivo*. Cela a déjà été réalisé *in vitro*, en calcium non-physiologique, montrant qu'il est possible d'induire de la LTP en présence de carbachol, un agoniste cholinergique (Isaac et al., 2009). Néanmoins, dans cette étude, l'induction de la LTD n'a pas été possible. Il y a de fortes raisons de croire que cela soit possible en calcium physiologique. Enfin, nous avons vu que le nombre de répétitions est étroitement lié à la probabilité d'induction de la plasticité. Quel est l'effet d'une diminution du calcium extracellulaire sur la probabilité d'induction ? Dans nos conditions, le grand nombre d'appariements utilisé, 100 pour la LTP et 150 pour la LTD, permet de s'assurer que la probabilité d'induire de la LTP ou LTD est assez élevée pour éviter de manquer un changement synaptique. Néanmoins, de nombreuses études utilisent un nombre plus faible d'appariements, en particulier dans le cortex où le nombre d'appariements est de 60 pour la LTP et la LTD (Froemke et al., 2006). La réévaluation de la règle de STDP dans ces structures devra prendre en compte le nombre d'appariements. Par ailleurs, beaucoup d'études, en particulier dans le cortex, utilisent déjà des fréquences élevées (Markram et al.,

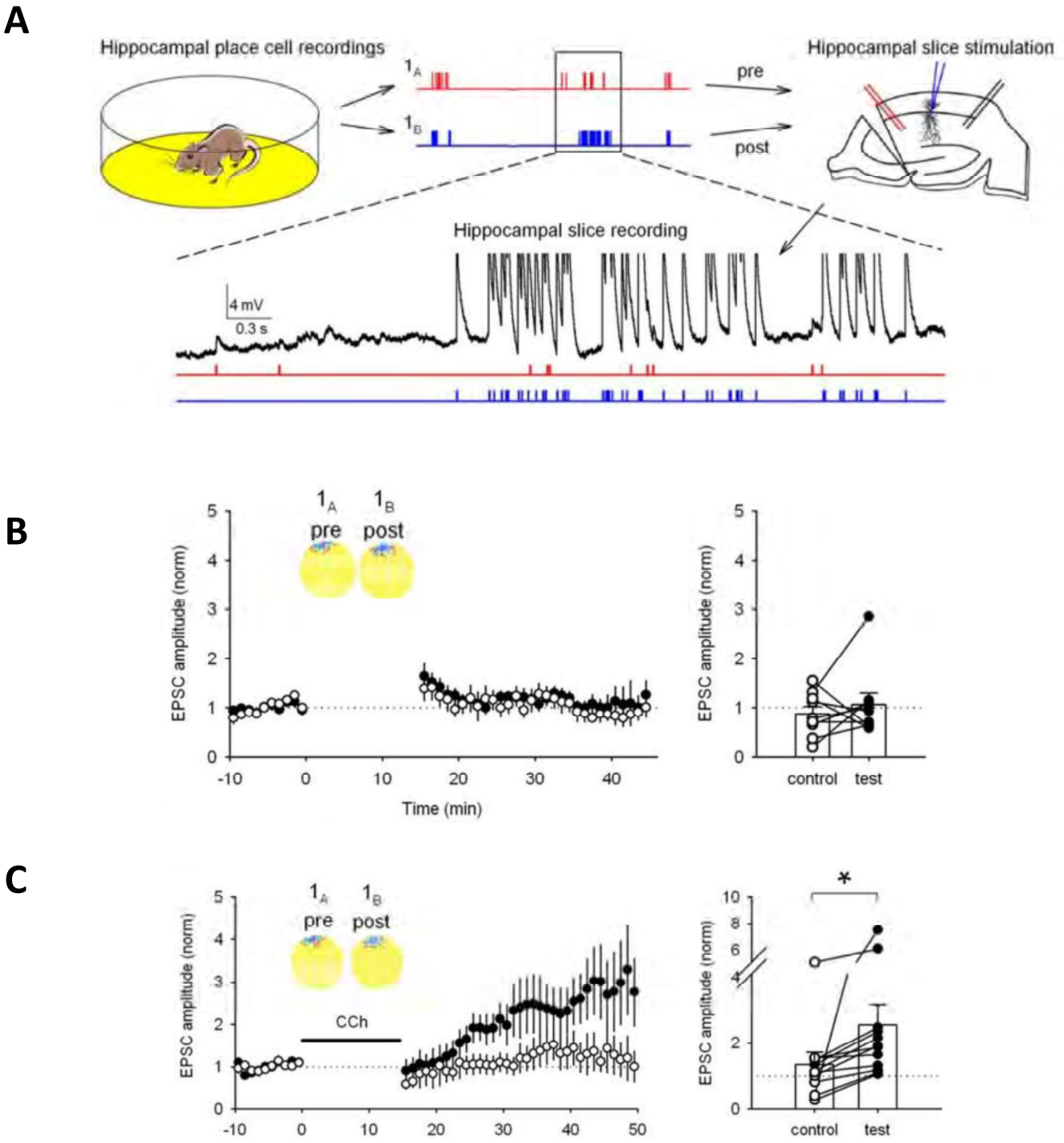

Isaac et al, 2009

Figure 22. L 'utilisation de patrons d'activités *in vivo* permet d'induire de la LTP

A. Les patrons d'activités provenant d'enregistrements des cellules de lieu sont utilisés pour induire de la plasticité dans la région CA1 de l'hippocampe.
B. L'utilisation du seul patron d'activité n'induit aucun changement synaptique.
C. En présence de carbachol, agoniste des récepteurs muscariniques de l'acétylcholine, une LTP est induite par le patron d'activité.

1997 ; Sjöström et al., 2001, 2003) pour induire la LTP en calcium non-physiologique. Il est probable que la réévaluation de la règle de STDP dans le cortex sera différente de l'hippocampe.

3. Le rôle des neuromodulateurs

Dopamine

Nos résultats indiquent que la perfusion de dopamine (DA) pendant l'appariement ne permet pas de récupérer la fenêtre de LTP, contrairement à ce qui a été montré dans une autre étude (Zhang et al., 2009). Plusieurs raisons peuvent expliquer cette différence : bien que la DA soit capable d'augmenter l'amplitude de la LTP dans des conditions de haut $[Ca^{2+}]_e$, ce n'est peut-être pas suffisant dans des conditions de $[Ca^{2+}]_e$ physiologique. De plus, l'étude de Zhang et collaborateurs (2009) a été réalisée sur cultures dissociées d'hippocampe, ce qui pourrait être une différence majeure pour les résultats observés. Les explorations futures du rôle de la DA devront probablement utiliser des agonistes spécifiques des récepteurs D1/D5 ou des bloqueurs des récepteurs D2, pour éventuellement observer un effet en calcium physiologique. Enfin, le rôle de l'inhibition devra être pris en compte, car dans les neurones pyramidaux de la couche 5 du cortex l'effet de la DA passe par une diminution de l'inhibition *via* l'activation des récepteurs D2 sur les interneurones (Xu and Yao, 2010).

Noradrénaline

Nos résultats montrent que la perfusion d'isoprénaline, un agoniste des récepteurs β-adrénergiques, permet de récupérer la fenêtre de LTP en $[Ca^{2+}]_e$ physiologique. Les études précédentes mettaient en évidence un rôle des récepteurs β-adrénergiques dans l'augmentation de la fenêtre temporelle d'induction de la LTP sans changement dans l'amplitude de la LTP (Lin et al., 2003). Nos données indiquent qu'elle aurait donc un rôle dans l'induction, et permet donc de diminuer le seuil d'induction de la LTP contrairement à des résultats

précédents (Edelmann and Lessmann, 2011). Néanmoins, quels sont les mécanismes sous-jacents à cette récupération ? Les effets de l'activation des récepteurs β-adrénergiques sont encore peu décrits dans le cadre de la plasticité synaptique. Bien qu'ils soient capable de permettre une augmentation du calcium intracellulaire (Seol et al., 2007), un travail important reste à faire sur les effets biophysiques concernant la rétro-propagation du potentiel d'action. On sait que les récepteurs β-adrénergiques peuvent améliorer la rétro-propagation par inhibition des canaux Kv 4.2 porteurs du courant I_A (Yuan et al., 2002), mais il reste à savoir si cela joue un rôle dans nos conditions. L'application de 4-amino-pyridine (4-AP), un bloqueur des canaux Kv 4.2, pourrait permettre d'identifier leurs rôles dans la récupération de la LTP en présence d'isoprénaline.

4. Aspect non-synaptique de la STDP

Nous avons vu que les changements synaptiques s'accompagnent de modifications de l'intégration dendritique et de l'excitabilité. En particulier, la LTP s'accompagne d'une E-S-Potentialisation et la LTD s'accompagne d'une E-S-Depression (Campanac and Debanne, 2008). Pour l'instant, nous n'avons pas étudié dans quelle mesure les changements synaptiques observés en $[Ca^{2+}]_e$ physiologique s'accompagnent de changements d'intégration dendritique. De plus, les changements synaptiques s'accompagnent de modifications de l'excitabilité intrinsèque du neurone pré- ou post-synaptique. Dans l'hippocampe, la LTP s'accompagne d'une augmentation de l'excitabilité du neurone pré-synaptique avec une augmentation du taux de décharge (Ganguly et al., 2000) mais d'une réduction de l'excitabilité pré-synaptique par une augmentation du courant I_h (Fan et al., 2005). La LTD s'accompagne d'une diminution de l'excitabilité du neurone post-synaptique (Li et al., 2004). Il serait donc intéressant de savoir si ces changements de l'intégration dendritique et de l'excitabilité se retrouvent dans des conditions physiologiques. Enfin, il a été montré qu'il existait une modulation différente du courant I_h, portée par les canaux HCN en fonction de

l'amplitude de la LTP ou LTD induite. Les fortes LTP s'accompagnent d'une diminution de l'excitabilité intrinsèque par une régulation à la hausse du courant I_h (Fan et al., 2005), alors que les faibles LTP s'accompagnent d'une augmentation de l'excitabilité intrinsèque par une régulation à la baisse du même courant (Campanac and Debanne, 2008). De la même manière, les fortes LTD s'accompagnent d'une augmentation de l'excitabilité intrinsèque par une régulation à la hausse du courant I_h (Brager and Johnston, 2007) alors que les faibles LTD s'accompagnent d'une diminution de l'excitabilité intrinsèque par une régulation à la baisse de ce courant (Gasselin et al., 2017). Il serait intéressant de savoir si ces changements homéostatiques se retrouvent dans nos conditions.

5. La seconde fenêtre de LTD

Nos résultats montrent une seconde fenêtre de LTD en haut calcium pour des délais positifs autour de +40/+60 ms. Ils s'ajoutent à deux études expérimentales (Nishiyama et al., 2000; Wittenberg and Wang, 2006) qui montraient elles aussi une fenêtre similaire. Néanmoins, ces études utilisaient une fréquence θ pour l'induction de la plasticité, ce qui pourrait augmenter la durée du potentiel d'action, activer des VDCC et induire une dépression synaptique (Zhou et al., 2005). Cependant, nos données proviennent de protocoles à faible fréquence. D'autres études seront nécessaires pour comprendre l'existence et les mécanismes sous-jacents à cette seconde fenêtre de dépression.

6. Le rôle des récepteurs NMDA pré-synaptiques

Nos résultats montrent que la LTP induite en haut calcium dépend des récepteurs NMDA post-synaptiques, alors que la LTD induite en bas calcium, pour le même protocole, semble plutôt reposer sur le récepteur NMDA pré-synaptique. Il est connu depuis longtemps que la LTP aux synapses CA3-CA1 repose sur le récepteur NMDA post-synaptique et son blocage empêche l'induction de LTP (Andrade-Talavera et al., 2016). Néanmoins, il semble que la LTD présente pour un appariement positif dépende des récepteurs NMDA pré-synaptiques.

Cela soulève beaucoup de questions sur les mécanismes sous-jacents et nécessitera des expériences approfondies, à l'image des travaux du groupe de Sjöström dans le cortex (Abrahamsson et al., 2017), pour établir le rôle joué par les récepteurs NMDA pré-synaptiques en $[Ca^{2+}]_e$ physiologique, et en particulier leurs voies de signalisation aux synapses CA3-CA1.

Conclusion

La règle de STDP est décrite dans de nombreuses structures, *in vitro* et *in vivo*. Néanmoins, un facteur important longtemps oublié est la concentration extracellulaire de calcium. Nous avons montré que l'utilisation de concentrations physiologiques (1.3 – 1.8 mM) de calcium altérait profondément la règle de STDP. Néanmoins, la modulation de l'activité pendant l'appariement ou l'application conjointe de neuromodulateurs a permis de récupérer une courbe classique de STDP aux synapses CA3-CA1 de l'hippocampe. Ces résultats poussent à une réévaluation de la règle de STDP dans l'ensemble des structures où elle a été décrite, mais apportent aussi des informations quant à son induction *in vivo*.

Annexes

1. Liste des communications scientifiques

- **12e Colloque de Neurosciences - du 19 au 22 mai 2015 - Société Française des Neurosciences – Montpellier.**
  Spike-timing dependent plasticity (STDP) rules in physiological extracellular calcium
  INGLEBERT Yanis, Dominique Debanne
- **International Neuroscience Conference 2016 – Linking cellular properties to neuronal network dynamics – 16-18 avril 2016 Marseille, France.**
  Spike-timing dependent plasticity (STDP) rules in physiological extracellular calcium
  INGLEBERT Yanis, Dominique Debanne
- **24th Annual Meeting of Doctoral School (19 mai 2016) UFR de Médecine La Timone, Marseille.**
  Homeostatic regulation of h-conductance controls intrinsic excitability and stabilizes the threshold for synaptic modification in CA1 neurons.
  Gasselin Célia, **Inglebert Yanis**, Dominique Debanne
- **10th FENS Forum of Neuroscience - Du 2-6 juillet 2016 Copenhague, Danemark.**
  Spike-timing dependent plasticity (STDP) rules in physiological extracellular calcium
  INGLEBERT Yanis, Dominique Debanne
- **CRCNS conference 2016 - 24 au 26 octobre 2016 - Agence Nationale de la Recherche (ANR) - Paris (Institut Pasteur)**
  Spike-timing dependent plasticity (STDP) rules in physiological extracellular calcium : experiments and theory.
  INGLEBERT Yanis, Yonatan Aljadeff, Nicolas Brunel, Dominique Debanne
- **COSYNE 2017 – Salt Lake City (USA) – 22 au 23 février 2017**
  STDP under physiological calcium concentration and implications for memory maintenance
  Yonatan Aljadeff **, INGLEBERT Yanis**, , Nicolas Brunel, Dominique Debanne
- **NeuroFrance 2017 - International meeting - 17 au 19 mai 2017 - Société Française des Neurosciences, Bordeaux, France**
  Spike-timing dependent plasticity (STDP) rules in physiological extracellular calcium: experiments and theory.
  INGLEBERT Yanis, Yonatan Aljadeff, Nicolas Brunel, Dominique Debanne
- **Annual Meeting Society of Neuroscience – 15-19 mai 2017 - Society of Neuroscience - Washington, D.C (USA)**
  Spike-timing dependent plasticity (STDP) rules in physiological extracellular calcium : experiments and theory.
  INGLEBERT Yanis, Yonatan Aljadeff, Nicolas Brunel, Dominique Debanne
- **INTERNATIONAL NEUROSCIENCE CONFERENCE 2018 – Neuroplasticity: from synapses to circuits – 15-16 avril 2018 – Marseille, France**
  Spike-timing dependent plasticity (STDP) rules in physiological extracellular calcium: experiments and theory.
  INGLEBERT Yanis, Yonatan Aljadeff, Nicolas Brunel, Dominique Debanne

2. Liste des publications

2.1 Homeostatic regulation of h-conductance controls intrinsic excitability and stabilizes the threshold for synaptic modification in CA1 neurons (J. Physiol 2015)

Célia Gasselin, **Yanis Inglebert**, Dominique Debanne

Journal of Physiology, 2015.

2.2 Plasticity of intrinsic excitability during LTD is mediated by bidirectional changes in h-channel activity (Scientific Reports 2017)

Célia Gasselin*, **Yanis Inglebert*,** Norbert Ankri & Dominique Debanne

Scientific Reports, 2017

* : co-premier auteur

2.3 Plasticity of intrinsic neuronal excitability (Curr. Op. in Neuro. 2019)

Dominique Debanne, **Yanis Inglebert**, Michaël Russier

Current Opinion in Neurobiology, 2019

JPn Neuroscience

The Journal of Physiology

J Physiol 593.22 (2015) pp 4855–4869

Homeostatic regulation of h-conductance controls intrinsic excitability and stabilizes the threshold for synaptic modification in CA1 neurons

Célia Gasselin[1,2,3], Yanis Inglebert[1,2,3] and Dominique Debanne[1,2,3]

[1] *INSERM, U-1072, Marseille, France*
[2] *Aix-Marseille University, Marseille, France*
[3] *Neurobiology of ion channels (UNIS), Marseille, France*

Key points

- We determined the contribution of the hyperpolarization-activated cationic (h) current (I_h) to the homeostatic regulation of CA1 pyramidal cells *in vitro* using chronic treatments (48 h) that either increase (picrotoxin) or decrease (kynurenate) neuronal activity.
- The h-conductance was found to be up- or down-regulated following chronic activity enhancement or activity deprivation, respectively. This bidirectional plasticity of I_h was found to subsequently alter both apparent input resistance and intrinsic neuronal excitability.
- Bidirectional homeostatic plasticity of I_h also determined EPSP waveform and EPSP summation tested at 5–30 Hz.
- Long-term synaptic modification induced by repetitive stimulation of the Schaffer collaterals was found to be constant across treatments in the presence of I_h but not when I_h was blocked pharmacologically. Thus, bidirectional homeostatic regulation of I_h stabilizes induction of long-term synaptic modification in CA1 pyramidal neurons that depends on EPSP summation.

Abstract The hyperpolarization-activated cationic (h) current is a voltage-shock absorber, highly expressed in the dendrites of CA1 pyramidal neurons. Up-regulation of I_h has been reported following episodes of intense network activity but the effect of activity deprivation on I_h and the functional consequence of homeostatic regulation of I_h remain unclear. We determined here the contribution of I_h to the homeostatic regulation of CA1 pyramidal cell excitability. Intrinsic neuronal excitability was decreased in neurons treated for 2–3 days with the $GABA_A$ channel blocker picrotoxin (PiTx) but increased in neurons treated (2–3 days) with the glutamate receptor antagonist kynurenate (Kyn). Membrane capacitance remained unchanged after treatment but the apparent input resistance was reduced for PiTx-treated neurons and enhanced for Kyn-treated neurons. Maximal I_h conductance was up-regulated after chronic hyperactivity but down-regulated following chronic hypoactivity. Up-regulation of I_h in PiTx-treated cultures was found to accelerate EPSP kinetics and reduce temporal summation of EPSPs whereas opposite effects were observed in Kyn-treated cultures, indicating that homeostatic regulation of I_h may control the induction of synaptic modification depending on EPSP summation. In fact, stimulation of the Schaffer collaterals at 3–10 Hz induced differential levels of plasticity in PiTx-treated and Kyn-treated neurons when I_h was blocked pharmacologically but not in control conditions. These data indicate that homeostatic regulation of I_h normalizes the threshold for long-term synaptic modification that depends on EPSP summation. In conclusion, bidirectional homeostatic regulation of I_h not only controls spiking activity but also stabilizes the threshold for long-term potentiation induced in CA1 pyramidal neurons by repetitive stimulation.

DOI: 10.1113/JP271369

(Resubmitted 27 July 2015; accepted after revision 15 August 2015; first published online 28 August 2015)
Corresponding author D. Debanne: Université de la Méditerranée, Boulevard Pierre Dramard, Marseille 13916, France. Email: dominique.debanne@univ-amu.fr

Abbreviations BCM, Bienenstock–Cooper–Monroe rule; fEPSP, field EPSP; I_h, hyperpolarization-activated cationic current; Kyn, kynurenate; LTD, long-term depression; LTP, long-term potentiation; PiTx, picrotoxin.

Introduction

Hebbian synaptic plasticity has a destabilizing effect on network activity, driving synaptic strength to extreme values (Turrigiano & Nelson, 2004). Extreme potentiation or depression may indeed lead to runaway excitation or extinction of spiking activity, respectively, in neural circuits. The functional synergy observed between synaptic and intrinsic plasticity in principal neurons (Daoudal *et al.* 2002; Wang *et al.* 2003; Campanac & Debanne, 2008) may further increase this destabilization. In order to prevent these extreme cases, compensatory mechanisms, called homeostatic plasticity, act to maintain neuronal activity within physiological bounds (Turrigiano & Nelson, 2004; Turrigiano, 2011). Synaptic transmission and intrinsic neuronal excitability are indeed adjusted following persistent changes in network activity. For instance, synaptic strength and intrinsic excitability are enhanced following chronic activity deprivation (Turrigiano *et al.* 1998; Desai *et al.* 1999; Karmarkar & Buonomano, 2006; Cudmore *et al.* 2010). Conversely, synaptic strength and intrinsic excitability are diminished after chronic hyperactivity of neuronal circuits (Karmarkar & Buonomano, 2006). Finally, synaptic transmission and intrinsic neuronal excitability are conjointly enhanced in parvalbumin-positive basket cells to stabilize the balance between synaptic excitation and inhibition (Campanac *et al.* 2013).

The substrate for homeostatic regulation of intrinsic neuronal excitability includes a wide range of voltage-gated ion channels including Na^+ (Desai *et al.* 1999; Aptowicz *et al.* 2004), Ca^{2+} (Desai *et al.* 1999) and K^+ channels (Desai *et al.* 1999; Cudmore *et al.* 2010; O'Leary *et al.* 2010; Kirchheim *et al.* 2013). The hyperpolarization-activated cationic current (I_h) is a major player in the control of intrinsic excitability. It determines membrane potential, input resistance, dendritic integration, EPSP summation and constrains synaptically evoked Ca^{2+} spikes (Maccaferri *et al.* 1993; Gasparini & DiFrancesco, 1997; Magee, 1998; Tsay *et al.* 2007; Shah, 2014). I_h is also involved in homeostatic modification of intrinsic neuronal excitability. While up-regulation of I_h has been reported upon enhanced neuronal activity (Chen *et al.* 2001; van Welie *et al.* 2004; Fan *et al.* 2005; Dyhrfjeld-Johnsen *et al.* 2008), it is still unclear whether I_h is down-regulated after activity deprivation (Breton & Stuart, 2009).

I_h controls temporal summation of EPSPs (Magee, 1998, 1999), suggesting that it might be able to set the threshold and magnitude of long-term synaptic modification induced by repetitive stimulation of afferent inputs. In fact, in the presence of h-channel blockers, the magnitude of long-term potentiation (LTP) is generally enhanced (Nolan *et al.* 2004; Campanac *et al.* 2008). However, the consequence of the homeostatic modulation of I_h on the induction of homosynaptic long-term synaptic plasticity is not clearly determined, principally because the homeostatic regulation of synaptic plasticity might interfere with the homeostatic regulation of voltage-gated conductances, including I_h.

In this study, we have therefore examined the contribution of I_h (1) to the homeostatic regulation of intrinsic neuronal excitability, and (2) to the induction of long-term synaptic plasticity. We show that I_h is bidirectionally regulated in CA1 pyramidal neurons by chronic manipulation of network activity in organotypic slice cultures of hippocampus. Maximal I_h conductance was found to be down-regulated after chronic (48–72 h) hypoactivity induced by the ionotropic glutamate receptor antagonist kynurenate, but up-regulated following chronic hyperactivity induced by the $GABA_A$ channel blocker picrotoxin. This bidirectional regulation of I_h is not limited to the control of intrinsic neuronal excitability. It also alters EPSP summation and subsequently compensates the up- and down-regulation of long-term synaptic modifications that result from homeostatic regulation of synaptic transmission. Our results thus indicate that homeostatic regulation of I_h therefore stabilizes the threshold for long-term synaptic modification in CA1 neurons induced by repetitive stimulation.

Methods

Organotypic hippocampal slice cultures

Interface hippocampal slice cultures were prepared as described previously (Stoppini *et al.* 1991; Boudkkazi *et al.* 2007; Debanne *et al.* 2008). All experimental procedures were carried out according to the European and Institutional guidelines for the care and use of laboratory animals (Council Directive 86/609/EEC and French National Research Council). Postnatal day 6–8 Wistar rats were deeply anaesthetized by intraperitoneal

injection of chloral hydrate (200 mg kg^{-1}) and killed by decapitation. The brain was removed and each hippocampus was individually dissected. Hippocampal slices (300–350 μm) were cut in an ice-cold solution containing (mM): 280 sucrose, 26 $NaHCO_3$, 10 D-glucose, 10 $MgCl_2$, 1.3 KCl, 1 $CaCl_2$, 1 kynurenate, and were bubbled with 95% O_2–5% CO_2. Penicillin–streptomycin was added. Slices were then transferred onto 20 mm latex membranes (Millicell, Merck Millipore, Darmstadt, Germany) inserted into 35 mm Petri dishes containing 1 ml of culture medium and maintained in an incubator at 37°C, 95% O_2–5% CO_2. The culture medium contained (in ml) 25 minimum essential medium (MEM), 12.5 Hank's balanced salt solution (HBSS), 12.5 horse serum, 0.5 penicillin–streptomycin, 0.6 glucose (1 M), 0.1 ascorbic acid (1 mg ml^{-1}), 0.4 Hepes (1 M), 0.5 B27 and 8.95 sterile H_2O. To limit glial proliferation, 5 μM cytosine arabinoside (AraC) was added to the culture medium starting at 3 DIV.

Electrophysiology and data acquisition

The slice cultures were transferred to a temperature-controlled recording chamber with oxygenated artificial cerebrospinal fluid (ACSF; in mM: NaCl, 125; KCl, 2.5; NaH_2PO_4, 0.8; $NaHCO_3$, 26; $CaCl_2$, 3; $MgCl_2$, 2; D-glucose, 10). CA1 pyramidal neurons were visualized by differential interference contrast (DIC) infrared (IR)-videomicroscopy. Pipettes were filled with an internal solution containing (in mM): potassium gluconate, 120; KCl, 20; Hepes, 10; EGTA, 0.5; $MgCl_2$, 2; Na_2ATP, 2.

Electrophysiological recordings were obtained using an Axoclamp-2B, an Axopatch-200B or a Multiclamp-700B amplifier (Molecular Devices, Sunnyvale, CA, USA), and pCLAMP v.8 or 10 (Molecular Devices). All the recordings of intrinsic neuronal excitability were obtained in the presence of kynurenate (2 mM) and picrotoxin (100 μM) to block excitatory and inhibitory synaptic transmission. Data were analysed with Igor Pro v.6 (Wavemetrics, Lake Oswego, OR, USA), and ClampFit (Molecular Devices).

Electrophysiological properties of recorded CA1 neurons were tested in current clamp by current injection (−155 to 155 pA; 800 ms). I_h was isolated in voltage clamp by subtraction of control records from those obtained with h-blockers (ZD-7288) in the bath and was measured by a voltage-clamp step from −50 mV to the test potential (−60 to −120 mV, 10 mV increment). EPSP summation was tested by injection of trains of five synaptic-like currents at frequencies ranging from 5 to 30 Hz. The profile of the synaptic-like current was given by $f(t) = a(1 - \exp(-t/\tau_{on}))\exp(-t/\tau_{off})$, with $\tau_{on} = 1$ ms and $\tau_{off} = 10$ ms.

Field potentials were recorded in the stratum radiatum of the CA1 region by using glass microelectrodes filled with 3 M NaCl. $GABA_A$ receptor-mediated inhibition was blocked with 100 μM picrotoxin and the area CA1 was surgically isolated from CA3 to avoid epileptiform activity. Glass stimulating electrodes filled with extracellular saline were placed in the stratum radiatum. Long-term synaptic modification was induced with 10 bursts of 10 shocks at 5, 10 or 100 Hz (Dudek & Bear, 1992). This procedure was slightly modified for 3 Hz stimulation (90 bursts of 10 shocks).

Data analysis

Apparent input resistance was determined by linearly fitting the voltage deflections induced by negative current pulses. Capacitance was calculated by exponential fitting of the voltage deflection ($y = A^*(1 - e^{-t/\tau})$) in the presence of ZD-7288 using LabVIEW 10.0 (National Instruments, Austin, TX, USA). The gain in the input-output curves was calculated on each cell by fitting the linear part of the curve. The I_h was characterized by comparing hyperpolarization-induced currents obtained in control conditions with those obtained in the presence of 10 μM ZD-7288. Activation was assessed by voltage steps from a holding potential of −50 mV to −60 - −120 mV. Subtraction of control records from those obtained after ZD-7288 application allowed isolation of I_h. Conductance was determined by $G_h = I_h/(V - E_h)$ with $E_h = -37.7$ mV (E_h is the reversal potential for I_h; Campanac *et al.* 2008). Spontaneous depolarizing activity was assessed by measuring EPSP area from the resting membrane potential with a semi-automatic procedure in which a horizontal cursor was adjusted on each trial to define the baseline.

Pooled data are presented as means ± SEM. Statistical comparisons were made using Mann–Whitney or Wilcoxon tests with SigmaPlot software (Systat Software Inc., San Jose, CA, USA).

Drugs

Kynurenate (Kyn, 2 mM) and picrotoxin (PiTx, 50 μM) were added to the culture medium 48–72 h before recording. Kynurenate and picrotoxin were purchased from Sigma (St. Louis, MO, USA), and ZD-7288 was obtained from Tocris Bioscience (Bristol, UK).

Results

Homeostatic regulation of intrinsic neuronal excitability in CA1 pyramidal neurons

The effect of chronic hyper- or hypoactivity on the excitability of CA1 pyramidal neurons was assessed in organotypic slice cultures of rat hippocampus. Cultures were treated for 48–72 h with either 2 mM Kyn (Kyn-treated), 50 μM PiTx (PiTx-treated) or with control

medium (Control). Acutely applied, these treatments blocked or increased spontaneous excitatory activity. Spontaneous activity was quantified in control and treated cultures by measuring the net area of excitatory synaptic activity. In fact, spontaneous depolarizing synaptic activity measured in CA1 pyramidal neurons was considerably reduced in the presence of Kyn (15 ± 5% of the control EPSP area, $n = 7$; $P < 0.001$), indicating that it was mediated by AMPA and NMDA receptors (Fig. 1*A* and *B*). In contrast, spontaneous depolarizing activity was augmented in the presence of PiTx and epileptiform bursting could be observed (760 ± 167% of the control depolarizing area, $n = 6$; $P < 0.001$; Fig. 1*A* and *B*).

Depolarizing current pulses (800 ms, 15–155 pA) were injected in the cell body of CA1 pyramidal neurons to compare intrinsic excitability of CA1 pyramidal cells in chronically treated cultures (Fig. 1*C*). In fact, the minimal current eliciting an action potential (i.e. rheobase) was reduced in Kyn-treated neurons (from 79 ± 3 pA, $n = 46$ in control neurons to 44 ± 2 pA, $n = 39$, Mann–Whitney, $P < 0.001$) but enhanced in PiTx-treated cells (130 ± 5 pA, $n = 34$, Mann–Whitney, $P < 0.001$; Fig. 1*D*). In addition, the gain of the input–output curves was enhanced in Kyn-treated neurons (from 0.23 ± 0.01 spikes pA^{-1}, $n = 46$ in control neurons to 0.34 ± 0.02 spikes pA^{-1}, $n = 39$; Mann–Whitney, $P < 0.001$; Fig. 1*E*) but reduced

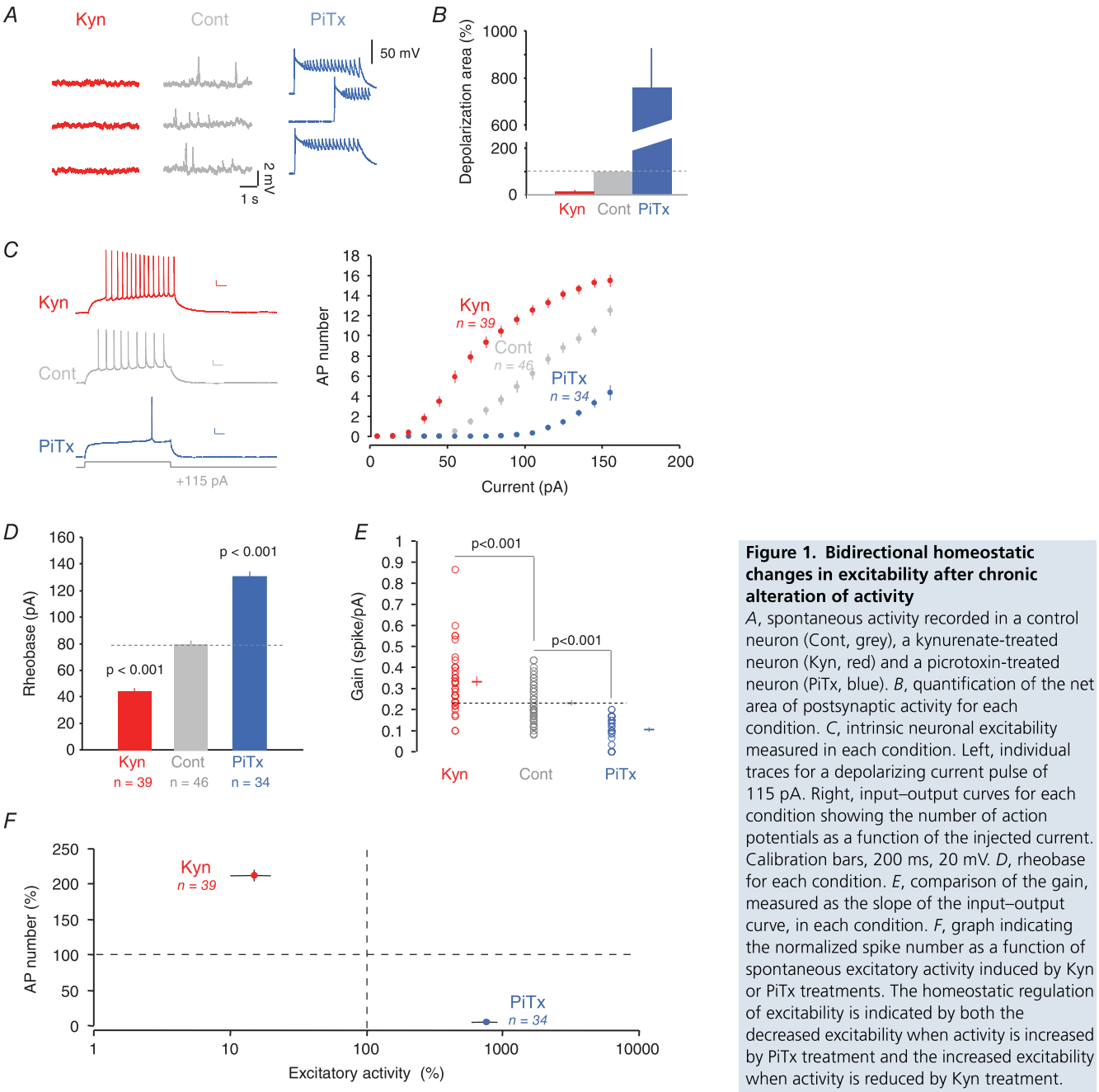

Figure 1. Bidirectional homeostatic changes in excitability after chronic alteration of activity
A, spontaneous activity recorded in a control neuron (Cont, grey), a kynurenate-treated neuron (Kyn, red) and a picrotoxin-treated neuron (PiTx, blue). *B*, quantification of the net area of postsynaptic activity for each condition. *C*, intrinsic neuronal excitability measured in each condition. Left, individual traces for a depolarizing current pulse of 115 pA. Right, input–output curves for each condition showing the number of action potentials as a function of the injected current. Calibration bars, 200 ms, 20 mV. *D*, rheobase for each condition. *E*, comparison of the gain, measured as the slope of the input–output curve, in each condition. *F*, graph indicating the normalized spike number as a function of spontaneous excitatory activity induced by Kyn or PiTx treatments. The homeostatic regulation of excitability is indicated by both the decreased excitability when activity is increased by PiTx treatment and the increased excitability when activity is reduced by Kyn treatment.

in PiTx-treated cells (0.10 ± 0.01 spikes pA^{-1}, $n = 34$). All the measurements were performed at comparable membrane potential (−65.0 ± 0.3 mV, $n = 39$ in control cultures, −64.6 ± 0.4 mV, $n = 46$ in Kyn-treated cultures and −64.2 ± 0.4 mV, $n = 34$ in PiTx cultures, Mann–Whitney U test, $P > 0.05$ in all cases). The holding current was comparable in the three conditions (−0.3 ± 1.9 pA in control cultures, −5.0 ± 2.0 pA in Kyn-treated neurons, and −1.0 ± 1.5 pA in PiTx-treated cultures; Mann–Whitney U test, $P > 0.1$ in all cases). The resting membrane potential (no holding current) has been measured in a subset of neurons. No difference was observed across categories (−65.3 ± 0.5 mV ($n = 19$) in control neurons, −64.3 ± 0.5 mV ($n = 16$) in Kyn-treated neurons and −65.0 ± 0.6 mV ($n = 17$) in PiTx-treated neurons; $P > 0.1$). In conclusion, changes in intrinsic excitability are negatively correlated with the variation in excitatory activity imposed during chronic treatments (Fig. 1*F*).

Bidirectional changes in apparent input resistance

In order to evaluate whether I_h was regulated, we also measured the apparent input resistance (R_{in}) with hyperpolarizing current pulses (800 ms, −5 to −155 pA) injected in the soma. Apparent R_{in} was calculated for each neuron as the linear slope of the voltage shift induced by each value of hyperpolarizing current. In PiTx-treated cultures, apparent R_{in} was found to be reduced (193 ± 6 MΩ in control, $n = 50$, *vs.* 154 ± 6 MΩ in PiTx-treated cultures, $n = 41$, Mann–Whitney U test, $P < 0.001$; Fig. 2*A*) but increased in Kyn-treated cultures (240 ± 6 MΩ in Kyn-treated cultures, $n = 53$, Mann–Whitney U test, $P < 0.001$; Fig. 2*A*). These variations in input resistance were strongly reduced when I_h was blocked with the h-channel blocker ZD-7288 (289 ± 14 MΩ, $n = 26$ in control neurons, 277 ± 9 MΩ, $n = 21$ in PiTx-treated neurons, Mann–Whitney, $P > 0.1$, and 331 ± 15 MΩ, $n = 24$ in Kyn-treated neurons, Mann–Whitney, $P > 0.01$; Fig. 2*B*), indicating that the observed differences in input resistance mostly result from the bidirectional regulation of h-channels. Nevertheless, there were still substantial changes present after h-channel block, suggesting that another conductance might be regulated in parallel. In addition, the membrane capacitance measured in the presence of ZD-7288 showed no change in control *vs.* Kyn-treated and PiTx-treated cultures (220 ± 14 pF, $n = 27$, in control neurons; 224 ± 11 pF, $n = 22$, in Kyn-treated neurons, Mann–Whitney, $P > 0.1$; 220 ± 9 pF, $n = 21$, in PiTx-treated neurons, Mann–Whitney, $P > 0.1$; Fig. 2*C*).

In CA1 pyramidal neurons, I_h not only determines apparent R_{in} but also resting membrane potential. All these pharmacological experiments were performed while membrane potential was kept constant (−65 mV, $P > 0.2$). However, consistent with the differential regulation of h-current, the amount of holding current applied to maintain the neuron at constant potential is not significantly changed in Kyn-treated neurons after application of ZD-7288, whereas it is superior to the control increase in PiTx-treated neurons (from −2 ± 3 pA to 9 ± 4 pA, $n = 25$, in control neurons, Mann–Whitney, $P = 0.021$; from −7 ± 4 pA to −5 ± 5 pA, $n = 23$, in Kyn-treated neurons, Mann–Whitney, $P > 0.1$; from −0.6 ± 3 pA to 17 ± 5 pA, $n = 20$, in PiTx-treated neurons, Mann–Whitney, $P < 0.001$; Fig. 2*D*). In conclusion, as for intrinsic neuronal excitability, changes in apparent R_{in} are negatively correlated with changes in excitatory activity (Fig. 2*E*).

Bidirectional changes in I_h

In order to further confirm the differential contribution of I_h after each treatment, the gain in apparent R_{in} due to ZD-7288 (10 μM) was compared in each condition. In these experiments, the initial voltage deflection measured in the soma was set to a constant value (−18.9 ± 0.07 mV) in order to activate the same amount of I_h in the three conditions. As expected, the increased apparent conductance induced by ZD-7288 was small in Kyn-treated neurons (135 ± 7%, $n = 28$, *vs.* 160 ± 9%, $n = 30$, in control neurons, Mann–Whitney, $P < 0.1$; Fig. 3*A*) but large in PiTx-treated neurons (177 ± 7%, $n = 25$, Mann–Whitney, $P < 0.1$; Fig. 3*A*).

Next, the biophysical properties of I_h were tested in the three conditions. CA1 pyramidal neurons were recorded in voltage clamp and negative steps of voltage (to −60 - −120 mV) were applied from a holding potential of −50 mV. The ZD-7288-sensitive maximal conductance was found to be reduced by ∼40% in Kyn-treated neurons (1.5 ± 0.2 nS, $n = 25$, in control neurons *vs.* 0.9 ± 0.1 nS, $n = 24$, in Kyn-treated neurons, Mann–Whitney, $P < 0.01$; Fig. 3*B* and *C*) but increased by ∼40% in PiTx-treated neurons (2.1 ± 0.2 nS, $n = 20$, Mann–Whitney, $P < 0.01$; Fig. 3*B* and *C*). Activation curves remained unchanged, however (Fig. 3*C*), indicating that the regulation of I_h cannot be explained by alteration in its voltage dependence. In conclusion, changes in maximal h-conductance are positively correlated with the changes in excitatory activity induced by the kynurenate and picrotoxin treatments (Fig. 3*D*).

I_h is implicated in excitability changes

We next examined the specific contribution of I_h regulation to intrinsic neuronal excitability. Blocking I_h with ZD-7288 increased intrinsic excitability in control cultures (Fig. 4*A*), reducing the rheobase from 89 ± 5 pA

to 67 ± 6 pA ($n = 19$, Wilcoxon, $P < 0.001$). Consistent with a weak h-conductance in Kyn-treated neurons, no significant changes in intrinsic excitability were observed in the presence of ZD-7288 (rheobase from 46 ± 2 pA to 45 ± 4 pA, $n = 14$, Wilcoxon, $P > 0.1$; Fig. 4*B*). In contrast, ZD-7288 application strongly increased the intrinsic excitability in PiTx-treated neurons (rheobase from 131 ± 8 pA to 80 ± 8 pA, $n = 10$, Wilcoxon, $P < 0.01$; Fig. 4*C*). These data indicate that a significant portion of the change in excitability results from the bidirectional regulation of I_h. In fact, the difference between the three input–output curves was strongly diminished in the presence of ZD-7288 (Fig. 4*D*). However, the difference was not totally abolished, indicating that in parallel to the bidirectional regulation of the h-current other conductances might be involved.

Homeostatic regulation of I_h determines synaptic waveform and EPSP summation

We next determined the consequence of bidirectional regulation of I_h on synaptic integration and EPSP summation. In a first step, we compared the EPSP waveform recorded extracellularly in the dendrites of CA1 pyramidal neurons in control, Kyn- and PiTx-treated cultures. The experiments were performed

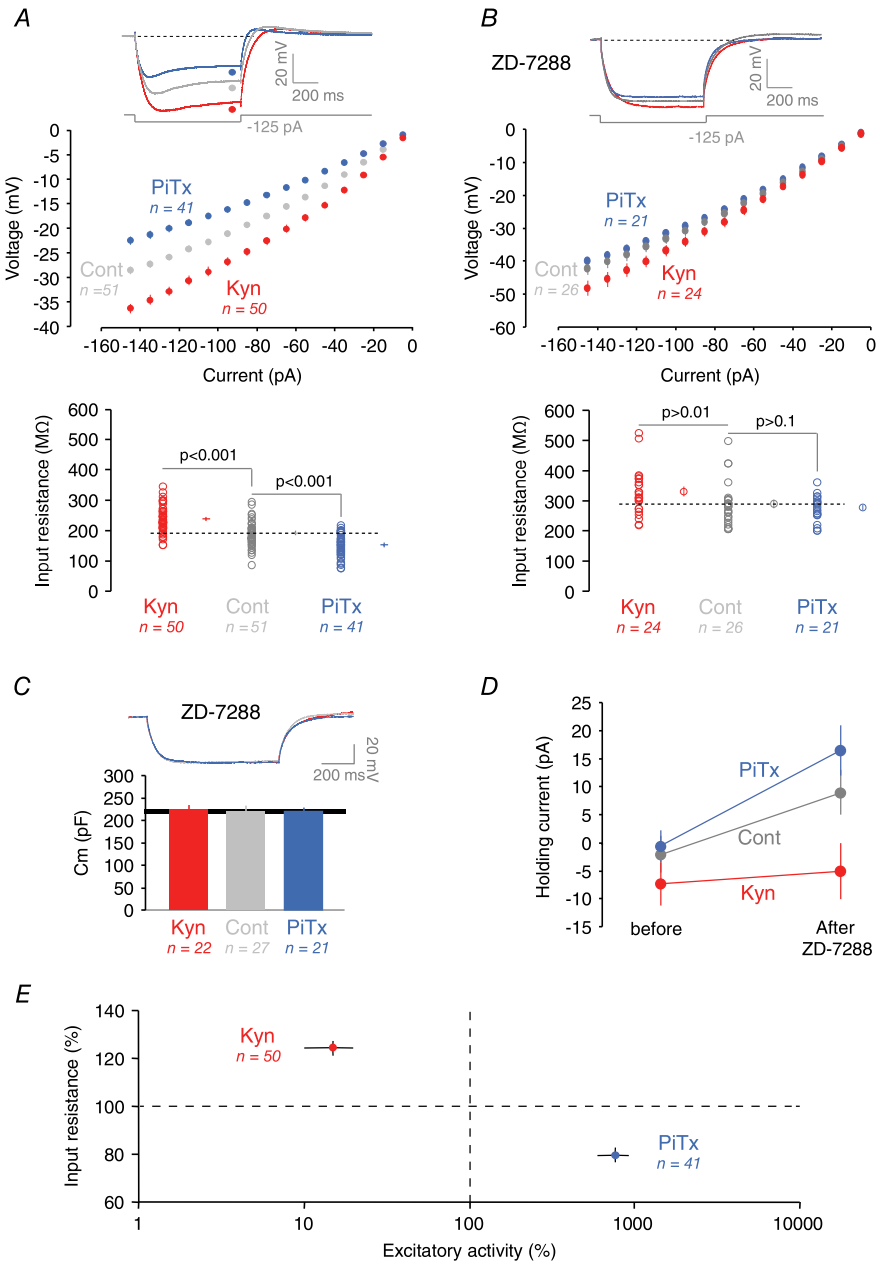

Figure 2. Bidirectional regulation of apparent R_{in}
A, input resistance in control, Kyn- and PiTx-treated CA1 neurons. Top, individual traces for a hyperpolarization of −125 pA for each condition (Cont, grey; PiTx, blue; Kyn, red). Middle, voltage measured at the steady-state phase of the hyperpolarization as a function of the current injected for each condition. Bottom, input resistance for each condition, measured by fitting. Membrane potential: −64.8 ± 0.3 mV, $n = 51$ in control neurons; −64.3 ± 0.3 mV, $n = 50$ in Kyn-treated neurons and −64.1 ± 0.4, $n = 41$ in PiTx-treated cells ($P > 0.1$ for all comparisons). *B*, R_{in} in the presence of ZD-7288 (10 μM). Membrane potential: −65.0 ± 0.6 mV, $n = 26$ in control; −64.5 ± 0.5 mV, $n = 24$ in Kyn; −63.3 ± 0.5, $n = 21$ in PiTx ($P > 0.05$ for all). *C*, effects of chronic treatments on membrane capacitance. Top, representative traces. Bottom, quantitative data. *D*, holding current injected to maintain the pyramidal neurons at a resting potential of −65 mV before and after ZD-7288 application for each condition. *E*, normalized input resistance as a function of spontaneous excitatory activity. The homeostatic regulation of input resistance is indicated by both the decreased R_{in} when activity is increased by PiTx treatment and the increased R_{in} when activity is reduced by Kyn treatment.

in the presence of PiTx (100 μM) to block $GABA_A$ receptor-mediated inhibition. The EPSP half-width measured extracellularly was significantly broader in Kyn-treated cultures compared to control and PiTx-treated cultures (3.6 ± 0.6 ms, $n = 9$ in Kyn-treated cultures *vs.* 2.4 ± 0.6 ms, $n = 8$ in control, $P = 0.075$ Mann–Whitney U test and 1.2 ± 0.2 ms, $n = 9$ in PiTx-treated cultures, $P < 0.001$ Mann–Whitney U test; Fig. 5*A*). To determine whether these differential effects resulted from a change in the waveform of glutamatergic synaptic currents or from the shaping of these currents by voltage-gated conductances downstream from the synapse, synaptic-like current was injected in the soma and the kinetics of the resulting simulated EPSP was compared among treatments. Confirming previous results obtained with biological field EPSPs, simulated intracellular EPSPs displayed significantly different time courses. Compared to controls, EPSPs were broader in Kyn-treated CA1 neurons but faster in PiTx-treated neurons (half-width: 50 ± 2 ms in control cultures, $n = 22$, *vs.* 65 ± 3 ms in Kyn-treated cultures, $n = 28$, $P < 0.001$, Mann–Whitney U test and 43 ± 2 ms in PiTx-treated cultures, $n = 24$, $P < 0.01$, Mann–Whitney U test; Fig. 5*B*).

Next, temporal summation of simulated EPSPs (5–30 Hz) was tested in CA1 pyramidal neurons recorded in the three experimental conditions. Compared to control neurons, EPSP summation was found to significantly increase in Kyn-treated neurons at 10, 15, 20 and 30 Hz, whereas a significant loss in EPSP summation was obtained in PiTx-treated neurons at 15, 20 and 30 Hz

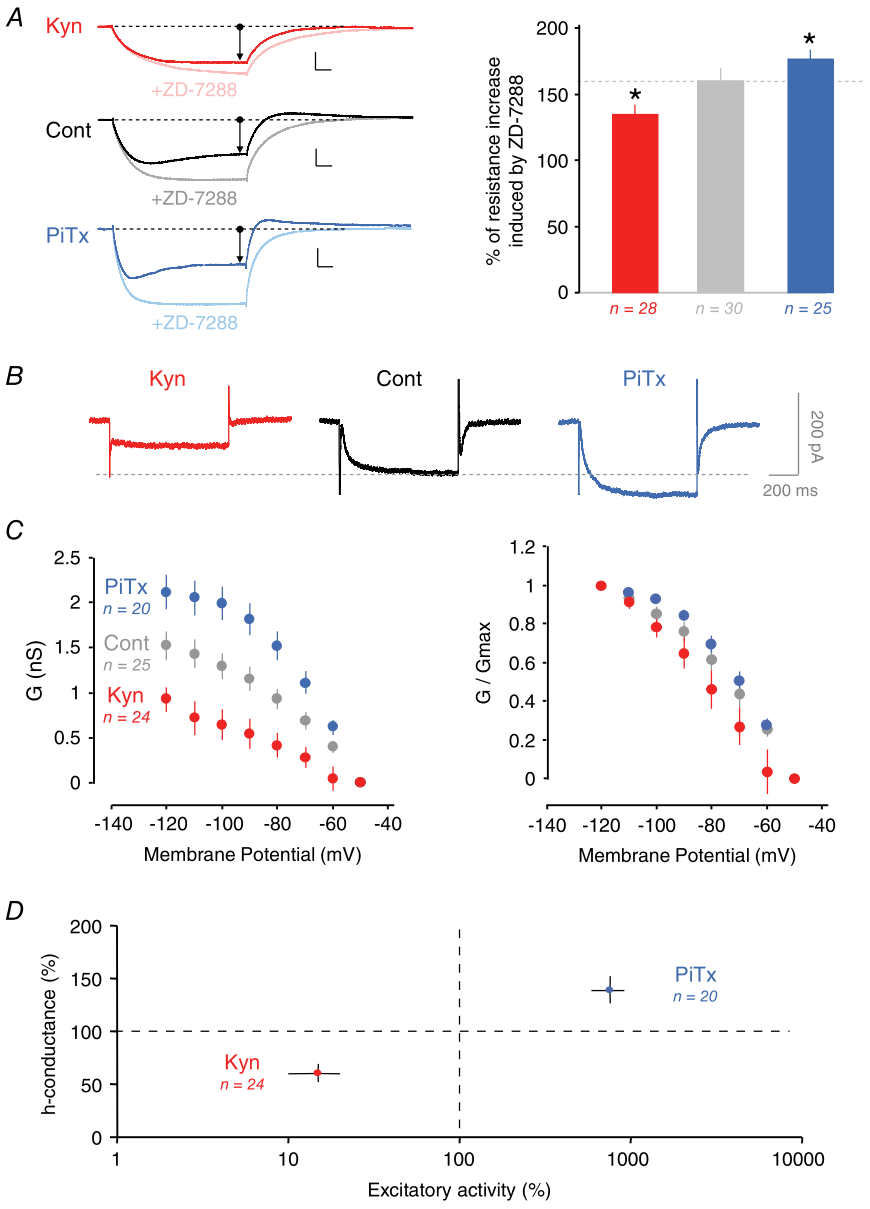

Figure 3. Bidirectional regulation of h-current
A, effects of ZD-7288 on input resistance in Kyn- and PiTx-treated neurons. Left, individual traces before and after ZD-7288 application for each condition. The initial input resistance is identical for each condition. Right, percentage of input resistance increase after ZD-7288 application. Membrane potential before ZD-7288: −64.7 ± 0.4 mV in control, −64.2 ± 0.4 mV in Kyn- and −64.0 ± 0.4 mV in PiTx-treated neurons ($P > 0.1$ for all). Membrane potential after ZD-7288: −65.3 ± 0.6 mV in control, −64.3 ± 0.5 in Kyn- and −64.5 ± 0.6 in PiTx-treated neurons ($P > 0.1$ for all comparisons). *B*, voltage-clamp recording of h-current in each condition. These traces were obtained by subtracting from control traces recorded after ZD-7288 application to the control ones. *C*, activation curve of h-current. Left, differences in the maximal conductance of I_h are observed between each condition. Right, normalized conductance allowed no changes to be seen in the biophysical properties of activation. *D*, h-conductance as a function of spontaneous excitatory activity. Note the increased h-conductance when activity is increased by PiTx treatment and the decreased h-conductance when activity is reduced by Kyn treatment.

(Fig. 5*C*). These differential changes in EPSP summation most likely resulted from the regulation of I_h. To test this hypothesis, we compared the effect of blocking I_h with ZD-7288 in neurons in the three conditions. ZD-7288 induced a significant increase in EPSP summation in hyperactive neurons (PiTx-treated) but no significant change in hypoactive cells (Kyn-treated, Fig. 5*D*), thus confirming the major contribution of I_h in the differential regulation of EPSP summation.

Homeostatic regulation of I_h and induction of long-term synaptic modification

Because homeostatic regulation of I_h largely affects EPSP summation, we next wondered what could be the consequence of this regulation on synaptic plasticity induced with repetitive stimulation of excitatory inputs. The Schaffer collaterals were stimulated at 10 Hz, a critical frequency for the induction of long-term synaptic modification (Dudek & Bear, 1992). Surprisingly, no significant change in synaptic plasticity was observed among treatments (changes in EPSP slope measured 10–30 min after 10 Hz stimulation: 128 ± 10% of the control field EPSP (fEPSP) slope, $n = 10$ in Kyn-treated neurons, 133 ± 21%, $n = 9$ in control neurons and 128 ± 10%, $n = 9$ in PiTx-treated cells; $P > 0.1$ for all comparisons; Fig. 6*A*, left and Fig. 6*C*, left). However, blocking h-channels in the same experiments with ZD-7288 (1 μM) induced differential plasticity in PiTx neurons (145 ± 29%, $n = 8$ in PiTx-treated cells *vs.* 93 ± 11%, $n = 9$ in Kyn-treated cells, and 102 ± 8%, $n = 9$ in control; Fig. 6*A*, right). The use of ZD-7288 at 1 μM does not directly affect the synaptic transmission (Gastrein *et al.* 2011). To avoid any saturating effect of two sequential synaptic plasticity inductions, we directly applied ZD-7288 on naive cultures and stimulated the Schaffer collaterals at 10 Hz. Significant long-term synaptic potentiation was observed in PiTx-treated cells compared to control or Kyn-treated neurons (146 ± 12%, $n = 8$ in PiTx-treated cells *vs.* 94 ± 7%, $n = 8$, $P = 0.002$ Mann–Whitney *U* test, in Kyn-treated cells, and 106 ± 6%, $n = 7$, $P = 0.02$, in control cells; Fig. 6*B* and *C*, right). The effects of Schaffer collateral stimulation at 3, 5

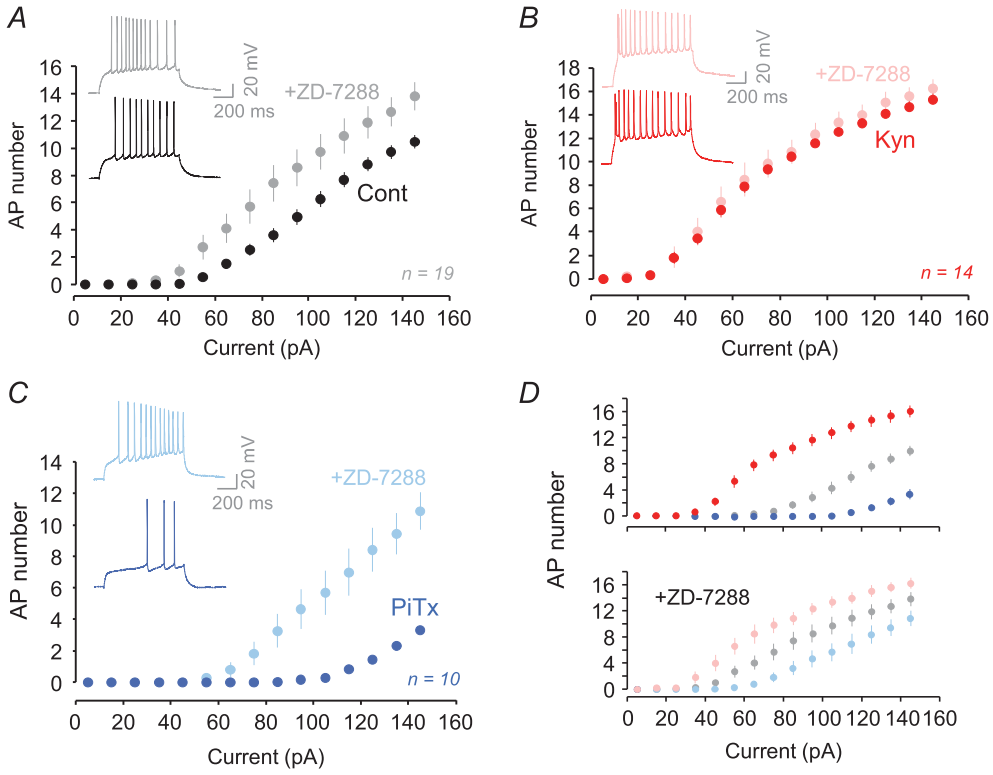

Figure 4. Role of I_h in the homeostatic regulation of cell excitability
A, number of action potentials fired for each current injection before and after ZD-7288 application in control neurons. Inset, representative traces. Membrane potential before ZD-7288: −65.2 ± 0.4 mV in control, −63.9 ± 0.5 mV in Kyn- and −63.3 ± 0.6 mV in PiTx-treated neurons ($P > 0.01$ for all comparisons). Membrane potential after ZD-7288: −65.5 ± 0.7 mV in control, −64.7 ± 0.6 mV in Kyn- and −63.6 ± 0.5 mV in PiTx-treated neurons ($P > 0.05$ for all comparisons). *B*, as in *A* with Kyn-treated neurons. *C*, as in *A* with PiTx-treated neurons. *D*, ZD-7288 application reduced the divergence of the input–output curves (top, before ZD-7288; bottom, after ZD-7288).

and 100 Hz was also tested in control, Kyn-treated and PiTx-treated cultures in the absence or in the presence of ZD-7288 (Fig. 6*D*). Confirming our results, in the presence of I_h (control condition), the level of plasticity was found to be similar across treatments (Fig. 6*D*, left). In contrast, blocking h-channels with ZD-7288 unmasked a differential potentiation in PiTx-treated cultures at 3 and 5 Hz but not at 100 Hz (Fig. 6*D*, right). It is well established that ZD-7288 induces a hyperpolarization of the membrane potential that cannot be controlled in field potential recording. This hyperpolarization may interfere with LTP induction. We therefore explored the effects of 10 Hz stimulation in whole-cell recordings. In fact, blocking h-channels with ZD-7288 had virtually no effect on LTP in Kyn-treated neurons (141 ± 24%, $n = 8$ in control and 142 ± 11%, $n = 6$ in ZD-7288; $P > 0.1$ Mann–Whitney test) but increased LTP in PiTx-treated neurons (from 123 ± 15%, $n = 10$ to 176 ± 36%, $n = 7$; $P < 0.05$ Mann–Whitney test; Fig. 6*E*).

We then examined the possible origin of this differential plasticity. A major determinant of the magnitude of long-term synaptic modification is the initial strength of the synapse (Debanne *et al.* 1999) and homeostatic treatments are known to modify AMPA receptor

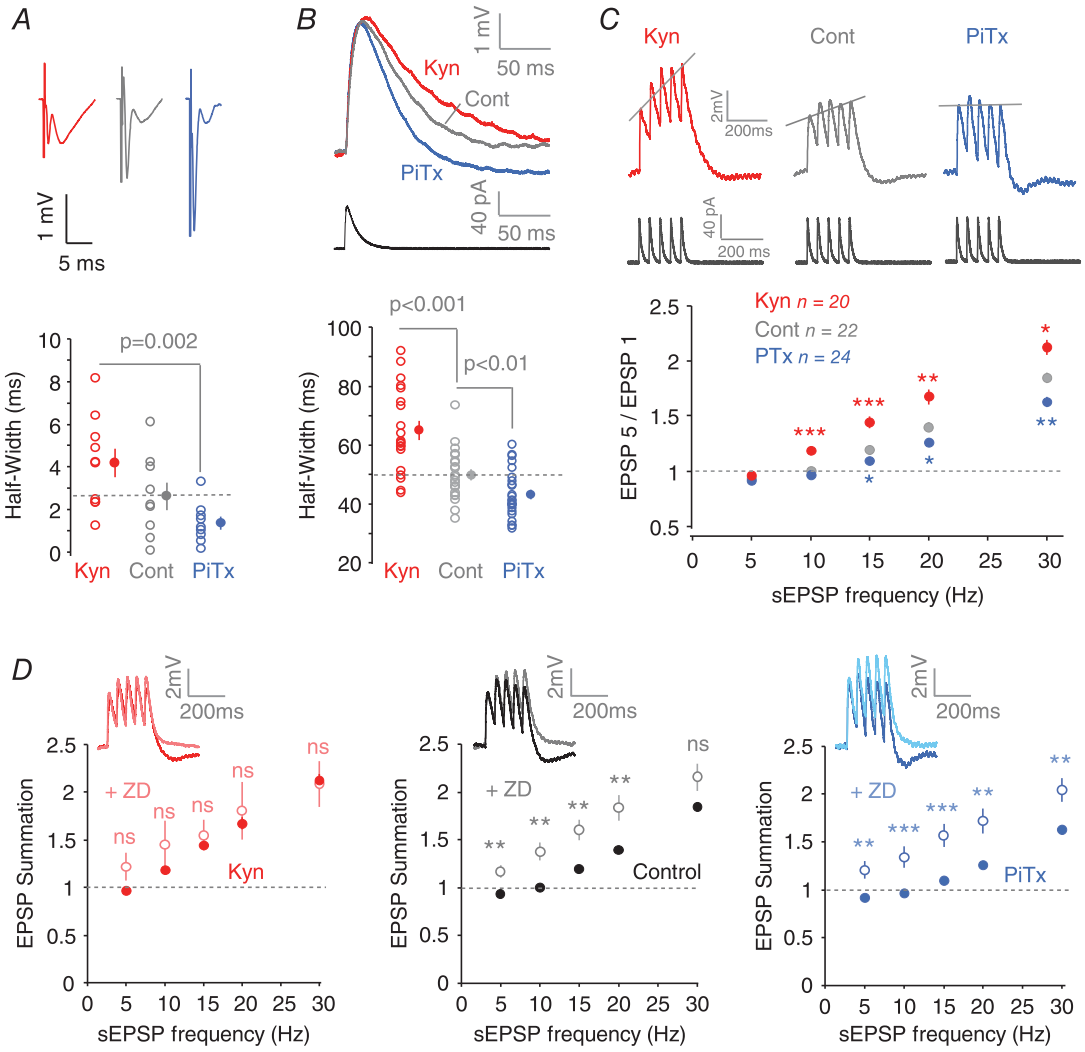

Figure 5. EPSP waveform and EPSP summation is altered after homeostatic regulation of I_h
A, changes in field EPSP waveform after each treatment. Top, representative fEPSP evoked by stimulation of the Schaffer collaterals. Bottom, quantification of fEPSP half-width for each treatment. *B*, simulated EPSPs generated by the injection of a simulated synaptic current in CA1 pyramidal neurons recorded in whole-cell configuration. *C*, EPSP summation of simulated trains of EPSPs at 20 Hz for each condition. Top, representative traces. Bottom, quantification of the summation by normalizing the fifth EPSP to the first. *D*, differential EPSP summation before and after ZD-7288 application for each condition. Representative traces for EPSP trains at 20 Hz before and after ZD-7288 application. Note the maximal effect for PiTx-treated neurons and the minimal effect for Kyn-treated neurons.

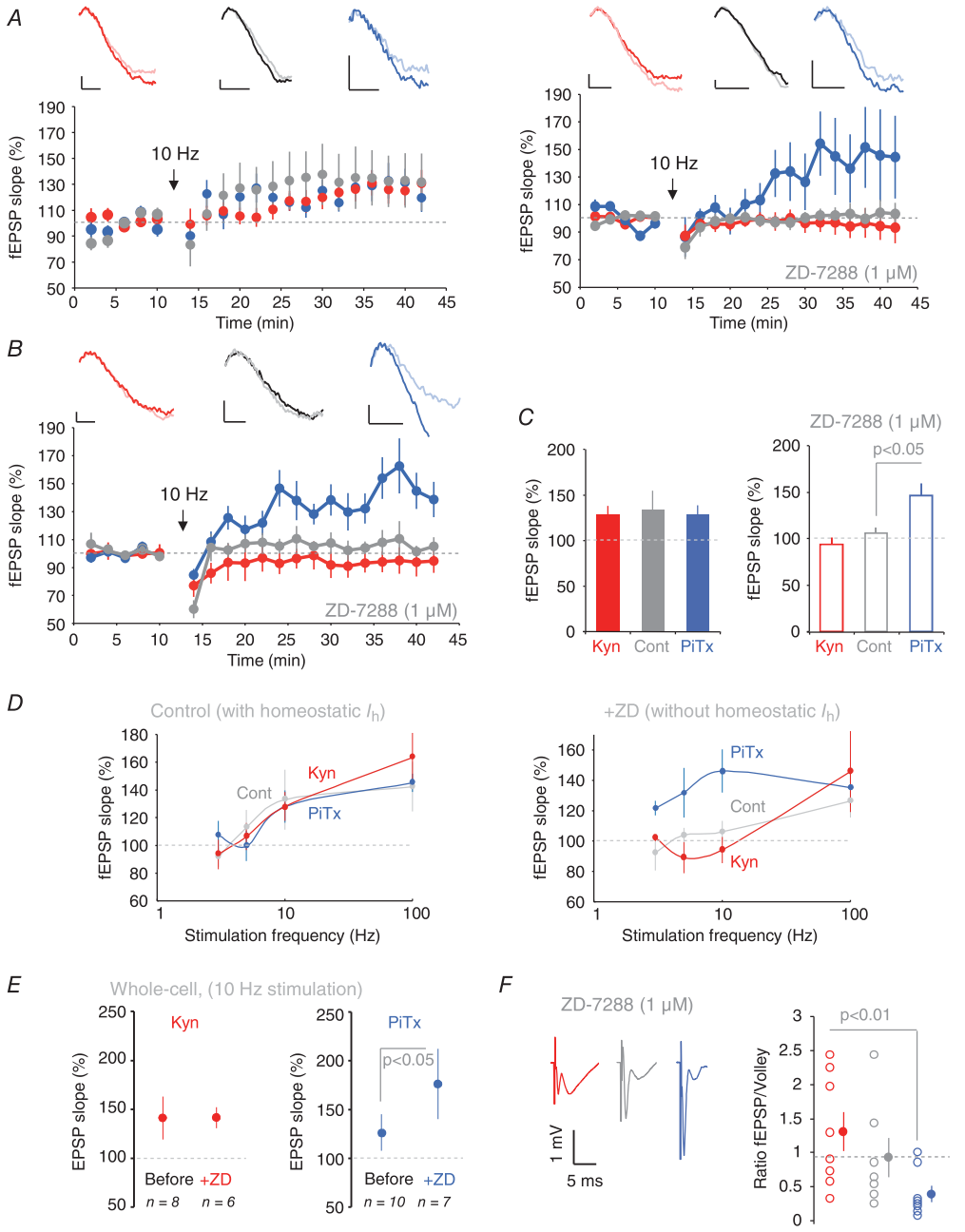

Figure 6. Homeostatic regulation of I_h stabilizes induction of long-term synaptic modification
A, induction of synaptic modification by 10 Hz stimulation. Left: time course of fEPSP slope before and after 10 Hz stimulation of synaptic afferents for each condition. Note the similar level of plasticity in each case. Right: time course of fEPSP slope before and after a second 10 Hz stimulation in the presence of ZD-7288 application (1 μM). Note the selective induction of LTP in PiTx-treated neurons. Top: representative examples of fEPSP slope changes for each condition before (light trace) and after (dark trace) 10 Hz stimulation (scale bars 0.1 mV, 0.5 ms). *B*, time course of fEPSP slope before and after 10 Hz stimulation of synaptic afferents for each condition in the presence of ZD-7288 application (1 μM) in the same slices. Note the selective induction of LTP in PiTx-treated cells. Top: representative examples of fEPSP slope changes for each condition before (light trace) and after (dark trace) 10 Hz stimulation (scale bars 0.1 mV, 0.5 ms). *C*, quantification of synaptic modification. Left, bar graph of fEPSP slope modifications after 10 Hz stimulation in the presence of ZD-7288. Right, quantification of fEPSP slope modifications after 10 Hz stimulation. *D*, BCM curves in control and in the presence of ZD-7288 for control, PiTx- and Kyn-treated neurons. *E*, LTP induced by 10 Hz stimulation in whole-cell configuration with or without functional h-channels. Note the similar level of LTP for Kyn-treated neurons but the differential effect for PiTx-treated neurons. *F*, comparison of the ratio of fEPSP slope to presynaptic volley for each condition. Left, representative fEPSP for each condition. Note the difference in the volley amplitude compared to the fEPSP size. Right, plot of the fEPSP slope normalized to the presynaptic volley amplitude for each condition.

accumulation at the synapse (O'Brien *et al.* 1998). In fact, the amplitude of the AMPA receptor-mediated component normalized to the presynaptic volley was very low in PiTx-treated cultures but high in Kyn-treated ones (0.39 ± 0.12, $n = 8$ in PiTx *vs.* 0.93 ± 0.28, $n = 7$ in control and 1.31 ± 0.28, $n = 8$ in Kyn-treated cultures; Fig. 6*D*), suggesting that low levels of AMPA receptors are expressed in synapses of PiTx-treated cultures whereas higher levels of AMPA receptors are found in synapses of Kyn-treated neurons.

Altogether, these data suggest that chronic network hyperactivity induced by PiTx causes a synaptic rearrangement which favours induction of long-term synaptic potentiation. Thus, homeostatic regulation of h-channels stabilizes the induction of synaptic plasticity by compensating the homeostatic propensity of glutamatergic synapses to express long-term modification.

Discussion

I_h is a major determinant of input resistance, resting membrane potential, EPSP summation and intrinsic neuronal excitability in CA1 pyramidal neurons (Maccaferri *et al.* 1993; Magee, 1998, 1999; Poolos *et al.* 2002). It is naturally an important factor in the activity-dependent regulation of intrinsic neuronal excitability. We show here that chronic manipulations of network activity induced homeostatic regulation of intrinsic neuronal excitability in CA1 pyramidal neurons. This plasticity is associated with the regulation of h-channel activity. h-conductance was found to be down-regulated after chronic hypoactivity (Kyn treatment), thus enhancing both input resistance and intrinsic excitability. In contrast, maximal h-conductance was up-regulated after chronic hyperactivity induced by the $GABA_A$ receptor antagonist picrotoxin, subsequently

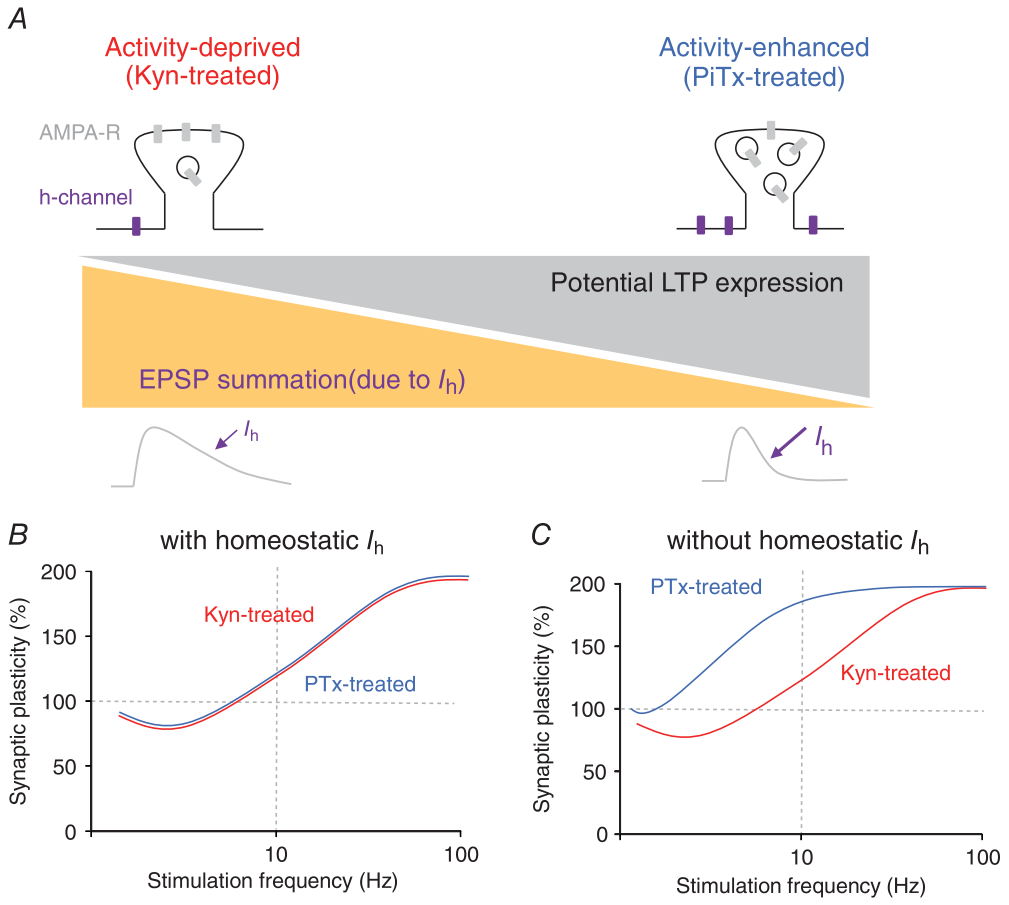

Figure 7. Interplay between regulation of I_h and synaptic plasticity: a hypothesis
A, the homeostatic regulation of EPSP summation compensates for the different potential for LTP expression. Kyn-treated dendritic spines (top left) express a large number of AMPA receptors but very few h-channels. Their potential for LTP is small and the EPSP summation in the 3–10 Hz range is high. PiTx-treated dendritic spines (top right) express very few AMPA receptors but a large number of h-channels. Their potential for LTP is therefore high but EPSP summation at 10 Hz is low. *B*, BCM curves with homeostatic regulation of I_h. Red curve, hypothetical curve obtained in Kyn-treated neurons. Blue curve, hypothetical curve obtained in PiTx-treated neurons. No difference is observed in each condition. *C*, BCM curves without homeostatic regulation. The curve obtained in PiTx-treated neurons is shifted to the left and LTP induction is facilitated.

decreasing both apparent input resistance and intrinsic neuronal excitability. We also showed that homeostatic regulation of I_h controls the induction of long-term synaptic modification and counteracts the propensity of synapses to undergo variable levels of synaptic plasticity. Thus, our results indicate that I_h is a key factor in the homeostatic regulation of intrinsic neuronal excitability in hippocampal neurons and normalizes induction of synaptic plasticity.

Activity deprivation causes homeostatic regulation of I_h in CA1 pyramidal neurons

We report here a 40% decrease in h-conductance in CA1 pyramidal neurons after activity deprivation induced by chronic blockade of ionotropic glutamate receptors with kynurenate for 48–72 h. The down-regulation of h-conductance caused homeostatic increases in apparent input resistance, intrinsic neuronal excitability and EPSP summation. All these changes result from the biophysical properties of I_h. Input resistance tested with hyperpolarizing pulses of current is controlled by the activation of h-channels causing a depolarization and subsequently a reduction in apparent input resistance. Since h-channels are open at resting membrane potential, they produce a constant depolarizing current. Any depolarization will deactivate I_h, therefore producing a hyperpolarization. Thus, I_h attenuates both EPSPs and depolarization induced by depolarizing current steps. Therefore the enhanced intrinsic excitability observed in our experiments is totally consistent with the homeostatic down-regulation of I_h.

Regulation of h-channel localization has been previously reported in hippocampal slice cultures following activity deprivation for 48 h with the voltage-dependent sodium (Na_v) channel blocker TTX, the AMPA receptor antagonist CNQX, or the NMDA receptor antagonist D-APV (Shin & Chetkovich, 2007). In particular, the gradient of h-channels along the apical dendrites of CA1 pyramidal neurons was lost after chronic reduction of excitatory synaptic drive. However, the functional consequence was not characterized. Our data are totally compatible with the reorganization of h-channels reported by Shin & Chetkovich (2007). In fact, the reduced maximal conductance together with the lack of change in activation voltage fits well with a reduced number of functional channels at the membrane. A reduction in the number of HCN1, a subunit of h-channels, has been reported after chronic activity deprivation induced by TTX (Arimitsu *et al.* 2009). In addition to the reduction in the total expression of h-channels, the expression of h-channels at the plasma membrane might be highly regulated. In fact, several isoforms of the h-channel auxiliary subunit TRIP8b also control the expression of HCN subunits at the membrane of CA1 pyramidal neurons (Santoro *et al.* 2009).

Induction of a large synaptic depression (long-term depression, LTD) has been shown to down-regulate h-channel activity in CA1 pyramidal neurons (Brager & Johnston, 2007). This regulation requires the activation of metabotropic glutamate receptor 1 (mGluR1) and protein kinase C. Although the induction mechanisms might be different from those responsible for the homeostatic regulation produced by chronic activity deprivation, it should be underlined that both correspond to a massive reduction in excitatory synaptic drive to CA1 pyramidal neurons, suggesting the existence of common homeostatic rules for the regulation of h-channel activity.

The homeostatic regulation of h-channels plays a major role in the increased intrinsic neuronal excitability observed after chronic activity deprivation. In the presence of the h-channel blocker ZD-7288 the difference between control and Kyn-treated neurons is reduced but not totally eliminated (Fig. 4*D*). This suggests that other voltage-gated conductances might be also regulated in parallel. In fact, chronic activity deprivation up-regulates the Na^+ current in neocortical neurons (Desai *et al.* 1999) and increases the number of Na_v channels in the CA3 area (Aptowicz *et al.* 2004). In addition, kynurenate treatment down-regulates voltage-gated K^+ channel K_{v1} activity in CA3 neurons (Cudmore *et al.* 2010). Chronic hyperactivity also enhances barium-sensitive leak potassium conductance in hippocampal neurons (O'Leary *et al.* 2010). Thus, although the modulation of h-channels is a major component in the homeostatic regulation of CA1 excitability, co-regulation of other voltage-gated conductances may occur in parallel (Marder & Goaillard, 2006). These regulations could be responsible for the remaining differences between the conditions after I_h blockade, as well as the lack of effect on the resting membrane potential upon I_h decrease.

Epileptiform activity induces up-regulation of I_h in CA1 pyramidal neurons

Our study indicates that the h-conductance is enhanced following epileptiform bursting produced by the $GABA_A$ receptor antagonist picrotoxin. This facilitation contributes to dampen apparent input resistance, intrinsic neuronal excitability and EPSP summation. Here again, the maximal h-conductance was found to be enhanced by ~40% and the voltage-dependent activation of the current was found to be unchanged. Our data are compatible with previous findings showing that in young rats, hyperthermia-induced seizures produced an up-regulation of I_h in CA1 neurons (Chen *et al.* 2001). In contrast with our findings, this study reported a significant shift in the activation of I_h. In adult rats, a reduction

in I_h was reported in entorhinal neurons after induction of status epilepticus (Shah *et al.* 2004), indicating that regulation of h-channels by epileptiform activity might be more complex. The homeostatic regulation of I_h reported here may determine the level of functional h-current *in vivo*. In fact, intrinsically bursting neurons display a larger h-current compared to regular spiking cells (van Welie *et al.* 2006).

The mechanisms underlying the up-regulation of h-channel activity by glutamatergic synaptic activity are complex and require AMPA receptor activation and post-synaptic calcium elevation (van Welie *et al.* 2004). In addition, h-channel trafficking at the membrane can be up-regulated by several isoforms of the auxiliary subunit TRIP8b expressed in the CA1 region (Santoro *et al.* 2009). Furthermore, the mobility of HCN1 subunits is highly regulated by stimulation of glutamatergic receptors (Noam *et al.* 2010). It will be important to determine how neuronal or synaptic activity modulates expression of specific TRIP8b subunits in CA1 pyramidal neurons.

Induction of a large synaptic potentiation (LTP) has been shown to up-regulate h-channel activity in CA1 pyramidal neurons (Fan *et al.* 2005; Campanac *et al.* 2008). This regulation requires the activation of NMDA receptors and the calcium/calmodulin protein kinase II (Fan *et al.* 2005). Although the induction mechanisms might be different from those responsible for the homeostatic regulation produced by chronic hyperactivity, it should be noted that both correspond to a massive increase in excitatory synaptic drive to CA1 pyramidal neurons, suggesting the existence of common homeostatic rules for regulation of h-channel activity.

The homeostatic regulation of I_h plays a major role in the decreased excitability observed after chronic epileptiform bursting. First, the h-channel blocker ZD-7288 induced a robust increase in the excitability of neurons treated for 48 h with PiTx (Fig. 4*C*). However, the gap between control and PiTx-treated neurons was not totally filled in the presence of ZD-7288, indicating that other channels might be also regulated. In fact, $K_{v2.1}$ channels mediating the delayed rectifier potassium current are located in the perisomatic region of hippocampal neurons. They are upregulated after epileptiform activity and also contribute to the reduction in intrinsic excitability (Misonou *et al.* 2004).

I_h controls resting membrane potential in CA1 neurons. Yet, homeostatic regulation of I_h was not associated with significant changes in membrane potential. This lack of effect could be the result of co-regulated channels that also control membrane potential. For instance, the increase in h-conductance induced by chronic hyperactivity should, in theory, depolarize the membrane potential. However, this depolarization could be compensated by the up-regulation of the leak potassium current (Brickley *et al.* 2001). In fact, chronic hyperactivity augments by a factor of 2 the barium-sensitive leak current, causing a hyperpolarization of the resting membrane potential (O'Leary *et al.* 2010). The stability of the resting membrane potential observed in our experiments can be considered as a homeostatic regulation aiming at maintaining neuronal excitability in a stable range.

Homeostatic regulation *of* I_h and the modulation of long-term synaptic modification

We show here that homeostatic regulation of the h-channel might interfere with the induction of long-term synaptic modification by stimulating the Schaffer collaterals at different frequencies (3–100 Hz). The frequency of 10 Hz is particularly interesting not only because it corresponds to the threshold between LTD and LTP in the Bienenstock–Cooper–Monroe (BCM) curve linking synaptic changes to stimulation frequency (Dudek & Bear, 1992), but also because at this frequency EPSP summation is significantly affected by I_h (see Fig. 5).

In control conditions, the plasticity curves for control, Kyn- and PiTx-treated cultures were virtually superimposed. When h-channels are blocked with ZD-7288, stimulation at 3, 5 and 10 Hz induced LTP that was larger in PiTx-treated neurons compared to control or Kyn-treated neurons. In contrast, no differential effect was observed across treatments in the presence of ZD-7288 after 100 Hz stimulation, suggesting that h-channels control the induction of synaptic modification in the low frequency range. Importantly, when the membrane potential was controlled and kept constant in whole-cell recordings, LTP was selectively enhanced after blocking h-channels in PiTx-treated but not in Kyn-treated neurons, thus confirming the results obtained in field potential.

Our data suggest that the propensity of CA3–CA1 synapses to express LTP is higher in PiTx-treated cultures compared to control or Kyn-treated cultures. We found that the ratio of the AMPA response to the presynaptic volley amplitude was significantly reduced in PiTx-treated neurons compared to Kyn-treated neurons, indicating that the number of AMPA receptors per synapse might be strongly regulated after chronic manipulation of network activity. The reduction in postsynaptic AMPA receptors has been observed in cortical neurons after chronic hyperactivity (Turrigiano *et al.* 1998). Moreover, the large facilitation observed in PiTx neurons expressing a reduced EPSP/volley ratio is compatible with previous findings indicating that the magnitude of LTP is maximal at hippocampal connections exhibiting small AMPA responses (Bi & Poo, 1998; Debanne *et al.* 1999).

Because AMPA receptors are known to be regulated by chronic activity (O'Brien *et al.* 1998; Turrigiano *et al.* 1998), we hypothesized that a strong internalization of AMPA receptors occurs during chronic treatment with

PiTx, making glutamatergic synapses particularly prone to the expression of LTP (Fig. 7*A*). However, this high potential for LTP expression in PiTx-treated neurons can be revealed only if the dampening of EPSP summation by h-current is blocked. Our results therefore point to the fact that homeostatic regulation of I_h may compensate the considerable potential of glutamatergic synapse to express LTP and normalize the induction of long-term synaptic modification (Fig. 7*B*). Our data therefore suggest that in the absence of h-channels, the BCM plasticity curve for PiTx-treated neurons would be shifted in relation to that of Kyn-treated neurons because of the differential content in AMPA receptors at dendritic spines (Fig. 7*C*).

Homeostatic regulation of h-channels appears therefore as a mechanism for regulating the sliding modification threshold of the BCM-like learning rule of synaptic modification (Narayanan & Johnston, 2010). A similar modification of the synaptic plasticity induction threshold has already been observed following the regulation of ionic currents (Ramakers & Storm, 2002; Chen *et al.* 2006). Moreover, the homeostatic plasticity of intrinsic excitability observed here seems to play an essential metaplastic role in the homeostasis of synaptic plasticity.

References

Aptowicz CO, Kunkler PE & Kraig RP (2004). Homeostatic plasticity in hippocampal slice cultures involves changes in voltage-gated Na^+ channel expression. *Brain Res* **998**, 155–163.

Arimitsu T, Nuriya M, Ikeda K, Takahashi T & Yasui M (2009). Activity-dependent regulation of HCN1 protein in cortical neurons. *Biochem Biophys Res Commun* **387**, 87–91.

Bi GQ & Poo MM (1998). Synaptic modifications in cultured hippocampal neurons: dependence on spike timing, synaptic strength, and postsynaptic cell type. *J Neurosci* **18**, 10464–10472.

Boudkkazi S, Carlier E, Ankri N, Caillard O, Giraud P, Fronzaroli-Molinieres L & Debanne D (2007). Release-dependent variations in synaptic latency: a putative code for short- and long-term synaptic dynamics. *Neuron* **56**, 1048–1060.

Brager DH & Johnston D (2007). Plasticity of intrinsic excitability during long-term depression is mediated through mGluR-dependent changes in I_h in hippocampal CA1 pyramidal neurons. *J Neurosci* **27**, 13926–13937.

Breton JD & Stuart GJ (2009). Loss of sensory input increases the intrinsic excitability of layer 5 pyramidal neurons in rat barrel cortex. *J Physiol* **587**, 5107–5119.

Brickley SG, Revilla V, Cull-Candy SG, Wisden W & Farrant M (2001). Adaptive regulation of neuronal excitability by a voltage-independent potassium conductance. *Nature* **409**, 88–92.

Campanac E, Daoudal G, Ankri N & Debanne D (2008). Downregulation of dendritic I_h in CA1 pyramidal neurons after LTP. *J Neurosci* **28**, 8635–8643.

Campanac E & Debanne D (2008). Spike timing-dependent plasticity: a learning rule for dendritic integration in rat CA1 pyramidal neurons. *J Physiol* **586**, 779–793.

Campanac E, Gasselin C, Baude A, Rama S, Ankri N & Debanne D (2013). Enhanced intrinsic excitability in basket cells maintains excitatory-inhibitory balance in hippocampal circuits. *Neuron* **77**, 712–722.

Chen K, Aradi I, Thon N, Eghbal-Ahmadi M, Baram TZ & Soltesz I (2001). Persistently modified h-channels after complex febrile seizures convert the seizure-induced enhancement of inhibition to hyperexcitability. *Nat Med* **7**, 331–337.

Chen X, Yuan LL, Zhao C, Birnbaum SG, Frick A, Jung WE, Schwarz TL, Sweatt JD & Johnston D (2006). Deletion of Kv4.2 gene eliminates dendritic A-type K^+ current and enhances induction of long-term potentiation in hippocampal CA1 pyramidal neurons. *J Neurosci* **26**, 12143–12151.

Cudmore RH, Fronzaroli-Molinieres L, Giraud P & Debanne D (2010). Spike-time precision and network synchrony are controlled by the homeostatic regulation of the D-type potassium current. *J Neurosci* **30**, 12885–12895.

Daoudal G, Hanada Y & Debanne D (2002). Bidirectional plasticity of excitatory postsynaptic potential (EPSP)-spike coupling in CA1 hippocampal pyramidal neurons. *Proc Natl Acad Sci USA* **99**, 14512–14517.

Debanne D, Boudkkazi S, Campanac E, Cudmore RH, Giraud P, Fronzaroli-Molinieres L, Carlier E & Caillard O (2008). Paired-recordings from synaptically coupled cortical and hippocampal neurons in acute and cultured brain slices. *Nat Protoc* **3**, 1559–1568.

Debanne D, Gahwiler BH & Thompson SM (1999). Heterogeneity of synaptic plasticity at unitary CA3-CA1 and CA3-CA3 connections in rat hippocampal slice cultures. *J Neurosci* **19**, 10664–10671.

Desai NS, Rutherford LC & Turrigiano GG (1999). Plasticity in the intrinsic excitability of cortical pyramidal neurons. *Nat Neurosci* **2**, 515–520.

Dudek SM & Bear MF (1992). Homosynaptic long-term depression in area CA1 of hippocampus and effects of *N*-methyl-D-aspartate receptor blockade. *Proc Natl Acad Sci USA* **89**, 4363–4367.

Dyhrfjeld-Johnsen J, Morgan RJ, Foldy C & Soltesz I (2008). Upregulated h-current in hyperexcitable CA1 dendrites after febrile seizures. *Front Cell Neurosci* **2**, 2.

Fan Y, Fricker D, Brager DH, Chen X, Lu HC, Chitwood RA & Johnston D (2005). Activity-dependent decrease of excitability in rat hippocampal neurons through increases in I_h. *Nat Neurosci* **8**, 1542–1551.

Gasparini S & DiFrancesco D (1997). Action of the hyperpolarization-activated current (I_h) blocker ZD 7288 in hippocampal CA1 neurons. *Pflugers Arch* **435**, 99–106.

Gastrein P, Campanac E, Gasselin C, Cudmore RH, Bialowas A, Carlier E, Fronzaroli-Molinieres L, Ankri N & Debanne D (2011). The role of hyperpolarization-activated cationic current in spike-time precision and intrinsic resonance in cortical neurons *in vitro*. *J Physiol* **589**, 3753–3773.

Karmarkar UR & Buonomano DV (2006). Different forms of homeostatic plasticity are engaged with distinct temporal profiles. *Eur J Neurosci* **23**, 1575–1584.

Kirchheim F, Tinnes S, Haas CA, Stegen M & Wolfart J (2013). Regulation of action potential delays via voltage-gated potassium Kv1.1 channels in dentate granule cells during hippocampal epilepsy. *Front Cell Neurosci* **7**, 248.

Maccaferri G, Mangoni M, Lazzari A & DiFrancesco D (1993). Properties of the hyperpolarization-activated current in rat hippocampal CA1 pyramidal cells. *J Neurophysiol* **69**, 2129–2136.

Magee JC (1998). Dendritic hyperpolarization-activated currents modify the integrative properties of hippocampal CA1 pyramidal neurons. *J Neurosci* **18**, 7613–7624.

Magee JC (1999). Dendritic I_h normalizes temporal summation in hippocampal CA1 neurons. *Nat Neurosci* **2**, 508–514.

Marder E & Goaillard JM (2006). Variability, compensation and homeostasis in neuron and network function. *Nat Rev Neurosci* **7**, 563–574.

Misonou H, Mohapatra DP, Park EW, Leung V, Zhen D, Misonou K, Anderson AE & Trimmer JS (2004). Regulation of ion channel localization and phosphorylation by neuronal activity. *Nat Neurosci* **7**, 711–718.

Narayanan R & Johnston D (2010). The h current is a candidate mechanism for regulating the sliding modification threshold in a BCM-like synaptic learning rule. *J Neurophysiol* **104**, 1020–1033.

Noam Y, Zha Q, Phan L, Wu RL, Chetkovich DM, Wadman WJ & Baram TZ (2010). Trafficking and surface expression of hyperpolarization-activated cyclic nucleotide-gated channels in hippocampal neurons. *J Biol Chem* **285**, 14724–14736.

Nolan MF, Malleret G, Dudman JT, Buhl DL, Santoro B, Gibbs E, Vronskaya S, Buzsaki G, Siegelbaum SA, Kandel ER & Morozov A (2004). A behavioral role for dendritic integration: HCN1 channels constrain spatial memory and plasticity at inputs to distal dendrites of CA1 pyramidal neurons. *Cell* **119**, 719–732.

O'Brien RJ, Kamboj S, Ehlers MD, Rosen KR, Fischbach GD & Huganir RL (1998). Activity-dependent modulation of synaptic AMPA receptor accumulation. *Neuron* **21**, 1067–1078.

O'Leary T, van Rossum MC & Wyllie DJ (2010). Homeostasis of intrinsic excitability in hippocampal neurones: dynamics and mechanism of the response to chronic depolarization. *J Physiol* **588**, 157–170.

Poolos NP, Migliore M & Johnston D (2002). Pharmacological upregulation of h-channels reduces the excitability of pyramidal neuron dendrites. *Nat Neurosci* **5**, 767–774.

Ramakers GM & Storm JF (2002). A postsynaptic transient K^+ current modulated by arachidonic acid regulates synaptic integration and threshold for LTP induction in hippocampal pyramidal cells. *Proc Natl Acad Sci USA* **99**, 10144–10149.

Santoro B, Piskorowski RA, Pian P, Hu L, Liu H & Siegelbaum SA (2009). TRIP8b splice variants form a family of auxiliary subunits that regulate gating and trafficking of HCN channels in the brain. *Neuron* **62**, 802–813.

Shah MM (2014). Cortical HCN channels: function, trafficking and plasticity. *J Physiol* **592**, 2711–2719.

Shah MM, Anderson AE, Leung V, Lin X & Johnston D (2004). Seizure-induced plasticity of h channels in entorhinal cortical layer III pyramidal neurons. *Neuron* **44**, 495–508.

Shin M & Chetkovich DM (2007). Activity-dependent regulation of h channel distribution in hippocampal CA1 pyramidal neurons. *J Biol Chem* **282**, 33168–33180.

Stoppini L, Buchs PA & Muller D (1991). A simple method for organotypic cultures of nervous tissue. *J Neurosci Methods* **37**, 173–182.

Tsay D, Dudman JT & Siegelbaum SA (2007). HCN1 channels constrain synaptically evoked Ca^{2+} spikes in distal dendrites of CA1 pyramidal neurons. *Neuron* **56**, 1076–1089.

Turrigiano G (2011). Too many cooks? Intrinsic and synaptic homeostatic mechanisms in cortical circuit refinement. *Annu Rev Neurosci* **34**, 89–103.

Turrigiano GG, Leslie KR, Desai NS, Rutherford LC & Nelson SB (1998). Activity-dependent scaling of quantal amplitude in neocortical neurons. *Nature* **391**, 892–896.

Turrigiano GG & Nelson SB (2004). Homeostatic plasticity in the developing nervous system. *Nat Rev Neurosci* **5**, 97–107.

van Welie I, Remme MW, van Hooft JA & Wadman WJ (2006). Different levels of I_h determine distinct temporal integration in bursting and regular-spiking neurons in rat subiculum. *J Physiol* **576**, 203–214.

van Welie I, van Hooft JA & Wadman WJ (2004). Homeostatic scaling of neuronal excitability by synaptic modulation of somatic hyperpolarization-activated I_h channels. *Proc Natl Acad Sci USA* **101**, 5123–5128.

Wang Z, Xu NL, Wu CP, Duan S & Poo MM (2003). Bidirectional changes in spatial dendritic integration accompanying long-term synaptic modifications. *Neuron* **37**, 463–472.

Additional information

Competing interests

None declared.

Author contributions

C.G. and D.D. conceived the project. C.G. and Y.I. collected the data and C.G., Y.I. and D.D. analysed the data. C.G., Y.I. and D.D. drafted the manuscript. All authors approved the final version of the manuscript, agree to be accountable for all aspects of the work and all persons designated as authors qualify for authorship. All experiments were carried out in U1072, Marseille, France.

Funding

This work was supported by INSERM, CNRS, French Ministry of Research (doctoral grant to C.G.), Fondation Recherche Médicale (doctoral grant to C.G.), and Agence Nationale de la Recherche (doctoral grant to Y.I.).

Acknowledgements

We thank Norah Boumedine-Guignon and Laure Fronzaroli-Molinieres for excellent technical assistance, and Jean-Marc Goaillard, Oussama El Far and Michael Seagar for helpful comments on the manuscript.

SCIENTIFIC REPORTS

OPEN

Plasticity of intrinsic excitability during LTD is mediated by bidirectional changes in h-channel activity

Received: 29 March 2017
Accepted: 18 October 2017
Published online: 31 October 2017

Célia Gasselin, Yanis Inglebert, Norbert Ankri & Dominique Debanne

The polarity of excitability changes associated with induction of Long-Term synaptic Depression (LTD) in CA1 pyramidal neurons is a contentious issue. Postsynaptic neuronal excitability after LTD induction is found to be reduced in certain cases (i.e. synergistic changes) but enhanced in others (i.e. compensatory or homeostatic). We examined here whether these divergent findings could result from the activation of two separate mechanisms converging onto a single learning rule linking synergistic and homeostatic plasticity. We show that the magnitude of LTD induced with low frequency stimulation (LFS) of the Schaffer collaterals determines the polarity of intrinsic changes in CA1 pyramidal neurons. Apparent input resistance (R_{in}) is reduced following induction of moderate LTD (<20–30%). In contrast, R_{in} is increased after induction of large LTD (>40%) induced by repetitive episodes of LFS. The up-regulation of I_h observed after moderate LTD results from the activation of NMDA receptors whereas the down-regulation of I_h is due to activation of mGluR1 receptors. These changes in R_{in} were associated with changes in intrinsic excitability. In conclusion, our study indicates that changes in excitability after LTD induction follow a learning rule describing a continuum linking synergistic and compensatory changes in excitability.

In central neurons, changes in intrinsic neuronal excitability have been shown to occur in parallel with synaptic modifications, thus affecting synergistically synaptic strength and dendritic integration in the post-synaptic neuron[1,2]. Induction of Long-Term synaptic Potentiation (LTP) is associated with an increase in the firing probability of the postsynaptic neuron[3–7], whereas induction of Long-Term synaptic Depression (LTD) is associated with a reduced firing probability in response to the test input[4,5,8].

Induction of synaptic plasticity has also been associated with non-synergistic (i.e. homeostatic) modifications of intrinsic excitability[9,10]. One of the key players in CA1 pyramidal cells is the hyperpolarization-activated cationic h-current (I_h), a major determinant of input resistance and intrinsic neuronal excitability[11,12]. Very large LTP (≈+300%) was found to up-regulate I_h to counteract excessive synaptic excitation[13,14] whereas large LTD (≈−60%) was found to down-regulate I_h to counteract excessive synaptic depression[15].

These two homeostatic regulations of I_h are not compatible with the synergistic changes in excitability and synaptic strength reported earlier[4,5,16]. The discrepancy for the LTP side was resolved by showing that h-channel regulation depended on LTP amplitude[17]. In fact, it was shown in this study that physiological LTP (i.e. +20–50%) produced a *decrease* in I_h seen as an increase in R_{in} whereas extreme LTP (i.e. +200–300%) produced an *increase* in I_h and the two extrema were linked by a continuum of synergistic and homeostatic plasticity. However, the discrepancy still remained for LTD. We examined whether a similar continuum also exists for homeostatic and synergistic changes in intrinsic neuronal excitability for the LTD side.

We show here that R_{in} also depends on the magnitude of LTD, with a decrease following induction of moderate LTD but an increase after induction of strong LTD. This dependence of R_{in} on the magnitude of LTD is abolished by the h-channel blocker ZD-7288. The decrease in R_{in} (due to an up-regulation of I_h) is mediated by NMDA receptor activation whereas the increase in R_{in} (i.e. due to a down-regulation of I_h) is mediated by activation of mGluR1. We show here that induction of LTD in the presence of the NMDA receptor antagonist D-AP5

UNIS, INSERM U-1072, Aix-Marseille University, Marseille, France. Célia Gasselin and Yanis Inglebert contributed equally to this work. Correspondence and requests for materials should be addressed to D.D. (email: dominique.debanne@inserm.fr)

enhanced neuronal excitability whereas LTD induction in the presence of the mGluR antagonist LY341485 diminished excitability of CA1 pyramidal neurons. We conclude that intrinsic plasticity induced by LTD also describes a continuum between synergistic and homeostatic plasticity in CA1 pyramidal neurons, involving different sets of glutamate receptors.

Results

LTD magnitude determines changes in R_{in} in CA1 pyramidal neurons. All experiments were performed in the presence of the GABA receptor antagonist PiTx (100 µM). EPSPs were evoked in CA1 pyramidal neurons recorded in whole-cell configuration by stimulating the Schaffer collaterals at 0.1 Hz. After obtaining a stable base line, Long-Term Depression (LTD) of synaptic transmission was induced by stimulation of the Schaffer collaterals at 3 Hz during 3 or 5 min. Input resistance (R_{in}) measured with large hyperpolarizing current pulses to recruit h-current (−120 pA, 800 ms) was found to be reduced to ~95.7% of the control value ($n = 33$, t-test $p < 0.01$) following LTD induction (Fig. 1A). But more interestingly a negative correlation was observed between the normalized R_{in} and the synaptic change ($y = -0.198x - 91.1$; $r = 0.36$; $p < 0.05$; Fig. 1B). This negative correlation was further confirmed by the difference in the mean R_{in} change observed after 3 or 5 min at 3 Hz (after 3 min at 3 Hz: 93 ± 3%, $n = 11$ for a mean EPSP change of −9 ± 4%; after 5 min at 3 Hz: 97 ± 2% for an EPSP change of −31 ± 3%; Fig. 1B).

To confirm the correlation observed with one train of 3 Hz stimulation, synaptic depressions of larger magnitudes were induced by repeated episodes of 3 Hz stimulation with ten minutes intervals. A progressive decrease in EPSP slope and a parallel changes in apparent R_{in} were observed (Fig. 1C). While R_{in} decreased after the first stimulation episode (see also Fig. 1A), it progressively increased after each stimulation episode (Fig. 1C). The analysis of the trajectories of individual cells showed in all cases an anti-correlation (Fig. 1D). The plot of R_{in} versus EPSP change revealed a significant anti-correlation ($r = 0.66$; $p < 0.001$; Fig. 1E). R_{in} was reduced to 90 ± 3% for moderate LTD (<20%) but increased to 116 ± 4% for large LTD (>50%; Fig. 1E). As previously reported for LTP[17], modulation of R_{in} was not associated with significant change in V_m following induction of LTD (−62.3 ± 0.9 mV in control and −61.8 ± 0.6 mV after the 3rd episode of 3 Hz stimulation, $p > 0.1$; Supplementary Figure 1). In conclusion, the magnitude of LTD determines the polarity of R_{in} change in CA1 pyramidal neurons.

Temporal stability of synaptic transmission and R_{in}. In order to eliminate any non-specific R_{in} changes, we repeated the same protocol with 0.1 Hz stimulation to test the temporal stability of synaptic strength and R_{in} in CA1 pyramidal neurons. No changes in EPSP slope were observed after 1 (Fig. 2A & B) or several repetitive episodes of 0.1 Hz stimulation (−4 ± 3% of control EPSP slope; Fig. 2C). Furthermore R_{in} remained unchanged throughout the experiment (103 ± 1%; Fig. 2C). Finally, no linear correlation was observed between normalized R_{in} and EPSP slope at the level of individual cells (Fig. 2D) or all taken together ($r = 0.05$; $p > 0.05$; Fig. 2E).

Regulation of I_h is responsible for changes in R_{in}. R_{in} is mainly governed by the h-current in CA1 pyramidal neurons. We therefore tested the role of I_h in the observed changes in R_{in}. We repeated the same protocol in the presence of the pharmacological blocker of h-channels ZD-7288 (1 µM). This concentration of ZD-7288 has been shown to block I_h without altering excitatory synaptic transmission[18]. In the presence of ZD-7288, stimulation of the Schaffer collaterals at 3 Hz still induced LTD (−23 ± 9%, $n = 8$; Fig. 3A) but R_{in} remained unchanged (98 ± 2% of control R_{in}, $n = 8$, Fig. 3A & B). Similarly, no change in R_{in} occurred following induction of incremental LTD by repeated low frequency stimulation at 3 Hz (Fig. 3C & D). No linear correlation was found between LTD magnitude and R_{in} changes in the presence of ZD-7288 ($r = 0.18$; $p > 0.05$; Fig. 3E). These results indicate that I_h is directly involved in the bidirectional regulation of R_{in} following induction of LTD.

To further confirm the implication of h-channels, the sag produced by activation of I_h was analysed. The sag was found to decrease after the 1st episode of 3 Hz stimulation and remained reduced by ~15% thereafter (Supplementary Figure 2A). Interestingly, a significant correlation between the normalized sag change and the magnitude of LTD was observed (Supplementary Figure 2B). But, surprisingly, no increase in the sag amplitude was observed following induction of LTD. We thus developed a simplified model of hippocampal neuron in which h conductance (G_h) increased from 0 to 10 nS (Supplementary Figure 2C). Importantly, while R_{in} provided a good description of changes in G_h, the sag increased when G_h increased in the 0–2 nS range but it was found to decrease when G_h increased in the 2–10 nS range. This result indicates that the sag is a not an index appropriate for evaluating activity-dependent regulation of h-channels.

Reduction of R_{in} depends on NMDAR. Induction of LTD requires both N-methyl-D-aspartate receptor (NMDAR)[19–21] and/or metabotropic glutamate receptor (mGluR)[15,22–24]. To dissect the role of NMDAR in the regulation in R_{in}, we applied the specific antagonist D-AP5 (50 µM) in the bath. In the presence of D-AP5, the magnitude of LTD induced by the first episode of 3 Hz stimulation was found to be reduced (93 ± 7% of control EPSP slope, $n = 6$ versus 72 ± 4%, $n = 16$, in control condition; Fig. 4A & B). In contrast with what was observed in control conditions, R_{in} was increased in 5 out of 6 cells after the first stimulation episode (110 ± 4% of control R_{in}, Fig. 4A & B).

The following stimulation episodes produced, however, comparable levels of LTD and R_{in} was found to augment up to 130% after the last episode of 3 Hz stimulation (128 ± 1%; Fig. 4C & D). Compared to the control situation, the plot of normalized R_{in} against EPSP change in D-AP5 indicates an upward shift of the linear anti-correlation ($r = 0.47$; $p < 0.05$; Fig. 4E). These data suggest that NMDARs are implicated in the down-regulation of R_{in} observed for moderate LTD. The remaining increase in R_{in} might result from the stimulation of mGluRs.

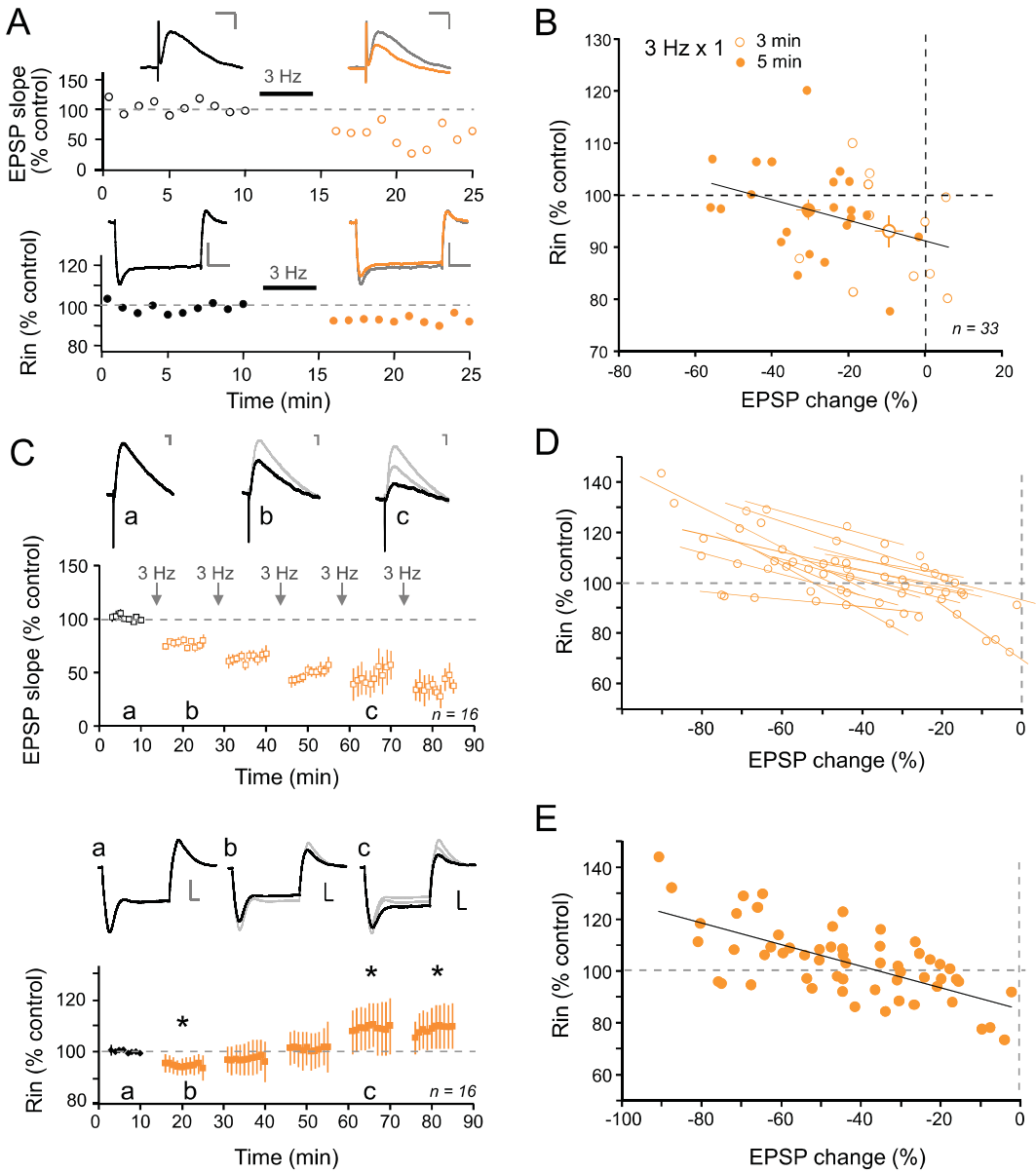

Figure 1. LTD magnitude determines changes in R_{in}. (**A**) Time-courses of EPSP slope (top) and R_{in} (bottom) in a single experiment showing a reduction in R_{in} following induction of LTD. Scale bars: top, 2 mV & 20 ms; bottom, 5 mV & 200 ms. (**B**) Plot of R_{in} as a function of EPSP change induced by 3 Hz stimulation for 3 or 5 minutes. Note the negative correlation ($y = 0.198x + 91.096$, $r = 0.36$; $p < 0.01$). (**C**) Top, EPSP slope time course pooled over sixteen experiments. Arrows indicate 3 Hz stimulation episodes. Representative EPSP traces in control (a), after the first stimulation episode (b) and after the third (c). Scale bars: 1 mV, 10 ms. Bottom, time course of apparent input resistance (R_{in}) after each stimulation episode. R_{in} is reduced after the first 3 Hz stimulation (a, b) and increased for the third (c). Stars indicate statistical significance ($p < 0.05$) Top, representative R_{in} traces in control (a), after the first stimulation episode (b) and after the third (c). Scale bars: 10 mV, 100 ms. (**D**) Normalized R_{in} as a function of EPSP change for each cell. Note that correlations for each cell are all negatively oriented. (**E**) Normalized R_{in} changes versus normalized LTD level for each stimulation episode. A significant linear negative correlation was observed ($y = -0.414x + 85.487$; $r = 0.66$; $p < 0.001$).

Enhancement of R_{in} depends on mGluR1. We next tested whether mGluRs were implicated in the up-regulation of R_{in}. We first applied the mGluR1/5 agonist DHPG (50–100 µM) during 5 min[23]. DHPG induced synaptic LTD (74 ± 6% of the control EPSP slope, n = 12; Fig. 5A). Interestingly, this mGluR-induced LTD was associated with a long-lasting increase of R_{in} (116 ± 4% of the control R_{in}; Fig. 5A & B).

Next, we induced LTD with 3 Hz stimulation of the Schaffer collaterals in the presence of the broad spectrum mGluR antagonist, LY341495 (100 µM). In this condition, synaptic LTD was still induced by 3 Hz stimulation (68 ± 12% of control EPSP slope, n = 7 after the 3rd episode of stimulation; Fig. 5C) but importantly R_{in} was found to be reduced (to 85 ± 7% of control R_{in}, n = 7 after the 3rd episode of 3 Hz stimulation; Fig. 5C). Furthermore, the plot of normalized R_{in} against EPSP change in LY341495 was found to follow a linear anti-correlation ($r = 0.64$;

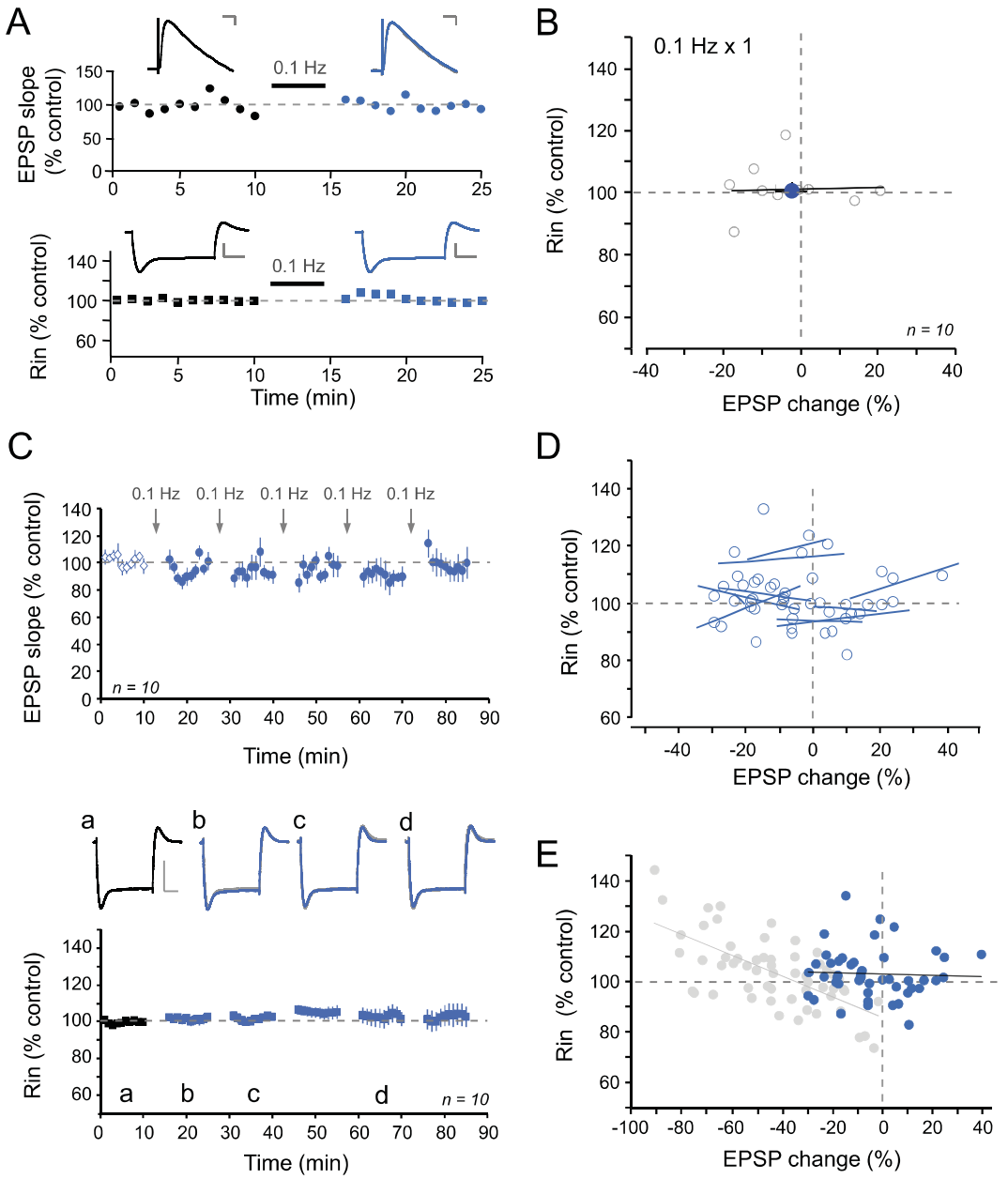

Figure 2. Temporal stability. (**A**) Time-courses of EPSP slope (top) and R_{in} (bottom) after 0.1 Hz stimulation. Scale bars; top, 2 mV & 20 ms; bottom, 10 mV & 200 ms. (**B**) Plot of R_{in} versus EPSP change. No correlation was observed ($y = 0.021x + 101.31$, $r = 0.10$). (**C**) Top, EPSP slope time-course pooled over ten experiments. Arrows indicate 0.1 Hz stimulation episodes. Bottom, time-course of R_{in}. Representative R_{in} traces in control (a), and after stimulation episodes (b, c & d). Scale bars: 10 mV, 100 ms. No statistically significant changes were observed. (**D**) Correlation between R_{in} and EPSP change for each cell after 0.1 Hz stimulation. (**E**) Normalized R_{in} versus normalized EPSP change for all episodes of 0.1 Hz stimulation (blue dots). Compared to the control condition (grey dots, see Fig. 1B), no linear correlation was observed ($y = -0.027x + 102.79$; $r = 0.05$, $p > 0.05$).

Fig. 5D). In contrast, R_{in} was found to be still enhanced when LTD was induced in the presence of the specific mGluR5 antagonist, MPEP (10 μM; Supplementary Figure 3), suggesting that mGluR1 and not mGluR5 is responsible for the increase in R_{in}.

In conclusion, the stimulation of NMDARs induces a decrease in R_{in} (i.e. up-regulation of I_h) whereas the stimulation of mGluR1 is responsible for an increase in R_{in} (i.e. down-regulation of I_h).

Changes in excitability associated with LTD. Next, we tested whether these changes in Rin were associated with changes in intrinsic excitability following induction of LTD. To better dissect the implication of bidirectional changes in R_{in} we pharmacologically isolated the mGluR- and NMDAR-mediated component of R_{in} changes associated with LTD induced by 3 Hz stimulation of the Schaffer collateral for 10 min with either D-AP5 or LY341495 in the bath. Consistent with the increase in R_{in} after 3 Hz stimulation in the presence of D-AP5,

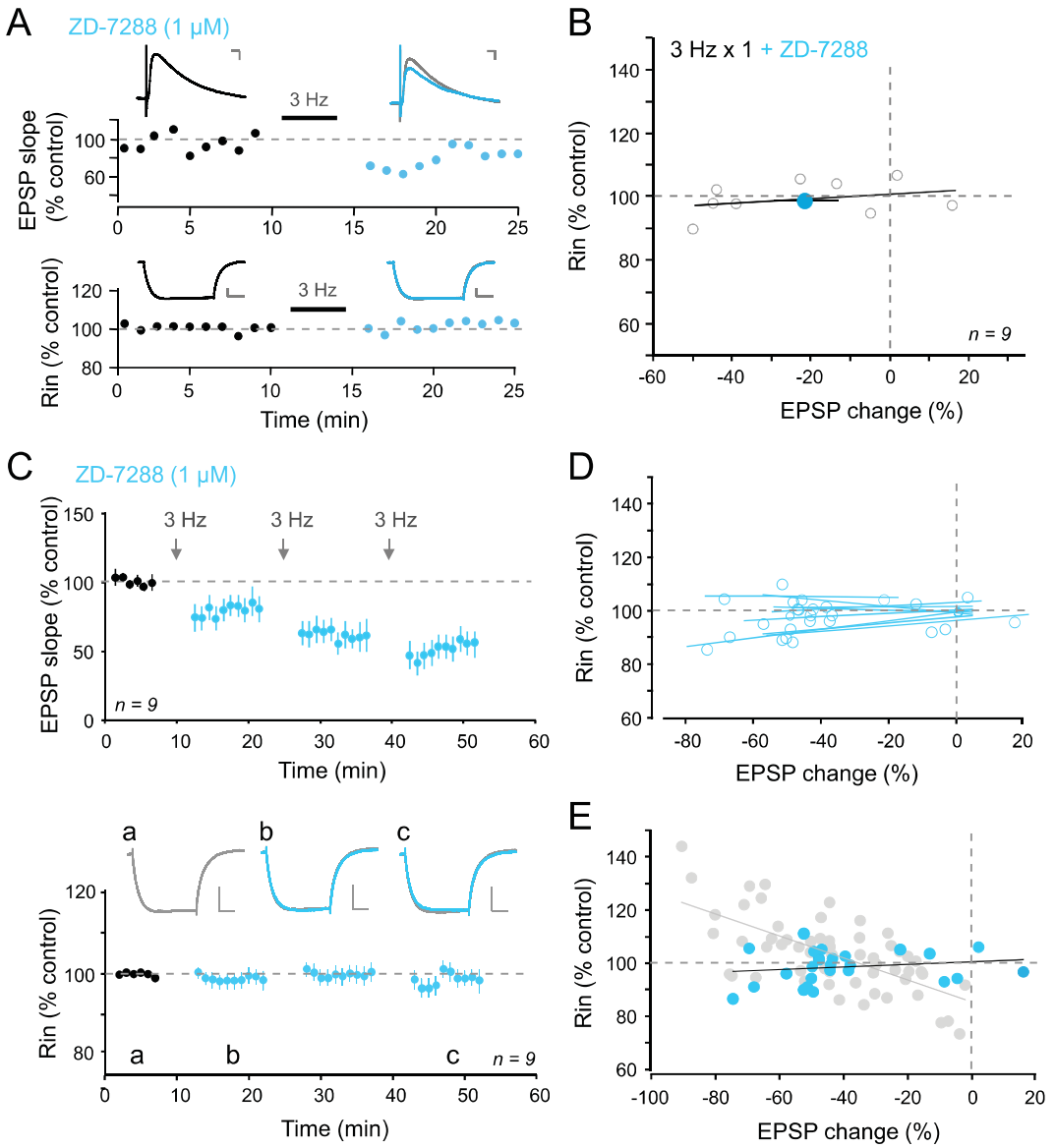

Figure 3. Blockade of h-channels ZD-7288 impairs regulation of R_{in}. (**A**) Time-courses of EPSP slope (top) and R_{in} (bottom) following 3 Hz stimulation for 5 min in the presence of ZD-72288. Scale bars: top, 2 mV & 20 ms; bottom, 5 mV & 200 ms. (**B**) Plot of R_{in} as a function of EPSP change. Note the lack of correlation ($y = 0.072 + 100.61$; $r = 0.31$). (**C**) Top, EPSP slope time-course pooled over nine experiments with ZD7288 (1 µM) in the bath. Note that ZD7288 does not alter synaptic plasticity. Bottom, R_{in} time course. Representative traces in control (a), after the first stimulation episode (b) and after the third (c). Scale bars: 10 mV, 100 ms. No R_{in} changes were observed. (**D**) Negative correlations between R_{in} changes and LTD levels for each cell in the presence of ZD-7288. (**E**) Normalized R_{in} versus EPSP change levels in control (grey dots) and in the presence of ZD-7288 (blue dots). No significant linear correlation was observed ($y = 0.05x + 100.6$; $r = 0.18$; $p > 0.05$).

excitability was found to be increased following LTD induction in D-AP5 (Fig. 6A & B). Conversely, in the presence of LY341495 excitability was found to be significantly reduced following induction of LTD (Fig. 6C & D).

In conclusion, LTD induced with 3 Hz stimulation activates NMDAR and mGluR that in turn regulate both R_{in} and intrinsic excitability in CA1 pyramidal cells.

Discussion

We show here that in CA1 pyramidal neurons, LTD magnitude determines the changes in input resistance (R_{in}) and hence, the direction of I_h regulation. Moderate LTD induces an increase in I_h (seen as a decrease in R_{in}) while strong LTD results in a decrease of I_h (i.e. an increase in R_{in}). LTD induction in the presence of the NMDA receptor antagonist D-AP5 suppressed the reduction in R_{in}, suggesting that it is mediated by NMDA receptors (Fig. 7A). In contrast, LTD induced by activation of mGluR1/5 with DHPG is associated with an increase in R_{in} (i.e. decrease in I_h). Furthermore, LTD induced in the presence of the mGluR antagonist LY341495 suppressed the increase in R_{in} and left it reduced by ~15%. However, no reduction in R_{in} was observed when LTD was induced

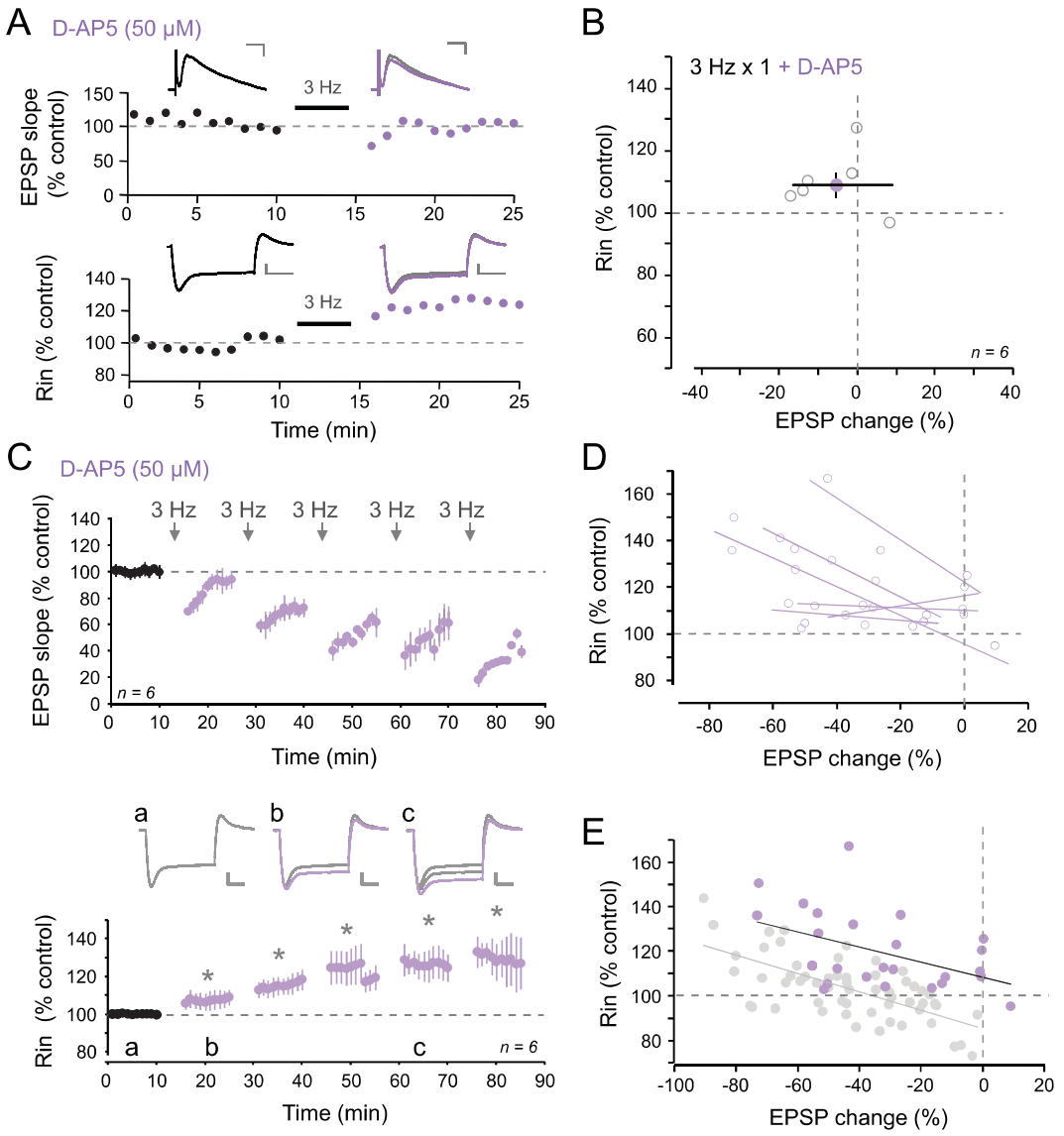

Figure 4. Blockade of NMDAR prevents decrease in R_{in}. (**A**) Time-courses of EPSP slope (top) and R_{in} (bottom) following 3 Hz stimulation for 5 min in the presence of D-AP5. Scale bars: top, 2 mV & 20 ms; bottom, 5 mV & 200 ms. (**B**) Plot of R_{in} as a function of EPSP change. (**C**) Top, EPSP slope time-course induced by repetitive 3 Hz stimulation in the presence of 50 µM D-AP5 in the bath. Bottom, corresponding R_{in} time-course after each stimulation episode. R_{in} is increased from the first episode to the last one. Stars indicate statistical significance ($p < 0.05$). Representative R_{in} traces in control (a), after the first stimulation episode (b) and after the third (c). Scale bars: 10 mV, 100 ms. (**D**) Individual linear correlations between R_{in} changes and EPSP slope modifications induced by 3 Hz stimulation in the presence of D-AP5. (**E**) Normalized R_{in} changes versus normalized LTD size for control condition (grey dots) and in presence of D-AP5 (purple dots). Note the shift to higher values of R_{in} when D-AP5 is present during the plasticity induction (correlation: $y = -0.34x + 108.7$, $r = 0.47$; $p < 0.05$).

in the presence of the mGluR5 antagonist, MPEP, suggesting that activation of mGluR1 and not mGluR5 triggers an increase in R_{in} (Fig. 7A). Finally, excitability was found to be increased when LTD was induced in the presence of D-AP5 whereas it was reduced when LTD was induced in the presence of LY341495. These results suggest that changes in intrinsic excitability follow a single learning rule linking synergistic changes induced by synaptic modification in the physiological range to homeostatic changes induced by large synaptic modification (Fig. 7B). Thus, our results bring strong evidence for fast compensatory processes in Hebbian plasticity[25].

LTD induces NMDAR-dependent up-regulation of I_h. Our results show that a single episode of 3 Hz stimulation for 3–5 min decreases R_{in} in CA1 pyramidal neurons. Blocking I_h with ZD-7288 prevents changes in R_{in} following 3 Hz stimulation, indicating that R_{in} is decreased through an increase of I_h. This component could be isolated by blocking mGluRs with LY341495. Because a reduction of R_{in} causes a decrease in intrinsic excitability[12], this regulation is functionally synergic to the long-lasting depression of synaptic transmission.

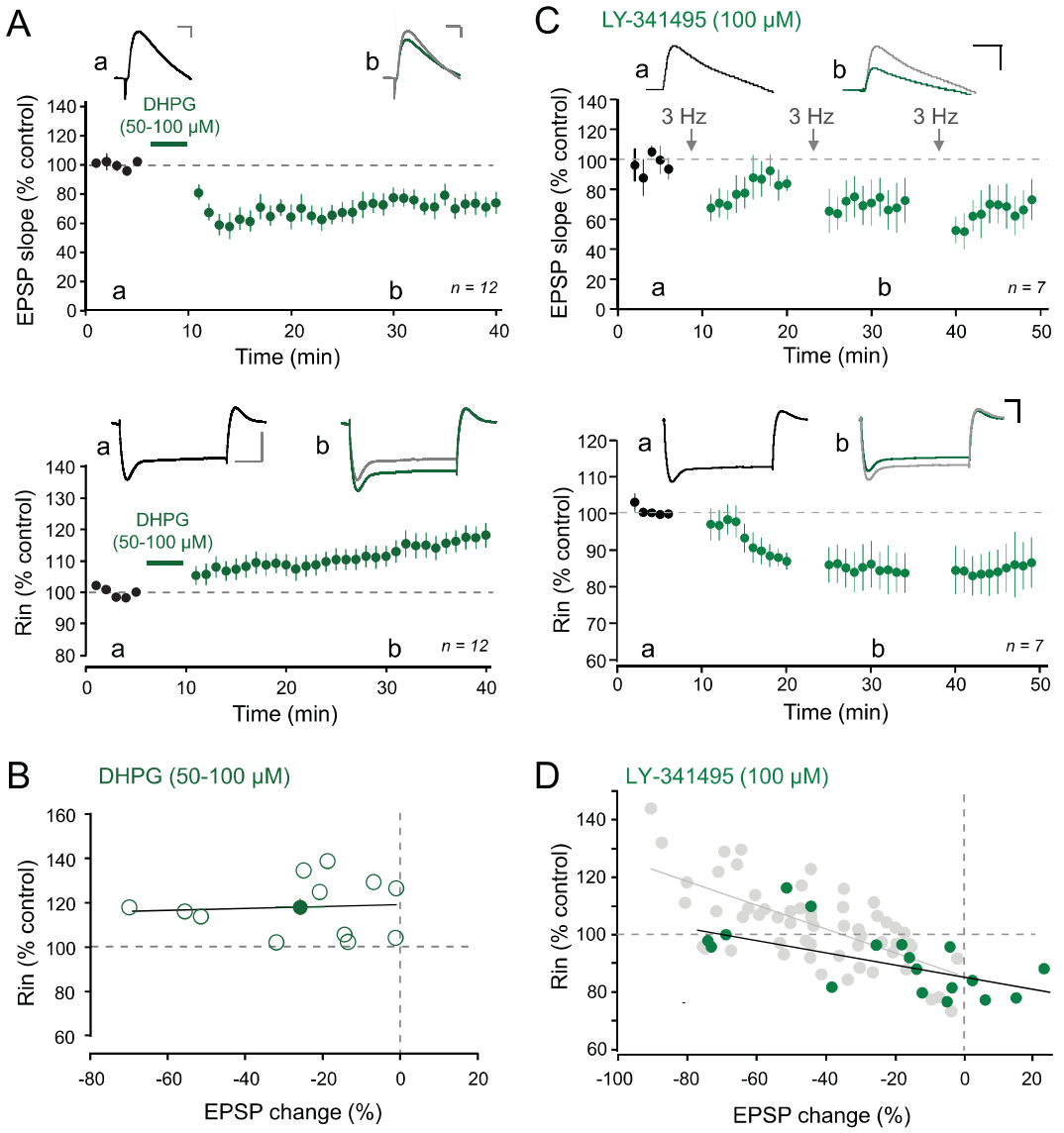

Figure 5. Blockade of mGluRs prevents increase in R_{in}. (**A**) Top, time-course of synaptic changes induced by bath application of 50–100 µM DHPG during 5 minutes (pooled data from 12 cells). Upper traces, representative examples of EPSPs before and after DHPG. Scale bars: top, 2 mV & 20 ms. Bottom, normalized R_{in} changes induced by DHPG. Upper traces, representative traces. Scale bars: 10 mV, 100 ms. (**B**) Plot of R_{in} as a function of EPSP changes. No correlation is observed ($r = 0.06$). (**C**) Top, time-course of synaptic changes induced by 3 Hz stimulation in the presence of 100 µM LY341495. Upper traces, representative examples of EPSPs before and after 3 Hz stimulation. Scale bars: 5 mV & 30 ms. Bottom, normalized R_{in} changes induced by 3 Hz stimulation in the presence of 100 µM LY341495. Scale bars: 10 mV & 50 ms. (**D**) Plot, of R_{in} as a function of EPSP changes (linear correlation, $y = -0.203x + 85.1$, $r = 0.64$; $p < 0.01$).

Such a Hebbian regulation of neuronal excitability has already been reported following LTD induction in CA1 neurons[4,5,16], but this had not been reported in previous studies in which very large LTD was induced[15]. We show that in the presence of the NMDA receptor antagonist D-AP5, no decrease in R_{in} was observed. Rather, R_{in} was enhanced, indicating that stimulation of non-NMDA receptors triggers the down-regulation of h-channel activity.

From Hebbian to homeostatic. Increasing LTD magnitude through repetition of 3 Hz stimulation episodes revealed that R_{in} could be regulated in the other direction. In fact, after the 3rd or 4th stimulation episode, large LTD was induced and R_{in} was found to be increased. This increase in R_{in} was prevented by the presence of ZD-7288 in the bath indicating that it was due to the down-regulation of I_h. A reduction of I_h has already been demonstrated in CA1 pyramidal cells following LTD induction of large magnitude[15]. This regulation is supposed to counteract the reduction in synaptic efficiency in a homeostatic manner. In fact, other experimental studies have shown that sensory deprivation or chronic inactivity leads to the down-regulation of I_h in pyramidal neurons of the barrel cortex[26] or the hippocampus[27]. The down-regulation of I_h could be induced by stimulation of group

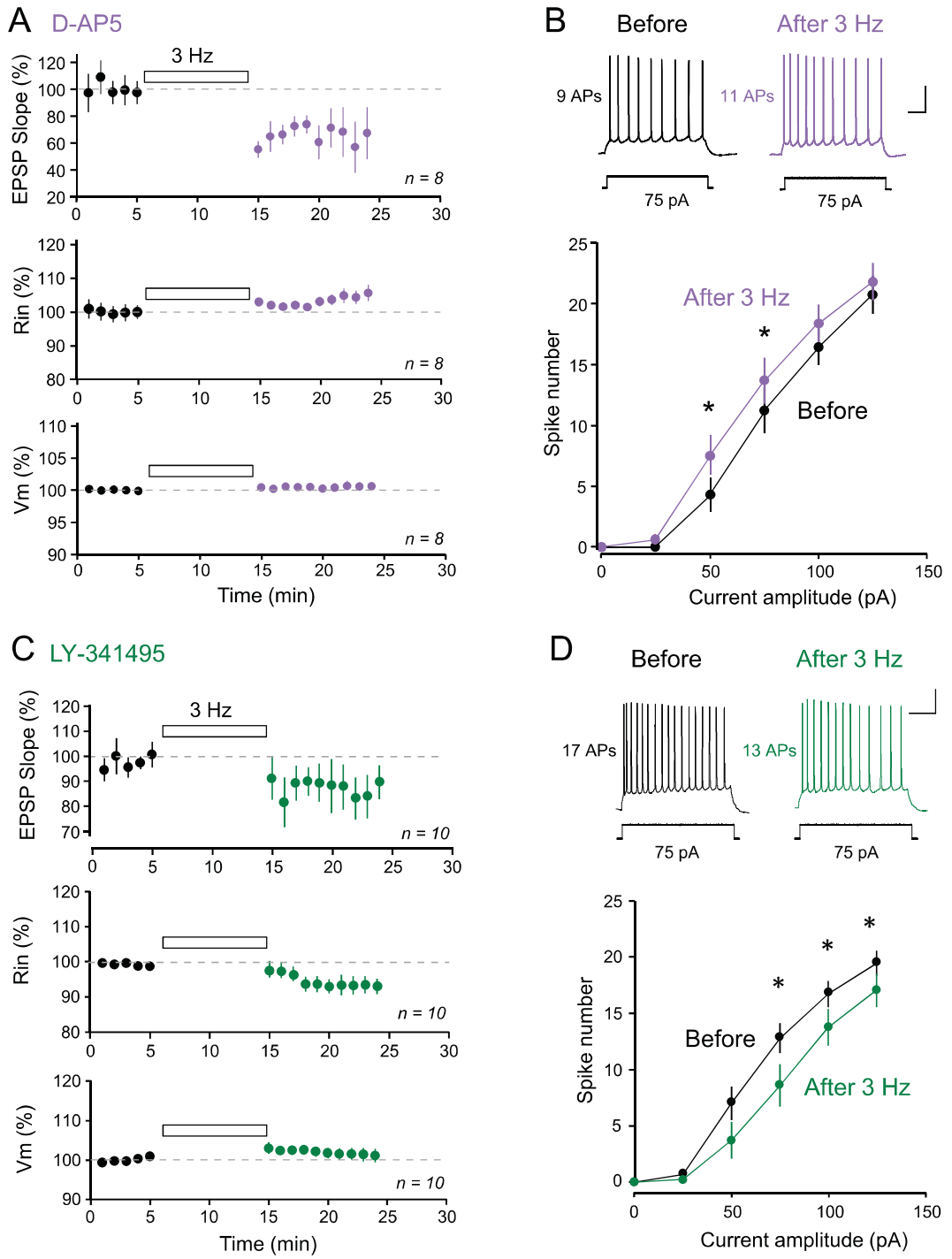

Figure 6. LTD is associated with bidirectional changes in excitability. (**A**) & (**B**) LTD induced in the presence of D-AP5 is associated with an increased excitability. (**A**) Top, time-course of LTD induced by 3 Hz stimulation of the glutamatergic inputs for 10 minutes in the presence of 50 µM D-AP5. Middle, time-course of the increased R_{in}. Bottom, time-course of V_m. (**B**) Top, representative example of firing induced by a current step of 75 pA before and after LTD induction with 3 Hz stimulation in the presence of D-AP5. Scale bars: 20 mV & 100 ms. Bottom, input-output curves before (black) and after (purple) LTD induction. Stars indicate significant change ($p < 0.05$). (**C**) & (**D**) LTD induced in the presence of LY341495 is associated with a decreased excitability. (**C**) Top, time-course of LTD induced by 3 Hz stimulation of the glutamatergic inputs for 10 minutes in the presence of 100 µM LY341495. Middle, time-course of the increased R_{in}. Bottom, time-course of V_m. (**D**) Top, representative example of firing induced by a current step of 75 pA before and after LTD induction with 3 Hz stimulation in the presence of LY341495. Scale bars: 20 mV & 200 ms. Bottom, input-output curves before (black) and after (dark green) LTD induction. Stars indicate significant change ($p < 0.05$).

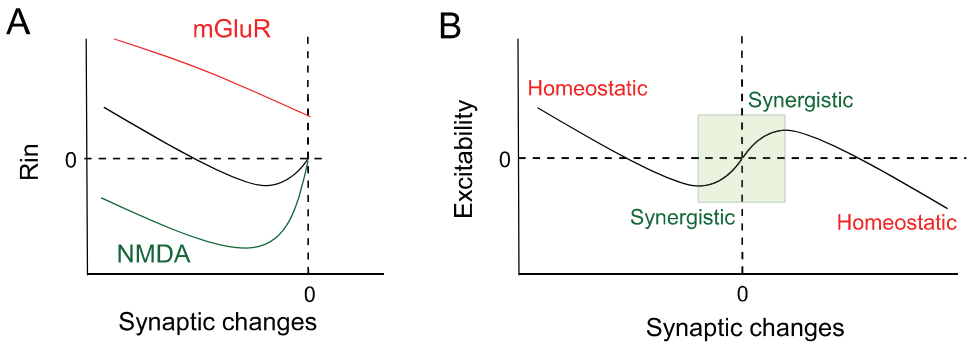

Figure 7. The continuum rule: linking synergistic plasticity with homeostatic plasticity. (**A**) Summary of the glutamate-receptor induced changes in R_{in} as a function of synaptic changes. Green curve illustrates the NMDA-dependent change in R_{in}. Red curve shows the mGluR-dependent change in R_{in}. Black curve illustrates the sum of the green and red curves. (**B**) Unifying rule for intrinsic plasticity. In a physiological range (defined by the green square), modulation of neuronal activity results in a conjugated modification in intrinsic excitability (synergistic). Out of this range, persisting increases (right) or decreases (left) in synaptic efficacy induce compensatory changes in intrinsic excitability (homeostatic). Adapted from Campanac *et al.* 2008 and from the present study.

I mGluR. We indeed show that DHPG induced LTD associated with an increase in R_{in}. In addition, we show that R_{in} diminished when LTD was induced by 3 Hz stimulation in the presence of the broad spectrum mGluR antagonist LY341495 but not in the presence of the specific mGluR5 antagonist MPEP, suggesting that activation of mGluR1 mediates the homeostatic increase in R_{in}. These results are consistent with the mGluR-dependent increase in both R_{in} and intrinsic excitability reported by Brager & Johnson (2007) and suggest that two sets of receptors might be able to up-regulate and down-regulate h-channel activity depending on the magnitude of synaptic modification.

mGluR5 has been shown to mediate enhanced excitability induced by stimulation of glutamatergic inputs in L5 pyramidal neurons[28] and in hippocampal parvalbumin-positive basket cells[7]. In these cases, the changes in excitability were synergistic to synaptic modification. Here, we show that stimulation of mGluR1 appears as the main factor responsible for the switch of synergistic to homeostatic regulation of intrinsic excitability.

Pharmacological[11] or activity-dependent[15] reduction in h-channel activity is usually associated with a hyperpolarizing shift in membrane potential. No change in membrane potential was, however, observed in the experiments reported here (see also Campanac *et al.*, 2008). The apparent discrepancy with the results of Brager & Johnston (2007) might be due to the much larger increase in input resistance obtained in this study following LTD induction (+100% versus + 20% in our case).

Compared to Hebbian plasticity, homeostatic regulation is generally considered as a slow process. In fact, most of the regulations of intrinsic excitability reported so far have been obtained with manipulating network activity for 2–3 days[10,27,29–31]. Here, we report induction of homeostatic plasticity of intrinsic excitability that can be induced in parallel with Hebbian synaptic plasticity on a much faster time-scale. Such rapid compensatory processes are thought to be necessary to stabilize neuronal activity[32,33].

Bidirectional regulation of I_h has already been revealed following LTP induction in CA1 pyramidal neurons[17]. The present study not only reconciles contradictive experimental results[4,15] but it also shows that Hebbian and homeostatic regulations of I_h occur in the same neuron after LTD induction and follow a single rule establishing a continuum between functionally opposite forms of intrinsic plasticity that target h-channels (Fig. 7B)[34].

Mechanisms of h-channels regulation. The existence of a learning rule linking synergistic and homeostatic changes implies multiple modes of h-channel regulation. Although further experimental investigations will be required, the mechanisms of molecular regulation of h-channels are multiple[35]. Activity of h-channels can be regulated by a change in their density (i.e. by insertion or removal of HCN subunits), by a change in the distribution of h-channels at the surface of the neuron[36] or by changes in their sensitivity to cyclic nucleotides[37]. Trip8b (Tetratricopeptide-Repeat containing Rab8b-interacting protein) has been identified as an important binding partner of HCN[38]. Interestingly, Trip8b undergo alternative splicing and its isoforms have been demonstrated to differently affect I_h density[39,40] and the sensitivity of h-channels to cyclic AMP[40,41]. In fact, while most isoforms of Trip8b enhance expression of dendritic HCN subunits[39,40], some Trip8b isoforms, however, suppress HCN subunit expression[42]. As dendrites are able to locally translate mRNA following LTD[43] and promote alternative splicing[44], Trip8b isoforms offer an attractive mechanism to explain the bidirectional regulation of I_h. Interestingly, it has recently been shown that h-channel upregulation that normally occurs after induction of large LTP[13] is absent in Trip8b knock-out mice[45]. Similar experiments should be conducted on the LTD side.

A remaining question is: what is the molecular link between activation of NMDAR/mGluR1 and the regulation of h-channels? The activation of different protein kinases such as Ca^{2+}/CaMKII or PKC results in the modulation of h-channel activity in response to different patterns of neuronal activity[13,15,46] but precise data on the regulation of Trip8b by either NMDAR or mGluR1 through Ca^{2+}/CaMKII or PKC are still missing today.

Experimental procedures

Slice preparation. Hippocampal slices were obtained from 14- to 20- day-old rats according to institutional guidelines for the care and use of laboratory animals (Directive 86/609/EEC and French National Research Council) an approved by the local health authority (# D1305508, Préfecture des Bouches-du-Rhône, Marseille). Rats were deeply anaesthetized with chloral hydrate (intraperitoneal 400 mg/kg) and killed by decapitation. Slices (350 µm) were cut in a solution containing a reduced concentration of sodium (in mM: 280 sucrose, 26 $NaHCO_3$, 10 D-glucose, 1.3 KCl, 1 $CaCl_2$, and 10 $MgCl_2$) on a vibratome (Leica VT1000S) and were maintained for 1 h at room temperature in oxygenated (95% O_2/5% CO_2) Artificial Cerebro-Spinal Fluid (ACSF; in mM: 125 NaCl, 2.5 KCl, 0.8 NaH_2PO_4, 26 $NaHCO_3$, 3 $CaCl_2$, 2 $MgCl_2$, and 10 D-glucose) with foetal bovine serum (4%). For recording, each slice was transferred to a temperature-controlled (30 °C) chamber with oxygenated ACSF. $GABA_A$ channels were blocked with picrotoxin (PiTX, 100 µM) and the CA3 area was surgically removed.

Electrophysiology. Neurons were identified with an Olympus BX 50WI microscope using infrared video microscopy and Differential Interference Contrast (DIC) × 60 optics.

Whole-cell recordings were made from CA1 pyramidal neurons with electrodes filled with a solution containing the following (in mM): 120 K-gluconate, 20 KCl, 10 HEPES, 0.5 EGTA, 2 $MgCl_2$ $6H_2O$, and 2 Na_2ATP. Stimulating pipettes filled with extracellular saline were placed in the *stratum radiatum* to stimulate the Schaffer collaterals.

In control and test conditions, Excitatory Post-Synaptic Potentials (EPSPs) were elicited at 0.1 Hz by a digital stimulator (NEURO DATA PG4000, Instruments corp.) or by pCLAMP (Molecular devices). LTD was induced with continuous shocks delivered at 3 Hz during 5 min. Apparent input resistance was tested by current injection (−120 pA; 800 ms). Series resistance was monitored throughout the recording and only experiments with stable resistance were kept (changes <10%).

Intrinsic excitability has been measured before and after 3 Hz stimulation with input-output curves consisting in plotting spike number in response to incrementing steps of current pulses[27,28]. Changes in membrane potential (V_m) were measured in the absence of any holding current.

Drugs. Drugs were bath applied. Picrotoxin (PiTx) was purchased from Sigma. [4-(*N*-ethyl-*N*-phenylamino)-1,2-dimethyl-6-(methylamino) pyrimidinium chloride] (ZD-7288), D-(-)-2-Amino-5-phosphonopentanoic acid (D-AP5), 3,5-Dihydroxyphenylglycine (DHPG), (2 S)-2-Amino-2-[(1 S,2 S)-2-carboxycycloprop-1-yl]-3-(xanth-9-yl) propanoic acid (LY341495) and 2-methyl-6-(phenylethylyl)pyridine (MPEP) were purchased from Tocris Bioscience.

Data acquisition and analysis. Recordings were obtained using an Axoclamp-2B (Molecular Devices) or a MultiClamp 700B (Molecular Devices) amplifier and pClamp10 software. Data were sampled at 10 kHz, filtered at 3 kHz, and digitized by a Digidata1322A (Molecular Devices). All data analyses were performed with custom written software in Igor Pro 6 (Wavemetrics).

Apparent input resistance was determined by the subtraction of the steady-state voltage change during hyperpolarizing current injection from the baseline.

Pooled data are presented as mean ± SEM. Statistical comparisons were made using Wilcoxon or Mann-Whitney test as appropriate with Sigma Plot software. Statistical correlations were tested using Spearman test. Data were considered as significant when $p < 0.05$.

Modelling. A simple Hodgkin-Huxley-type model of hippocampal neuron was developed under LabView (LabView 7). The model had no dimension and included only the h conductance with parameters taken from Campanac *et al.*, 2008. The leak resistance was set to 1 GΩ. The h-current was given by:

$$I_h = G_h * (V_m - E_h) \quad (1)$$

with V_m the membrane potential, $E_h = -37.7$ mV, and the h-conductance given by the following equation:

$$G_h = G_{h,\,max} * n \quad (2)$$

The activation and deactivation time constants were determined by fitting experimental data from Campanac *et al.* (2008). The following differential equation was solved,

$$dn(V, t)/dt = \alpha_n(V) * [1 - n(V, t)] \quad (3)$$

This equation corresponds to:

$$d(V, t)/dt = [n_\infty(V) - n(V, t)]/\tau(V) \quad (4)$$

$$n_\infty(V) = \alpha_n(V)/[\alpha_n(V) + \beta_n(V)] \quad (5)$$

$$\tau(V) = 1 \text{ for } V > -30 \text{ mV} \quad (6)$$

otherwise

$$\tau(V) = 1/[\alpha_n(V) + \beta_n(V)] \quad (7)$$

$$\alpha_n = 0.0204/(1 + \exp[(V + 98.68)/13.24]) \quad (8)$$

$$\beta_n = 0.0176/(1 + \exp[-(V + 57.96)/13.2]) \quad (9)$$

where $n_\infty(V)$ is the steady-state activation parameter and $\tau(V)$ the activation time constant.

References

1. Debanne, D. & Poo, M. M. Spike-timing dependent plasticity beyond synapse - pre- and post-synaptic plasticity of intrinsic neuronal excitability. *Front Synaptic Neurosci* **2**, 21 (2010).
2. Titley, H. K., Brunel, N. & Hansel, C. Toward a Neurocentric View of Learning. *Neuron* **95**, 19–32 (2017).
3. Abraham, W. C., Gustafsson, B. & Wigstrom, H. Long-term potentiation involves enhanced synaptic excitation relative to synaptic inhibition in guinea-pig hippocampus. *J Physiol* **394**, 367–80 (1987).
4. Daoudal, G., Hanada, Y. & Debanne, D. Bidirectional plasticity of excitatory postsynaptic potential (EPSP)-spike coupling in CA1 hippocampal pyramidal neurons. *Proc Natl Acad Sci USA* **99**, 14512–7 (2002).
5. Campanac, E. & Debanne, D. Spike timing-dependent plasticity: a learning rule for dendritic integration in rat CA1 pyramidal neurons. *J Physiol* **586**, 779–93 (2008).
6. Lopez-Rojas, J., Heine, M. & Kreutz, M. R. Plasticity of intrinsic excitability in mature granule cells of the dentate gyrus. *Sci Rep* **6**, 21615 (2016).
7. Campanac, E. *et al*. Enhanced intrinsic excitability in basket cells maintains excitatory-inhibitory balance in hippocampal circuits. *Neuron* **77**, 712–22 (2013).
8. Shim, H. G. *et al*. Long-Term Depression of Intrinsic Excitability Accompanied by Synaptic Depression in Cerebellar Purkinje Cells. *J Neurosci* **37**, 5659–5669 (2017).
9. Turrigiano, G. G. & Nelson, S. B. Homeostatic plasticity in the developing nervous system. *Nat Rev Neurosci* **5**, 97–107 (2004).
10. Desai, N. S., Rutherford, L. C. & Turrigiano, G. G. Plasticity in the intrinsic excitability of cortical pyramidal neurons. *Nat Neurosci* **2**, 515–20 (1999).
11. Gasparini, S. & DiFrancesco, D. Action of the hyperpolarization-activated current (Ih) blocker ZD 7288 in hippocampal CA1 neurons. *Pflugers Arch* **435**, 99–106 (1997).
12. Poolos, N. P., Migliore, M. & Johnston, D. Pharmacological upregulation of h-channels reduces the excitability of pyramidal neuron dendrites. *Nat Neurosci* **5**, 767–74 (2002).
13. Fan, Y. *et al*. Activity-dependent decrease of excitability in rat hippocampal neurons through increases in I(h). *Nat Neurosci* **8**, 1542–51 (2005).
14. Narayanan, R. & Johnston, D. Long-term potentiation in rat hippocampal neurons is accompanied by spatially widespread changes in intrinsic oscillatory dynamics and excitability. *Neuron* **56**, 1061–75 (2007).
15. Brager, D. H. & Johnston, D. Plasticity of intrinsic excitability during long-term depression is mediated through mGluR-dependent changes in I(h) in hippocampal CA1 pyramidal neurons. *J Neurosci* **27**, 13926–37 (2007).
16. Wang, Z., Xu, N. L., Wu, C. P., Duan, S. & Poo, M. M. Bidirectional changes in spatial dendritic integration accompanying long-term synaptic modifications. *Neuron* **37**, 463–72 (2003).
17. Campanac, E., Daoudal, G., Ankri, N. & Debanne, D. Downregulation of dendritic I(h) in CA1 pyramidal neurons after LTP. *J Neurosci* **28**, 8635–43 (2008).
18. Gastrein, P. *et al*. The role of hyperpolarization-activated cationic current in spike-time precision and intrinsic resonance in cortical neurons *in vitro*. *J Physiol* **589**, 3753–73 (2011).
19. Dudek, S. M. & Bear, M. F. Homosynaptic long-term depression in area CA1 of hippocampus and effects of N-methyl-D-aspartate receptor blockade. *Proc Natl Acad Sci USA* **89**, 4363–7 (1992).
20. Mulkey, R. M. & Malenka, R. C. Mechanisms underlying induction of homosynaptic long-term depression in area CA1 of the hippocampus. *Neuron* **9**, 967–75 (1992).
21. Debanne, D., Gahwiler, B. H. & Thompson, S. M. Asynchronous pre- and postsynaptic activity induces associative long-term depression in area CA1 of the rat hippocampus *in vitro*. *Proc Natl Acad Sci USA* **91**, 1148–52 (1994).
22. Oliet, S. H., Malenka, R. C. & Nicoll, R. A. Two distinct forms of long-term depression coexist in CA1 hippocampal pyramidal cells. *Neuron* **18**, 969–82 (1997).
23. Huber, K. M., Roder, J. C. & Bear, M. F. Chemical induction of mGluR5- and protein synthesis–dependent long-term depression in hippocampal area CA1. *J Neurophysiol* **86**, 321–5 (2001).
24. Bashir, Z. I., Jane, D. E., Sunter, D. C., Watkins, J. C. & Collingridge, G. L. Metabotropic glutamate receptors contribute to the induction of long-term depression in the CA1 region of the hippocampus. *Eur J Pharmacol* **239**, 265–6 (1993).
25. Zenke, F. & Gerstner, W. Hebbian plasticity requires compensatory processes on multiple timescales. *Philos Trans R Soc Lond B Biol Sci* **372** (2017).
26. Breton, J. D. & Stuart, G. J. Loss of sensory input increases the intrinsic excitability of layer 5 pyramidal neurons in rat barrel cortex. *J Physiol* **587**, 5107–19 (2009).
27. Gasselin, C., Inglebert, Y. & Debanne, D. Homeostatic regulation of h-conductance controls intrinsic excitability and stabilizes the threshold for synaptic modification in CA1 neurons. *J Physiol* **593**, 4855–69 (2015).
28. Sourdet, V., Russier, M., Daoudal, G., Ankri, N. & Debanne, D. Long-term enhancement of neuronal excitability and temporal fidelity mediated by metabotropic glutamate receptor subtype 5. *J Neurosci* **23**, 10238–48 (2003).
29. Karmarkar, U. R. & Buonomano, D. V. Different forms of homeostatic plasticity are engaged with distinct temporal profiles. *Eur J Neurosci* **23**, 1575–84 (2006).
30. Cudmore, R. H., Fronzaroli-Molinieres, L., Giraud, P. & Debanne, D. Spike-time precision and network synchrony are controlled by the homeostatic regulation of the D-type potassium current. *J Neurosci* **30**, 12885–95 (2010).
31. Kuba, H., Yamada, R., Ishiguro, G. & Adachi, R. Redistribution of Kv1 and Kv7 enhances neuronal excitability during structural axon initial segment plasticity. *Nat Commun* **6**, 8815 (2015).
32. Honnuraiah, S. & Narayanan, R. A calcium-dependent plasticity rule for HCN channels maintains activity homeostasis and stable synaptic learning. *PLoS One* **8**, e55590 (2013).
33. Zenke, F., Gerstner, W. & Ganguli, S. The temporal paradox of Hebbian learning and homeostatic plasticity. *Curr Opin Neurobiol* **43**, 166–176 (2017).
34. Debanne, D., Daoudal, G., Sourdet, V. & Russier, M. Brain plasticity and ion channels. *J Physiol Paris* **97**, 403–14 (2003).
35. Shah, M. M. Cortical HCN channels: function, trafficking and plasticity. *J Physiol* **592**, 2711–9 (2014).
36. Shin, M. & Chetkovich, D. M. Activity-dependent regulation of h channel distribution in hippocampal CA1 pyramidal neurons. *J Biol Chem* **282**, 33168–80 (2007).
37. Luthi, A. & McCormick, D. A. Modulation of a pacemaker current through Ca(2+)-induced stimulation of cAMP production. *Nat Neurosci* **2**, 634–41 (1999).
38. Santoro, B., Wainger, B. J. & Siegelbaum, S. A. Regulation of HCN channel surface expression by a novel C-terminal protein-protein interaction. *J Neurosci* **24**, 10750–62 (2004).

39. Lewis, A. S. *et al*. Alternatively spliced isoforms of TRIP8b differentially control h channel trafficking and function. *J Neurosci* **29**, 6250–65 (2009).
40. Santoro, B. *et al*. TRIP8b splice variants form a family of auxiliary subunits that regulate gating and trafficking of HCN channels in the brain. *Neuron* **62**, 802–13 (2009).
41. Zolles, G. *et al*. Association with the auxiliary subunit PEX5R/Trip8b controls responsiveness of HCN channels to cAMP and adrenergic stimulation. *Neuron* **62**, 814–25 (2009).
42. Santoro, B. *et al*. TRIP8b regulates HCN1 channel trafficking and gating through two distinct C-terminal interaction sites. *J Neurosci* **31**, 4074–86 (2011).
43. Huber, K. M., Kayser, M. S. & Bear, M. F. Role for rapid dendritic protein synthesis in hippocampal mGluR-dependent long-term depression. *Science* **288**, 1254–7 (2000).
44. Glanzer, J. *et al*. RNA splicing capability of live neuronal dendrites. *Proc Natl Acad Sci USA* **102**, 16859–64 (2005).
45. Brager, D. H., Lewis, A. S., Chetkovich, D. M. & Johnston, D. Short- and long-term plasticity in CA1 neurons from mice lacking h-channel auxiliary subunit TRIP8b. *J Neurophysiol* **110**, 2350–7 (2013).
46. van Welie, I., van Hooft, J. A. & Wadman, W. J. Homeostatic scaling of neuronal excitability by synaptic modulation of somatic hyperpolarization-activated Ih channels. *Proc Natl Acad Sci USA* **101**, 5123–8 (2004).

Acknowledgements

Supported by INSERM, CNRS, French Ministry of Research (doctoral grant to CG), ANR NEUC 2014 (ANR-14-NEUC-0004) and Fondation pour la Recherche Médicale (FDT20120925075, doctoral grant to CG & FDT20170437059, doctoral grant to YI).

Author Contributions

C.G. & Y.I. collected and analyzed the data. N.A. performed computer simulations, C.G. Y.I. & D.D. wrote the manuscript and prepared the figures, & D.D. supervised the project.

Additional Information

Supplementary information accompanies this paper at https://doi.org/10.1038/s41598-017-14874-z.

Competing Interests: The authors declare that they have no competing interests.

Publisher's note: Springer Nature remains neutral with regard to jurisdictional claims in published maps and institutional affiliations.

Available online at www.sciencedirect.com

ScienceDirect

Current Opinion in Neurobiology

Plasticity of intrinsic neuronal excitability

Dominique Debanne, Yanis Inglebert and Michaël Russier

Long-term synaptic modification is not the exclusive mode of memory storage, and persistent regulation of voltage-gated ion channels also participates in memory formation. Intrinsic plasticity is expressed in virtually all neuronal types including principal cells and interneurons. Activation of synaptic glutamate receptors initiates long-lasting changes in neuronal excitability at presynaptic and postsynaptic side. As synaptic plasticity, intrinsic plasticity is bi-directional and expresses a certain level of input-specificity or cell-specificity. We discuss here the nature of the learning rules shared by intrinsic and synaptic plasticity and the impact of intrinsic plasticity on temporal processing.

Address
UNIS, UMR1072 INSERM – AMU, Marseille, France

Corresponding author: Debanne, Dominique (dominique.debanne@inserm.fr)

Current Opinion in Neurobiology 2019, **54**:73–82

This review comes from a themed issue on **Neurobiology of learning and plasticity**

Edited by **Scott Waddell** and **Jesper Sjotrom**

https://doi.org/10.1016/j.conb.2018.09.001

Introduction

Long-lasting plasticity of chemical synaptic transmission is usually considered as the main mechanism accounting for information storage in the brain. Synapse-specific changes in transmission from a large array of inputs appears particularly appealing for maintaining a high computational capacity in the brain. However, this appears not to be the whole story and many other factors involved in the transfer of neuronal information occupy today a key position in functional plasticity. Voltage-gated channels located at the input or output side of neurons are involved in a form of activity-dependent plasticity called intrinsic plasticity (for review, see Refs. [1–5]).

Here, we review recent *in vitro* works devoted to the study of intrinsic plasticity in mammalian neurons. First, we will discuss new expression mechanisms of graded persistent firing, a form of short-term plasticity that may account for working memory. Second, we review some recent findings that illustrate cellular correlates of learning mediated by changes in intrinsic excitability. Next, we will describe different ways of modulating input–output function at the neuronal scale. Then, we will consider the learning rules of intrinsic plasticity on the basis of those defined for synaptic modifications. Next, we will review recently identified mechanisms of intrinsic plasticity in GABAergic interneurons. Finally, we will discuss the consequences of intrinsic plasticity on temporal processing.

Graded firing: a cellular analog of working memory

Working memory is an ephemeral retention of information whose neurobiological substrate can be seen as a stimulus-specific modulation of neural activity that lasts until a new stimulus is presented (Figure 1a). The neuronal basis for this form of memory was first identified in associative cortices of the monkey (for review, see Ref. [6]). In the prefrontal cortex, the posterior parietal cortex or the inferotemporal cortex, a subset of neurons called 'memory neurons' show persistent activity during a delayed response task, in which the animal is required to retain information of a sensory cue across a delay period between the stimulus and the behavioral response. In contrast with long-lasting forms of memory requiring molecular and/or structural changes, this form of short-term memory (or working memory) is a dynamic and ephemeral process. According to the classical view, the stimulation is memorized through reverberating activity within interconnected groups of neurons (Figure 1b). Inhibition of one of the neurons may stop activity within interconnected neurons. Egorov *et al.* [7] discovered that single isolated neurons are able to memorize the stimulus that was transiently applied (Figure 1b). During basal stimulation of muscarinic acetylcholine receptors (mAChR), neurons from the entorhinal cortex may, upon brief stimulation, generate sustained increases in their electrical activity that are graded in frequency and reversible by hyperpolarization. Persistent firing is cell-specific [8] and it has been also reported in CA3 [9] and CA1 [10] hippocampal pyramidal neurons, mitral cells from the olfactory bulb [11] and L5 cortical pyramidal neurons [8,12••] under stimulation of mAChR. Graded persistent firing requires postsynaptic calcium influx mediated by spiking activity. The original mechanism of graded firing was thought to be mediated by calcium-activated non-selective (CAN) cationic current that in turn depolarizes the cell [7] (Figure 1c). But, the molecular identity of CAN channels remains elusive and alternative mechanisms have been considered. The inversion of the Na^+/Ca^{2+} exchanger activity by accumulation of intracellular Na^+ has been proposed to account for persistent firing in

Figure 1

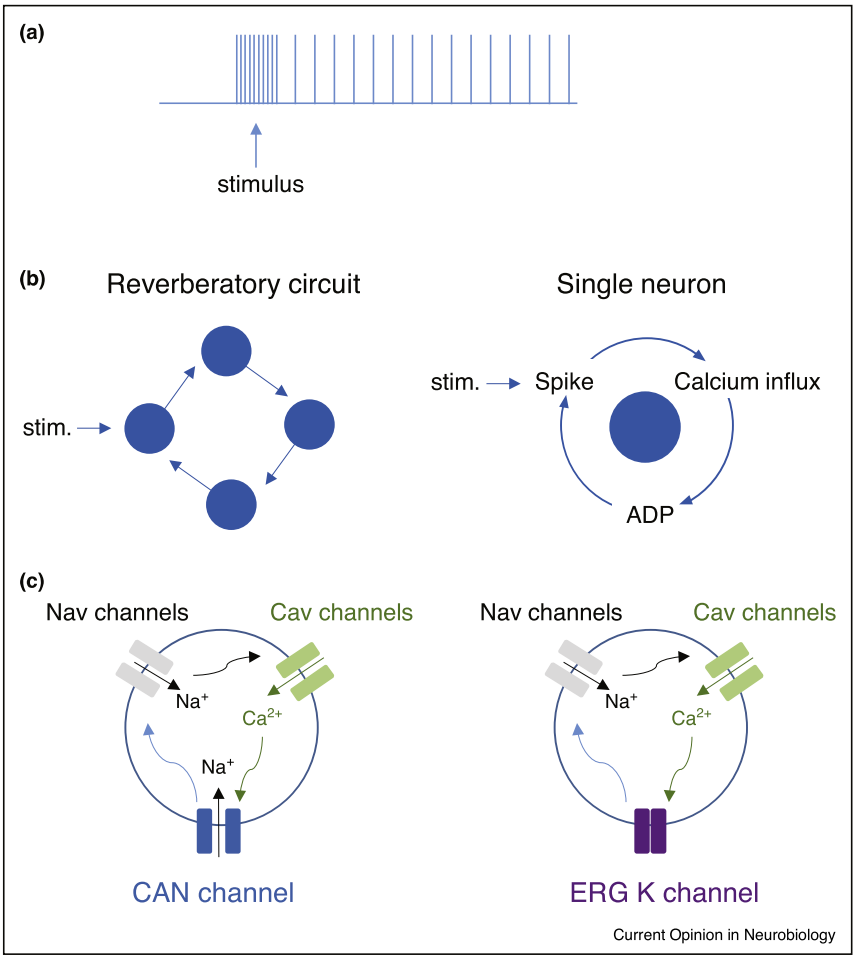

Persistent firing as a cellular model of working memory.
(a) Brief excitation of the neuron by the stimulus leads to persistent firing that is persistently maintained at the same rate. Adapted from Ref. [7] **(b)** Reverberatory circuit versus single neuron mnemonics. In both cases, an external stimulation leads to persistent activity through synaptic connections (reverberatory circuit) or through a calcium-dependent afterdepolarization (ADP). **(c)** Two possible mechanisms for ADP. Left, the opening of CAN channel leads to sustained firing through Na^+ influx (adapted from Ref. [7]). Right, the closure of an ether-à-gogo related gene (ERG) channel leads to persistent firing through a depolarization of the membrane conjugated with an increase in input resistance (adapted from Ref. [12••]).

mitral cells of the olfactory bulb [11]. Although attractive, this mechanism seems unable to explain all forms of persistent firing since in neocortical pyramidal neurons, persistent firing is still observed in the presence of tetrodotoxin, a potent Nav channel blocker [12••] (in this case, calcium spikes replace sodium spikes). In this study, persistent firing is mediated by the modulation of ether-à-Go-Go related gene (ERG) K^+ channel [12••]. ERG channels mediate a leak potassium current that is downregulated by calcium entry induced with repetitive spiking (Figure 1c).

Cellular correlates of learning

The search for cellular excitability correlates of learning and memory in the mammalian brain has focused on neurons that are thought to be active during learning. Since the pioneering work of C. Woody, many studies have shown that classical conditioning alters intrinsic excitability (IE) in neurons from the pericruciate cortex [13], hippocampus [14,15] or cerebellum [16]. All these studies indicate that intrinsic plasticity occurs in neurons following learning but the activity of the recorded cell was not accurately controlled during learning. A recent study went a step further by showing using a fluorescent activity-reporter that intrinsic excitability is altered only in cells that are active during learning [17••].

Regulations of neuronal excitability have been involved in others forms of learning such as spatial learning [18], fear conditioning [19–22], odor discrimination [23–25].

Experiencing new or enriched environment is also known to affect intrinsic excitability [26,27]. Following learning, usually after-hyperpolarization (AHP), AP threshold and accommodation are decreased resulting in an enhancement of AP firing and neuronal IE in the hippocampus (spatial and fear conditioning), amygdala (fear conditioning and odor discrimination), or prefrontal cortex (fear conditioning). While most of excitability changes discussed so far corresponds to enhanced IE, *decrease* in IE has been observed in mitral cells of the accessory olfactory bulb following social learning [17••]. In fact, mitral cells showed an unusual reduction in cell firing during repetitive stimulation. The reason why polarity is changes in this particular case is not yet elucidated but it may act to filter sustained or repetitive signals.

Multiple mechanisms for modulating input–output function

Input–output function is a critical operation achieved by synaptic and intrinsic mechanisms. Whereas expression mechanisms of synaptic plasticity are rather simple and involve either presynaptic change in neurotransmitter release or postsynaptic change in glutamate receptor density or function, plasticity of IE can be expressed through at least three different types of functional modulation (Figure 2). Ion channels located in dendrites shape EPSP waveform by either boosting or attenuating the synaptic response. Thus, a given EPSP may lead to an action potential if the net amplification is enhanced. Two ion channels located in the dendrites, the hyperpolarization-activated cyclic nucleotide-gated (HCN) channel and the voltage-gated potassium channel (Kv4.2) attenuate the EPSP amplitude. Their downregulation following induction of synaptic potentiation enhances input–output function [28–31]. As synaptic plasticity, the modulation of EPSP amplification is generally *local* as other inputs remain unchanged [28,32].

Input–output function may be altered via modulation of spike threshold (Figure 2). The spike threshold is determined by voltage-gated Na^+ (Nav) and K^+ (Kv) channels. Shift of Nav activation towards hyperpolarized values lowers the spike threshold and increases excitability following induction of synaptic potentiation in CA1 pyramidal neurons [33]. Similarly, downregulation of Kv1 channels, as observed in auditory neurons following cochlea removal, lowers the spike threshold and increases intrinsic excitability [34••]. This type of modulation is *global* since it may affect all incoming inputs.

Figure 2

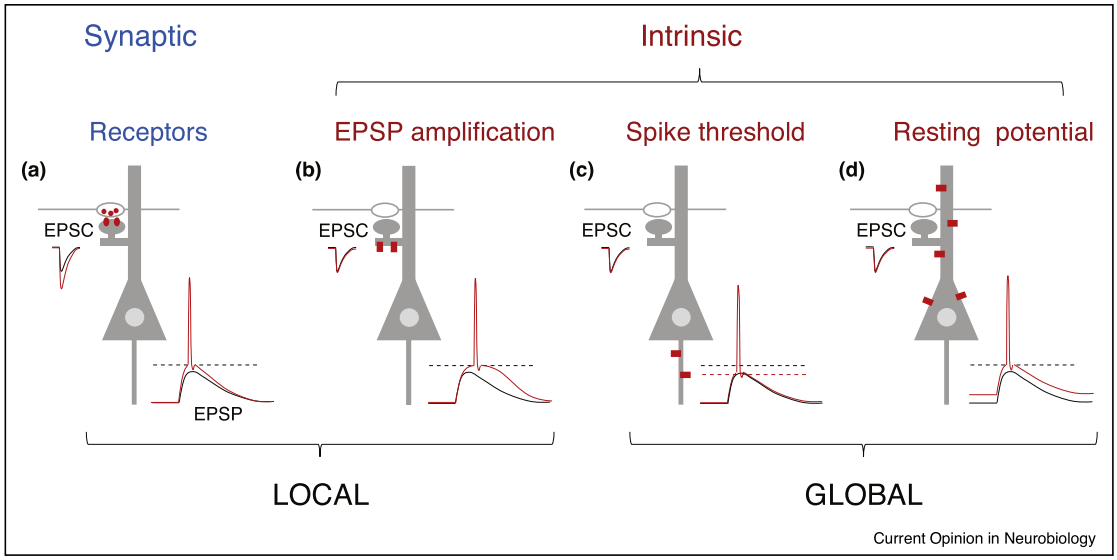

Mechanisms of input–output function modulation.
(a) Synaptic modification of input–output function. Local potentiation of synaptic transmission by increase in transmitter release and/or postsynaptic receptor density is characterized by an enhanced excitatory post-synaptic current (EPSC). At the initial segment, the excitatory post-synaptic potential (EPSP) becomes large enough to cross the action potential (AP) threshold and to elicit a postsynaptic spike. Note the larger EPSP slope. **(b)** Change in EPSP amplification. When dendritic channels (red) are regulated, the resulting EPSP is amplified and crosses the spike threshold. Note that here the synaptic current (EPSC) is kept constant to clearly distinguish intrinsic from synaptic changes and the initial EPSP slope remains unchanged. These first two modifications are *local* because they do not affect all synaptic inputs. **(c)** Change in spike threshold. An increase in spike firing is obtained when the AP threshold is hyperpolarized through the regulation of voltage-gated ion channels located at the axon initial segment. Here again, synaptic current (EPSC) remains unchanged. **(d)** Change in resting membrane potential. Following modulation of voltage-gated channels, the resting membrane potential of the neuron is depolarized leading to the triggering of an action potential by the EPSP. Note that here again, synaptic current (EPSC) remains unchanged. These last two modifications are *global* because they affect all synaptic inputs.

Input–output function can be modulated by changing the resting membrane potential (RMP) of the neuron (Figure 2). Hippocampal granule cells display long-term depolarization (LT-Depol) of the RMP by approximately 8–10 mV following high frequency firing [35]. LT-Depol in granule cells is mediated by a protein kinase A-dependent upregulation of HCN channels. While, the regulation of HCN channels leads to attenuated EPSP amplitude and therefore to a reduction in intrinsic excitability (see above), the net effect here is however an increase in excitability. In fact, the large depolarization of resting membrane potential (8–10 mV) largely dominates the excitability reduction caused by the attenuation of excitatory synaptic inputs. This sustained depolarization may not only lead to granule cell firing in response to incoming excitatory inputs but also to the facilitation of transmission at their mossy-fiber boutons through an analog-digital signaling mechanism [36]. Here again, this modulation is *global* as all inputs will be equally affected.

Learning rules of intrinsic plasticity

Hebbian changes in IE

Hebbian plasticity has been first defined for synaptic transmission in the form of the Bienenstock-Cooper-Munro (BCM) rule. BCM rule stipulates that synaptic modification correlates with the activity modulation during learning (for a recent review, see Ref. [37]; Figure 3a). Hebbian synaptic modification in the hippocampus and neocortex is also induced by the degree of correlation between presynaptic and postsynaptic activity and is referred to as spike-timing dependent plasticity or STDP [38]. Both types of Hebbian plasticity are associated with

Figure 3

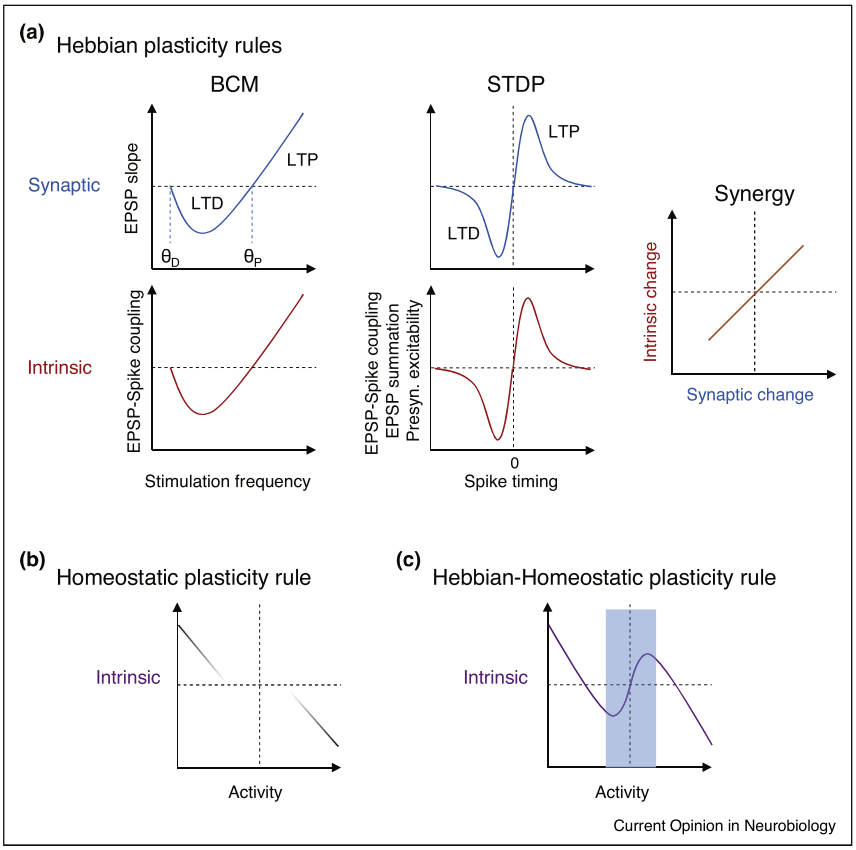

Cooperation between synaptic and intrinsic plasticity rules.
(a) Synergistic changes in synaptic and intrinsic plasticity (Hebbian). Left, BCM (Bienenstock-Cooper-Munro) rule defines synergistic synaptic and intrinsic modification following low ($\theta_D <$ frequency $< \theta_P$) or high ($>\theta_P$) stimulation frequency. θ_D = LTD threshold, θ_P = LTP threshold. Adapted from Ref. [41]. Middle, STDP (spike-timing dependent plasticity) rule defines synergistic synaptic and intrinsic modification following negative or positive spike timing. Adapted from Refs. [28,32,50,51]. Right, synaptic and intrinsic plasticity change synergistically. Adapted from Refs. [32,41]. **(b)** Homeostatic plasticity rule. Increase in synaptic activity induces an opposite decrease in excitability whereas reduction in synaptic drive induces an elevation in excitability. Note that homeostatic plasticity rule only accounts for intrinsic excitability changes following low or high, but not for intermediate changes in synaptic activity. Adapted from Refs. [56,63,64]. **(c)** Hebbian-homeostatic plasticity rule. This plasticity rule links homeostatic plasticity as defined in panel (b) to Hebbian changes in intrinsic excitability as defined in panel (a). Adapted from Refs. [29,69•].

intrinsic plasticity that are synergistic to the induced synaptic changes (Figure 3a).

At the postsynaptic side, synaptic modifications are associated with synergistic plasticity of IE that affects the input–output function of the neuron (i.e. excitatory postsynaptic potential-spike (or EPSP-spike) coupling; see for review Refs. [1,39]). In CA1 pyramidal neurons, long-term synaptic potentiation (LTP) is associated with an increased firing probability in response to the tetanized or paired input [32,40,41] whereas long-term synaptic depression (LTD) is associated with a decreased firing probability in response to the stimulated input [32,41]. EPSP summation is changed synergistically with synaptic modifications induced by STDP protocols [28] (Figure 3a). All these Hebbian modifications in IE require NMDA-receptor activation and are input-specific, that is no modification occurs on other inputs. Hebbian intrinsic plasticity is not specific to hippocampal neurons and long-lasting increase in IE has been induced in neocortical neurons following synaptic [42] or intrinsic [43,44,45•] activation paradigms.

Intrinsic plasticity has been reported in at least three different types of cerebellar neurons. In deep cerebellar nuclei, granule and Purkinje neurons, IE is enhanced following high frequency stimulation that induces LTP [46–48]. Here again, NMDA-receptor activation is required for induction of intrinsic plasticity. In Purkinje cells, enhanced IE is mediated by the downregulation of SK channels and requires activation of PKA and casein kinase 2 (CK2). As in cortical neurons, the reciprocal is true and long-lasting decrease in IE is observed following LTD induction [49]. This LTD-IE is mediated by the upregulation of HCN channels.

Synergistic changes in IE have been also identified at the presynaptic side when LTP or LTD is induced by STDP protocols in hippocampal and neocortical neurons [50,51] (Figure 3a). IE in the presynaptic neuron was found to be enhanced following induction of synaptic LTP by positive correlation whereas IE of the presynaptic cell was decreased following induction of LTD by negative correlation. Presynaptic intrinsic plasticity involves yet unidentified retrograde messengers and might be of great importance for the dynamics of neural circuits by creating privileged pathways of activity in the brain where presynaptic and postsynaptic excitability as well as synaptic transmission change harmoniously.

Homeostatic plasticity of IE

Hebbian mechanisms appear insufficient to explain activity-dependent plasticity during development because they tend to reinforce active circuits and depress inactive ones and are thus destabilizing. In fact, stability in neural circuits can be achieved by introducing homeostatic plasticity that adjust synaptic strength and intrinsic excitability [52]. Initially reported in cultured visual cortical neurons [53], homeostatic plasticity of IE has been observed in virtually all neuronal types. IE is enhanced in response to chronic activity deprivation induced pharmacologically [54–57] or by sensory deprivation [34••,58,59], whereas it is reduced in response to elevated network activity [54,56,60], leading to a homeostatic plasticity rule that is globally anti-Hebbian (Figure 3b).

While many ion channels are regulated in parallel [61], two inhibitory channels have recently retain attention: Kv1 channels located in the axon that determine spike threshold and intrinsic excitability [62], and HCN channels located in the dendrites that dampens all depolarizing events such as EPSPs. Downregulation of Kv1 channel activity has been identified as a major mechanism for the increased excitability observed in CA3 pyramidal neurons after chronic blockade of glutamate receptors [55] and in auditory neurons following cochlear removal [34••]. Conversely, Kv1 currents are upregulated following epileptiform activity [60], indicating that Kv1 channel activity is bi-directionally regulated. In CA1 pyramidal neurons, HCN channels are homeostatically regulated following bidirectional chronic manipulation of network activity [56] or following induction of large synaptic modification [63,64].

Whereas homeostatic plasticity in cortical pyramidal cells is usually induced by persistent modulation of activity lasting few tens of hours [53–56], homeostatic potentiation of IE can be induced by a transient hyperpolarization (20–300 s) in vestibular neurons [65] and cerebellar Golgi cells [66]. Both forms of plasticity involve the downregulation of BK channel activity. It should be noted that in contrast to pyramidal cells that are silent at rest, these cells correspond to pacemaker neurons that continuously fire at 5–10 Hz. Interestingly, vestibular sensory loss triggers rapid potentiation of excitability in vestibular neurons thus enabling adaptive compensatory increases in optokinetic reflex gain [67•].

Linking Hebbian and homeostatic intrinsic plasticity

Despite their apparent antagonistic feature, Hebbian and homeostatic plasticity are thought to work hand-in-hand [68]. The modulation of HCN channel following induction of synaptic modification provides a good example for such interaction. Whereas large LTP is associated with decreased IE due to the upregulation of HCN channel activity [63], small LTP is combined with increased IE resulting from downregulation of HCN channel [32]. The opposite is true for LTD with a HCN-dependent increase in IE induced in parallel of large LTD [64] and a HCN-dependent decrease in IE for small LTD [69•]. The multiple regulation of HCN channel implies distinct induction and expression pathways [63,64,69•,70]. Thus,

IE follows a single plasticity rule linking Hebbian and homeostatic plasticity (Figure 3c).

Intrinsic plasticity in GABAergic interneurons

Intrinsic plasticity is not exclusively expressed in principal neurons and GABAergic interneurons also display several forms of long-term intrinsic plasticity. Basket cells of the dentate gyrus exhibit LT-Depol of their resting membrane potential following high-frequency stimulation of the glutamatergic inputs [71]. As in granule cells, LT-Depol enhances the efficacy of EPSPs to fire the interneuron but in basket cells LT-Depol results from changes in the Na^+/K^+ ATPase pump function and requires the activation of calcium-permeable AMPA receptor.

Voltage-dependent excitability is also finely tuned in basket cells by Kv1-dependent modulation of the spike threshold to adjust inhibition levels in cortical circuits. Stimulation of the Neuregulin 1 receptor ErbB4 has been shown to strongly regulate Kv1 channel activity and

Figure 4

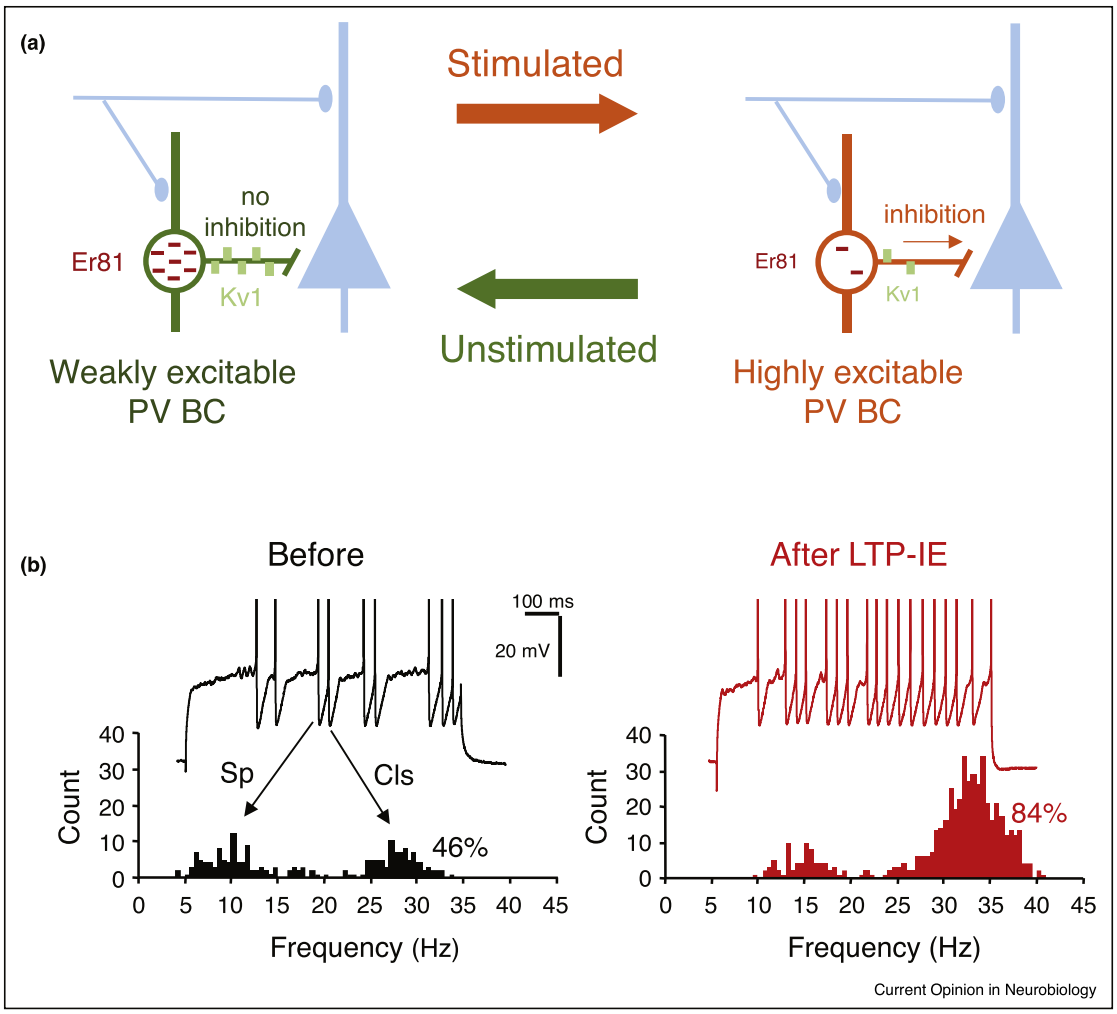

Intrinsic plasticity in GABAergic interneurons.
(a) Bidirectional regulation of intrinsic excitability in parvalbumin positive basket cells (PV-BC). Left, in unstimulated conditions, no inhibition is observed because the PV-BC is not recruited by the circuit as the consequence of elevated levels of Kv1 channels in the axon through activity-dependent elevation of the transcription factor Er81. Right, in stimulated conditions, PV-BC is recruited because of reduced levels Kv1 channels through activity-dependent reduction in Er81, leading to functional inhibition that counterbalance enhanced excitation. Adapted from Refs. [73••,74•,75•].
(b) Modulation of temporal processing in PV-BC. In control conditions, PV-BC display a specific mode of firing composed of sparse spikes (Sp) typically occurring after a slow depolarizing ramp of potential at an instantaneous frequency of ~10 Hz (i.e. theta frequency) and clustered spikes (Cls) that immediately follow a spike at an instantaneous frequency of ~30 Hz (i.e. gamma frequency). After induction of long-term potentiation of intrinsic excitability (LTP-IE), the proportion of Cls increases from 46 to 84% indicating a gain of spiking activity in the gamma frequency range. Adapted from Ref. [73••].

intrinsic excitability in parvalbumin positive basket cells (PV-BC) [72]. Likewise, PV-BCs exhibit potentiation of IE mediated by the downregulation of Kv1 channel activity and induced by synaptic activation of metabotropic glutamate receptor subtype 5 (mGluR5) [73••] (Figure 4a). This facilitation is responsible for most of the increased firing and is thought to compensate enhanced synaptic and intrinsic excitation in pyramidal neurons. The reciprocal modulation has been recently observed in somatosensory PV interneuron following activity-deprivation [74•], indicating that Kv1-dependent regulation of neuronal excitability is bidirectional (Figure 4a). In the cortex, most PV interneurons express Er81, a transcription factor involved in the activation pathway of Ca^{2+}/calmodulin-dependent kinase I [75•]. Noteworthy, Er81 is highly regulated by activity and controls levels of Kv1.1 channel in PV interneurons [75•]. In fact, Er81 level is high in weakly active circuits whereas it is low in highly active circuits (Figure 4a).

Incidence of intrinsic plasticity on temporal processing

Temporal processing is thought to represent a key factor in brain function and is controlled by synaptic circuits and by intrinsic properties [76,77]. For example, during initial storage of fear learning, spiking activity among adjacent CA1 pyramidal neurons becomes more synchronized [78]. At a cellular scale, spike-timing, membrane resonance and pacemaker activity are all controlled by voltage-gated ion channels including those involved in intrinsic plasticity [55,79,80]. Both Hebbian and homeostatic regulations of IE are associated with improved spike-time precision [42,45•,55]. In all cases, improved precision results from an ion channel-dependent enhancement of the voltage rising-slope preceding the action potential.

HCN channels set resonance frequency in hippocampal CA1 neurons in the θ range. Following large synaptic modifications, the resonance frequency is modulated as the sign of the induced synaptic change through modifications in HCN channel properties [64,81]. This shows that oscillatory intrinsic dynamics in the hippocampus can be finely tuned under homeostatic plasticity of IE.

Modulation of the temporal structure of firing has been described in two cell types. In Purkinje cells, SK-dependent enhancement of intrinsic excitability leads to increased burst firing in response to climbing fiber discharge and shortening of spike pauses [82•]. As Purkinje cells inhibit deep cerebellar nuclei, these briefer spike pauses are seen as enhanced excitation at the output side of the cerebellum. Likewise, enhanced IE in PV-BC promotes clustered spiking activity in the gamma-frequency range [73••] (Figure 4b). As PV-BC represents the main cell-type orchestrating network oscillations in the hippocampus, this modulation in the temporal structure of PV-BC firing suggests use-dependent modulation of gamma oscillations [83].

Conclusion and perspective

Remarkable progress in understanding learning rules and in identifying mechanisms of intrinsic plasticity has been made these recent years. However, many issues remain. For instance, most studies reported in this review comes from *in vitro* works and very few studies have been performed *in vivo* [44,45•] with physiologically realistic induction protocols. One may dream in the nearest future of monitoring IE in cortical or cerebellar neurons during the acquisition of a simple behavioral task. To achieve this goal, development of new tools will be required. Another challenge will consist in identifying why opposite changes in intrinsic excitability is observed in different types of neuron within the same structure following sensory deprivation [58,84]. Whereas changes in IE are clearly homeostatic in layer 2/3 principal neurons [58], they are Hebbian in layer five pyramidal cells [84]. The future will probably help to answer all these questions.

Conflict of interest statement

Nothing declared.

Acknowledgements

Supported by INSERM, CNRS, AMU, FRM (FDT2170437059 & DVS20131228768) and ANR NEUC 2014 (ANR-14-NEUC-0004).

References and recommended reading

Papers of particular interest, published within the period of review, have been highlighted as

- • of special interest
- •• of outstanding interest

1. Zhang W, Linden DJ: **The other side of the engram: experience-driven changes in neuronal intrinsic excitability.** *Nat Rev Neurosci* 2003, **4**:885-900.
2. Daoudal G, Debanne D: **Long-term plasticity of intrinsic excitability: learning rules and mechanisms.** *Learn Mem* 2003, **10**:456-465.
3. Sjostrom PJ, Rancz EA, Roth A, Hausser M: **Dendritic excitability and synaptic plasticity.** *Physiol Rev* 2008, **88**:769-840.
4. Titley HK, Brunel N, Hansel C: **Toward a neurocentric view of learning.** *Neuron* 2017, **95**:19-32.
5. Lisman J, Cooper K, Sehgal M, Silva AJ: **Memory formation depends on both synapse-specific modifications of synaptic strength and cell-specific increases in excitability.** *Nat Neurosci* 2018, **21**:309-314.
6. Zylberberg J, Strowbridge BW: **Mechanisms of persistent activity in cortical circuits: possible neural substrates for working memory.** *Annu Rev Neurosci* 2017, **40**:603-627.
7. Egorov AV, Hamam BN, Fransen E, Hasselmo ME, Alonso AA: **Graded persistent activity in entorhinal cortex neurons.** *Nature* 2002, **420**:173-178.
8. Rahman J, Berger T: **Persistent activity in layer 5 pyramidal neurons following cholinergic activation of mouse primary cortices.** *Eur J Neurosci* 2011, **34**:22-30.
9. Jochems A, Yoshida M: **Persistent firing supported by an intrinsic cellular mechanism in hippocampal CA3 pyramidal cells.** *Eur J Neurosci* 2013, **38**:2250-2259.

10. Knauer B, Jochems A, Valero-Aracama MJ, Yoshida M: **Long-lasting intrinsic persistent firing in rat CA1 pyramidal cells: a possible mechanism for active maintenance of memory.** *Hippocampus* 2013, **23**:820-831.

11. Zylbertal A, Kahan A, Ben-Shaul Y, Yarom Y, Wagner S: **Prolonged intracellular Na+ dynamics govern electrical activity in accessory olfactory bulb mitral cells.** *PLoS Biol* 2015, **13**e1002319.

12. •• Cui ED, Strowbridge BW: **Modulation of ether-a-go-go related gene (ERG) current governs intrinsic persistent activity in rodent neocortical pyramidal cells.** *J Neurosci* 2018, **38**:423-440.
This study shows that persistent firing in neocortical pyramidal neurons is mediated by the reduction of the ether-à-gogo related gene (ERG) K^+ channel. Calcium accumulation during triggering stimuli appears to attenuate ERG currents, leading to depolarization of the membrane potential and increased input resistance.

13. Woody CD, Black-Cleworth P: **Differences in excitability of cortical neurons as a function of motor projection in conditioned cats.** *J Neurophysiol* 1973, **36**:1104-1116.

14. Disterhoft JF, Coulter DA, Alkon DL: **Conditioning-specific membrane changes of rabbit hippocampal neurons measured in vitro.** *Proc Natl Acad Sci U S A* 1986, **83**:2733-2737.

15. Coulter DA, Lo Turco JJ, Kubota M, Disterhoft JF, Moore JW, Alkon DL: **Classical conditioning reduces amplitude and duration of calcium-dependent afterhyperpolarization in rabbit hippocampal pyramidal cells.** *J Neurophysiol* 1989, **61**:971-981.

16. Schreurs BG, Tomsic D, Gusev PA, Alkon DL: **Dendritic excitability microzones and occluded long-term depression after classical conditioning of the rabbit's nictitating membrane response.** *J Neurophysiol* 1997, **77**:86-92.

17. •• Gao Y, Budlong C, Durlacher E, Davison IG: **Neural mechanisms of social learning in the female mouse.** *Elife* 2017, **6.**
This study shows how social learning affects intrinsic excitability in two cell types of the accessory olfactory bulb. Mitral cells show an unusual attenuation of IE during repetitive firing whereas inhibitory interneurons display an enhanced IE.

18. Oh MM, Kuo AG, Wu WW, Sametsky EA, Disterhoft JF: **Watermaze learning enhances excitability of CA1 pyramidal neurons.** *J Neurophysiol* 2003, **90**:2171-2179.

19. Rosenkranz JA, Grace AA: **Dopamine-mediated modulation of odour-evoked amygdala potentials during pavlovian conditioning.** *Nature* 2002, **417**:282-287.

20. Santini E, Quirk GJ, Porter JT: **Fear conditioning and extinction differentially modify the intrinsic excitability of infralimbic neurons.** *J Neurosci* 2008, **28**:4028-4036.

21. Kaczorowski CC, Disterhoft JF: **Memory deficits are associated with impaired ability to modulate neuronal excitability in middle-aged mice.** *Learn Mem* 2009, **16**:362-366.

22. Song C, Ehlers VL, Moyer JR Jr: **Trace fear conditioning differentially modulates intrinsic excitability of medial prefrontal cortex-basolateral complex of amygdala projection neurons in infralimbic and prelimbic cortices.** *J Neurosci* 2015, **35**:13511-13524.

23. Saar D, Grossman Y, Barkai E: **Reduced after-hyperpolarization in rat piriform cortex pyramidal neurons is associated with increased learning capability during operant conditioning.** *Eur J Neurosci* 1998, **10**:1518-1523.

24. Zelcer I, Cohen H, Richter-Levin G, Lebiosn T, Grossberger T, Barkai E: **A cellular correlate of learning-induced metaplasticity in the hippocampus.** *Cereb Cortex* 2006, **16**:460-468.

25. Motanis H, Maroun M, Barkai E: **Learning-induced bidirectional plasticity of intrinsic neuronal excitability reflects the valence of the outcome.** *Cereb Cortex* 2014, **24**:1075-1087.

26. Malik R, Chattarji S: **Enhanced intrinsic excitability and EPSP-spike coupling accompany enriched environment-induced facilitation of LTP in hippocampal CA1 pyramidal neurons.** *J Neurophysiol* 2012, **107**:1366-1378.

27. Valero-Aracama MJ, Sauvage MM, Yoshida M: **Environmental enrichment modulates intrinsic cellular excitability of hippocampal CA1 pyramidal cells in a housing duration and anatomical location-dependent manner.** *Behav Brain Res* 2015, **292**:209-218.

28. Wang Z, Xu NL, Wu CP, Duan S, Poo MM: **Bidirectional changes in spatial dendritic integration accompanying long-term synaptic modifications.** *Neuron* 2003, **37**:463-472.

29. Campanac E, Daoudal G, Ankri N, Debanne D: **Downregulation of dendritic I(h) in CA1 pyramidal neurons after LTP.** *J Neurosci* 2008, **28**:8635-8643.

30. Frick A, Magee J, Johnston D: **LTP is accompanied by an enhanced local excitability of pyramidal neuron dendrites.** *Nat Neurosci* 2004, **7**:126-135.

31. Losonczy A, Makara JK, Magee JC: **Compartmentalized dendritic plasticity and input feature storage in neurons.** *Nature* 2008, **452**:436-441.

32. Campanac E, Debanne D: **Spike timing-dependent plasticity: a learning rule for dendritic integration in rat CA1 pyramidal neurons.** *J Physiol* 2008, **586**:779-793.

33. Xu J, Kang N, Jiang L, Nedergaard M, Kang J: **Activity-dependent long-term potentiation of intrinsic excitability in hippocampal CA1 pyramidal neurons.** *J Neurosci* 2005, **25**:1750-1760.

34. •• Kuba H, Yamada R, Ishiguro G, Adachi R: **Redistribution of Kv1 and Kv7 enhances neuronal excitability during structural axon initial segment plasticity.** *Nat Commun* 2015, **6**:8815.
The authors show that auditory deprivation by removing the cochlea in the chick leads to the elongation of the axon initial segment associated to the switch from Kv1 to Kv7 channels.

35. Mellor J, Nicoll RA, Schmitz D: **Mediation of hippocampal mossy fiber long-term potentiation by presynaptic Ih channels.** *Science* 2002, **295**:143-147.

36. Alle H, Geiger JR: **Combined analog and action potential coding in hippocampal mossy fibers.** *Science* 2006, **311**:1290-1293.

37. Cooper LN, Bear MF: **The BCM theory of synapse modification at 30: interaction of theory with experiment.** *Nat Rev Neurosci* 2012, **13**:798-810.

38. Feldman DE: **The spike-timing dependence of plasticity.** *Neuron* 2012, **75**:556-571.

39. Debanne D, Poo MM: **Spike-timing dependent plasticity beyond synapse - pre- and post-synaptic plasticity of intrinsic neuronal excitability.** *Front Synaptic Neurosci* 2010, **2**:21.

40. Andersen P, Sundberg SH, Sveen O, Swann JW, Wigstrom H: **Possible mechanisms for long-lasting potentiation of synaptic transmission in hippocampal slices from guinea-pigs.** *J Physiol* 1980, **302**:463-482.

41. Daoudal G, Hanada Y, Debanne D: **Bidirectional plasticity of excitatory postsynaptic potential (EPSP)-spike coupling in CA1 hippocampal pyramidal neurons.** *Proc Natl Acad Sci U S A* 2002, **99**:14512-14517.

42. Sourdet V, Russier M, Daoudal G, Ankri N, Debanne D: **Long-term enhancement of neuronal excitability and temporal fidelity mediated by metabotropic glutamate receptor subtype 5.** *J Neurosci* 2003, **23**:10238-10248.

43. Cudmore RH, Turrigiano GG: **Long-term potentiation of intrinsic excitability in LV visual cortical neurons.** *J Neurophysiol* 2004, **92**:341-348.

44. Paz JT, Mahon S, Tiret P, Genet S, Delord B, Charpier S: **Multiple forms of activity-dependent intrinsic plasticity in layer V cortical neurones in vivo.** *J Physiol* 2009, **587**:3189-3205.

45. • Mahon S, Charpier S: **Bidirectional plasticity of intrinsic excitability controls sensory inputs efficiency in layer 5 barrel cortex neurons in vivo.** *J Neurosci* 2012, **32**:11377-11389.
The authors show that rhythmic firing can trigger long-lasting increase or decrease in intrinsic excitability in layer five pyramidal neurons of the rat barrel cortex*in vivo*. The direction of plasticity depends on initial cell excitability.

46. Aizenman CD, Linden DJ: **Rapid, synaptically driven increases in the intrinsic excitability of cerebellar deep nuclear neurons.** *Nat Neurosci* 2000, **3**:109-111.

47. Armano S, Rossi P, Taglietti V, D'Angelo E: **Long-term potentiation of intrinsic excitability at the mossy fiber-granule cell synapse of rat cerebellum.** *J Neurosci* 2000, **20**:5208-5216.

48. Belmeguenai A, Hosy E, Bengtsson F, Pedroarena CM, Piochon C, Teuling E, He Q, Ohtsuki G, De Jeu MT, Elgersma Y *et al.*: **Intrinsic plasticity complements long-term potentiation in parallel fiber input gain control in cerebellar Purkinje cells.** *J Neurosci* 2010, **30**:13630-13643.

49. Shim HG, Jang DC, Lee J, Chung G, Lee S, Kim YG, Jeon DE, Kim SJ: **Long-term depression of intrinsic excitability accompanied by synaptic depression in cerebellar Purkinje cells.** *J Neurosci* 2017, **37**:5659-5669.

50. Ganguly K, Kiss L, Poo M: **Enhancement of presynaptic neuronal excitability by correlated presynaptic and postsynaptic spiking.** *Nat Neurosci* 2000, **3**:1018-1026.

51. Li CY, Lu JT, Wu CP, Duan SM, Poo MM: **Bidirectional modification of presynaptic neuronal excitability accompanying spike timing-dependent synaptic plasticity.** *Neuron* 2004, **41**:257-268.

52. Turrigiano GG, Nelson SB: **Homeostatic plasticity in the developing nervous system.** *Nat Rev Neurosci* 2004, **5**:97-107.

53. Desai NS, Rutherford LC, Turrigiano GG: **Plasticity in the intrinsic excitability of cortical pyramidal neurons.** *Nat Neurosci* 1999, **2**:515-520.

54. Karmarkar UR, Buonomano DV: **Different forms of homeostatic plasticity are engaged with distinct temporal profiles.** *Eur J Neurosci* 2006, **23**:1575-1584.

55. Cudmore RH, Fronzaroli-Molinieres L, Giraud P, Debanne D: **Spike-time precision and network synchrony are controlled by the homeostatic regulation of the D-type potassium current.** *J Neurosci* 2010, **30**:12885-12895.

56. Gasselin C, Inglebert Y, Debanne D: **Homeostatic regulation of h-conductance controls intrinsic excitability and stabilizes the threshold for synaptic modification in CA1 neurons.** *J Physiol* 2015, **593**:4855-4869.

57. Shim HG, Jang SS, Jang DC, Jin Y, Chang W, Park JM, Kim SJ: **mGlu1 receptor mediates homeostatic control of intrinsic excitability through Ih in cerebellar Purkinje cells.** *J Neurophysiol* 2016, **115**:2446-2455.

58. Maffei A, Turrigiano GG: **Multiple modes of network homeostasis in visual cortical layer 2/3.** *J Neurosci* 2008, **28**:4377-4384.

59. Milshtein-Parush H, Frere S, Regev L, Lahav C, Benbenishty A, Ben-Eliyahu S, Goshen I, Slutsky I: **Sensory deprivation triggers synaptic and intrinsic plasticity in the hippocampus.** *Cereb Cortex* 2017, **27**:3457-3470.

60. Kirchheim F, Tinnes S, Haas CA, Stegen M, Wolfart J: **Regulation of action potential delays via voltage-gated potassium Kv1.1 channels in dentate granule cells during hippocampal epilepsy.** *Front Cell Neurosci* 2013, **7**:248.

61. Marder E, Goaillard JM: **Variability, compensation and homeostasis in neuron and network function.** *Nat Rev Neurosci* 2006, **7**:563-574.

62. Rama S, Zbili M, Fekete A, Tapia M, Benitez MJ, Boumedine N, Garrido JJ, Debanne D: **The role of axonal Kv1 channels in CA3 pyramidal cell excitability.** *Sci Rep* 2017, **7**:315.

63. Fan Y, Fricker D, Brager DH, Chen X, Lu HC, Chitwood RA, Johnston D: **Activity-dependent decrease of excitability in rat hippocampal neurons through increases in I(h).** *Nat Neurosci* 2005, **8**:1542-1551.

64. Brager DH, Johnston D: **Plasticity of intrinsic excitability during long-term depression is mediated through mGluR-dependent changes in I(h) in hippocampal CA1 pyramidal neurons.** *J Neurosci* 2007, **27**:13926-13937.

65. Nelson AB, Krispel CM, Sekirnjak C, du Lac S: **Long-lasting increases in intrinsic excitability triggered by inhibition.** *Neuron* 2003, **40**:609-620.

66. Hull CA, Chu Y, Thanawala M, Regehr WG: **Hyperpolarization induces a long-term increase in the spontaneous firing rate of cerebellar Golgi cells.** *J Neurosci* 2013, **33**:5895-5902.

67. • Nelson AB, Faulstich M, Moghadam S, Onori K, Meredith A, du Lac S: **BK channels are required for multisensory plasticity in the oculomotor system.** *Neuron* 2017, **93**:211-220.
This paper shows that unilateral vestibular deafferentation triggers rapid potentiation of IE in vestibular neurons and occludes induction of intrinsic plasticity, concomitant with an increase in the gain of the optokinetic reflex.

68. Zenke F, Gerstner W: **Hebbian plasticity requires compensatory processes on multiple timescales.** *Philos Trans R Soc Lond B Biol Sci* 2017, **372.**

69. • Gasselin C, Inglebert Y, Ankri N, Debanne D: **Plasticity of intrinsic excitability during LTD is mediated by bidirectional changes in h-channel activity.** *Sci Rep* 2017, **7**:14418.
This study shows that the magnitude of LTD determines the polarity of intrinsic changes in CA1 pyramidal neurons, thus providing support to a continuum rule linking synergistic (Hebbian) and compensatory (homeostatic) changes in excitability.

70. Santoro B, Piskorowski RA, Pian P, Hu L, Liu H, Siegelbaum SA: **TRIP8b splice variants form a family of auxiliary subunits that regulate gating and trafficking of HCN channels in the brain.** *Neuron* 2009, **62**:802-813.

71. Ross ST, Soltesz I: **Long-term plasticity in interneurons of the dentate gyrus.** *Proc Natl Acad Sci U S A* 2001, **98**:8874-8879.

72. Li KX, Lu YM, Xu ZH, Zhang J, Zhu JM, Zhang JM, Cao SX, Chen XJ, Chen Z, Luo JH *et al.*: **Neuregulin 1 regulates excitability of fast-spiking neurons through Kv1.1 and acts in epilepsy.** *Nat Neurosci* 2011, **15**:267-273.

73. •• Campanac E, Gasselin C, Baude A, Rama S, Ankri N, Debanne D: **Enhanced intrinsic excitability in basket cells maintains excitatory-inhibitory balance in hippocampal circuits.** *Neuron* 2013, **77**:712-722.
This study shows that high frequency stimulation of the Schaffer collaterals that induces LTP and intrinsic excitability in CA1 pyramidal cells also enhances intrinsic excitability in PV-BC through an mGluR5-dependent reduction of Kv1 channel activity. Enhanced intrinsic excitability promotes spiking activity at the gamma frequency.

74. • Gainey MA, Aman JW, Feldman DE: **Rapid disinhibition by adjustment of PV intrinsic excitability during whisker map plasticity in mouse S1.** *J Neurosci* 2018, **38**:4749-4761.
The authors show that brief sensory deprivation rapidly weakens excitability of PV interneurons in the barrel cortex through the upregulation of Kv1 channel activity.

75. • Dehorter N, Ciceri G, Bartolini G, Lim L, del Pino I, Marin O: **Tuning of fast-spiking interneuron properties by an activity-dependent transcriptional switch.** *Science* 2015, **349**:1216-1220.
The authors show that network activity modulates intrinsic excitability of neocortical PV-BC through the post-mitotic expression of the transcriptional regulator Er81 and the regulation of Kv1.1 channels.

76. Eichenbaum H: **Time cells in the hippocampus: a new dimension for mapping memories.** *Nat Rev Neurosci* 2014, **15**:732-744.

77. Paton JJ, Buonomano DV: **The neural basis of timing: distributed mechanisms for diverse functions.** *Neuron* 2018, **98**:687-705.

78. Liu YZ, Wang Y, Shen W, Wang Z: **Enhancement of synchronized activity between hippocampal CA1 neurons during initial storage of associative fear memory.** *J Physiol* 2017, **595**:5327-5340.

79. Fricker D, Miles R: **EPSP amplification and the precision of spike timing in hippocampal neurons.** *Neuron* 2000, **28**:559-569.

80. Gastrein P, Campanac E, Gasselin C, Cudmore RH, Bialowas A, Carlier E, Fronzaroli-Molinieres L, Ankri N, Debanne D: **The role of hyperpolarization-activated cationic current in spike-time**

precision and intrinsic resonance in cortical neurons in vitro. *J Physiol* 2011, **589**:3753-3773.

81. Narayanan R, Johnston D: **Long-term potentiation in rat hippocampal neurons is accompanied by spatially widespread changes in intrinsic oscillatory dynamics and excitability.** *Neuron* 2007, **56**:1061-1075.

82. • Grasselli G, He Q, Wan V, Adelman JP, Ohtsuki G, Hansel C: **Activity-dependent plasticity of spike pauses in cerebellar Purkinje cells.** *Cell Rep* 2016, **14**:2546-2553.

This study demonstrates that in cerebellar Purkinje cells the pauses following spike bursts can be modulated by the activity-dependent regulation of SK2, thus altering the spike output pattern of these neurons.

83. Whittington MA, Traub RD, Jefferys JG: **Synchronized oscillations in interneuron networks driven by metabotropic glutamate receptor activation.** *Nature* 1995, **373**:612-615.

84. Nataraj K, Le Roux N, Nahmani M, Lefort S, Turrigiano G: **Visual deprivation suppresses L5 pyramidal neuron excitability by preventing the induction of intrinsic plasticity.** *Neuron* 2010, **68**:750-762.

Bibliographie

Abbott, L.F., and Nelson, S.B. (2000). Synaptic plasticity: taming the beast. *3*, 6.

Abrahamsson, T., Chou, C.Y.C., Li, S.Y., Mancino, A., Costa, R.P., Brock, J.A., Nuro, E., Buchanan, K.A., Elgar, D., Blackman, A.V., et al. (2017). Differential Regulation of Evoked and Spontaneous Release by Presynaptic NMDA Receptors. Neuron *96*, 839-855.e5.

Albuquerque, E.X., Pereira, E.F.R., Alkondon, M., and Rogers, S.W. (2009). Mammalian nicotinic acetylcholine receptors: from structure to function. Physiol. Rev. *89*, 73–120.

Andrade-Talavera, Y., Duque-Feria, P., Paulsen, O., and Rodríguez-Moreno, A. (2016). Presynaptic Spike Timing-Dependent Long-Term Depression in the Mouse Hippocampus. Cereb. Cortex *26*, 3637–3654.

Banerjee, A., Meredith, R.M., Rodríguez-Moreno, A., Mierau, S.B., Auberson, Y.P., and Paulsen, O. (2009). Double dissociation of spike timing-dependent potentiation and depression by subunit-preferring NMDA receptor antagonists in mouse barrel cortex. Cereb. Cortex N. Y. N 1991 *19*, 2959–2969.

Banerjee, A., González-Rueda, A., Sampaio-Baptista, C., Paulsen, O., and Rodríguez-Moreno, A. (2014). Distinct mechanisms of spike timing-dependent LTD at vertical and horizontal inputs onto L2/3 pyramidal neurons in mouse barrel cortex. Physiol. Rep. *2*, e00271.

Bear, M.F., and Abraham, W.C. (1996). Long-term depression in hippocampus. Annu. Rev. Neurosci. *19*, 437–462.

Benardo, L.S., and Prince, D.A. (1982). Dopamine modulates a Ca2+-activated potassium conductance in mammalian hippocampal pyramidal cells. Nature *297*, 76–79.

Bender, V.A. (2006). Two Coincidence Detectors for Spike Timing-Dependent Plasticity in Somatosensory Cortex. J. Neurosci. *26*, 4166–4177.

Bender, K.J., Ford, C.P., and Trussell, L.O. (2010). Dopaminergic Modulation of Axon Initial Segment Calcium Channels Regulates Action Potential Initiation. Neuron *68*, 500–511.

Berretta, N., Berton, F., Bianchi, R., Capogna, M., Francesconi, W., and Brunelli, M. (1990). Effects of dopamine, D-1 and D-2 dopaminergic agonists on the excitability of hippocampal CA1 pyramidal cells in guinea pig. Exp. Brain Res. *83*.

Bi, G., and Poo, M. (1998). Synaptic Modifications in Cultured Hippocampal Neurons: Dependence on Spike Timing, Synaptic Strength, and Postsynaptic Cell Type. J. Neurosci. *18*, 10464–10472.

Bienenstock, E.L., Cooper, L.N., and Munro, P.W. (1982). Theory for the development of neuron selectivity: orientation specificity and binocular interaction in visual cortex. J. Neurosci. Off. J. Soc. Neurosci. *2*, 32–48.

Birtoli, B., and Ulrich, D. (2004). Firing mode-dependent synaptic plasticity in rat neocortical pyramidal neurons. J. Neurosci. Off. J. Soc. Neurosci. *24*, 4935–4940.

Bissière, S., Humeau, Y., and Lüthi, A. (2003). Dopamine gates LTP induction in lateral amygdala by suppressing feedforward inhibition. Nat. Neurosci. *6*, 587–592.

Bittner, K.C., Milstein, A.D., Grienberger, C., Romani, S., and Magee, J.C. (2017). Behavioral time scale synaptic plasticity underlies CA1 place fields. Science *357*, 1033–1036.

Blitzer, R.D., Connor, J.H., Brown, G.P., Wong, T., Shenolikar, S., Iyengar, R., and Landau, E.M. (1998). Gating of CaMKII by cAMP-regulated protein phosphatase activity during LTP. Science *280*, 1940–1942.

Blokland, A. (1995). Acetylcholine: a neurotransmitter for learning and memory? Brain Res. Rev. *21*, 285–300.

Bock, T., and Stuart, G.J. (2016). Impact of calcium-activated potassium channels on NMDA spikes in cortical layer 5 pyramidal neurons. J. Neurophysiol. *115*, 1740–1748.

Bouvier, G., Larsen, R.S., Rodríguez-Moreno, A., Paulsen, O., and Sjöström, P.J. (2018). Towards resolving the presynaptic NMDA receptor debate. Curr. Opin. Neurobiol. *51*, 1–7.

Brager, D.H., and Johnston, D. (2007). Plasticity of intrinsic excitability during long-term depression is mediated through mGluR-dependent changes in I(h) in hippocampal CA1 pyramidal neurons. J. Neurosci. Off. J. Soc. Neurosci. *27*, 13926–13937.

Brandalise, F., and Gerber, U. (2014). Mossy fiber-evoked subthreshold responses induce timing-dependent plasticity at hippocampal CA3 recurrent synapses. Proc. Natl. Acad. Sci. *111*, 4303–4308.

Brandalise, F., Carta, S., Helmchen, F., Lisman, J., and Gerber, U. (2016). Dendritic NMDA spikes are necessary for timing-dependent associative LTP in CA3 pyramidal cells. Nat. Commun. *7*, 13480.

Bringuier, V., Fregnac, Y., Debanne, D., Shulz, D., and Baranyi, A. (1992). Synaptic origin of rhythmic visually evoked activity in kitten area 17 neurones. Neuroreport *3*, 1065–1068.

Brzosko, Z., Schultz, W., and Paulsen, O. (2015). Retroactive modulation of spike timing-dependent plasticity by dopamine. ELife *4*.

Brzosko, Z., Zannone, S., Schultz, W., Clopath, C., and Paulsen, O. (2017). Sequential neuromodulation of Hebbian plasticity offers mechanism for effective reward-based navigation. ELife *6*.

Campanac, E., and Debanne, D. (2008). Spike timing-dependent plasticity: a learning rule for dendritic integration in rat CA1 pyramidal neurons: STDP and plasticity of dendritic integration. J. Physiol. *586*, 779–793.

Campanac, E., Daoudal, G., Ankri, N., and Debanne, D. (2008). Downregulation of Dendritic Ih in CA1 Pyramidal Neurons after LTP. J. Neurosci. *28*, 8635–8643.

Cantrell, A.R., Smith, R.D., Goldin, A.L., Scheuer, T., and Catterall, W.A. (1997). Dopaminergic modulation of sodium current in hippocampal neurons via cAMP-dependent phosphorylation of specific sites in the sodium channel alpha subunit. J. Neurosci. Off. J. Soc. Neurosci. *17*, 7330–7338.

Carroll, R.C., and Zukin, R.S. (2002). NMDA-receptor trafficking and targeting: implications for synaptic transmission and plasticity. Trends Neurosci. *25*, 571–577.

Carter, B.C., and Jahr, C.E. (2016). Postsynaptic, not presynaptic NMDA receptors are required for spike-timing-dependent LTD induction. Nat. Neurosci. *19*, 1218–1224.

Cassenaer, S., and Laurent, G. (2007). Hebbian STDP in mushroom bodies facilitates the synchronous flow of olfactory information in locusts. Nature *448*, 709–713.

Cassenaer, S., and Laurent, G. (2012). Conditional modulation of spike-timing-dependent plasticity for olfactory learning. Nature *482*, 47–52.

Chavez-Noriega, L.E., Bliss, T.V., and Halliwell, J.V. (1989). The EPSP-spike (E-S) component of long-term potentiation in the rat hippocampal slice is modulated by GABAergic but not cholinergic mechanisms. Neurosci. Lett. *104*, 58–64.

Chevaleyre, V., Takahashi, K.A., and Castillo, P.E. (2006). Endocannabinoid-mediated synaptic plasticity in the CNS. Annu. Rev. Neurosci. *29*, 37–76.

Cho, K., Aggleton, J.P., Brown, M.W., and Bashir, Z.I. (2001). An experimental test of the role of postsynaptic calcium levels in determining synaptic strength using perirhinal cortex of rat. J. Physiol. *532*, 459–466.

Conn, P.J., and Pin, J.P. (1997). Pharmacology and functions of metabotropic glutamate receptors. Annu. Rev. Pharmacol. Toxicol. *37*, 205–237.

Corlew, R., Wang, Y., Ghermazien, H., Erisir, A., and Philpot, B.D. (2007). Developmental switch in the contribution of presynaptic and postsynaptic NMDA receptors to long-term depression. J. Neurosci. Off. J. Soc. Neurosci. *27*, 9835–9845.

Couey, J.J., Meredith, R.M., Spijker, S., Poorthuis, R.B., Smit, A.B., Brussaard, A.B., and Mansvelder, H.D. (2007). Distributed Network Actions by Nicotine Increase the Threshold for Spike-Timing-Dependent Plasticity in Prefrontal Cortex. Neuron *54*, 73–87.

Cui, Y., Paillé, V., Xu, H., Genet, S., Delord, B., Fino, E., Berry, H., and Venance, L. (2015). Endocannabinoids mediate bidirectional striatal spike-timing-dependent plasticity. J. Physiol. *593*, 2833–2849.

Cui, Y., Prokin, I., Xu, H., Delord, B., Genet, S., Venance, L., and Berry, H. (2016). Endocannabinoid dynamics gate spike-timing dependent depression and potentiation. ELife *5*.

Cull-Candy, S.G., and Leszkiewicz, D.N. (2004). Role of distinct NMDA receptor subtypes at central synapses. Sci. STKE Signal Transduct. Knowl. Environ. *2004*, re16.

Dan, Y., and Poo, M.-M. (2006). Spike Timing-Dependent Plasticity: From Synapse to Perception. Physiol. Rev. *86*, 1033–1048.

Daoudal, G. (2003). Long-Term Plasticity of Intrinsic Excitability: Learning Rules and Mechanisms. Learn. Mem. *10*, 456–465.

Daoudal, G., Hanada, Y., and Debanne, D. (2002). Bidirectional plasticity of excitatory postsynaptic potential (EPSP)-spike coupling in CA1 hippocampal pyramidal neurons. Proc. Natl. Acad. Sci. *99*, 14512–14517.

Debanne, D., and Thompson, S. (1994). Calcium: A Trigger for Long-Term Depression and Potentiation in the Hippocampus. Physiology *9*, 256–260.

Debanne, D., Gähwiler, B.H., and Thompson, S.M. (1994). Asynchronous pre- and postsynaptic activity induces associative long-term depression in area CA1 of the rat hippocampus in vitro. Proc. Natl. Acad. Sci. U. S. A. *91*, 1148–1152.

Debanne, D., Gähwiler, B.H., and Thompson, S.M. (1998a). Long-term synaptic plasticity between pairs of individual CA3 pyramidal cells in rat hippocampal slice cultures. J. Physiol. *507 (Pt 1)*, 237–247.

Debanne, D., Shulz, D.E., and Fregnac, Y. (1998b). Activity-dependent regulation of “on” and “off” responses in cat visual cortical receptive fields. J. Physiol. *508 (Pt 2)*, 523–548.

Debanne, D., Gähwiler, B.H., and Thompson, S.M. (1999). Heterogeneity of synaptic plasticity at unitary CA3-CA1 and CA3-CA3 connections in rat hippocampal slice cultures. J. Neurosci. Off. J. Soc. Neurosci. *19*, 10664–10671.

Debanne, D., Inglebert, Y., and Russier, M. (2018). Plasticity of intrinsic neuronal excitability. Curr. Opin. Neurobiol. *54*, 73–82.

Debanne, D., Guerineau, N.C., Giihwiler, B.H., and Thompson, S.M. Paired-pulse facilitation and depression at unitary synapses in rat hippocampus: quantal fluctuation affects subsequent release. 14. J Physiol. 1996 Feb 15;491 (Pt 1):163-76.

Delgado, J.Y., Coba, M., Anderson, C.N.G., Thompson, K.R., Gray, E.E., Heusner, C.L., Martin, K.C., Grant, S.G.N., and O’Dell, T.J. (2007). NMDA receptor activation dephosphorylates AMPA receptor glutamate receptor 1 subunits at threonine 840. J. Neurosci. Off. J. Soc. Neurosci. *27*, 13210–13221.

Derkach, V., Barria, A., and Soderling, T.R. (1999). Ca2+/calmodulin-kinase II enhances channel conductance of alpha-amino-3-hydroxy-5-methyl-4-isoxazolepropionate type glutamate receptors. Proc. Natl. Acad. Sci. U. S. A. *96*, 3269–3274.

Ding, F., O'Donnell, J., Xu, Q., Kang, N., Goldman, N., and Nedergaard, M. (2016). Changes in the composition of brain interstitial ions control the sleep-wake cycle. Science *352*, 550–555.

Drever, B.D., Riedel, G., and Platt, B. (2011). The cholinergic system and hippocampal plasticity. Behav. Brain Res. *221*, 505–514.

Dudek, S.M., and Bear, M.F. (1992). Homosynaptic long-term depression in area CA1 of hippocampus and effects of N-methyl-D-aspartate receptor blockade. Proc. Natl. Acad. Sci. U. S. A. *89*, 4363–4367.

Duguid, I., and Sjöström, P.J. (2006). Novel presynaptic mechanisms for coincidence detection in synaptic plasticity. Curr. Opin. Neurobiol. *16*, 312–322.

Dunwiddie, T., and Lynch, G. (1978). Long-term potentiation and depression of synaptic responses in the rat hippocampus: localization and frequency dependency. J. Physiol. *276*, 353–367.

Edelmann, E., and Lessmann, V. (2011). Dopamine Modulates Spike Timing-Dependent Plasticity and Action Potential Properties in CA1 Pyramidal Neurons of Acute Rat Hippocampal Slices. Front. Synaptic Neurosci. *3*, 6.

Emptage, N., Bliss, T.V.P., and Fine, A. (1999). Single Synaptic Events Evoke NMDA Receptor–Mediated Release of Calcium from Internal Stores in Hippocampal Dendritic Spines. Neuron *22*, 115–124.

Epsztein, J., Lee, A.K., Chorev, E., and Brecht, M. (2010). Impact of spikelets on hippocampal CA1 pyramidal cell activity during spatial exploration. Science *327*, 474–477.

Faber, E.S.L., Delaney, A.J., Power, J.M., Sedlak, P.L., Crane, J.W., and Sah, P. (2008). Modulation of SK channel trafficking by beta adrenoceptors enhances excitatory synaptic transmission and plasticity in the amygdala. J. Neurosci. Off. J. Soc. Neurosci. *28*, 10803–10813.

Fan, Y., Fricker, D., Brager, D.H., Chen, X., Lu, H.-C., Chitwood, R.A., and Johnston, D. (2005). Activity-dependent decrease of excitability in rat hippocampal neurons through increases in Ih. Nat. Neurosci. *8*, 1542–1551.

Feldman, D.E. (2000). Timing-Based LTP and LTD at Vertical Inputs to Layer II/III Pyramidal Cells in Rat Barrel Cortex. Neuron *27*, 45–56.

Fino (2010). Spike-timing dependent plasticity in the striatum. Front. Synaptic Neurosci.

Fino, E., Glowinski, J., and Venance, L. (2005). Bidirectional activity-dependent plasticity at corticostriatal synapses. J. Neurosci. Off. J. Soc. Neurosci. *25*, 11279–11287.

Fino, E., Deniau, J.-M., and Venance, L. (2008). Cell-specific spike-timing-dependent plasticity in GABAergic and cholinergic interneurons in corticostriatal rat brain slices. J. Physiol. *586*, 265–282.

Fisher, S.D., Robertson, P.B., Black, M.J., Redgrave, P., Sagar, M.A., Abraham, W.C., and Reynolds, J.N.J. (2017). Reinforcement determines the timing dependence of corticostriatal synaptic plasticity in vivo. Nat. Commun. *8*, 334.

Foncelle, A., Mendes, A., Jędrzejewska-Szmek, J., Valtcheva, S., Berry, H., Blackwell, K.T., and Venance, L. (2018). Modulation of Spike-Timing Dependent Plasticity: Towards the Inclusion of a Third Factor in Computational Models. Front. Comput. Neurosci. *12*.

Frégnac, Y., Shulz, D., Thorpe, S., and Bienenstock, E. (1988). A cellular analogue of visual cortical plasticity. Nature *333*, 367–370.

Frégnac, Y., Pananceau, M., René, A., Huguet, N., Marre, O., Levy, M., and Shulz, D.E. (2010). A Re-Examination of Hebbian-Covariance Rules and Spike Timing-Dependent Plasticity in Cat Visual Cortex in vivo. Front. Synaptic Neurosci. *2*.

Frey, U., Schroeder, H., and Matthies, H. (1990). Dopaminergic antagonists prevent long-term maintenance of posttetanic LTP in the CA1 region of rat hippocampal slices. Brain Res. *522*, 69–75.

Frick, A., Magee, J., and Johnston, D. (2004). LTP is accompanied by an enhanced local excitability of pyramidal neuron dendrites. Nat. Neurosci. *7*, 126–135.

Froemke, R.C., Poo, M.-M., and Dan, Y. (2005). Spike-timing-dependent synaptic plasticity depends on dendritic location. Nature *434*, 221–225.

Froemke, R.C., Tsay, I.A., Raad, M., Long, J.D., and Dan, Y. (2006). Contribution of Individual Spikes in Burst-Induced Long-Term Synaptic Modification. J. Neurophysiol. *95*, 1620–1629.

Fu, Y.-X. (2004). Asymmetry in Visual Cortical Circuits Underlying Motion-Induced Perceptual Mislocalization. J. Neurosci. *24*, 2165–2171.

Fuenzalida, M., Fernández de Sevilla, D., Couve, A., and Buño, W. (2010). Role of AMPA and NMDA receptors and back-propagating action potentials in spike timing-dependent plasticity. J. Neurophysiol. *103*, 47–54.

Ganguly, K., Kiss, L., and Poo, M. (2000). Enhancement of presynaptic neuronal excitability by correlated presynaptic and postsynaptic spiking. Nat. Neurosci. *3*, 1018–1026.

Gasselin, C., Inglebert, Y., Ankri, N., and Debanne, D. (2017). Plasticity of intrinsic excitability during LTD is mediated by bidirectional changes in h-channel activity. Sci. Rep. *7*.

Giessel, A.J., and Sabatini, B.L. (2010). M1 Muscarinic Receptors Boost Synaptic Potentials and Calcium Influx in Dendritic Spines by Inhibiting Postsynaptic SK Channels. Neuron *68*, 936–947.

Glass, M., and Felder, C.C. (1997). Concurrent stimulation of cannabinoid CB1 and dopamine D2 receptors augments cAMP accumulation in striatal neurons: evidence for a Gs linkage to the CB1 receptor. J. Neurosci. Off. J. Soc. Neurosci. *17*, 5327–5333.

Golding, N.L., Staff, N.P., and Spruston, N. (2002). Dendritic spikes as a mechanism for cooperative long-term potentiation. Nature *418*, 326–331.

Graupner, M., and Brunel, N. (2010). Mechanisms of induction and maintenance of spike-timing dependent plasticity in biophysical synapse models. Front. Comput. Neurosci. *4*.

Graupner, M., and Brunel, N. (2012). Calcium-based plasticity model explains sensitivity of synaptic changes to spike pattern, rate, and dendritic location. Proc. Natl. Acad. Sci. *109*, 3991–3996.

Gribkoff, V.K., and Ashe, J.H. (1984). Modulation by dopamine of population responses and cell membrane properties of hippocampal CA1 neurons in vitro. Brain Res. *292*, 327–338.

Guo, Y., Huang, S., de Pasquale, R., McGehrin, K., Lee, H.-K., Zhao, K., and Kirkwood, A. (2012). Dark exposure extends the integration window for spike-timing-dependent plasticity. J. Neurosci. Off. J. Soc. Neurosci. *32*, 15027–15035.

Gustafsson, B., Wigstrom, H., Abraham, W., and Huang, Y. (1987). Long-term potentiation in the hippocampus using depolarizing current pulses as the conditioning stimulus to single volley synaptic potentials. J. Neurosci. *7*, 774–780.

Hamilton, T.J., Wheatley, B.M., Sinclair, D.B., Bachmann, M., Larkum, M.E., and Colmers, W.F. (2010). Dopamine modulates synaptic plasticity in dendrites of rat and human dentate granule cells. Proc. Natl. Acad. Sci. *107*, 18185–18190.

Harris, R.J., Symon, L., Branston, N.M., and Bayhan, M. (1981). Changes in extracellular calcium activity in cerebral ischaemia. J. Cereb. Blood Flow Metab. Off. J. Int. Soc. Cereb. Blood Flow Metab. *1*, 203–209.

Hashimotodani, Y., Ohno-Shosaku, T., Tsubokawa, H., Ogata, H., Emoto, K., Maejima, T., Araishi, K., Shin, H.-S., and Kano, M. (2005). Phospholipase Cbeta serves as a coincidence detector through its Ca2+ dependency for triggering retrograde endocannabinoid signal. Neuron *45*, 257–268.

Hasselmo, M.E. (1999). acetylcholine and memory consolidation. Trends Cogn. Sci. *3*, 9.

Hayashi, Y., Shi, S.H., Esteban, J.A., Piccini, A., Poncer, J.C., and Malinow, R. (2000). Driving AMPA receptors into synapses by LTP and CaMKII: requirement for GluR1 and PDZ domain interaction. Science *287*, 2262–2267.

He, K., Huertas, M., Hong, S.Z., Tie, X., Hell, J.W., Shouval, H., and Kirkwood, A. (2015). Distinct Eligibility Traces for LTP and LTD in Cortical Synapses. Neuron *88*, 528–538.

Heinemann, U., Lux, H.D., and Gutnick, M.J. (1977). Extracellular free calcium and potassium during paroxsmal activity in the cerebral cortex of the cat. Exp. Brain Res. *27*, 237–243.

Higgins, D., Graupner, M., and Brunel, N. (2014). Memory Maintenance in Synapses with Calcium-Based Plasticity in the Presence of Background Activity. PLoS Comput. Biol. *10*, e1003834.

Hoffman, D.A., Magee, J.C., Colbert, C.M., and Johnston, D. (1997). K+ channel regulation of signal propagation in dendrites of hippocampal pyramidal neurons. Nature *387*, 869–875.

Holbro, N., Grunditz, A., Wiegert, J.S., and Oertner, T.G. (2010). AMPA receptors gate spine Ca(2+) transients and spike-timing-dependent potentiation. Proc. Natl. Acad. Sci. U. S. A. *107*, 15975–15980.

Hollmann, M., Hartley, M., and Heinemann, S. (1991). Ca2+ permeability of KA-AMPA--gated glutamate receptor channels depends on subunit composition. Science *252*, 851–853.

Holmgren, C.D., and Zilberter, Y. (2001). Coincident Spiking Activity Induces Long-Term Changes in Inhibition of Neocortical Pyramidal Cells. J. Neurosci. *21*, 8270–8277.

Huang, S., Huganir, R.L., and Kirkwood, A. (2013). Adrenergic gating of Hebbian spike-timing-dependent plasticity in cortical interneurons. J. Neurosci. Off. J. Soc. Neurosci. *33*, 13171–13178.

Huang, S., Rozas, C., Treviño, M., Contreras, J., Yang, S., Song, L., Yoshioka, T., Lee, H.-K., and Kirkwood, A. (2014). Associative Hebbian synaptic plasticity in primate visual cortex. J. Neurosci. Off. J. Soc. Neurosci. *34*, 7575–7579.

Hudmon, A., and Schulman, H. (2002). Structure-function of the multifunctional Ca2+/calmodulin-dependent protein kinase II. Biochem. J. *364*, 593–611.

Huerta, P.T., and Lisman, J.E. (1993). Heightened synaptic plasticity of hippocampal CA1 neurons during a cholinergically induced rhythmic state. Nature *364*, 723–725.

Isaac, J.T.R., Buchanan, K.A., Muller, R.U., and Mellor, J.R. (2009). Hippocampal place cell firing patterns can induce long-term synaptic plasticity in vitro. J. Neurosci. Off. J. Soc. Neurosci. *29*, 6840–6850.

Ismailov, I. (2004). The Kinetic Profile of Intracellular Calcium Predicts Long-Term Potentiation and Long-Term Depression. J. Neurosci. *24*, 9847–9861.

Jacob, V., Brasier, D.J., Erchova, I., Feldman, D., and Shulz, D.E. (2007). Spike Timing-Dependent Synaptic Depression in the In Vivo Barrel Cortex of the Rat. J. Neurosci. *27*, 1271–1284.

Jay, T.M., Gurden, H., and Yamaguchi, T. (1998). Rapid increase in PKA activity during long-term potentiation in the hippocampal afferent fibre system to the prefrontal cortex in vivo. Eur. J. Neurosci. *10*, 3302–3306.

Jester, J.M., Campbell, L.W., and Sejnowski, T.J. (1995). Associative EPSP--spike potentiation induced by pairing orthodromic and antidromic stimulation in rat hippocampal slices. J. Physiol. *484 (Pt 3)*, 689–705.

Jones, H.C., and Keep, R.F. (1988). Brain fluid calcium concentration and response to acute hypercalcaemia during development in the rat. J. Physiol. *402*, 579–593.

Kampa, B.M., Clements, J., Jonas, P., and Stuart, G.J. (2004). Kinetics of Mg2+ unblock of NMDA receptors: implications for spike-timing dependent synaptic plasticity. J. Physiol. *556*, 337–345.

Karmarkar, U.R., and Buonomano, D.V. (2002). A Model of Spike-Timing Dependent Plasticity: One or Two Coincidence Detectors? J. Neurophysiol. *88*, 507–513.

Kempadoo, K.A., Mosharov, E.V., Choi, S.J., Sulzer, D., and Kandel, E.R. (2016). Dopamine release from the locus coeruleus to the dorsal hippocampus promotes spatial learning and memory. Proc. Natl. Acad. Sci. U. S. A. *113*, 14835–14840.

Kim, J., Jung, S.-C., Clemens, A.M., Petralia, R.S., and Hoffman, D.A. (2007). Regulation of Dendritic Excitability by Activity-Dependent Trafficking of the A-Type K+ Channel Subunit Kv4.2 in Hippocampal Neurons. Neuron *54*, 933–947.

Kirkwood, A., Dudek, S.M., Gold, J.T., Aizenman, C.D., and Bear, M.F. (1993). Common forms of synaptic plasticity in the hippocampus and neocortex in vitro. Science *260*, 1518–1521.

Lengyel, I., Voss, K., Cammarota, M., Bradshaw, K., Brent, V., Murphy, K.P.S.J., Giese, K.P., Rostas, J. a. P., and Bliss, T.V.P. (2004). Autonomous activity of CaMKII is only transiently increased following the induction of long-term potentiation in the rat hippocampus. Eur. J. Neurosci. *20*, 3063–3072.

Lezcano, N., and Bergson, C. (2002). D1/D5 Dopamine Receptors Stimulate Intracellular Calcium Release in Primary Cultures of Neocortical and Hippocampal Neurons. J. Neurophysiol. *87*, 2167–2175.

Li, C., Lu, J., Wu, C., Duan, S., and Poo, M. (2004). Bidirectional Modification of Presynaptic Neuronal Excitability Accompanying Spike Timing-Dependent Synaptic Plasticity. Neuron *41*, 257–268.

Lin, Y.-W., Min, M.-Y., Chiu, T.-H., and Yang, H.-W. (2003). Enhancement of associative long-term potentiation by activation of beta-adrenergic receptors at CA1 synapses in rat hippocampal slices. J. Neurosci. Off. J. Soc. Neurosci. *23*, 4173–4181.

Lisman, J., Yasuda, R., and Raghavachari, S. (2012). Mechanisms of CaMKII action in long-term potentiation. Nat. Rev. Neurosci. *13*, 169–182.

Liu, Y., Cui, L., Schwarz, M.K., Dong, Y., and Schlüter, O.M. (2017). Adrenergic Gate Release for Spike Timing-Dependent Synaptic Potentiation. Neuron *93*, 394–408.

Losonczy, A., Makara, J.K., and Magee, J.C. (2008). Compartmentalized dendritic plasticity and input feature storage in neurons. Nature *452*, 436–441.

Lu, J. -t., Li, C. -y., Zhao, J.-P., Poo, M. -m., and Zhang, X. -h. (2007). Spike-Timing-Dependent Plasticity of Neocortical Excitatory Synapses on Inhibitory Interneurons Depends on Target Cell Type. J. Neurosci. *27*, 9711–9720.

Malenka, R.C., and Bear, M.F. (2004). LTP and LTD: an embarrassment of riches. Neuron *44*, 5–21.

Malenka, R.C., and Nicoll, R.A. (1986). Dopamine decreases the calcium-activated afterhyperpolarization in hippocampal CA1 pyramidal cells. Brain Res. *379*, 210–215.

Malinow, R., and Malenka, R.C. (2002). AMPA receptor trafficking and synaptic plasticity. Annu. Rev. Neurosci. *25*, 103–126.

Markram, H., Lübke, J., Frotscher, M., and Sakmann, B. (1997). Regulation of synaptic efficacy by coincidence of postsynaptic APs and EPSPs. Science *275*, 213–215.

McNamara, C.G., Tejero-Cantero, Á., Trouche, S., Campo-Urriza, N., and Dupret, D. (2014). Dopaminergic neurons promote hippocampal reactivation and spatial memory persistence. Nat. Neurosci. *17*, 1658–1660.

Mehta, M.R., Quirk, M.C., and Wilson, M.A. (2000). Experience-Dependent Asymmetric Shape of Hippocampal Receptive Fields. Neuron *25*, 707–715.

Meliza, C.D., and Dan, Y. (2006). Receptive-Field Modification in Rat Visual Cortex Induced by Paired Visual Stimulation and Single-Cell Spiking. Neuron *49*, 183–189.

Miller, R. (1981). Meaning and purpose in the intact brain: a philosophical, psychological, and biological account of conscious processes (Oxford : New York: Clarendon Press ; Oxford University Press).

Min, R., and Nevian, T. (2012). Astrocyte signaling controls spike timing-dependent depression at neocortical synapses. Nat. Neurosci. *15*, 746–753.

Mothet, J.-P., Le Bail, M., and Billard, J.-M. (2015). Time and space profiling of NMDA receptor co-agonist functions. J. Neurochem. *135*, 210–225.

Mukherjee, S., and Manahan-Vaughan, D. (2013). Role of metabotropic glutamate receptors in persistent forms of hippocampal plasticity and learning. Neuropharmacology *66*, 65–81.

Mulkey, R.M., and Malenka, R.C. (1992). Mechanisms underlying induction of homosynaptic long-term depression in area CA1 of the hippocampus. Neuron *9*, 967–975.

Mulkey, R.M., Endo, S., Shenolikar, S., and Malenka, R.C. (1994). Involvement of a calcineurin/inhibitor-1 phosphatase cascade in hippocampal long-term depression. Nature *369*, 486–488.

Neve, K.A., Seamans, J.K., and Trantham-Davidson, H. (2004). Dopamine Receptor Signaling. J. Recept. Signal Transduct. Res. *24*, 165–205.

Neveu, D., and Zucker, R.S. (1996). Postsynaptic Levels of [Ca2+]i Needed to Trigger LTD and LTP. Neuron *16*, 619–629.

Nevian, T., and Sakmann, B. (2006). Spine Ca2+ Signaling in Spike-Timing-Dependent Plasticity. J. Neurosci. *26*, 11001–11013.

Nguyen, P.V., and Kandel, E.R. (1997). Brief theta-burst stimulation induces a transcription-dependent late phase of LTP requiring cAMP in area CA1 of the mouse hippocampus. Learn. Mem. Cold Spring Harb. N *4*, 230–243.

Nicholson, C., Bruggencate, G.T., Steinberg, R., and Stöckle, H. (1977). Calcium modulation in brain extracellular microenvironment demonstrated with ion-selective micropipette. Proc. Natl. Acad. Sci. U. S. A. *74*, 1287–1290.

Nishiyama, M., Hong, K., Mikoshiba, K., Poo, M., and Kato, K. (2000). Calcium stores regulate the polarity and input speci®city of synaptic modi®cation. *408*, 5.

O'Connor, D.H., Wittenberg, G.M., and Wang, S.S.-H. (2005). Graded bidirectional synaptic plasticity is composed of switch-like unitary events. Proc. Natl. Acad. Sci. *102*, 9679–9684.

O'Dell, T.J., Connor, S.A., Guglietta, R., and Nguyen, P.V. (2015). β-Adrenergic receptor signaling and modulation of long-term potentiation in the mammalian hippocampus. Learn. Mem. Cold Spring Harb. N *22*, 461–471.

Otmakhova, N.A., Otmakhov, N., and Lisman, J.E. (2002). Pathway-specific properties of AMPA and NMDA-mediated transmission in CA1 hippocampal pyramidal cells. J. Neurosci. Off. J. Soc. Neurosci. *22*, 1199–1207.

Paille, V., Fino, E., Du, K., Morera-Herreras, T., Perez, S., Kotaleski, J.H., and Venance, L. (2013). GABAergic circuits control spike-timing-dependent plasticity. J. Neurosci. Off. J. Soc. Neurosci. *33*, 9353–9363.

Palacios-Filardo, J., and Mellor, J.R. (2019). Neuromodulation of hippocampal long-term synaptic plasticity. Curr. Opin. Neurobiol. *54*, 37–43.

Pawlak, V. (2010). Timing is not everything: neuromodulation opens the STDP gate. Front. Synaptic Neurosci. *2*.

Pawlak, V., and Kerr, J.N.D. (2008). Dopamine Receptor Activation Is Required for Corticostriatal Spike-Timing-Dependent Plasticity. J. Neurosci. *28*, 2435–2446.

Pedarzani, P., and Storm, J.F. (1995). Dopamine modulates the slow Ca(2+)-activated K+ current IAHP via cyclic AMP-dependent protein kinase in hippocampal neurons. J. Neurophysiol. *74*, 2749–2753.

Petersen, C.C.H., Malenka, R.C., Nicoll, R.A., and Hopfield, J.J. (1998). All-or-none potentiation at CA3-CA1 synapses. Proc. Natl. Acad. Sci. *95*, 4732–4737.

Petrovic, M.M., Nowacki, J., Olivo, V., Tsaneva-Atanasova, K., Randall, A.D., and Mellor, J.R. (2012). Inhibition of post-synaptic Kv7/KCNQ/M channels facilitates long-term potentiation in the hippocampus. PloS One *7*, e30402.

Pike, F.G., Meredith, R.M., Olding, A.W., and Paulsen, O. (1999). Rapid report: postsynaptic bursting is essential for "Hebbian" induction of associative long-term potentiation at excitatory synapses in rat hippocampus. J. Physiol. *518 (Pt 2)*, 571–576.

Pin, J.P., and Duvoisin, R. (1995). The metabotropic glutamate receptors: structure and functions. Neuropharmacology *34*, 1–26.

Ramos, B.P., and Arnsten, A.F.T. (2007). Adrenergic pharmacology and cognition: focus on the prefrontal cortex. Pharmacol. Ther. *113*, 523–536.

Rodríguez-Moreno, A., and Paulsen, O. (2008). Spike timing-dependent long-term depression requires presynaptic NMDA receptors. Nat. Neurosci. *11*, 744–745.

Rosen, Z.B., Cheung, S., and Siegelbaum, S.A. (2015). Midbrain dopamine neurons bidirectionally regulate CA3-CA1 synaptic drive. Nat. Neurosci. *18*, 1763–1771.

Rosenkranz, J.A. (2006). Dopaminergic Regulation of Neuronal Excitability through Modulation of Ih in Layer V Entorhinal Cortex. J. Neurosci. *26*, 3229–3244.

Rosenmund, C., Feltz, A., and Westbrook, G.L. (1995). Calcium-dependent inactivation of synaptic NMDA receptors in hippocampal neurons. J. Neurophysiol. *73*, 427–430.

Safo, P., and Regehr, W.G. (2008). Timing dependence of the induction of cerebellar LTD. Neuropharmacology *54*, 213–218.

Salgado, H., Köhr, G., and Treviño, M. (2012). Noradrenergic 'Tone' Determines Dichotomous Control of Cortical Spike-Timing-Dependent Plasticity. Sci. Rep. *2*.

Sanhueza, M., McIntyre, C.C., and Lisman, J.E. (2007). Reversal of synaptic memory by Ca2+/calmodulin-dependent protein kinase II inhibitor. J. Neurosci. Off. J. Soc. Neurosci. *27*, 5190–5199.

Sara, S.J. (2009). The locus coeruleus and noradrenergic modulation of cognition. Nat. Rev. Neurosci. *10*, 211–223.

Schiller, J., and Schiller, Y. (2001). NMDA receptor-mediated dendritic spikes and coincident signal amplification. Curr. Opin. Neurobiol. *11*, 343–348.

Schiller, J., Schiller, Y., Stuart, G., and Sakmann, B. (1997). Calcium action potentials restricted to distal apical dendrites of rat neocortical pyramidal neurons. J. Physiol. *505*, 605–616.

Schiller, J., Schiller, Y., and Clapham, D.E. (1998). NMDA receptors amplify calcium influx into dendritic spines during associative pre- and postsynaptic activation. Nat. Neurosci. *1*, 114–118.

Schuett, S., Bonhoeffer, T., and Hübener, M. (2001). Pairing-Induced Changes of Orientation Maps in Cat Visual Cortex. Neuron *32*, 325–337.

Schultz, W. (1998). Predictive reward signal of dopamine neurons. J. Neurophysiol. *80*, 1–27.

Seol, G.H., Ziburkus, J., Huang, S., Song, L., Kim, I.T., Takamiya, K., Huganir, R.L., Lee, H.-K., and Kirkwood, A. (2007). Neuromodulators Control the Polarity of Spike-Timing-Dependent Synaptic Plasticity. Neuron *55*, 919–929.

Shen, W., Flajolet, M., Greengard, P., and Surmeier, D.J. (2008). Dichotomous dopaminergic control of striatal synaptic plasticity. Science *321*, 848–851.

Shin, R.-M., Tsvetkov, E., and Bolshakov, V.Y. (2006). Spatiotemporal asymmetry of associative synaptic plasticity in fear conditioning pathways. Neuron *52*, 883–896.

Shinoe, T. (2005). Modulation of Synaptic Plasticity by Physiological Activation of M1 Muscarinic Acetylcholine Receptors in the Mouse Hippocampus. J. Neurosci. *25*, 11194–11200.

Shouval, H.Z., Bear, M.F., and Cooper, L.N. (2002). A unified model of NMDA receptor-dependent bidirectional synaptic plasticity. Proc. Natl. Acad. Sci. *99*, 10831–10836.

Shulz, D., and Frégnac, Y. (1992). Cellular analogs of visual cortical epigenesis. II. Plasticity of binocular integration. J. Neurosci. Off. J. Soc. Neurosci. *12*, 1301–1318.

Silver, I.A. (1990). Intracellular and extracellular changes of [Ca2+] in hypoxia and ischemia in rat brain in vivo. J. Gen. Physiol. *95*, 837–866.

Sjöström, P.J., and Häusser, M. (2006). A Cooperative Switch Determines the Sign of Synaptic Plasticity in Distal Dendrites of Neocortical Pyramidal Neurons. Neuron *51*, 227–238.

Sjöström, P.J., Turrigiano, G.G., and Nelson, S.B. (2001). Rate, Timing, and Cooperativity Jointly Determine Cortical Synaptic Plasticity. Neuron *32*, 1149–1164.

Sjöström, P.J., Turrigiano, G.G., and Nelson, S.B. (2003). Neocortical LTD via Coincident Activation of Presynaptic NMDA and Cannabinoid Receptors. Neuron *39*, 641–654.

Sourdet, V. (1999). The Role of Dendritic Filtering in Associative Long-Term Synaptic Plasticity. Learn. Mem. *6*, 422–447.

Spruston, N. (2008). Pyramidal neurons: dendritic structure and synaptic integration. Nat. Rev. Neurosci. *9*, 206–221.

Stefan, K. (2000). Induction of plasticity in the human motor cortex by paired associative stimulation. Brain *123*, 572–584.

Stefan, K., Kunesch, E., Benecke, R., Cohen, L.G., and Classen, J. (2002). Mechanisms of enhancement of human motor cortex excitability induced by interventional paired associative stimulation. J. Physiol. *543*, 699–708.

Stefani, M.R., and Gold, P.E. (2001). Intrahippocampal Infusions of K-ATP Channel Modulators Influence Spontaneous Alternation Performance: Relationships to Acetylcholine Release in the Hippocampus. J. Neurosci. *21*, 609–614.

Steinberg, J.P., Takamiya, K., Shen, Y., Xia, J., Rubio, M.E., Yu, S., Jin, W., Thomas, G.M., Linden, D.J., and Huganir, R.L. (2006). Targeted in vivo mutations of the AMPA receptor subunit GluR2 and its interacting protein PICK1 eliminate cerebellar long-term depression. Neuron *49*, 845–860.

Stuart, G.J., and Häusser, M. (2001). Dendritic coincidence detection of EPSPs and action potentials. Nat. Neurosci. *4*, 63–71.

Sugisaki, E., Fukushima, Y., Tsukada, M., and Aihara, T. (2011). Cholinergic modulation on spike timing-dependent plasticity in hippocampal CA1 network. Neuroscience *192*, 91–101.

Sugisaki, E., Fukushima, Y., Fujii, S., Yamazaki, Y., and Aihara, T. (2016). The effect of coactivation of muscarinic and nicotinic acetylcholine receptors on LTD in the hippocampal CA1 network. Brain Res. *1649*, 44–52.

Suri, R.E., and Schultz, W. (1999). A neural network model with dopamine-like reinforcement signal that learns a spatial delayed response task. Neuroscience *91*, 871–890.

Thiele, A. (2013). Muscarinic signaling in the brain. Annu. Rev. Neurosci. *36*, 271–294.

Thomas, M.J., Moody, T.D., Makhinson, M., and O'Dell, T.J. (1996). Activity-dependent beta-adrenergic modulation of low frequency stimulation induced LTP in the hippocampal CA1 region. Neuron *17*, 475–482.

Tomasulo, R.A., and Ramirez, J.J. (1993). Activity-mediated changes in feed-forward inhibition in the dentate commissural pathway: relationship to EPSP/spike dissociation in the converging perforant path. J. Neurophysiol. *69*, 165–173.

Tong, G., Shepherd, D., and Jahr, C.E. (1995). Synaptic desensitization of NMDA receptors by calcineurin. Science *267*, 1510–1512.

Tzounopoulos, T., Kim, Y., Oertel, D., and Trussell, L.O. (2004). Cell-specific, spike timing–dependent plasticities in the dorsal cochlear nucleus. Nat. Neurosci. *7*, 719–725.

Tzounopoulos, T., Rubio, M.E., Keen, J.E., and Trussell, L.O. (2007). Coactivation of pre- and postsynaptic signaling mechanisms determines cell-specific spike-timing-dependent plasticity. Neuron *54*, 291–301.

Valtcheva, S., Paillé, V., Dembitskaya, Y., Perez, S., Gangarossa, G., Fino, E., and Venance, L. (2017). Developmental control of spike-timing-dependent plasticity by tonic GABAergic signaling in striatum. Neuropharmacology *121*, 261–277.

Wang, F. (2004). Steering growth cones with a CaMKII/calcineurin switch. Neuron *43*, 760–762.

Wang, H.-X., Gerkin, R.C., Nauen, D.W., and Bi, G.-Q. (2005). Coactivation and timing-dependent integration of synaptic potentiation and depression. Nat. Neurosci. *8*, 187–193.

Watts, V.J., and Neve, K.A. (1997). Activation of type II adenylate cyclase by D2 and D4 but not D3 dopamine receptors. Mol. Pharmacol. *52*, 181–186.

Weber, J.P., Andrásfalvy, B.K., Polito, M., Magó, Á., Ujfalussy, B.B., and Makara, J.K. (2016). Location-dependent synaptic plasticity rules by dendritic spine cooperativity. Nat. Commun. *7*, 11380.

Wickens, J. (1990). Striatal dopamine in motor activation and reward-mediated learning: steps towards a unifying model. J. Neural Transm. Gen. Sect. *80*, 9–31.

Winder, D.G., and Sweatt, J.D. (2001). Roles of serine/threonine phosphatases in hippocampal synaptic plasticity. Nat. Rev. Neurosci. *2*, 461–474.

Wittenberg, G.M., and Wang, S.S.-H. (2006). Malleability of Spike-Timing-Dependent Plasticity at the CA3-CA1 Synapse. J. Neurosci. *26*, 6610–6617.

Wolters, A., Sandbrink, F., Schlottmann, A., Kunesch, E., Stefan, K., Cohen, L.G., Benecke, R., and Classen, J. (2003). A Temporally Asymmetric Hebbian Rule Governing Plasticity in the Human Motor Cortex. J. Neurophysiol. *89*, 2339–2345.

Wong, R.P., and Bradbury, M.W. (1975). Permeability of the blood-brain barrier to calcium in adrenal insufficiency. Brain Res. *84*, 361–364.

Woodin, M.A., Ganguly, K., and Poo, M. (2003). Coincident pre- and postsynaptic activity modifies GABAergic synapses by postsynaptic changes in Cl- transporter activity. Neuron *39*, 807–820.

Wyllie, D.J., and Nicoll, R.A. (1994). A role for protein kinases and phosphatases in the Ca(2+)-induced enhancement of hippocampal AMPA receptor-mediated synaptic responses. Neuron *13*, 635–643.

Xu, J. (2005). Activity-Dependent Long-Term Potentiation of Intrinsic Excitability in Hippocampal CA1 Pyramidal Neurons. J. Neurosci. *25*, 1750–1760.

Xu, T.-X., and Yao, W.-D. (2010). D1 and D2 dopamine receptors in separate circuits cooperate to drive associative long-term potentiation in the prefrontal cortex. Proc. Natl. Acad. Sci. *107*, 16366–16371.

Yamamuro, Y., Hori, K., Tanaka, J., Iwano, H., and Nomura, M. (1995). Septo-hippocampal cholinergic system under the discrimination learning task in the rat: a microdialysis study with the dual-probe approach. Brain Res. *684*, 1–7.

Yang, K., and Dani, J.A. (2014). Dopamine D1 and D5 Receptors Modulate Spike Timing-Dependent Plasticity at Medial Perforant Path to Dentate Granule Cell Synapses. J. Neurosci. *34*, 15888–15897.

Yang, S.-N., Tang, Y.-G., and Zucker, R.S. (1999). Selective Induction of LTP and LTD by Postsynaptic $[Ca^{2+}]_i$ Elevation. J. Neurophysiol. *81*, 781–787.

Yao, H., and Dan, Y. (2001). Stimulus Timing-Dependent Plasticity in Cortical Processing of Orientation. Neuron *32*, 315–323.

Yao, H., Shen, Y., and Dan, Y. (2004). Intracortical mechanism of stimulus-timing-dependent plasticity in visual cortical orientation tuning. Proc. Natl. Acad. Sci. *101*, 5081–5086.

Yuan, L.-L., Adams, J.P., Swank, M., Sweatt, J.D., and Johnston, D. (2002). Protein kinase modulation of dendritic K+ channels in hippocampus involves a mitogen-activated protein kinase pathway. J. Neurosci. Off. J. Soc. Neurosci. *22*, 4860–4868.

Zhang, J.-C., Lau, P.-M., and Bi, G.-Q. (2009). Gain in sensitivity and loss in temporal contrast of STDP by dopaminergic modulation at hippocampal synapses. Proc. Natl. Acad. Sci. *106*, 13028–13033.

Zhang, L.I., Tao, H.W., Holt, C.E., Harris, W.A., and Poo, M. (1998). A critical window for cooperation and competition among developing retinotectal synapses. Nature *395*, 37–44.

Zhou, Y.-D., Acker, C.D., Netoff, T.I., Sen, K., and White, J.A. (2005). Increasing Ca2+ transients by broadening postsynaptic action potentials enhances timing-dependent synaptic depression. Proc. Natl. Acad. Sci. *102*, 19121–19125.